Support structure for offshore solar

The proposal of a new concept

A.B.Z. Feys

Report number: SDPO.20.007

TU Delft

Support structure for offshore solar

The proposal of a new concept

by

A.B.Z. Feys

to obtain the degree of Master of Science
at the Delft University of Technology,
to be defended publicly on Friday June 26, 2020 at 10:00 AM.

Student number:	4303830	
Project duration:	April 23, 2019 – June 26, 2020	
Thesis committee:	Prof. ir. J.J. Hopman,	TU Delft, chairman
	Dr.-Ing. S. Schreier,	TU Delft , supervisor
	Dr. ir. G.H. Keetels	
	Dr. ir. O. Isabella	

An electronic version of this thesis is available at http://repository.tudelft.nl/.
Cover picture was obtained from Ekrullia [8]

TU Delft

Preface

Thank you for your interest in my thesis. I wrote this thesis for the completion of my master in Marine Technology at the Delft University of Technology. After studying in Delft since September 2013, I will graduate on the twenty-sixth of June in the design track of my studies. Over my study period, I was always actively involved in the educational program and the association for marine technology students: S.G. ”William Froude”.

Finishing this thesis leaves me with a sigh of relieve. I must honestly confess that, at the beginning of this thesis, I could not predict how challenging this endeavour would be. The process of learning and discovering was highly rewarding. I learned a lot about myself and about doing research. Finishing this thesis and my master gives me a feeling of fulfilment and pride.

Thanks to the support I got during the thesis, I could bring this thesis to the right end. The long conversations and discussions with my supervisor Sebastian provided me with the scientific structure and knowledge that was needed for the completion of this task. His analytical and humane approach was an indispensable contribution to the success of my thesis. Furthermore, I want to thank my supervising professor, professor Hopman, for this overview and feedback on the monthly feedback meetings. Furthermore, I would like to thank Mr. Keertels and Mr. Isabella for reading my thesis, providing me with feedback and questions during the green light meetings and my, currently upcoming, defence. Moreover, I want to thank all my teachers and professor who helped me with obtaining knowledge that led to my master degree.

During the challenging period of writing my thesis and during all the steps that lead to this point I also got great support from outside of the university. Therefore I want to thank my parents, my brother and my girlfriend. Furthermore, I want to thank my friends. You were a great support! Especially many people who provided feedback on my sometimes hard to understand and complicated and to read writing styles?!

I hope you enjoy reading,
Thank you, Andreas

Delft, June 2020

Summary

This thesis presents the potential of solar energy to answer the increasing demand for sustainable energy. Multiple floating solar parks are installed on inland water bodies. This trend is a result of the lack of surface for Photo Voltaic systems and a result of legislation on national and international governmental levels, for the reduction of greenhouse gasses. This inland technology is currently well established. Still, in densely populated areas such as the Netherlands supplementary surface could be beneficial to unlock the full potential of solar energy. Ocean and sea surfaces are a possible, but challenging solution to this problem. These offshore water surfaces could be used for electricity or synthetic fuel production.

Offshore locations are attractive because of the abundant availability of surface. Still, an Offshore Floating PV-system needs to overcome multiple technical and non-technical challenges and requirements. This challenge demands technical solution within the constraints of a suitable business case. Furthermore, the impact on people and ecology also needs to stay within ethical borders.

An Offshore Floating PV can be subdivided into three physical subsystems: an energy converting system, a position monitoring or mooring system and a floating support structure. Multiple concepts were proposed in literature or by the industry. All proposed concepts are variations of support systems that provide a surface for conventional Photo Voltaic-technology. It also was concluded that none of the proposed concepts is fully developed. Currently, only one system is in the testing phase. The current state of the technology, and the high potential of an Offshore Floating PV are the drivers behind the search for a new concept design.

In this thesis, the requirements for an Offshore Floating PV support structure were formulated, and a brainstorm resulted in the buoy and beam concept for further research. The buoy and beam structure is a system in which submerged beams form a triangle grid are held together by floating buoys. The buoys support triangle platforms, by carrying the corners of the platforms. All connections between the buoys, beams and platforms are fully hinged. Because of the hinges, the structure can move with the waves and therefore mitigates the loads it experiences.

In the second part of this thesis, the feasibility of the buoy and beam structure was assessed. It was concluded that the heave response is the most critical response to the feasibility of the concept. When the platform would heave too much, the waves will slam into the platforms and the solar panels, leading to damage and excessive loads on the structure. Consequently, the heave response and the relative wave height seen from the moving triangle platform are researches and modelled.

The structure was identified as a hydrodynamic transparent structure. Consequently, the relevant hydrodynamic loads are obtained with the Morison equation and Airy wave theory. All damping terms are linearised. A differential equation incorporated the constrains for both, the construction and the hydromechanic loads. The mechanical equations can be linearised by assuming small angular displacements of the beams.

This differential equation is implemented in a calculation tool in MATLAB. The code is verified over multiple steps. The tool made it possible to obtain the response based on the topology and the main dimensions of the buoys and the beams.

With this calculation tool relations between the dimensions of the buoys and beams on one side and the frequency response, on the other hand, are identified by simulating different variations of a simplified starting design. The following conclusions were made on the eigenfrequencies. Firstly, it was noted that the eigenfrequencies of the system are in proximity to each other. Secondly, it was shown that the first and second eigenfrequency could be calculated in a simplified manner. Thirdly, it was seen that the buoy diameter to mass ratio has a positive linear correlation with respect to the eigenfrequency, i.e. the stiffness to mass ratio of the system severely influences the eigenfrequency. Furthermore, it was seen that an increasing beam length has a slight linear correlation with the eigenfrequency. Also, it was concluded that a large hexagon system (for example, nineteen buoys) could be beneficial because a hexagon structure creates a large surface with respect to the number of buoys. Moreover, in reality, the response should be lower than the model prediction, as a result of the high number of beams that cause damping. Additionally, a hexagon system should have a minimal change in response for differ-

ent incoming wave angle.
To obtain a feasible system, the response peaks of the structure should not overlap with the wave spectrum. Based on the additional simulation, it was concluded that it should be possible to design a system with a low eigenfrequency resulting in a system that will only slightly move with the waves. Additional relations between the dimensions of the buoys and beams and the response peaks were found. The requirements to obtain a low eigenfrequency and a modest response match, which positively influences the feasibility.
Some further steps on the research of the heave response and the relative wave height are needed. The calculation tool can still be improved. A preciser estimation of the response peaks is of significant importance. Some further iterations must be executed to determine the full potential and feasibility of the concept design. Furthermore, in a scientific point of view, it will be highly interesting to validate the model on a model scale.
In the development of the buoy and beam structure, additional critical responses need to be researched. The forces in the hinges and the response in horizontal direction need to be known for further assessment of the feasibility. Next to the technical aspects, the human, ecological and economic implications of the buoy and beam structure need to be researched.

Goal and outline of the thesis

In this thesis an extensive introduction to the topic Offshore Floating PV is written in chapter 1, 2 and 3. To better guide the reader the goal and the thesis outline will be introduced hereafter.

Goal of the thesis

The goal of this thesis is to develop a new concept design for an Offshore Floating PV support structure and demonstrate its feasibility. First, the necessity of developing a new floating support structure for Offshore Floating PV is argued. This necessity leads to the first subgoal of this thesis: the proposition of a new concept. This new concept will have multiple pitfalls and responses. A second subgoal is to identify the most critical response for the feasibility of the proposed concept. The development of a modelling tool for the assessment of the most critical response of the proposed concept is the third subgoal of this thesis. This modelling tool should indicate the response and should be simple and fast so that it can be used as a design tool. Based on this tool, the influence of the design parameters, of the new concept, on the critical response should be examined, which is a last subgoal of the thesis. This will make it possible to assess the feasibility of the concept with respect to the most critical response.

Outline of the thesis

The first three chapters form together an introduction to the topic of Offshore Floating PV. This helps to define the goal of this thesis. Chapter 1 gives a motivation and presents background on the need for floating solar. Societal trends that support and push this new technology will be discussed. In chapter 2, the requirements for an Offshore Floating PV structure will be identified based on a triple bottom line assessment. The found requirements will be grouped and are used in chapter 3 (section 5.2) to assess the existing concepts. Later these requirements are reused to assess the concepts resulting from the brainstorm.

In chapter 3, the state of the art of floating solar energy is discussed. Relevant literature related to Offshore Floating PV will be discussed. And as said above, the currently existing concepts found in the literature will be compared and assessed with the defined requirements. This chapter will conclude the substantial introduction of this thesis and will lead up to the definition of the research goal presented in chapter 4.

The research definition sets the goal of this thesis on finding a feasible new concept design for an Offshore Floating PV support structure. A brainstorm and selection process is presented in chapter 5, furthermore, the most critical response of this new concept will be identified. In section 5.4, the modelling approach and requirements for the calculation tool are discussed. A more detailed description of the outline of the modelling part of the report can be found in section 5.4. This outline is visualised by Figure 5.10 on page 45.

The mechanical aspects of the modelling will be discussed, followed by the hydrodynamical elements, in chapter 6 and chapter 7 respectively. Substitution of these two theoretical approaches will be executed in chapter 8. The implementation of the model in the MATLAB code and the procedure of stepwise verification of the model are discussed in chapter 9 and chapter 10.

With the full model, that can be used as a design tool, variations on the design parameters will be carried out in chapter 11. These variations will identify the influence of the design parameters on the most critical response. This analysis will lead to a proposition of design guidelines. With these design guidelines, a concept for low eigenfrequency is presented and simulated in section 11.3. Chapter 12 will discuss the proposed design and the calculation tool. Recommendations on the model and the concept design will be formulated. Chapter 13 gives an overall conclusion of the presented work of this thesis.

Contents

1

Background on floating solar

In current society, there are many trends and pressures for carbon-free energy generation. An alternative energy form is the capture and conversion of solar irradiance by, for example, Photo Voltaic (PV) technology. Solar power tends to be space-intensive because of the relatively low energy density per square meter compared to conventional carbon energy. Therefore, there are multiple solutions found to overcome this surface hunger. One of the proposed solutions is floating solar and offshore floating solar [64].
This chapter gives an introduction to these ecological and societal trends. Furthermore, it discusses the basic setup and the advantages and disadvantages of Floating Photo Voltaic (FPV).

1.1. Societal trends behind floating solar

The increasing world population needs an increasing amount of energy to sustain and improve living quality. Energy is currently, for the majority, sourced by consuming fossil fuels which emit CO_2 into the atmosphere. Not only has CO_2 a major influence on global warming, but the carbon energy resource is also limited. [24] Global and local policies are adopted to minimise and mitigate global warming and climate change. The Paris Agreement formulates these global intentions. At the time of writing, 185 countries have ratified the convention that set the aims to keep the global warming well under 2°C and do efforts to lower it even further under 1.5°C [45]. In 2019, 10.9% of the global energy consumed was coming from renewable sources [41, p.31]. [39]
On a local level, these ambitions are converted into laws and policies. The EU, China and many other countries are actively stimulating green energy alternatives to minimise the CO_2 emission, such as solar power, hydropower and wind energy. The EU has set targets on increasing renewable energy, reduction of greenhouse gas emission and the increase of energy efficiency for 2020 and 2030. As a long term goal the EU wants to “cut its emissions [by 2050] substantially – by 80-95% compared to 1990 levels” [9, 10].[10, 38]
Specifically, in the Netherlands, the target is to produce 14% and 27% of all used energy from sustainable sources by respectively 2020 and 2030. In 2050, all energy should come from sustainable sources [42]. In the Netherlands and other Western European countries, the space requirements are challenging due to the high population density.
The increasing world population needs an increasing land resource. The land is needed for agriculture and living but also for renewable energy harvesting, which is land-intensive. Some renewable energy systems have moved to alternative places to cope with, on the one hand, land scarcity and, on the other hand, to be realised on large scales for maximum efficiency. Offshore wind farms and solar fields in deserted areas are examples of this trend. In both cases, the potential of the technologies enlarges as these locations have respectively more wind than inland installations and they have larger solar irradiance then regions that are more frequently cloudy. [13, 56]
A second trend related to the increasing world population is the demographic shift from the countryside towards the major cities. As cities are ever-growing, the energy need in these densely populated areas is increasing simultaneously. Most of these cities are located in coastal areas or the proximity of large water bodies. These water bodies are often used for several economic activities. [59]

The storage of energy in the energy transition towards more sustainable energy poses a technical challenge. Akinyele and Rayudu [1] indicates the potential of different energy storage methods. However, the technologies available in this instance still have multiple downsides and challenges to overcome before they can be widely applied. Not only storage is difficult (as indicated in the paper of Akinyele and Rayudu). Transport over longer distances is also relatively hard compared with carbon fuels. The unpredictability and the challenges with transport create the need for diversified renewable energy sources close to the consumer. Solar energy can be used on a sunny day, and wind energy is used during the night for example.
The need for a fast energy transition, as indicated by the national and international goals on greenhouse gasses, is a great opportunity for solar energy. Solar energy has a high potential due to the abundance of solar irradiance. Solar energy provides energy during the day when energy demand is higher. Combining solar energy with other renewable energy sources creates a diverse renewable energy generation system. The average solar irradiance at the earth surface varies between 60 and $250W/m^2$ [20]. Certainly between a latitude of -45 to +45 °the technology is highly interesting because of the relatively high solar irradiance [55]. “Research has shown that “black dot” areas could provide more than the entire world’s total primary energy demand, assuming that a conversion efficiency as low as 8% is achieved” as can be observed in Figure 1.1 [20]. There are multiple solar energy converting technologies of which concentrated solar technology and PV are the most common.

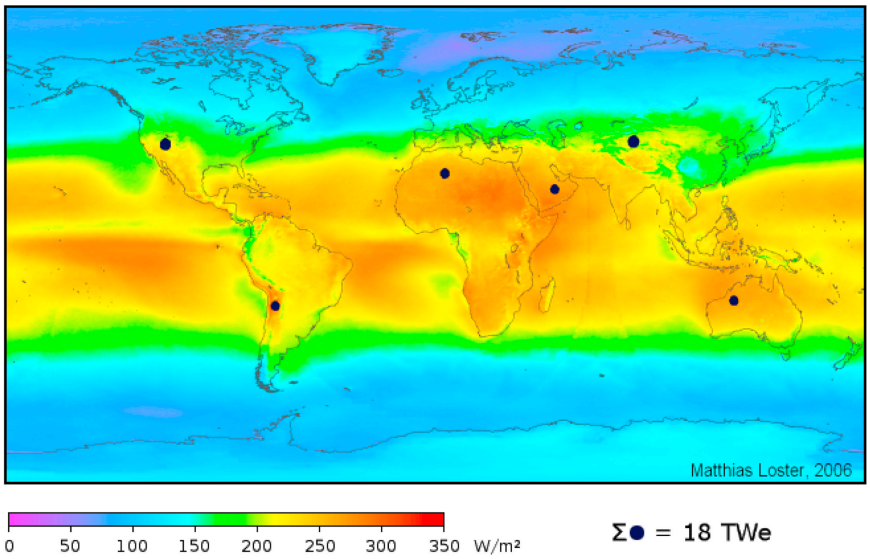

Figure 1.1: “Annual average solar irradiance distribution over the surface of the Earth” “Research has shown that “black dot” areas could provide more than the entire world’s total primary energy demand, assuming that a conversion efficiency as low as 8% is achieved.” [20]

Contrary to what Figure 1.1 shows, is that solar energy is space-intensive. Certainly, with the pressure of urbanisation, it is hard to provide space for solar energy in the proximity of the many end-users in large urban areas. Large cities and densely populated countries are often located on sea or ocean shores. Consequently, there is an opportunity to explore energy generation on the less used surface of the seas and oceans. Over the last 20 years, offshore wind energy increased [16]. Multiple reasons drive offshore wind energy; one of them is the space requirement [16]. The pressures mentioned above (sustainable energy need and surface requirements) could result in an opportunity for Offshore Floating PV (OFPV) applications. The potential of FPV is discussed by multiple sources: Hogerwaard et al. [17], Patterson et al. [37], Solanki et al. [47], Trapani [55], Trapani and Millar [56], World Bank [64].

1.2. Floating solar power

PV is a solar energy converting technology that, in case of FPV, is located on the water surface to convert solar irradiance to electricity. A conceptualisation of Inland Floating PV (IFPV) will follow to in-

troduce the concept of FPV. All IFPV installations consist of three basic parts, as can be seen in Figure 1.2. These three parts are a floating structure an anchoring system and a system that converts, combines and transport the energy. The floating platform provides a surface for the PV-panels. Cabling, combiner boxes, inverters and transformers combine the energy to add it to the electricity network or use it in another way.

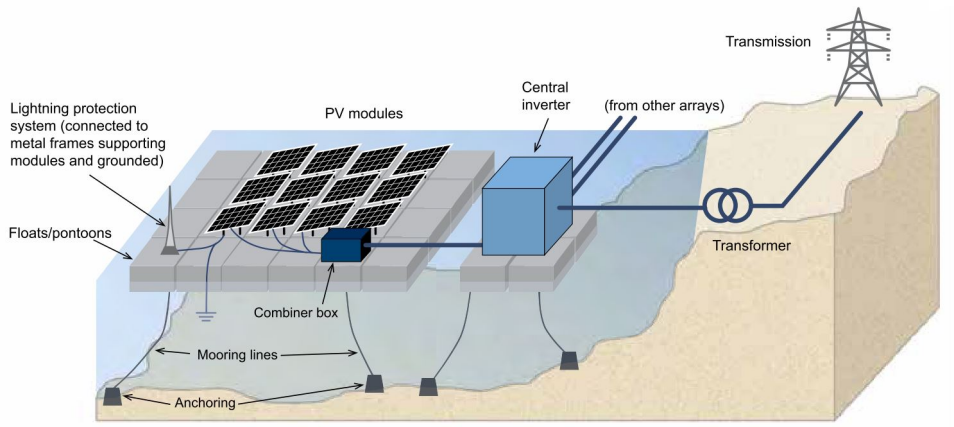

Figure 1.2: “Schematic representation of a typical large-scale [inland] FPV system with its key component”[65, p10]

In this thesis, a distinction will be made between IFPV farms and OFPV farms. IFPV are FPV’s installed on inland water bodies. These inland water bodies are all water bodies that are not classified as oceans or seas, which are mostly freshwater. There, no violent waves will occur. OFPV is located on seas and oceans. The division between offshore and inland is made as the loads, exerted on the construction, in offshore installations are notably higher. Therefore significantly different solution and design are needed.
To discuss the advantages and disadvantages of the technology Table 1.1 is made based on literature and discussed in detail in the sequel. For some instances, there are differences between offshore and inland application. In these situations, “i” indicates inland installations, “o” indicates offshore installations.

Table 1.1: Advantages and disadvantages of floating solar. (o): applicable on OFPV, (i): applicable on IFPV.

Advantages	**Disadvantages**
I) Renewable energy	a) Interference with ecology
II) Reduction of evaporation	b) Interference with economic activities
III) Cooling of PV-panels	c) Complex environment (o)
IV) Usage of obsolete surface	d) Energy gain is latitude dependent
V) Less shading	e) In a concept stage (o)
VI) Proven technology on short term (i)	
VII) Modular character	
VIII) Close to population hubs	
IX) Integration in other renewable energy	
X) No moving parts	

These advantages and disadvantages need some more background. Therefore the number and letters indicated in Table 1.1 is used as a cross-reference. (I) Solar energy is a renewable energy that could contribute to the global aim for the reduction of greenhouse gasses. (II) In hot climates, FPV farms can cover (drinking or irrigation) water reservoirs to reduce water evaporation [52, 64]. (III) At the same time, the water can reduce the module operating temperature, which improves efficiency. The natural cooling is especially interesting in regions with a hot climate since the PV panels tend to heat faster. In literature and commerce, the cooling advantage (claims of 10 % efficiency increase as a result of cooling [5, 58]) is widely used to promote the technology. These claims need some reluctance as they

are coming from tests in hot climates. In these hot climates, the cooling effect is most probably higher than in relative cooler climates.
(IV) In multiple cases, such as water reservoirs, hydropower lakes, offshore waters, etc. the water surface is not used, or current activities will not be hindered by dual-use for FPV farms. Furthermore, Folkerts et al. [14] indicates that for The Netherlands, surface for solar is a limiting factor for solar energy, and that FPV could be a potential solution. (V) In most situations, there are no obstacles on the water surface that cause shade.
(VI) PV technology is a proven technology for land-based energy generation and has been installed in large quantity, reaching an overall quantity of 500 GW [41]. Furthermore, the FPV farms on inland water bodies became a proven technology over the last decade with over 1GW installed in September 2018 [64]. Due to the novelty of the technology, a longer track record is still missing so far point. (VII) The modular character and the relatively easy installation of the technology are most probably one of the reasons for the fast growth. The floating structure consists of components of manageable size, similar to the size of a conventional industrial PV panel, which is easily on-site assembled. [64]
(VIII) Most megacities are located in the proximity of seas or drinking water basins. These water surfaces could be used to generate energy close to these cities. (IX) On the other hand, the FPV can be integrated and combined with current renewable energy sources by installing them on hydropower lakes or in offshore wind parks. (X) Another advantage is that the PV technology has no moving parts for power generation, which reduces the maintenance. [64]
(a) However, a downside could be the impact on the ecological environment. There are no publications on in-depth studies of the impact on marine and other wildlife. Nevertheless, it is believed that the reduction of the contact surface between water and air and the creation of underwater shade could influence the ecology. FPV could, therefore, generate safe havens and breeding ground for species. Observations of offshore wind farms have shown that some species flourish as a result of the absence of fishing. The positive impact on the ecology is arguable since the main progress could be related to the removal of overfishing. (b) The system competes with other water surface-related (economic) activities. Options for mutual benefits need to be found or generated.
(c) For OFPV, the technology is less mature than for inland applications [64]. So far, only one test is in execution on the possibilities for offshore installation. An offshore environment is challenging due to the larger loads and the more complex and demanding environment that is involved with the offshore operation. The wind, waves and currents exert loads on the structure, which makes it difficult. It is also more complicated because of a higher risk of biofouling and the corrosive environment. (d) Yet, the energy gain is for all PV technologies dependent on the specific solar irradiance at the location.

1.3. Arguments for offshore solar research

There are strong reasons to advocate research into offshore floating solar farms. There is a need for sustainable and green energy due to the impact of greenhouse gasses on the climate. Therefore a shift needs to be made in the coming decades. There are multiple sources of renewable and sustainable energy. Of these sources, solar energy is a highly interesting option because of its abundance of solar irradiance. Currently, solar energy is mainly applied in land-based installations. Still, big steps are necessary as defined in multiple policy documents on climate change. To meet the targets on the reduction of greenhouse gasses interests have been growing in the use of IFPV.
Placing FPV on hydropower lakes, water reservoirs and other water bodies have significant advantages. Also, here the available surface is limited. For that reason, researchers start to look at the largest water bodies on this planet: such as oceans and seas. Placing solar power on seas and oceans will create multiple challenges, considering the harsh environment. There is currently no dominant or proven concept for OFPV. This makes OFPV an interesting topic for research, and it establishes the opportunity to come up with new concepts that can perform better in a challenging offshore environment. Therefore the current state of the art on FPV should be researched, for OFPV and IFPV.

2

Requirements for an offshore solar system

Offshore Floating PV (OFPV) was identified as a technology that could meet the requirements for future sustainable energy without using the land surface. An OFPV concept needs to fulfil multiple demands to be a success. These requirements are the result of the interaction with its context. Prerequisites imposed by the context are identified by a "Triple Bottom Line (TBL)" analysis (People Planet Profit). The requirements and their interconnections will be identified in this chapter. Finding a system that meets the demands should make it possible to compete and contribute to future energy provision.

2.1. A qualitative triple bottom line analysis

"The TBL is an accounting framework that incorporates three dimensions of performance: social, environmental and financial" Slaper [46, p.1]. TBL is known as the triple "P" which refers to People Planet Profit. It is a procedure to assess not only the financial requirements but also includes other aspects of sustainability. Some other procedures or assessments such as the sustainable or the millennium development goals, do not fully/sufficiently take the economic aspects into account. [46]
In literature, some sources try to quantify the advantages and disadvantages of the three pillars [27, 54]. Accurate quantification is in all instances complex since the pillars of People and Planet can not easily be expressed in a common (monetary) unit. Moreover, the technology of OFPV is undeveloped and undefined. Therefore the assessment of the system itself is not yet achievable. [46]
The TBL analysis will identify the requirements for an OFPV system. These three P's represent the context of the system. A qualitative analysis shall be executed. Implying that the TBL analysis will be used as a guideline and basis to find the demands imposed by the context. These requirements are the basis and benchmark for a feasible and possible successful system. The interaction will work in mutual directions. This means, for example, that the planet (and environment) aspect will not only be influenced by the presence of a FPV system, but the environment will also affect the system. An OFPV can create opportunities that have a positive impact on all aspects of the TBL assessment. When these opportunities are utilised, and the requirements are met, a competitive and relevant design can be obtained.
Figure 2.1 presents the system and its boundaries. The system within the boundaries is to be determined, and performance can be assessed based on the requirements. The context, or what is outside of the system boundaries, will impose demands on the system. The figure also partly displays items within the system. These represent subsystems of the FPV-system. There are three physical systems: the energy converting system (A), the position keeping or monitoring system (B) and the (floating) support system (C). Lastly, there is a management system (D).

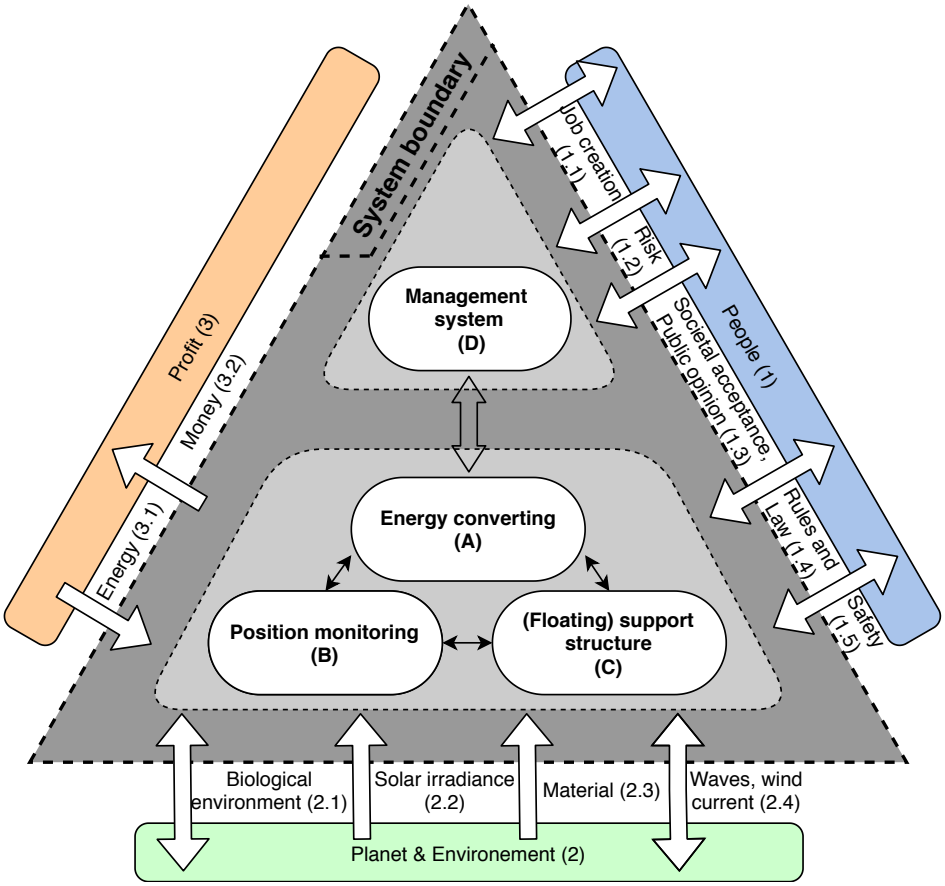

Figure 2.1: System diagram of an OFPV system including context, based on quantitative TBL-analysis

The main purpose of the system is to convert the solar irradiation to usable energy. Solar irradiance coming from the system's environmental context is of major influence on the system. Section 2.1 stated that a certain amount of energy inflow per surface area would be present at a certain time and location. Because of the small inflow of energy per square meter, the system has to cover a large surface area. So, the system consists of three physical subsystems:

A The energy converting subsystem that will capture the energy emitted by the sun and transfer it to usable energy. Inherent to the relatively low energy density per square meter, this means that the subsystem most probably will extend over a large surface. The energy will be transformed and will be emitted over the system boundaries.

B A position monitoring subsystem is needed. It does not mean that all concepts or solutions will need to have a fixed position over time. It is still necessary to know the location of the system when the construction is not fixated on a specific location. Lastly, there is a management subsystem required

C The need for a large surface area to collect significant energy implies that the large energy converting subsystem will need some kind of support. This support system is the second subsystem.

D The management subsystem is not a physical subsystem. It includes all management steps over its lifetime.

The TBL analysis can assess these four systems and their interaction.

People (1)
In all aspects, climate change will have a significant effect on people and society. A shift is simply a necessity for humanity. A successful FPV concept could be part of the energy transition. Thus, a FPV concept should contribute positively to the desired energy transition. Additionally, the new activities

related to OFPV should have a positive socio-economic impact by creating jobs and business opportunities. Contrary, the new technology also brings challenges to the people aspect. Firstly, the influence of public opinion will have an impact. There is resistance against offshore wind farms and IFPV farms [12, 34, 35]. A similar resistance can occur for OFPV applications. Another major requirement for the success of the technology is the absence of failure. When during the testing period or after the installation, failure appears, it will largely impact public opinion. Not only public opinion will be impacted, but it can also greatly affect people's safety. Thus the technology should be safe and resist the environmental conditions. Safety does not only emphasise on the integrity of the structure. It also stresses the safety related to all aspects of the installation during its lifetime. When considering surface usage, FPV should not compete, or it should win the competition with the current users of the space. Lastly, there is a need for the development of new knowledge and expertise. The new developments can then cascade to potential other new technologies.

Planet & environment (2)
The usage of space or surface of an organisation, individual, society, technology, etc. over its lifetime is a representation of the impact on the planet[62]. Solar energy inevitably needs significant surface. The technology creates shading underwater, and it generates a barrier for wildlife that operates on the surface of the sea. For this reason, again, the technology needs to be compact and space-efficient. However, the FPV can positively affect its environment by generating safe havens for fish, as discussed in section 1.2.
The FPV generates renewable energy. This still does not make it a sustainable technology. Over the life cycle (the production and extraction of material to the decommissioning and recycling) the technology should have a low (environmental) impact. The material selection also needs to be done sustainably, taking recycling into account. During the lifetime, no parts or pieces should break loose or should dissolve (things such as microplastics, oils, etc.), and it should not harm or pollute nature in any other way. Furthermore, the technology should minimise (underwater)noise during installation, operation and removal as this highly impacts wildlife.
The solar irradiance does not only have benefits, but it also stresses the system due to harmful UV-light. Other loads coming from the environment are wind, waves and currents. Depending on the position relative to the water surface, the construction will experience more or less stresses from these environmental loads. Finally, there is the interaction with the biological environment. The present fauna and flora around the system can impact the construction in the form of biofouling. The installation should be able to handle all environmental loads on the installation as waves, winds, currents, UV light, biofouling,...

Profit (3)
The main driver for the technology will be the potential profitability. This is of major importance for the success of a new design. Making compromises on people and planet to increase profitability should be done with great caution and within the ethical boundaries. Subtracting the cost from the revenues approximates the profitability. Yet, other aspects need to be taken into account, such as risk, time, lifetime, etc. The price of energy will define revenues. The costs could be subdivided base on the life cycle in (0)[1] the development cost of the technology; (a) material, production and installation costs of the platform; (b) the operation and maintenance cost of the platform; and (c) the recycling and decommissioning costs. The design choices made early in the process will highly impact all these parameters. The system aim is minimising the cost over the economic life and maximise the revenue over the process and its lifetime, within the ethical borders stated in the people and planet sections. The profitability depends both on the system itself and on the market and the environment in which it operates.
In Figure 2.1 highly simplifies the profitability by indicating an investment inflow that then results in an energy outflow in a not yet determined energy form.

Discussion
An installation that can resist the offshore conditions is vital for multiple reasons: to minimise the risk of environmental pollution, to guarantee people's safety and to maximise economic benefits. The survivability and risk of failure are highly related to the maintenance (cost) of the system. The system should

[1] Zero indicates that it does not need to be included once the technology is established.

be cost-effective; material choice and usage is an important factor in this. Material selection and usage affect the pressure on the environment, and it impacts the business case. The ability to survive harsh conditions might conflict with the minimisation of material usage and needs to be balanced. Lastly, there is a need for an installation that is easy to produce, install, maintain and manage.

2.2. Requirements for offshore solar system

When providing a new design for an OFPV system, the design should fulfil the requirements discussed in the qualitative TBL analysis in section 2.1. The requirements will be discussed separately and reformulated. These requirements will form a guideline in the assessment of current concepts and the development of potential new concepts. Therefore the requirements will be grouped. Main requirements can have subrequirements. Multiple requirements will be applied to multiple stages of the system's lifetime. The lifetime of the system is defined in Figure 2.2. The operational period should be taken into consideration.

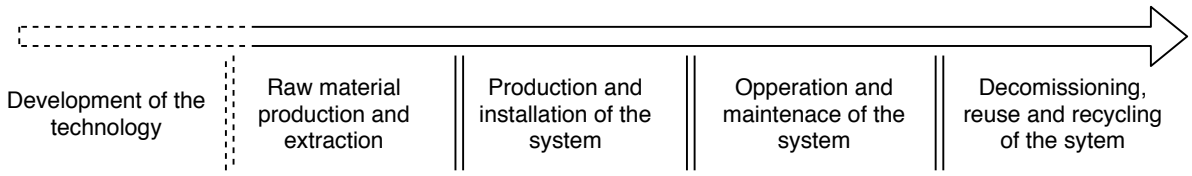

Figure 2.2: Timeline of an OFPV system

Produce energy conform market price

A successful system needs to be able to compete with alternative energy-producing systems. Here the importance of the business case or economic viability comes into play. The system-boundary currently excludes energy consumption. The business case could include an extra energy conversion or energy need on a specific location. For example, in the paper of Patterson et al. [37], the consumption and price of methanol should be included in the business case. This thesis excludes the consumption of energy.

The timeline defined in Figure 2.2 will be used to structure the costs involved in the system. All costs should be limited, taking into account the boundaries set by the other requirements.

- **Development costs of the technology**
  In Figure 2.2, the development cost is not included. The development costs depend on the state of the art of the technologies in cooperated in the new design.

- **Minimal material costs**
  The material choice has a strong interconnected dependency with other requirements. As other requirements will also determine the materials of choice.

- **Production and installation costs**
  Depending on the complexity and the exact design of the system production and installation costs will differ.

- **Operation and maintenance costs**
  This cost is related to the risk of failure and its components and the complexity of the repair.

- **Decommissioning and recycling**
  The cost of decommissioning and recycling should not be disregarded as the afterlife highly influences the performance on the TBL analysis.

On the other hand, there is the revenue side of the business case. Figure 2.1 states that the output will be energy.

- **Energy gain**
  The energy gain needs to be maximised and should account for the invested cost. The energy gains both need to be maximised over the costs and surface usage.

Environmental conditions
For multiple aspects of the TBL analysis, the installation must be able to cope with its environment. Surviving the environmental conditions can be translated to minimising the risk of failure due to the loads caused by the environment. Firstly, the environmental loads can be related to the wind, the waves and currents and the response of the system. Secondly, biological interaction will exert loads. Thirdly, the installation will age over time; this includes potential corrosion, wear, fatigue, etc. The three main environmental conditions to be considered, are listed hereafter:

- Survive the loads related to:
  - waves,
  - wind and
  - current.
- Minimise the negative impact of biological interaction, such as biofouling and bird dropping.
- Handle the aspects of ageing over its lifetime. This includes corrosion, fatigue and change of material properties.

Overcoming and surviving these environmental conditions over a certain timespan is a necessity for a valuable business case as a failing system will hold increasing maintenance costs and will limit the revenues. Thus, it is directly related to economic validity. Furthermore, a failing installation can have a high impact on the people and planet aspects when, for example, parts break loose.

Lifetime
As long as the system can fulfil the other requirements, there is no need to indicate a minimal or maximum lifetime. Still, the economic factors will demand a certain lifetime. For example, a certain production or installation cost and the energy input power by the sun is limited. Therefore a certain lifetime is required to earn back your expenditure by your revenue for your output energy. Current offshore projects give a reasonable indication of possible lifespan. Most offshore wind farms or ships have an engineering lifetime of 20 years.

Minimisation of ecological impact
Regarding the TBL analyses, the urge of a system with minimal ecological impact can be concluded. As mentioned in section 2.1, it is highly difficult to quantify or translate the ecological impact to a monetary value. Therefore, it is hard to compare it with economic gain. But this should not lead to concessions on the ecological impact. Some methods are suggested to assess the ecological impact.

- Life cycle analysis
  The ISO-definition of LCA is the “compilation and evaluation of the inputs, outputs and the potential environmental impacts of a product system throughout its life cycle” [15]. It is often used to investigate the effects of materials mainly. The life cycle analysis focuses on the impact of the used materials and the reuse and recycling after the economic lifetime.
- Ecological impact assessment
  “Ecological impact assessment is the process of identifying, quantifying and evaluating the potential impacts of defined actions on ecosystems or their components. If properly implemented, it provides a scientifically defensible approach to ecosystem management.”[15]
- Additional research on legal or policy guidelines
  Depending on the geographic location, the legal framework can generate some additional requirements on this topic.

Minimal development time
As said before, one of the drivers of this new technology is the desire to reduce greenhouse gasses. Therefore, there is a strong desire that the technology needs to be available within a certain time. It should be taken into account the time needed to integrate a new technology takes multiple years. In the early 1990s, the first offshore wind farm was installed after numerous years of research. Minimising the complexity of the technologies and focusing on incorporating established technologies will minimise development time. This way, it might be possible to contribute to the policy goals set for the reduction of greenhouse gasses.

Safe for people
People can be classified into two groups. First, the group that is actively involved during the lifetime of the installation. These are people involved from the production till the dismantling of the installation. Second, the people who are in the sphere of influence of the FPV installation, for example, fishermen or other seamen. The safety of the individuals in both groups should be a priority of the system at all times.

Other
Legal requirements should be actively regarded. specific legislation will depend on the location. The social resistance to the new technology should be minimised. Finally, the financing of new technology is a complicated factor in itself.

Concluding table
The requirements and the relations with the TBL analysis and the larger requirements are summarised in Table 2.1. An Analytic Hierarchy Process (AHP) analysis will execute a prioritisation on the requirements in the second part of the next chapter. In the right part indicates how certain requirements are combined under the categories cost, survivability, development time and safety. Items can only be categorised in one category. Combining and organising these requirements is used in the assessment of a feasible design based on the TBL assessment.

Table 2.1: Concluding table on the requirements of an OFPV system and the relations in respect to the TBL-assessment

	People (1)	Planet (2)	Profit (3)	Cost	Survivability	Development time	Safety
Development time		×	×			×	
Survive in current	×	×	×		×		
Survive in waves	×	×	×		×		
Survive in wind	×	×	×		×		
Ageing	×	×	×		×		
Operation and maintenance costs			×	×			
Safety	×		×				×
Decommissioning and recycling costs		×	×	×			
Production and installation costs			×	×			
Material costs			×	×			
biofouling	×	×	×		×		
Development costs			×	×			

3

State of the art of floating solar

This chapter discusses relevant concepts to give an overview of the current state of technology. Concepts and applications of Inland Floating PV (IFPV) are briefly covered first. Next, the chapter only discusses aspects of IFPV that are relevant for Offshore Floating PV (OFPV). Second, the proposed concepts and the current state of offshore applications will be discussed. The different concepts will be assessed based on the requirements found in section 2.2. This will lead to a comparison between the concepts and their advantages and disadvantages and potential. Furthermore, the most promising concepts in the perspective of this writer of this thesis will be pointed out.

3.1. Inland floating PV

Over the last decade, the cumulative installed power of FPV platforms on inland water bodies has been rising drastically. The first installation was deployed in 2007 in Japan for research purposes. Afterwards, many other small installations were deployed for demonstration or research purposes. Currently, larger commercial installations have been installed, mainly in Japan, Korea and China. A cumulative power of 1314 MWp was reached at the end of 2018 (see Figure 3.1) according to the World Bank. All of these projects were installed on inland water bodies except for some test or demonstration projects in protected coastal waters of Norway and The Maldives [65]. On the other hand, marine (or even offshore) application of PV is not new at all. There are solar-powered buoys for research and as navigation aids guiding ship traffic.

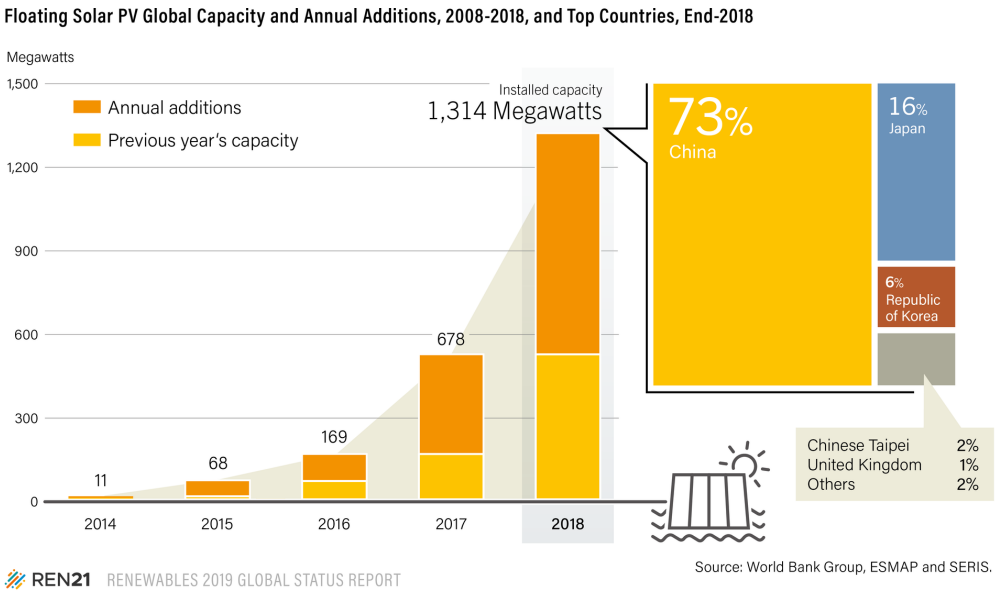

Figure 3.1: Increase of cumulative installed capacity of FPV on inland waters [64]

In the period between 2007 and 2013, the technology was in an exploratory phase. Multiple concepts were proposed and tested by mainly research groups. The concepts introduced can be split into two groups. Those who made use of large floaters (structures larger than two PV-panels) and those who use modules (that are the same size as one or two PV-panels).
In the first group, some concepts made use of pontoons [67] or other floating elements such as cubes, buoys or tubes reinforced with metal frames for the creation of a large platform. The first group was popular in the first stage of development. Trapani [55] created an overview of all projects executed between 2007 and 2014. Additionally, Sahu et al. [44] gives a more general overview of the different concepts. In this first group, some concepts tried to increase energy yield. Some were tracking the sun with rotation over one or two angels. Others were using lenses or reflectors to increase the solar irradiance. Others were using direct water cooling of the PV-panels by placing the PV modules directly in the water. Currently, there are still some projects executed that use larger tubular floating systems which track the sun, but this is rather seldom. [55]
The second group contains proven technology. The project of Ferrer-Gisbert et al. [11] was the first technology that contained small floats. A similar concept is later patented and commercialised by the French company Ciel et Terre. The platforms are made of different plastic floating modules that can be connected. Their construction consists of modules that hold the PV-panels, modules for walkways and extra modules. All modules are floating. They can all be connected to obtain one large IFPV field. The technology from Ciel et Terre (called Hydrelio) has been used for multiple projects. Chinese Sungrow and Dutch Profloating have produced similar products. The technology can be regarded as the winning concept for inland floating projects.
Based on the fast technology advancement of IFPV and the increasing applications, the World Bank created overview reports for the promotion and understanding of the new technology. For the report, they work together with the Singaporean research institute SERIS. SERIS is linked with the University of Singapore. SERIS runs a testbed for IFPV technologies. They published an extensive market report that gives insights for governments, policymakers, investors, etc. [64] The report contains a detailed overview of all the current concepts inland and offshore. Furthermore, they made a special and extensive handbook for practitioners. The handbook goes into detail on topics such as design, economic and legal considerations, construction, maintenance and many more. [66]

3.2. Offshore floating PV concepts

The development of OFPV is not as advanced yet as IFPV. Some projects and concepts have been proposed, and on an exceptional basis, the concept is tested. This section of the report will give an overview of the proposed concepts. Figure 3.2 gives an overview. Information that can be found will be summarised and shared. This thesis will indicate the issues or challenges of the technology that might arise according to the author. Lastly, the concepts will be analysed and compared based on the requirements set in section 2.2. It will indicate the potential of the different concepts.

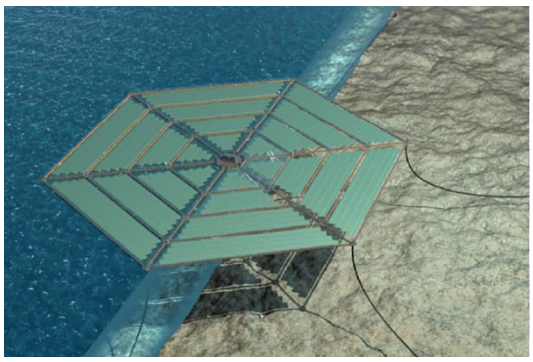

(a) SUNdy project of DNV [22]

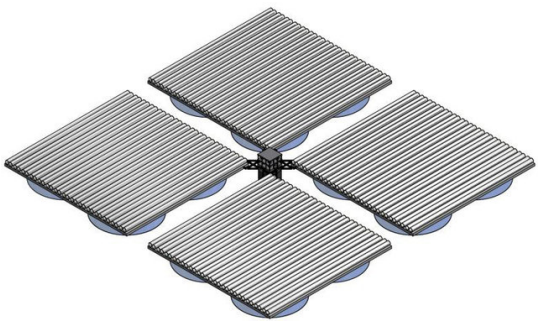

(b) Concept by Diendorfer et al. [7]

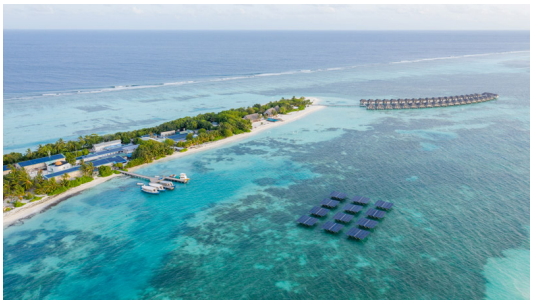

(c) Swimsol OFPV [51]

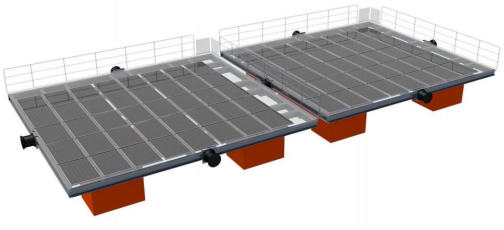

(d) Concept by Moss Maritime [29]

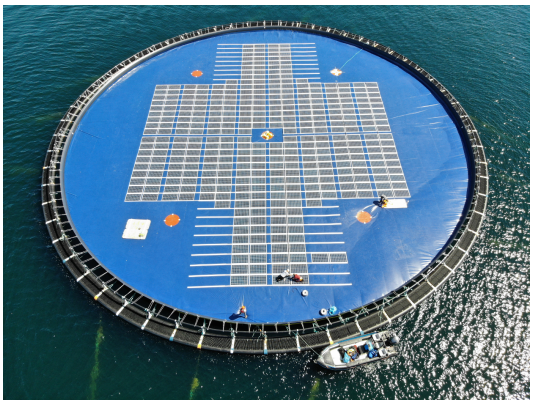

(e) Ocean Sun concept [31]

(f) Oceans of Energy concept [30]

Figure 3.2: Current proposed concepts and concepts in testing phase for FPV

3.2.1. SUNdy project, DNV

First, there is the concept generated by DNV KENA, a part of current DNV GL focussing on energy. The concept is called SUNdy (see Figure 3.2a). It was proposed in October 2012. It is a modular floating 2MW producing hexagon system. Twenty-five of these arrays should together form a system with a total power of 50 MWp. One hexagon consists of multiple onshore assembled modules of flexible, thin-film PV panel mounted onto a flexible floating mattress. The system contains all needed inverters and converters and is located in the middle of the hexagon. The information online does not specify if the hexagon is a stiff skeleton or a flexible line structure. The publication talks about a “tension only design”. The “tension design only” is most probably talking about the mooring system or the flexible PV panel mattresses in between the stiff beams. These mattresses are mounted in a spider web fashion. The system is moored in 20 to 100m water depth. According to the image, the hexagon does not deflect under the weight of the anchor lines suggesting that the hexagon skeleton is made of stiff beams. [22, 43, 55]

The publication and the project did not have any follow up. The KEMA department within DNV (now DNV GL) is not public anymore and is part of DNV GL Energy. Which suggests that they do not further develop the concept. The extensive report of SERIS and the World Bank did not mention the concept either. Due to the standstill and the commercial nature, not much is know about the system details. Thus, it is hard to study the realism behind the structural design. Freely discussing the design based on limited information, some remarks could be made. Assuming that the hexagon is made of a stiff skeleton to maintain its shape means that there will be large loads on the mattresses and PV-panels in heavy seas. In that case, the mattresses will operate as a parachute system in a fluid due to the response of the structure in waves resulting in probably unrealistic large loads. Assuming, the unlikely case of a flexible hexagon skeleton, the system has a large risk on wrinkling and folding. Yet, this theoretical excise points out the interest for FPV from some time ago.

“The panels themselves are envisaged to be laminated and added to a flexible foam surface, which gives the panels buoyancy and structure” [44]. Trapani [55] already executed the first test cases of flexible PV-panels in a water environment. However, the loads on the foam mattress could be a major

point of concern, both technologically and financially. The efficiency of flexible PV-panels is lower then the stiff ones [55]. The absence of a suitable, flexible material for the mattress could increase the development time drastically; especially, as result of the limited knowledge on flexible elements in offshore conditions related to failure mechanisms such as fatigue.
Due to the flexible nature, the material quantity needed to withstand the internal forces could be lower compared to rigid or stiff solutions, which might result in a rather cost-effective construction. Trapani [55] mentions the intention of adding walkways to the structure. When humans need to be on board, special safety requirements should be incorporated in the construction. Due to the position of the PV-panels, there is a risk of green water. This could lead to the impact of breaking waves and possibilities of biofouling on top of the panels.

3.2.2. Diendorfer et al., University of Vienna

A second project is proposed in 2013 by Diendorfer et al. at the University of Vienna in which multiple air chambers create support by flexible skirts for concentrated solar power, as indicated in Figure 3.2b. The flexible skirts are pulled down by weight at the bottom of the skirt. The paper focuses mainly on the performance of concentrated solar power, taking into account the dynamic behaviour of the floating structure in model scale. The paper concludes that the concentrated solar system on the proposed floater has the potential to have a similar performance as inland systems. [7]
The parer does not explain the development of the floater technology. The next steps in the development process that were suggested were further designing of the floating structure and estimation of financial performance. The realism and concept of the technical and structural layout are not argued in the paper presented by Diendorfer et al. [7]. No follow up has been published.
The authors of the paper doe do not discuss the realism of the concept on a large scale. Issues that could arise are related to the skirt that should provide the buoyancy. The paper indicates a weight of $50kg/m^2$ but does not indicate the dimensions of the system. Only from some graphs, a glimpse of the dimensions can be deduced, indicating a side of 150 meters. Assuming four cylinders per platform and therefore a cylinder diameter of $150/2 = 75meter$ results in a pressure of $624Pa$ within the skirt. [7] Assuming a flexible skirt thickness of $50mm$ results in a stress of $\frac{pD}{2t} = 939kPa$ for static situations (with p the pressure, D the diameter and t the skirt thickness). What seems like a reasonable and achievable option. But most probably the issue starts to occur in dynamic conditions. Additionally, no dimensions of the skirts are given, and the risk of the loss of pressure is not known. The structure is model tested in specific situations and does include heave motion and does not discuss extreme wave conditions. Yet the consequences of failure can be high. The authors think that the risk of failure of the skirt are likely and need further investigation. Failure mechanisms that could be identified are loss of pressure due to rupture, loss of pressure when part of the skirts comes out of the water, rupture of the skirt as a result of stress concentration, fatigue or interaction with other floating objects, etc. An additional issue with the skirt is the difficulty of finding and producing a material with suitable properties for the skirt. The technology might be delayed due to the absence of technology needed for the skirt. Lastly, the interconnection in the middle of the four platforms shown in Figure 3.2b will experience high loads that most probably are unrealistic in most offshore conditions.
On material cost, it is hard to indicate the performance. The indication off $50kg/m^2$ for the total weight could mean that the quantity of material is relatively low [7]. This weight indication is rather low in the perception of the author of this thesis. But the weight focused on the application of concentrated solar and could be different if other solar technologies are applied.
A later instance, the University of Vienna cooperated in the research of the Swimsol concept, discussed hereafter. Almost no similarities have been found between this concept and the concept of Swimsol. It supports the assumption that the concept was discarded.
Improvements to the basic concept can be suggested. First, it could use PV-panels. Secondary the number of skirts could be increased to improve redundancy. However, the challenges related to the skirt are not covered when these improvements are included.

3.2.3. Swimsol

The company Swimsol did research together with the University of Vienna and installed multiple FPV systems in the Maldives. Currently, they are testing a new prototype of 3.25 kWp, 1:2 scale model that should be able to handle up to 4 meter high waves shown in Figure 3.2c. The concept that they

developed is a rigid pontoon with a dedicated floating system. [51]
The solar farm is installed in protected waters, so it is disputable if it can be classified as a fully offshore installation. They patented a system that consists of a truss system providing the platform for the PV-panels. The patent focuses on the buoyancy mounted on the tubes of the trusses providing a stable platform for the PV-panels. The system is fully rigid and has no flexible character. The system has been installed on a small scale in protected waters. [40]
It seems to be a hard system to scale up. When scale-up was needed, an array of these small scale systems was installed. That is not a problem if they desire to only power small holiday islands, as they currently do. No plans or intentions for full offshore installation have been communicated. The main risk of failure that is identified was the risk of slamming. Due to the limited freeboard, the PV-panels may be damaged by larger waves. Therefore the author concludes that the system cannot be applied offshore with the current design. Even though it is a system that was shown to be technically and economically viable in protected waters.

3.2.4. MOSS Maritime

The next two concepts are coming from Norwegian companies. First, there is the concept of MOSS Maritime, which is proposed in the summer of 2019 (see Figure 3.2d). Hence, it is the most recently introduced concept. They designed a modular square pontoon (10m x 10m) concept. The pontoons are flexible connected. The connections are located in the middle of the sides of the square. So, the modules can move relatively with respect to each other. The module dimensions need to be adjusted for every location. The system is intended for offshore and inland applications. The complete system will be moored to the seabed. Every nine modules should have one platform that holds the electronics for all nine modules. On their social media channel, they mention that they will test on model scale. So far, no results have been communicated. [29]
It is unclear where they plan to install the systems. They only specify a case of a wave height of 3 to 4 meter and a period of 10 seconds resulting in a wavelength of 150 meters. In which one wavelength should at least have ten modules. The connection is made in the middle of the sides of the square. This is most probably done to provides a more flexible system for all incoming wave directions.
That design provokes a higher risk on slamming of the waves on the underside of the deck. As a result of the flexible nature on, the risk of slamming will be slightly altered. Furthermore, the construction is connected with hinges. The Space@Sea research project investigated other structures were with large pontoons. The Space@Sea project is a triangle concept the triangle concept to provide large floating areas at oceans and seas. The hinges connecting the triangle platforms experience unrealistically high loads. [61] As a result of the similarity with the MOSS Maritime concept, the connection of large pontoons with hinges is doubtful. The communicated wave height of 3 to 4 meter is relatively small for full offshore usage. The concept visualisation does already include walkways for people increasing the safety of people. Additionally, the system does not include complex, new technologies, except for the multiple hinged bodies and the connections.

3.2.5. Ocean Sun

The second Norwegian project is presented by the company Ocean Sun. The concept was proposed in 2017 and can be seen in Figure 3.2e. They developed a fully flexible system. A round-shaped ring tensions a flexible membrane. On that membrane, the PV-panels are mounted with a cumulative power of 200 kW or 500 kW. As far as known they are rigid PV slide in specific slots mounted on the fabric. The system is still in development and is meant for nearshore, protected and inland waters. The system is protected with patents. [25, 32]
The floating fish farms largely inspire the project. Some of the current fish farms are located on the shores of Norway. One of the fish farms' concepts also consists of round-shaped polyurethane tubes holding the nets that are underwater (see Figure 3.3c hereafter). The structure aims to work fully flexible to minimise and mitigate the loads. The advantage is that the knowledge of these fish farms can be used. The fish farms are also located in protected waters. Fish farms that are further offshore tent to use other designs. The author concludes that the flexible polyurethane tubes are not or not yet applicable in full offshore conditions. It could be forecasted that the loads due to the membrane further increase. One of the challenges with the concept is the strength and the loading for the membrane. It is unclear what happens with green water as this could be a potential. As a result of the movement of the flexible system, the change in shape can lead to large loads on the fabric. Additionally, the rigid

PV-panels will probably apply local stress concentrations on the fabric.

3.2.6. Oceans of Energy

Lastly, there is the concept of Oceans of Energy. They are currently executing a test on the North Sea. They want to test a 50 kWp system for one year. Currently, a 17kW system is installed. They aim to build a system that can survive in wave heights up to 13 meters. For now, they tested with a maximum wave height of 4 meters. [30, 60]
It is difficult to identify the risks in this concept. It is easier to focus on the unknown. Firstly, the module size is unknown, analysing the Figure 3.2f it seems that one module has dimensions in the range of 2 meters by 22 meters. It looks as if there is some kind of hinge between the modules. Similarly to the Moss Maritime concept, the hinges could experience high loads when interacting with the waves. Secondly, it is unknown how the buoyancy is arranged and what the effect is of green water on deck. Oceans of Energy states that it helps to remove bird droppings. However, it can also imply risks. The proximity between the PV-panels and the sea surface can bring difficulties with it. Breaking waves could result in relatively high loads on the surface, and constant contact with salty seawater can enhance corrosion. Moreover, regular water on deck could lead to biofouling. The limited freeboard indicates that there is only limited residual buoyancy, which means that it might be unsafe for people to walk on the platform. Extending the system further could mean that the middle platforms might not be accessible anymore.

3.2.7. Other tests and literature

Lastly, there are some other related technologies discussed in the literature. Trapani [55] proposed the use of flexible PV-panels. They specifically focus on the socio-economic case of Malta and target the technical application of flexible PV-panels in an aquatic environment. No specific concept for the layout and arrangement of the system is stated. According to the findings, the flexible PV-panels perform well in these conditions.
Patterson et al. [36] proposed an offshore system for the generation of synthetic methanol powered by the energy of OFPV. The design of the PV panel platform was based on the research done by Li [26] in his PhD thesis. Li [26] studied the wave-induced hydroelastic response of a circular floating collar in the context of fish farming. The research of Li [26] was then extended to FPV by Kristiansen and Borvik [23] by model testing a circular FPV with an air cushion supported island. The topology is similar to the Ocean Sun concept only here the PV-panels are now supported by entrapped air underneath the sail, which is then similar to the concept of Diendorfer et al.. The skirts are way shorter, which leads to even higher risks.

(a) Test of flexible PV-panels by Trapani and Millar [57]

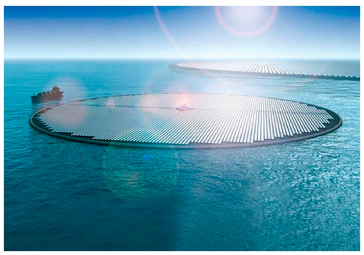

(b) Concept artist impression used by Patterson et al. [36]

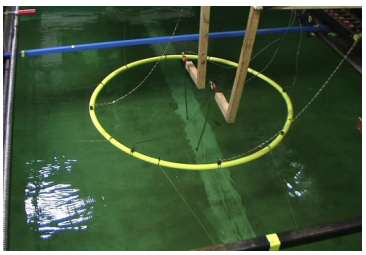

(c) Test set up for flexible fish farms executed by Li [26]

3.3. Comparison between concepts and assessing on requirements

In section 3.2 the published concepts are introduced. First, a qualitative and quantitative comparison will be made based on the available information. Second, these concepts will be assessed on the requirements set in section 2.2.
It can be concluded that the systems presented have considerable similarities. The following items need to be concluded. Firstly, all systems make use of buoyancy. This is the most logical system for support as creating buoyancy is a material-efficient way to create support in (deep) offshore waters. The option of bottom founded structures is not discussed or presented. Most probably due to the limited locations with shallow waters. Even in the commercial implementation of Swimsol, which is placed in

(shallow) atoll waters, a floating system was chosen. Secondly, the systems all consider conventional PV technology except for the concept of Diendorfer et al.. The distinction in concepts can be detected between flexible PV technology and more conventional rigid PV technology. The systems that are already in the application or testing phase (Swimsol, Ocean Sun and Oceans of Energy) apply the rigid PV-panels. PV technology is well established and is, therefore, the most logical choice. Thirdly, it is noticed no mooring system is discussed, except for the SUNdy project and the concept researched by Patterson et al.. The knowledge of mooring can be used from the offshore oil and gas industry. All systems behave in a flexible nature. Some systems have fully flexible elements other are flexible connected rigid bodies. Lastly, it must be pointed out that all concepts are still in the concept phase or in the first parts of the testing phase. The real challenge is the scale up to full scale.
The proposed solutions are all variations on a floating support structure for conventional PV technology. Conventional PV technology has clear advantages over other solar energy converting systems and support via buoyancy is an effective and efficient choice for a stable platform.
The quantitative comparison in table 3.1 will discuss the year of introduction and development period, the proposed power installation, whether the concept is tested, the level of flexibility and the modularity of the concept. From the previous discussion on the concepts, all concepts have some kind of flexibility introduced. Table 3.1 will subdivide the flexibility over three ranges: micro- $(< 2m)$, meso- $(2m - 20m)$ en macro-level $(> 20m)$. The categorisation is based on the currently proposed concepts, both inland and offshore. It can be concluded that multiple concepts have some kind of modularity system, which gives the possibility of easy assembly. The modality will also be included in the comparison.

Table 3.1: Quantitative comparison of existing projects and proposed concepts

	Years of activity	**System proposed size**	**Tested**	**Flexibility level**	**Modularity**
SUNdy	2012	2 MW (50MW)	No	All levels	Partly
University of Vienna	2013	Unknown	No	Not flexible	No
Swimsol	2014 - today	227 kWp	Protected water	Not flexible	No
Moss Maritime	2019 - today	9 709 kWp	Model scale	Macro level	Yes
Ocean Sun	2016 - today	200 or 500 kWp	Protected water	All levels	No
Oceans of Energy	2019 - today	1MW	Offshore	Macro level	Yes

Additionally, the systems are assessed on the requirements set in section 2.2. The comparison can not be made quantitatively. Therefore a 5 step scale will be made. The scale will indicate the influence on the validity of the concept positively with a "++" and negatively with "−−". This gives the following scale from respectively positive to negative "++", "+", "0", "−" and "−−". Often there will be no indication on the performance, which will then be indicated with a question marque. The assessment is based on the opinion of the writer of this thesis. Table 3.2 shows the results.
It should be noted that some requirements are vital for the success of the concept based on what was discussed in section 2.2. A concept should be both economically and technically feasible. All systems and subsystems should survive all environmental conditions to be technically feasible. Some general trends in the comparison in Table 3.2 can be seen. First of all, based on the author's opinion, there are no concepts that are expected to handle the interaction with waves in long times. Therefore, it is believed that obtaining a support structure that has an appropriate interaction and response in waves is highly challenging.
A feasible and appropriate floating support structure that is capable of resisting the offshore conditions is missing in today's market. The mooring system and the energy converting system are not in-depth discussed by literature and are assumed to not come up as issues, according to the author. These technologies have already experienced further development in other industries such as offshore energy and land-based PV.
Concepts of larger platforms, connected with hinges, are expected to experience high loads on those hinges (Oceans of Energy and Moss Maritime). This expectation is based on the conclusions of the research of Space@Sea, where large floating triangles are hinge connected [61]. Still, these concepts are the most promising. The Moss Maritime currently tests their system on model scale and the oceans of energy concept is tested in North Sea conditions.
Incorporating a flexible membrane in the design for offshore conditions is expected to be difficult. The

Table 3.2: Qualitative comparison of existing projects and proposed concepts

	SUNdy	University of Vienna	Swimsol	Moss Maritime	Ocean Sun	Oceans of Energy
Cost						
Development costs	–	−−	+	–	+	+
Material costs	?	?	+	+	++	+
Production and installation costs	0	+	++	++	++	++
Opperation and maintenance costs	?	?	++	++	+	+
Decomissioning and recycling costs	?	?	+	+	–	+
Surviving						
Wave	–	–	−−	–	−−	–
Wind	+	–	0	–	+	+
Current	+	–	+	+	+	?
Biofouling	−−	?	0	0	?	−−
Ageing	?	–	0	–	−−	–
Environmental impact	?	?	?	?	?	?
Development time	−−	−−	+	0	–	++
Safety	?	?	+	+	+	–

membrane needs to have properties that are complicated to achieve with the current technological standard. This is shown by the Ocean Sun concept, which is, so far, applied nearshore. Even in these conditions, doubts are raised on the feasibility of the concept. Hence, the application of flexible membranes or mattresses will need a long and/or expensive development track. Other concepts, such as Oceans Sun and Oceans of Energy where the PV-panels are placed close to the water. It could lead to wave impact or problems with biofouling.
Concepts such as Swimsol and Ocean Sun are designed for protected waters and will not survive offshore conditions. For Swimsol the scale-up of the platform is not achievable. Scaling up is done by placing multiple platforms next to each other. When scaling-up in offshore conditions, The platforms could probably interfere and crash into each other. Fish farms inspired the Ocean Sun concept; this fish farm concept is also not used offshore. When fish farms move offshore, they tend to use other concepts. This raises doubts on the concept of Ocean Sun.
Cost is often positively represented in table 3.2. Which could be confusion, as a positive representation with a “+” in this thesis, represents a relatively low cost. The positive indication does not imply that there will be a feasible business case. Due to the unknown business cases, profitability is hard to assess.

3.4. Conclusion on comparison

In general terms, it could be said that all concepts have their specific advantages and disadvantage. But none of the proposed concepts can overcome all its disadvantages to become a fully feasible system. A concept needs to meet a certain threshold of technical feasibility to become a viable system. Some tests are executed on a small scale. Still, challenges will arise when scaling up. Surviving offshore conditions, in particular the interaction with water and waves, is the most challenging.
The most promising concepts, concluding from the comparison, are the concepts of Moss Maritime and the concept of Oceans of Energy. Still, they have both their specific drawbacks. In both cases, there are worries about the loads that can occur in the hinges. Moreover, contact with the water surface can provoke risks. For the Oceans of Energy concept, there will be almost permanent contact with the water. This leads to breaking waves and possible biofouling. For the Moss Maritime concept, there

is the risk of slamming on the platforms. Again, these risks are dependent on the interaction with the waves.
It can also be concluded that all concepts are variations on floating support structures for mostly conventional PV technology. There are no concepts that make use of bottom founded structures or that are incorporating other forms of support. For the relatively low payload of PV technology, a floating system appears to be a promising solution for reasons of cost and material use. All concepts make use of conventional PV technology. A technology that is widely established. Except for the idea proposed by [7] which only researched the influence of platform motion on a concentrated solar system. The lack of an all fulfilling concept opens doors for further exploration and development of more concepts.

4

Research goal, scope and question

Deductive reasoning and analysis based on literature were executed in chapter 3. Some interesting conclusions were drawn on both the high potential for the Offshore Floating PV (OFPV) and on the current state. These steps identified some knowledge gaps and design deficiencies for Floating Photo Voltaic (FPV). Based on these findings, this chapter formulates the goal of the thesis. A scope and a research question to define the boarders on the research of this thesis will be identified. Subquestions are formulated to approach the overall research question in a manageable way.
In chapter 1 and section 1.3, it was concluded that there is an opportunity to propose a new FPV concept. Literature shows that for Inland Floating PV (IFPV) one particular solution is well established. For inland installations, multiple commercial projects were executed, and the technology becomes well established. The same trend is not yet seen for offshore applications as it has to endure a more difficult environment. Multiple concepts were proposed, but so far, none of the concepts is fully developed as was discussed in chapter 3. All OFPV-systems found in the literature have particular downsides that could block the concept, according to the author of this thesis. The main problem to realise OFPV is the lack of a feasible floating support structure.

4.1. Research goal

Based on the gaps as mentioned earlier and deficiencies the author believed that the current concepts would not fully overcome all challenges imposed on OFPV.
The following research goal is formulated: The goal is to

Develop a new design for an OFPV support structure and demonstrate its feasibility.

A floating support structure which could perform at least as good as the concepts proposed so far should be obtained. The concept has to meet the requirements drawn up in section 2.2 to be at least as good. The main conclusions were: (1) that the system should be cost-efficient and (2) that the system should survive the offshore conditions. The goal should be achieved within the ethical boundaries imposed by the TBL assessment (section 2.1).
Section 3.3 concluded that a floating structure has high potential. After proposing a new concept design, the main design parameters will be identified. These design parameters will influence the feasibility of the design and are hence essential to be determined. This leads to the scope of this thesis.

4.2. Scope

In the research goal, the thesis is limited to the development of a floating support structure and assess the feasibility. In that perspective, it is essential to identify response which is most critical for the feasibility of the concept. The critical and likely reasons for the failure of the new system need to be further researched. This research can be done by firstly assessing the system on the requirements build-up in section 2.2.
The second part of the research goal is to identify and quantify the design drivers that influence the feasibility of the system. The relations between the response and the design parameters need to be found.

If possible, only the support structure will be considered when examining the response by theoretical modelling. The different design parameters will be varied to see the effect on the specific response. This will give the first indication of the viability of the concept.
Based on the literature, it was concluded that the response of the construction in waves is often the most critical aspect in the design. The response depends on the specific design parameters of the concept. The support structure must be simplified to identify the main design parameters. The main loads exerted by the environment on the system are coming from the hydrodynamic interaction with the environment. The simulation of hydrodynamics environment will be limited to regular waves with different frequencies. The hydrodynamics lead to forces (pressures), added masses, hydrostatic stiffness and damping. These loads will be modelled theoretically, and these loads will have lead to dynamic response. The resulting response from the theoretical modelling will indicate the feasibility of the system.

4.3. Research question

The scope of the research is defined. Now, a dedicated research question is formulated within the borders of the set scope.

What is a feasible concept design for an offshore floating support structure for photovoltaics and what are the design parameters that influence the most critical response?

The aim is to find a new design for the support subsystem of an OFPV installation. Therefore, the design drivers that influence the most critical response must be identified. It is assumed that the interaction with waves will lead to a critical response. Subquestions are formulated to simplify the process of answering the research question.

1. **What is a promising concept design for an offshore floating support structure for offshore PV?**
   The aim is to come up with one or multiple new concept designs for support structures that have the potential to perform at least as good as the currently available concepts. The most promising design should be selected for further research.

2. **What is the most critical response that influences the feasibility of the new concept design of the offshore floating support structure?**
   The most critical response of the newly defined concept should be identified so that further research can be executed. The most critical response has the strongest influence on the feasibility of the concept.

3. **How can the most critical response of the concept efficiently be modelled for design purposes?**
   The aim is to investigate and argue which principles and theories can be used to estimate the response. Once these theories are implemented in a model, the model should be suitable to be used as a tool for design purposes. This requires a computational light tool that can give a first estimation of the relation between the design parameters and the most critical response.

4. **What are the important design parameters that influence the response?**
   After the response is modelled, the design parameters can be varied. Logic relations between the design parameters and the critical response need to be determined. Design solutions can be concluded using these relations.

5. **What are suitable main dimensions, magnitudes and ratios, to increase the feasibility of the concept in the perspective of the researched response?**
   The previous found relations will now be used to build up conclusions design parameters for a feasible system should be suggested.

The guideline described by the research question and subquestions, and limited by the scope will define the following research. The answers to the subquestions can be found in the following chapters: subquestion 1, 2 and 3 in chapter 5, subquestion 4 in section 5.4 and chapter 6, 7, 8, 9 and 10 and subquestion 5 in chapter 11 and 12.

5

New design

During chapter 3 no specific Offshore Floating PV (OFPV) design has shown to be successful based on the set criteria. Neither does one of the concepts show hard evidence to be compliant with all the requirements set in chapter 3. So this allows going back to the drawing board to create a new concept for a floating support structure that is at least as good as the currently existing concepts. Some of the concepts of the brainstorm will be selected and further discussed and designed. Then the selected concepts will be compared with the current concepts explained in chapter 3 to examine its' potential. The comparison will again be made based on the set requirements of chapter 3.

5.1. Brainstorm

A brainstorm to develop new concepts for OFPV was executed. The goal of the brainstorm is to find a floating support system that can carry a system to convert solar radiation of 60 to 250 W/m^2 (on average over 24 hours) to usable energy [20]. Figure 2.1 was adapted to illustrate the focus of the brainstorm. By smartly displacing the ocean's water, a stable platform could be provided that can support the relatively low payload of the PV-panels. Conventional PV technology is a proper energy conversion method for solar energy. The aim of the brainstorm is finding (new) floating support structures for conventional PV technology.

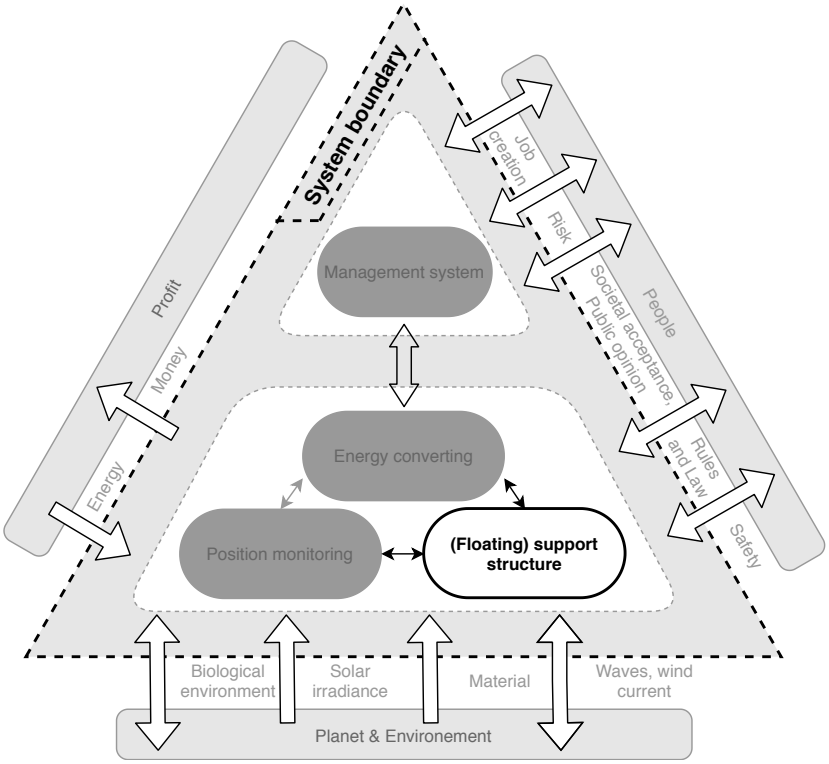

Figure 2.1: System diagram of an OFPV system with focus on floating support structure

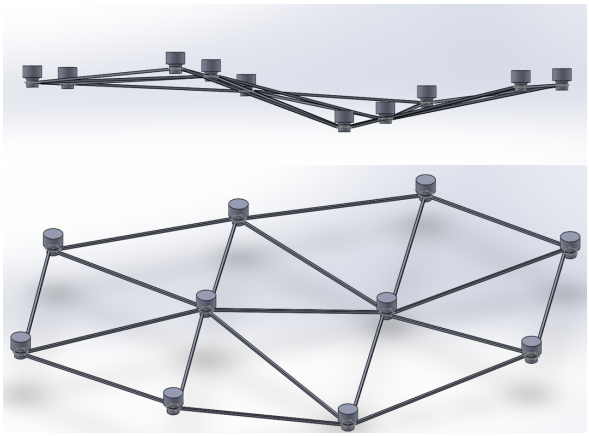

(a) Buoy and beam structure

(b) Full mattress [50]

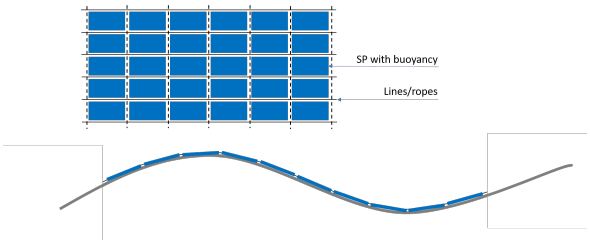

(c) Pontoon system

(d) Water lily [63]

(e) Ten(t)sioned sheet [33]

Figure 5.1: Visualisation of concepts from brainstorm

Buoy and beam structure
The first idea is a structure that connects multiple buoys by beams and hinges, shown in Figure 5.1a. The figure shows a system of triangles, which is favourable as three points define a plane in a 3D space. A triangle shape is preferred over a square or other polygon layout. As the three sides of the triangle fully define a triangle. By connecting the beams to the buoys by a hinge, the structure can move in waves. Connecting three buoys above the water will create a platform, which will be filled with PV-panels. The buoy and beam dimensions should be adopted to obtain a desirable behaviour in the waves of a specific location.

Full mattress
A second outcome is to develop a system that is a large mattress similar to Figure 5.1b. The mattress is flexible with a certain stiffness in all its directions. It follows the shape of the water surface. However, the risk of folding or wrinkling is rather high. Dynamically changing the stiffness of the pressure system might minimise the risk of folding. Moreover, the technical feasibility might be an issue, as there are not materials that could handle the load.

Pontoon system
A similar system as the Moss Maritime concept explained in section 3.2 has been presented in this brainstorm. The initial idea was inspired by the inland systems that have multiple pontoons with one PV panel. Smaller pontoons could result in less material use than the Moss Maritime system. All pontoons are connected with a line or rope to guide the loads (Figure 5.1c). In that way, the pontoons mainly take the vertical loads, and the lines take the horizontal loads. As a result of choice for the lines, the structure stays highly flexible.

Ten(t)sioned sheet
Getting inspiration from tents (see Figure 5.1e) used for camping, one could think of using a similar construction for a floating offshore support structure. In a tent, the groundsheet is often tensioned by the use of bend rods. Since the mattress mentioned earlier risks to fold easily, a combination with a tent-system could be a solution. However, building the system in large dimensions might be difficult to come up with an appropriate design.

Water lily
In nature, a water lily is an example of a structure that uses solar energy on the water surface to create energy. The water lily is located at the surface with its leaves and is connected with long branches to the bottom of the water. Still, this system has the disadvantage that in case of harder winds and waves, the plant does not survive that well and will grow its leaves back. A FPV, needs to rotate the leaves, so they to turn with the wind and waves.

Other response mitigation measures
All concepts take into account to mitigate and minimise the loads working on the system and the structure. Some additional measures could be taken to minimise the loads. These measures are applied to multiple concepts and are mentioned hereafter.

1. Porosity of platform: By introducing openings in between the PV-panels, water or air could move through the platform so that pressure does not further build-up. It could also make that the system could move through the wave in extreme environmental conditions, which could avoid severe damage in extreme conditions.

2. Reduced slamming loads: Known measures to prevent slamming peak pressure should be applied. Surfaces with a risk of high slamming loads are often equipped with ribs to lower the peak pressure.

3. Adaptive stiffness, mass or damping: If the PV panel platform is flexible, measures could be introduced to create adaptive stiffness to optimise the behaviour in different sea states. Also, in non-flexible solutions, it might be beneficial to adjust the dynamic properties.

4. Breakwater barriers: The whole structure could be placed behind a wave barrier. Yet, breakwaters are very costly. In case of an integrated floating wave barrier, the system will probably work suboptimally in rough seas as the barrier will not provide the needed protection.

5. Creation of buoyancy over the length of individual submerged elements to reduce the loads as buoyancy and gravity are balanced.

5.1.1. Discussion of brainstorm

The brainstorm, resulted in multiple futuristic and some incomplete concept. Going back to the criteria and reasoning behind the assessment of the current concept in section 3.3, some concepts of the brainstorm can easily be disregarded. The full mattress system and the ten(t)sioned sheet will be neglected due to the complexity, development time needed and the conversion efficiency of the flexible PV-panels. Similar reasoning holds for the SUNdy concept, and the water lily, which is naturally too weak to survive stronger winds. Therefore, the pontoon system and the buoy and beam structure are left. The pontoon system has high similarities with the Moss Maritime concept. Still, the location of the connection (at the corners) and the module size is different, and the choice for a rope-like system is both arguable and different.

5.2. Concept selection

When including the most promising concepts of literature, a total of four key systems was found. The outcome from the brainstorm is in a more conceptional state. Based on the AHP method, the concepts are ranked on their potential.

5.2.1. AHP-method

The AHP is a method used for pairwise comparison. The tool is ideal to select one out of multiple solutions when complex criteria are involved. Exclusively, the author's opinion is taken into account in the assessment process. The judgement is subjective and based on intuition, logic reasoning and knowledge found in the literature. Due to the novelty of multiple technologies, there is room for discussion on the choices made. Applying the AHP method should reduce the complexity of the judgement and thereby improves the quality. The explanation on the execution of the AHP method can be found in Appendix A. [21]
The criteria found in Table 3.2 on page 28 are based on the weighting and importance coming from the AHP analysis (see Table 5.1). Multiple aspects can be grouped into four main requirements: Survivability, cost, development time and safety. A lower ranking of a requirement does not mean it is not important. A concept needs to fulfil all requirements. Still, the requirement of surviving the offshore conditions needs more focus then achieving a rather cheap system.

Table 5.1: Prioritisation of requirements based on AHP of an OFPV system and the relations in respect to the TBL-assessment.

	People	Planet	Profit	AHP importance	Survivability	Cost	Development time	Safety
Development time		X	X	15%			15%	
Survive in current	X	X	X	13%	13%			
Survive in waves	X	X	X	13%	13%			
Survive in wind	X	X	X	13%	13%			
Ageing	X	X	X	7%	7%			
Operation and maintenance costs			X	7%		7%		
Safety	X		X	7%				7%
Decommissioning and recycling costs		X	X	5%		5%		
Production and installation costs			X	5%		5%		
Material costs			X	5%		5%		
Biofouling	X	X	X	5%	5%			
Development costs			X	4%		4%		
					50%	28%	15%	7%

Based on these weighting, the different concepts are assessed in the next step of the AHP process, which results in Table 5.2.

Table 5.2: Results of the selection of concept based on the AHP-method

Moss Maritime	27%
Buoy and beam	27%
Oceans of Energy	24%
Flexible connected pontoons	22%

Based on the outcomes of the AHP some conclusions can be drawn. Most importantly, there is no clear winner in the different concepts. The accuracy of the judgement used in the AHP-method is not accurate enough to conclude on a precise number one. One exception can be noticed: The technique to connect pontoons still include significant uncertainties. This means that all concepts have the potential of being at least as good as the other ones. As it is unclear how the connection could be made, the development time could be increased.

5.2.2. Selection of the buoy and beam structure

The three most promising concepts are the concepts of Moss Maritime, Oceans of Energy and the buoy and beam structure. The first two are currently commercially researched on their potential. The technology is pushed forward, with the support of in-house knowledge and dedicated research. According to the AHP analysis, the buoy and beam structure still has the potential to become at least as good or maybe even better system than the ones commercially proposed.
Going back to the requirements in section 2.2, a more elaborate indication to what extend the design can meet the requirements is given. These requirements were the basis for the coefficients used in the AHP analysis. Because of the hinge mechanism, the elements can move in respect to each other. In this way, the structure can follow the shape of the waves in case of limited wave steepness. This should minimise the contact between the water surface and the PV panel platform. Sufficient clearance between the water surface and the platform should be maintained.

Furthermore, there are some other novelties and interesting aspects related to the design. A triangle layout was chosen. Three points in space always define a plane. Moreover, three defined lengths also fully define a triangle, which means that with three beams the position of the three corners is fully described in respect to each other. The structure can also be executed with different polygon shapes, but the advantages of a triangle are supposed to be significant.
The rigid triangle shape and the rigid platform holding the PV-panels should avoid structural loading of the PV-panels. The PV-panels should be able to withstand loads coming from the wind and accidental water impact. The wave slamming can be significant and should be taken into account. The triangle structure also provides the possibility for a modular production and assembly method. Compared to rigidly connected pontoons, the buoyancy is created by introducing limited hydrostatic stiffness. The lower stiffness could lead to a limited response in waves.
The criteria of limited material costs and development time are maybe harder to defend for the other concepts. For now, it is unclear how much and what material must be used to produce the buoy and beam structure. Forces in the structure need to be calculated to define the dimension of the design. The development time and cost is predicted to be relatively low compared to the futuristic concepts that use flexible PV and mattresses. However, the hinge system could block the technology due to the large loads and a lack of solutions to hold these loads. Albeit, it could be that current technology is unable to develop and produce hinges that can handle the loads. The same hold for the Moss Maritime concept and the concept of Oceans of Energy. This potential drawback needs to be researched. The loads could be lower compared to the Moss Maritime concept, and the concept of Oceans of Energy as the hydrostatic characteristics are different.
A major difference between the buoy and beam structure and the other concepts is the hydrostatic stiffness of the elements at the water surface. As result of the relatively small water plane area the buoy and beam structure will behave significantly different in waves. This difference makes the buoy and beam structure interesting to further research.
It is reasonable to design further and research the buoy and beam structure. At this early concept stage of the design, the advantages and defaults of the system are impossible to assess fully. Therefore, it is necessary to further design and then identify potential drawbacks within the system. Then, these shortcomings need to be quantified to confirm or disprove the current expectations of the design.

5.3. The buoy and beam structure

An envisioning of the buoy and beam concept will introduced. This envisioning does not fix any design choice yet. It is favourable to delay design choices as much as possible and to first fully assess the consequences of the design options.

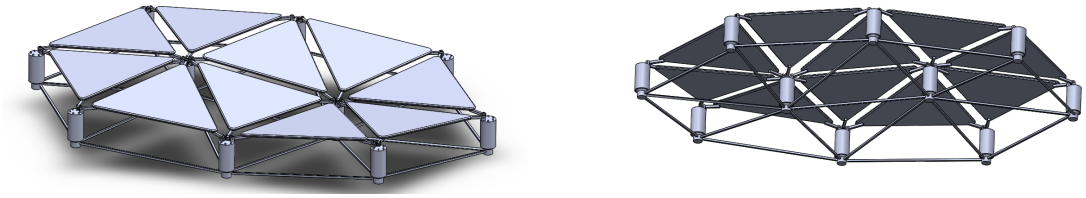

(a) View on the buoy and beam structure from above

(b) View on the buoy and beams structure from below

Figure 5.2: Impression of a possible system layout with buoys

The chosen concept can be found in Figure 5.2b and 5.2a. It consists out of four main parts: first, the PV and the electrical system (indicated as energy converting system with (A) in Figure 2.1); second, the platforms that support the PV; third, the skeleton that is in the water including the buoys and connecting beams (together indicated with (C) as a support structure in Figure 2.1). Additionally, to these four parts, there are still other parts that are not included in the design such as the operation and maintenance system (part of the management system in Figure 2.1), grid connection or energy transport system, and a mooring system (indicated as position monitoring in Figure 2.1).
The beams form triangles that have the same dimensions as the platforms above. The proportions and dimensions of the system are not defined at this stage. It could be beneficial to vary the dimensions

and dynamic properties of the buoys or triangles depending on the position within the platform.
On the triangle platforms, walkways for maintenance and installations could be included. The buoys could contain electrical equipment such as transformers, combiner boxes and other electrical components. An additional energy transformation could also be integrated into the buoys or could be mounted on the platforms. All triangles could have their dedicated transformer, so it becomes a modular plug and play layout. Likewise, multiple triangles form an independent system, which then later will be combined for transmission or transport, could be chosen. An optimum in the layout of the electrical system must be found. This optimisation depends on the size of the triangle platforms.

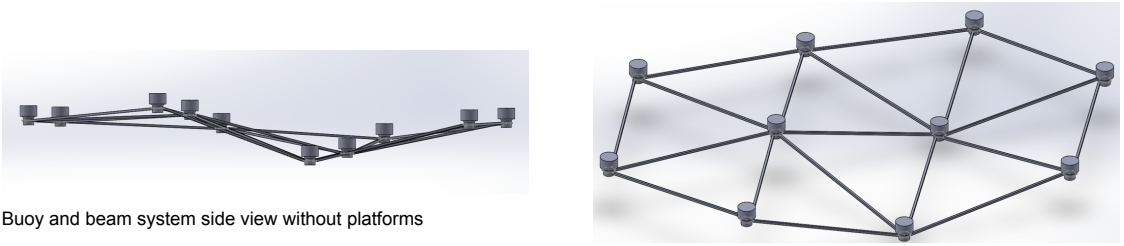

(a) Buoy and beam system side view without platforms

(b) Buoy and beam system top view without platforms

Figure 5.3: System without platforms

Figure 5.3a and 5.3b illustrate the skeleton construction. The buoys are visualised by cylinders and the beams between the buoys by tubes. The structure is fully hinged, and no restrictions on the movement of the hinges are applied, which provides flexibility in the structure. The beams are envisioned to be located underwater. By placing the beams underwater, damping will increases. Having the weight low will also increase the stability of the structure.

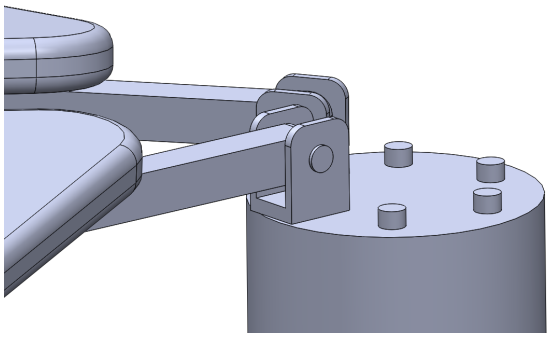

Figure 5.4: Visualisation of the hinge in the system

The PV-panels are supported by the platform. As the PV are relatively lightweight, the dedicated platform can be relatively light. The major loads on the platform might be: slamming of waves coming from underneath; the aerodynamic pressure caused by the movement of the structure in waves; or the load of the wind. The following ideas are proposed to reduce the magnitude of these loads. First, the platform should not be continuous. The gaps in the platform prevent air or water from being entrapped, leading to high loads, and it reduces material costs. Second, the air gap between the ocean surface and the platform must be significantly large so that slamming can be avoided.
The buoy-platform connection and the buoy-beam connection must be freely hinged. These hinges will most probably experience large forces, and therefore need to be calculated carefully. Due to the forces on the hinges, they should be engineered with great care. In this thesis, no movement restriction or stiffness or damping is envisioned on the hinges. Buoys will have up to six beams connected. Three buoys will support each platform.
The following dimensions could be envisioned. The beams are in the range of 10 to 40 meters, with buoys of a diameter of 1.5 meters and a draft of 5 meters. All dimensions, shapes and constrains still need to be researched. Part of this research will be done in this thesis.

5.3.1. Most critical response

Except for the graphical representations, the system has still many unknowns and possible unidentified infeasibilities. Multiple suggested solutions indicated in the previous section are open for debate. Making choices in an early design stage can have a significant impact on later design steps, which would lead to dependencies for further research. Thus, the harvesting potential is dependent on the size, and the mooring load is dependent on the interaction with the waves and currents. Therefore, the most critical aspects for the blockage of the technology need to be found. If these critical aspects can be solved, a feasible system is coming closer.
The first and most prominent requirement deducted from the triple bottom line analysis and the AHP was the survival in the offshore conditions indicated in Table 5.1. This means that the construction can handle the loads and related responses. The loads in offshore conditions are generated by wind, waves, currents, corrosive environment or biofouling. These environmental parameters results in static and dynamic loads. The dynamic loads of offshore waves are crucial as they will result in the movement of the structure. These loads are indicated in Figure 5.5. The loads will lead to responses. These responses determine the feasibility of the system. The loads indicated at the bottom of the stairs are expected to be the most complex response to overcome. All subsystems (A, B, C and D) marked in Figure 2.1 need to be able to handle the load. For now, the floating support subsystem is the main point of attention.

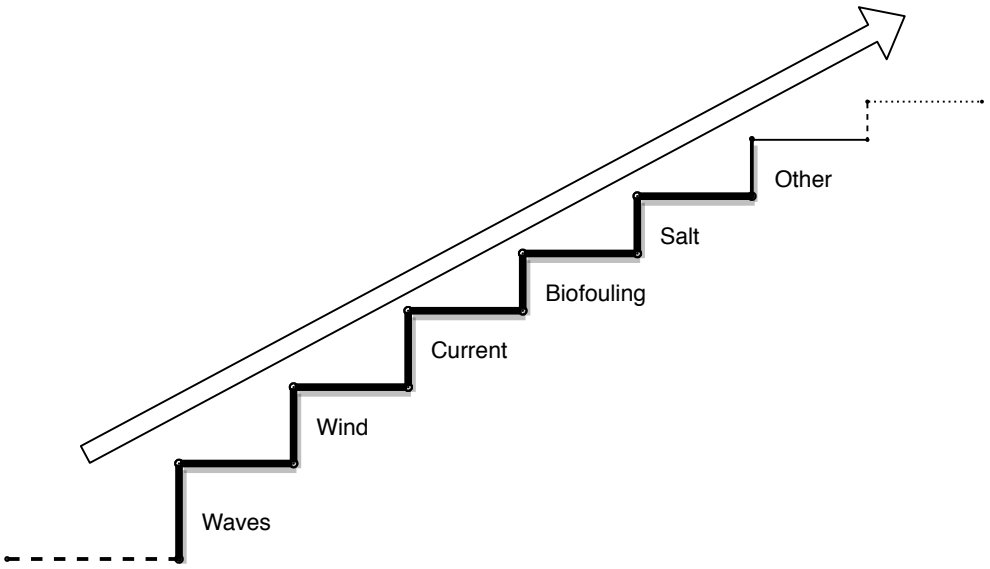

Figure 5.5: Loads on the system impacting that impact the survivability and feasibility

From all subsystems, the response in waves is a crucial part. The response in waves is dependent on the dimensions of the structure and its components. This means that the dimensions could be optimised for mitigation and minimisation of the critical response. The dimensions will determine where the range of frequencies where the response peak appears. The range is highly relevant, taking into account that the specific place of installation has a specific wave spectrum. When the response peak of the construction does not overlap with the peak of the wave spectrum, the response can be minimised. The structure and its structural elements will have a response in multiple degrees of freedom. A crucial aspect for survivability of the system is the heaving response of the construction. When part of the structure is heaving the air gap between the platform and the water surface could disappear. Contact with water can be violent and therefore damage the system. Additionally, in case of frequent contact between the platform and the water, this could lead to biofouling. Finding relations between the dimensions of the individual elements of the construction and their mutual proportions concerning the heave response in the wave will be a significant step forward in the design process. It will help to assess if the buoy and beam concept is a valid option. Therefore, the hydrodynamic environment and the heave response need to be researched. This assessment is one of the essential steps.

5.3.2. Estimation of weight

Optimising the dimensions of the system for a minimum response in heave direction could lead to an unrealistic design as the water displacement of the system is insufficient to keep the system afloat. Consequently a first weight estimation of the buoy and beam system based on the beam length is executed. For the first estimation, multiple assumptions were made. First, it is said that the dimensions of the individual elements over the system are equal. This means that a buoy at the centre has the same dimensions as a buoy at the sides. The buoys at the side have fewer platforms connected compared to the middle ones and therefore support less weight. It is assumed that ballast will be added on the exterior buoys to compensate for this. Additionally, the weight of the mooring system is not incorporated assuming that the mooring system is designed in a way that it is neutrally buoyant.
The weight of the PV-panels is based on literature. The total weight of the PV-panels is used to calculate the load on the platform. Thereby the gravity and the acceleration of the water surface in waves will be taken into account. The PV-panels weight is simplified by assuming a triangle-shaped distribution over the sides of the triangle, as indicated in Figure 5.7. It approximates that three I-beams support the PV-panels. The I-beams are assumed to have a height that is two times the base and the flange thickness in one-tenth of the beam base. Calculating the stress in the beam due to the bending moment determines the dimensions of the beam. Then the weight of the buoys is estimated. It assumes that the buoy has a draft of three times the diameter and buoy rises one times the diameter above the still water level, resulting in a total height of four times the diameter. The plate thickness of the buoys is estimated at 4 centimetres on average. As all weights are known, the water displacement can be estimated. Hereafter, the procedure described will be explained stepwise.

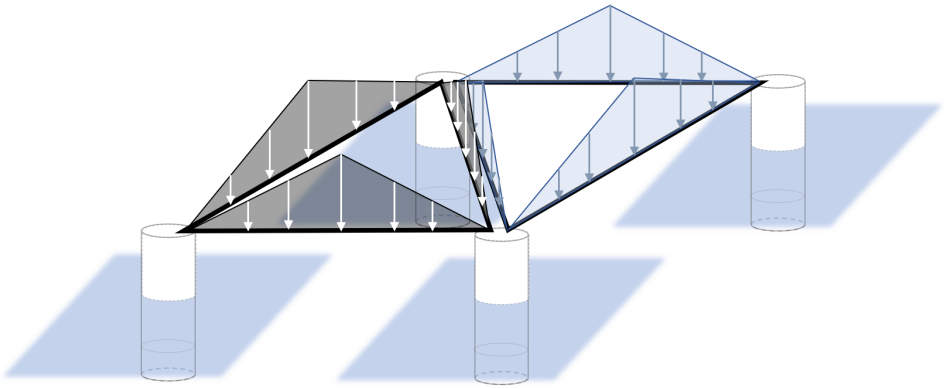

Figure 5.6: Visualisation of simplifications made to estimate the systems weight.

Because of these assumptions, a buoy in the middle of a larger system will be connected to six platforms. The buoy will carry six times one-third of the PV-panels weight of the platforms. This results in the equivalent weight of the PV-panels of two platforms. The platforms are approximated with three beams. The buoys will carry half of the weight of one beam. This results in an equivalent of six full beams.

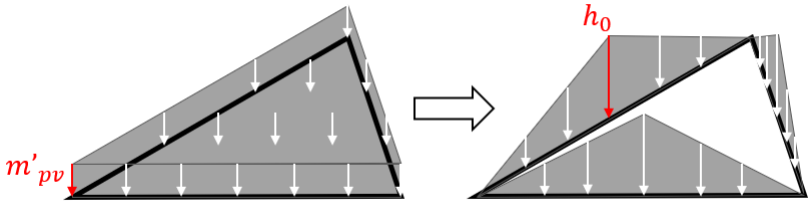

Figure 5.7: Visualisation of simplifications made to in the platforms weight distribution.

Commercial roof-mounted PV-panels weigh 10 to 25 kg/m^2 [2, 48, 49]. The higher end of 25 kg/m in-

cludes the mounting structure on the roof. The hostile offshore environment and the dynamic behaviour of the structure demand a stronger mounting. Therefore a value of 50 kg/m^2 is taken into account for the weight (m^*_{PV}). This weight should also account for the additional electric components. The total weight of the PV-panels and their mounts of one platform can be found in equation 5.1. L indicates the length of the side of one triangle.

$$m_{PV} = \frac{\sqrt{3}}{4} L^2 m^*_{PV} \tag{5.1}$$

Now the weight needs to be distributed over the platform. As this calculation holds the first estimation, the weight of the PV-panel platform will be distributed over three beams with a triangle shaped weight distribution. The distribution simplification is indicated in Figure 5.7. The total weight on the triangle (integration over the surface) will equal the total weight over the beams (integration over the length). The height of the triangle (indicated with h_0) can be calculated as indicated in equation 5.2.

$$\frac{\sqrt{3}}{4} L^2 m^*_{PV} = 3\frac{1}{2} L h_0 \rightarrow h_0 = \frac{\sqrt{3}}{6} L m^* \tag{5.2}$$

The value h_0 is indicated in kg/m and needs to be multiplied with the acceleration to obtain the force distribution. The acceleration, for the calculation of the force, is obtained by summing up the gravity with the acceleration of the water surface. With an amplitude of 7.5 meters and a period of 15s causing an acceleration of $1.32 m/s^2$ is obtained. The acceleration assumes that the structure follows the waves. The bending moment can be calculated, as indicated in equation 5.3. The first two terms show the bending moment resulting from the PV-panels. The last terms account for the mass of the beam.

$$M = -\frac{h_0 (g + a) L^2}{12} - \frac{1}{8} m^*_b (g + a) L^2 \tag{5.3}$$

Where the weight per meter of the beam (m^*_b) is estimated by equation 5.4. The cross sectional area of the beam is calculated in equation 5.5.

$$m^*_b = A_b \rho_{st} \tag{5.4}$$

$$A_b = (2B + H - 2t)t = (2B + 2B - 2\frac{B}{10})\frac{B}{10} = \frac{19}{50} B^2 \tag{5.5}$$

With the tensile stress of steel, the bending moment and the moment of inertia the dimensions of the I-beam (Figure 5.8) can be calculated as indicated in equation 5.6. Steel with a tensile stress of 355 Mpa and a weight of 7850 kg/m^3 was chosen. The dimensions of the I-beam are indicated in Figure 5.8.

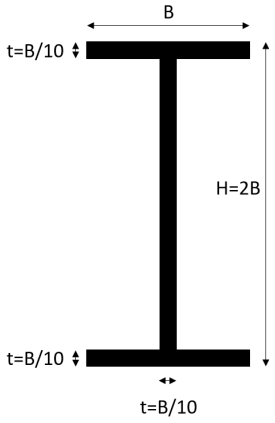

Figure 5.8: Dimensional proportions of the I-beam for the weight estimation.

$$I = \frac{BH^3}{12} - \frac{(B-t)(H-2t)^3}{12} = \frac{8B^4}{12} - \frac{8(B-t)^4}{12} = \frac{2}{3}B^4 - \frac{2}{3}B^4\left(\frac{9}{10}\right)^4 = \frac{2}{3}B^4\left(1 - \left(\frac{9}{10}\right)^4\right) \tag{5.6a}$$

$$\sigma = \frac{-M\frac{H}{2}}{I} = \frac{-MB}{I} = \frac{\left(\frac{h_0(g+a)}{12}L^2 + \frac{1}{8}\frac{19}{50}B^2\rho_{st}(g+a)L^2\right)B}{\frac{2}{3}B^4\left(1-\left(\frac{9}{10}\right)^4\right)} \tag{5.6b}$$

$$\sigma\frac{2}{3}B^3\left(1-\left(\frac{9}{10}\right)^4\right) = \frac{h_0(g+a)}{12}L^2 + \frac{1}{8}\frac{19}{50}B^2\rho_{st}(g+a)L^2 \tag{5.6c}$$

$$0 = -\sigma\frac{2}{3}\left(1-\left(\frac{9}{10}\right)^4\right)B^3 + \frac{1}{8}\frac{19}{50}\rho_{st}(g+a)L^2B^2 + \frac{h_0(g+a)}{12}L^2 \tag{5.6d}$$

Solving the cubic equation for the width (B) results in the dimensions of the I-beam and the beam length. The mass of the beam can be calculated with the beam length, as indicated in equation 5.7.

$$m_{beam} = m_b^* L = \frac{19}{50}B^2\rho_{st}L \tag{5.7}$$

Morover, the mass of the buoys needs to be calculated. The weight of the buoys can be calculated based on the surface of the cylinder, as indicated in equation 5.8. As said before a thickness of 4cm, a draft of three times the diameter and a buoy height of four times the buoy diameter was chosen. The volume of the submerged part of the buoy should create the buoyancy for the structure, as indicated in equation 5.10a. Substituting the masses of all elements gives a cubic equation.

$$m_{buoy} = A_{buoy}t_{buoy}\rho_{st} = \left(\pi DH + 2\frac{\pi D^2}{4}\right)t_{buoy}\rho_{st} = \left(\pi D4D + \frac{\pi D^2}{2}\right)t_{buoy}\rho_{st} = \frac{9\pi D^2}{2}t_{buoy}\rho_{st} \tag{5.8}$$

$$V = T\frac{\pi D^2}{4} = \frac{3\pi D^3}{4} \tag{5.9}$$

$$V_{buoy}\rho_{H2O} = m_{buoy} + 2m_{PV} + 6m_{beam} \tag{5.10a}$$

$$\frac{3\pi D^3}{4}\rho_{H2O} = \frac{9\pi D^2}{2}t_{buoy}\rho_{st} + 2m_{PV} + 6m_{beam} \tag{5.10b}$$

$$0 = -\frac{3\pi D^3}{4}\rho_{H20} + \frac{9\pi D^2}{2}t_{buoy}\rho_{st} + 2m_{PV} + 6m_{beam} \tag{5.10c}$$

Equation 5.10c can be solved for the buoy diameter. This relates the buoy diameter to the sides of the triangle. The diameter was substituted in equation 5.11. The result is an estimated mass of the system per buoy in the system. When multiplying this result with the number of buoys, the total weight is obtained.

$$m_{sys}^* = \frac{3\pi D^3}{4}V_{buoy}\rho_{H2O} \tag{5.11}$$

When plotting the weight over the increasing length of the platform Figure 5.9 is obtained.

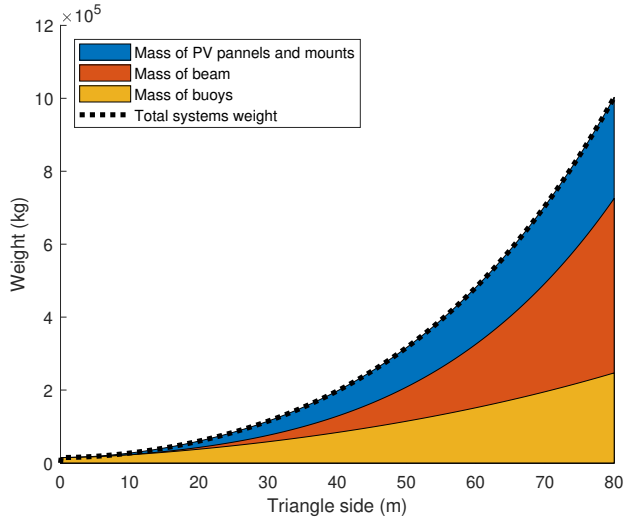

Figure 5.9: The weight contributions in relation to an increasing beam length

For a system where the buoys are 27 meters apart, a total weight of 95778 kg per buoy is found. The dimensions correspond with a diameter of 3.41 meters and a beamwidth of 0.16 meter. This result in relative height weights as result of the assumptions. At the end of this thesis future improvements will be discussed.

5.4. Modelling approach

So far, the two subquestions were answered. A new design was proposed, and the heave response of the structure is believed to be the most critical response. In this part of the report, a start will be made on answering the third subquestion. This was formulated as follows: “How can the response of the concept that was identified as most critical efficiently be modelled and calculated for design purposes?”. The scope (section 4.2) indicates that the structure will be simplified if possible. The main dimensions will be taken into account and varied to identify the main design drivers that influence the response.
The goal of the calculation tool is to find relations between dimensions of the buoy and beam structure and the heave response. The influence of the ratio’s of the particular dimensions and the impact of the structure size in respect to the wave characteristics, on the heave response, are highly relevant. Therefore a model will be build up to simulate the behaviour in waves. As said in the scope, this can be done in regular waves. The construction must be approximated where possible. Hence, the construction elements will be assumed to all be cylinders. Varying the main dimensions of these cylinders should indicate relations between the dimensions and the response.
The model will not assess the vertical balance of the system. A fixed location will be assumed. Based on the water displacement the mass will be determined. Therefore it must be separately checked if the water displacement is sufficient to keep the system floating.
The modelling approach and the structure of the following chapters are schematised in Figure 5.10.

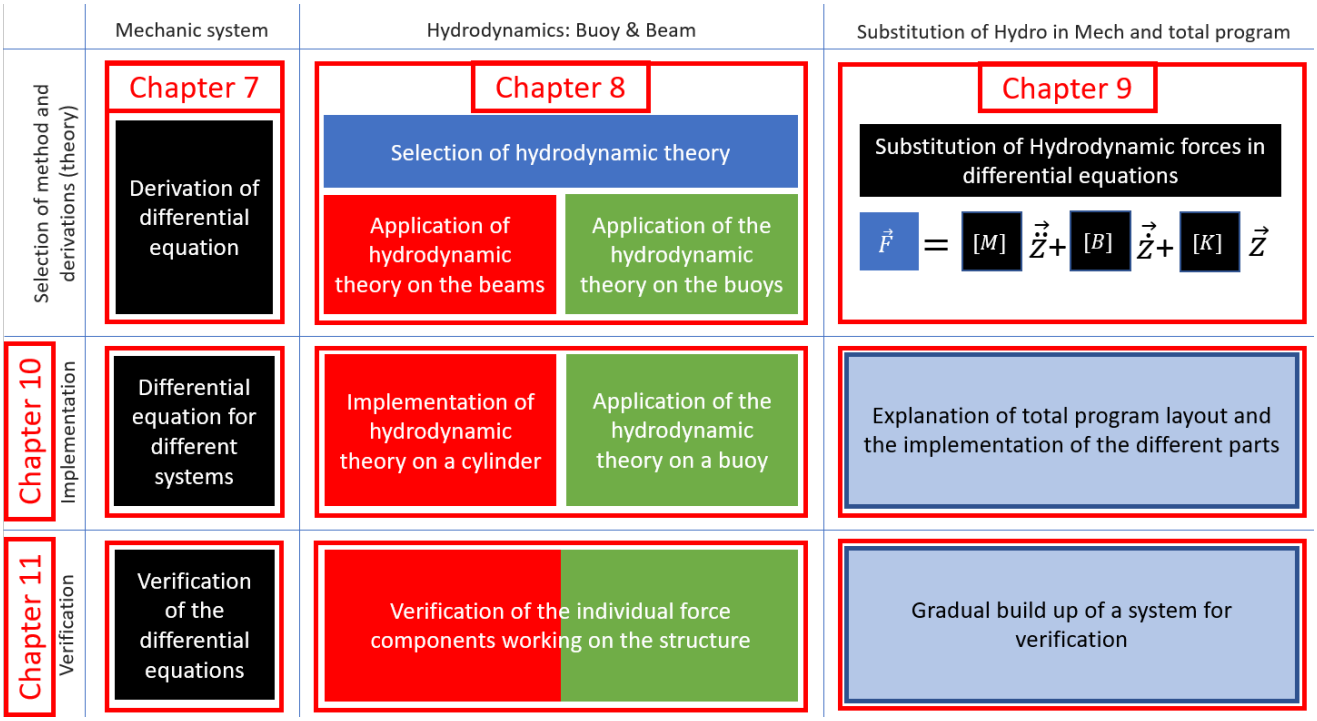

Figure 5.10: Scheme of structure report for the following chapter 6 till chapter 10

From a modelling point of view, there are two main physical aspects. First, there is a mechanical aspect. The mechanical part of the modelling deals with the external and internal forces and the masses. Combining these will determine the heave response. The internal forces are coming from interconnections and constraints in the construction. The theory on the mechanics will be discussed in chapter 6. This will lead to a differential equation that describes the response of the structure depending on the external forces. Second, the interaction of the buoy and beam structure with its hydromechanical environment generate external loads. These loads are discussed in chapter 7.
Furthermore, there are aerodynamic aspects. The platform will heave with the support structure and therefore move through the air. The movement will result in a force proportional to the square of the velocity. For now, this damping force is assumed to be minor. There are three reasons for. First, the density of air is lower than the density of water by a factor of 10^3. This difference in density results in smaller forces. Second, it is assumed that the platform will not be continuous. This will further decrease the force. It is assumed that the damping can partly be approximated by incorporating it with the general damping that is also present in the hydrodynamic environment. Therefore only the hydrodynamic loads are incorporated in the model. Then the obtained hydrodynamic forces can be substituted in the mechanical model. The mass and mass distribution of the system is estimated by the underwater volume of the structure times the water density. This will slightly overestimate the moment of inertia. Still this is an appropriate first step as the mass of the volume displaced must be the same as the total mass of the system. Consequently, the hydrodynamic forces on the individual elements will be estimated in the model. This is done in chapter 8.
When the theory is discussed, the physics will be implemented and coded in chapter 9. The same steps as before will be taken. First, it will be discussed how the mechanical theory is implemented after which the hydrodynamic theory is discussed. Chapter 9 explains the connecting pieces, and the total calculation tool. The implementation will be verified in chapter 9. The implemented parts will be checked. A buoy and beam structure will be build up bit by bit so that the working principles of the program become apparent.

5.4.1. Defining the variation space of the design

When the model is composed, the design drivers (inputs of the calculation tool) must be identified. Therefore potential design drivers must be incorporated in the calculation tool. Additionally, the desired output to assess the performance of the design are identified. The model needs to be build up to vary

the input and output parameters. The relation between the varying input and resulting output will lead to an identification and quantification of the design parameters within the main dimensions.

Input variations
The elements to vary can be split into two aspects. Firstly, the dimensions and properties of the buoys and beams. Secondly, the topology and layout of the structure. The buoys are modelled by vertically oriented cylinders that go through the water surface, and the connecting beams are horizontal fully submerged cylinders. The hydrostatic stiffnesses of the buoys are defined separately to extend the practicality of the model. This gives the possibility of more complex variations as it does not depend on the diameter of the buoy. By separating the stiffness, it is possible to have a different, but constant, diameter at the waterline. This shortcut does not incorporate the hydrodynamic effects of the varying diameter of the length of the buoy. Apart from the dimensions of the structure, the topology of the buoy and beam structure will be varied. The topology describes the number of buoys and the way the triangles are placed with respect to each other. Furthermore, the global position relative to the incoming waves needs to be varied.
A list of main dimensions and general aspects of the design that should be included in the model for variation are listed here:

- General:
  - Size of structure: number of buoys and triangles
  - Topology of structure
  - Wave direction relative to the structure
- Beam:
  - Length
  - Diameter
  - (Added) mass
  - Damping
  - Depth
- Buoy
  - Diameter
  - Draft
  - (Added) Mass
  - Stiffness

Moreover, the hydrodynamic environment needs to be varied. The number of variables will depend on the selected wave theory. Therefore, it will not be discussed here. Based on the assumption of regular waves, items such as wavelength, wave height need to be varied.

Desired output results
The following results and output should be obtained for every variation.

- Response in heave direction
- Relative wave height seen from the moving construction
- Proportions of the hydrodynamic loads
- Angles of the beams in the construction
- Eigenmodes and eigenfrequencies

The relative wave height and the angels in the construction will be calculated with the heave response of the structure. It will be useful to give an estimation of the loads within the construction. Now the in- and outputs of the model are clarified the model can be build up.
This modelling approach will result in a calculation tool where multiple variables can be varied. At the end of this thesis, some of these input variables will be varied.

6

Mechanical analysis of the support structure

This chapter discusses the derivations of the differential equations that describe the response of the structure in heave direction. The goal is to find a standard method for the derivation of the mechanical equations for a buoy and beam structure to obtain the heave response and other desired modelling outputs. In this chapter, the systematic derivation of the mechanical equations will be determined based on a relatively simple four buoy system. This will serve as an input in build up a system in section 9.1. In this chapter, the hydrodynamic loads are represented by external loads on the mechanical system. These will be addressed separately in chapter 7 and will then be combined into the complete models in chapter 8. In essence, the structure consists of multiple rigid bodies that are interconnected which all experience external forces. These interconnections can be described by constraints of the system. The constraints and the external environment result in forces, added masses, damping terms and spring stiffnesses. Together these form a system that can be described by multibody dynamics.
Analysing the structure can be done based on multiple theories within classical mechanics. The most straightforward system, in this case, is Newton-Euler mechanics. This is based on Newton's laws of motions. This is extended by Euler theory for point particles and rigid bodies. Within classical mechanics, there is a reformulation done resulting in Lagrange and Hamiltonian mechanics. Depending on the structure and the desired outcome, a one of these methods is preferable. For the modelling of the buoy and beam structure, classical Newton Euler theory will be used. This is a straightforward method that is familiar to the writer and covers all needs for the simulation.
The derivation of the differential equations will be executed as follows. First the forces on the individual elements are analysed in section 6.1. Then approximating small angular displacements of the connecting beams will be argued (section 6.2) after which a differential equation for a four beam system will be presented in section 6.3.

6.1. Forces on the individual elements

Before introducing the full structure, the two building blocks of the structure will be introduced separately. First, the beam will be discussed followed by the buoy. The aim is to discuss simplifications and assumptions that are made and the argumentation why these are valid. Furthermore, the loads relevant to the heave response will be identified. This introduction and conceptualisation are needed as input for the setting up the mechanical system.

6.1.1. Modelling of the beam

The beam is modelled as a line segment connecting the centres of two buoys. Meaning that the location, orientation and length are represented by the endpoints of the line segment (in cartesian coordinates x, y, z). On each end, forces from neighbouring elements are present. The hydrostatic and gravitational forces cancel out. Because it is assumed that the beam and the displaced water have the same mass. This mass is equally distributed over the length of the beam in this model. A diameter and a length define the beam. This results in a mass and a moment of inertia.

In Figure 6.1, a representation of the beam in its hydrodynamic environment along with external forces is given. No force and moment are present in the direction of the cylinder centre line as a result of the cylindrical shape and the relatively small diameter. An alternative frame of reference (o, p, z) is used where the z-axis has the same orientation as the global z-axis. The goal is to find a response in the z-direction. Therefore, only the relevant moment and forces are taken into account. These are the moment and force component in respectively the p- and z-direction. The length of the beam is calculated from the centre point to the centre point of the two connected buoys. This results in an overestimation of the length of the beam, which consequently results in an overestimation of the hydrodynamic forces. The figure indicates no damping or added mass. The damping and added mass terms are within the hydrodynamic forces.

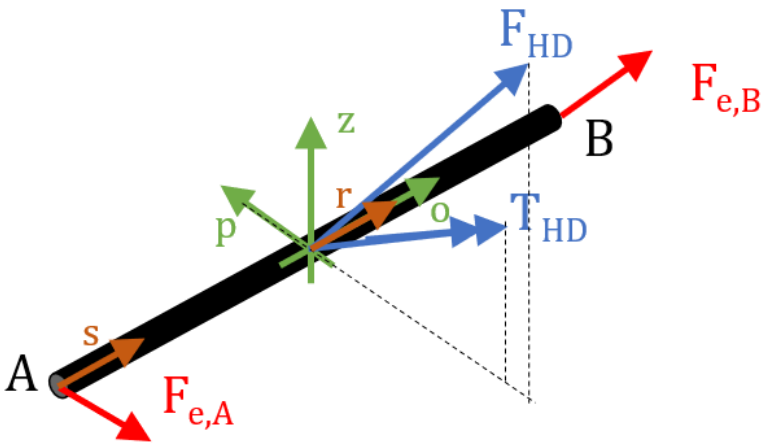

Figure 6.1: Modelling of the external forces on the beam (red: forces from connected buoys, blue: hydrodynamic loads, orange: tangent unit vector, green: local axis system, dotted line: decomposition of vectors.

6.1.2. Modelling of the buoy

Point masses are used to model the buoys of the structure, i.e. all loads will act on the centre of the buoy and no moment on the body is taken into account. The buoys are assumed to float stable and vertical. The buoy has a specific location in space (x, y, z), the diameter and draft (D, T). The dimensions determine the mass, and will initially determine the hydrostatic stiffness. Defining the stiffness separately from the defined diameter excludes the effect on the hydrodynamics coming from variations of the diameter over the buoy height. These effects are, for example, damping resulting from vertices and vertical forces on the surfaces created by a varying diameter. The buoy experiences loads by the hydrodynamic and hydrostatic environment, the gravity and from the connected beams.
A simple Free Body Diagram (FBD) is given in Figure 6.2a. On the left side of the figure, the FBD with multiple external forces is shown. The gravitational and hydrostatic force cancel each other out. The forces can be simplified, as represented in Figure 6.2b. Here the external forces are summed and the static forces are excluded as these are equal in magnitude and opposite in direction. For the analysis of the response in the vertical direction, the forces or force components in the vertical direction are relevant. Other forces are not taken into account. The hydrodynamic forces related to stiffness and damping are excluded from the hydrodynamic force. The stiffness and damping are incorporated separately represented by a spring and damper. The mass of the buoy incorporates the added mass force. For now, these are just arbitrary linear stiffness, dampers, (added)masses and dynamic forces. The stiffness is linear because the assumed constant diameter of buoys and the damping and added mass is assumed linear [6].

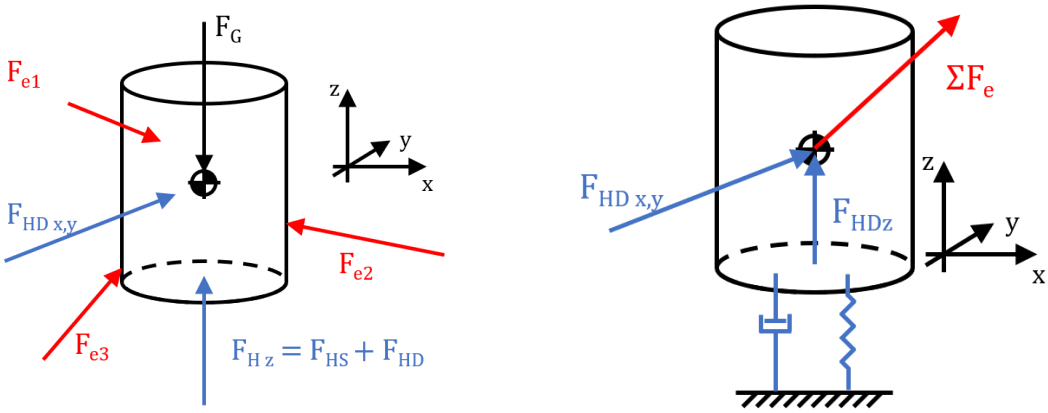

(a) Buoy external forces

(b) Buoy external forces with separated stiffness and damping

Figure 6.2: Modelling of the buoy.
G: the gravitational force, subscript $e1..n$: the external forces 1 to n from the connected elements, HV and HH: the vertical hydromechanic force (consists of the hydrostatic and hydrodynamic force) and the horizontal hydrodynamic force, HS and HD: Hydrostatic and hydrodynamic part of the force.

6.1.3. Modelling of the triangle platforms

As said in section 5.4, the platforms are not separately integrated in the mechanical model. The mass and mass distribution is estimated by the mass of the displaced water and the damping left out as it is estimated to be minor in repect to the other elements.

6.2. Small angle approximation

Before a 3D structure is assessed, a smaller 2D structure will be examined. The 2D environment will show some nonlinear behaviour that is present in the system. The goal is here to find to what extent the second- and higher-order effects are relevant in the analysis and modelling of the system. First, a FBD of a structure in 2D is shown in Figure 6.3. The moment balance, calculated in the middle of the beam, indicates some nonlinear behaviour. This can be seen in equation 6.1.

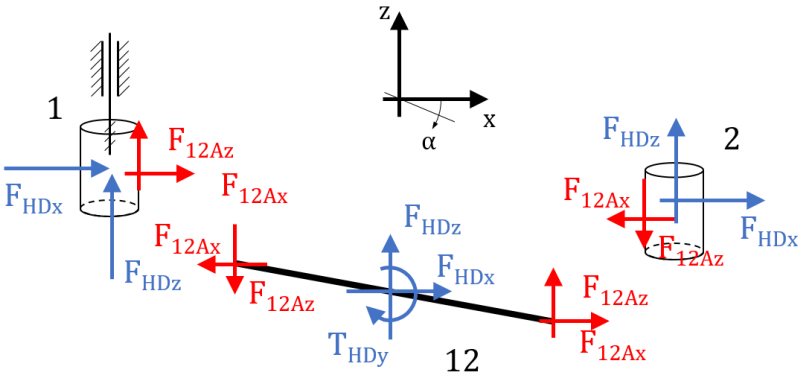

Figure 6.3: FBD of a two buoy structure in 2D
HD: hydrodynamic load, A/B forces in respectively connection A/B

$$\sum T_{12} = I\ddot{\alpha} \rightarrow T_{12} - \underbrace{(F_{12Ax} + F_{12Bx})\frac{L}{2}\sin(\alpha_{12})}_{1} - \underbrace{(F_{12Az} + F_{12Bz})\frac{L}{2}\cos(\alpha_{12})}_{2} = I_{12}\ddot{\alpha}_{12} \qquad (6.1)$$

The force of the neighbouring buoy, respectively the x- and the z- direction which, is multiplied with, respectively the sine and the cosine of the angle. This results in nonlinear behaviour in equation 6.1. Both the force and the angle are time-varying elements resulting in a term that is nonlinear (equation 6.2).

$$1: \rightarrow |F_{12Ax} + F_{12Bx}|\, e^{i\omega t} \frac{L}{2} \sin\left(|\alpha_{12}|\, e^{i\omega t}\right) \tag{6.2a}$$

$$2: \rightarrow |F_{12Az} + F_{12Bz}|\, e^{i\omega t} \frac{L}{2} \cos\left(|\alpha_{12}|\, e^{i\omega t}\right) \tag{6.2b}$$

Equation 6.1 could be approximated by a linear system by assuming that only small angles between the beam and the horizontal plane will occur. First, a realistic and feasible support structure should not have any response that has large angles. When large angles occur large forces in both horizontal and vertical direction will arise, this could lead to the infeasibility of the concept. Secondary, when analysing realistic waves in offshore conditions, only small steepness arises [19]. It can be assumed that the structure will follow the waves with a relative phase angle. Therefore small angles in the construction can be assumed.
The approach of assuming that $\sin(\alpha) = \alpha$ does not fully linearise the equation. α and the force both include a time-dependent part: $e^{i\omega t}$. Hence the nonlinearities shown in equation 6.3 are still in place. For that reason the assumption is made that the angles can be assumed as follows: $\sin(\alpha) = 0$ and $\cos(\alpha) = 1$. This results in a linear equation that should be sufficiently valid while simulating.

$$1: \rightarrow |F_{12Ax} + F_{12Bx}|\, e^{i\omega t} \frac{L}{2} \sin\left(|\alpha_{12}|\, e^{i\omega t}\right) \approx |F_{12Ax} + F_{12Bx}|\, e^{i\omega t} \frac{L}{2} \left(|\alpha_{12}|\, e^{i\omega t}\right) \tag{6.3}$$

$$1: \rightarrow \approx 0 \tag{6.4a}$$

$$2: \rightarrow |F_{12Az} + F_{12Bz}|\, e^{i\omega t} \frac{L}{2} \tag{6.4b}$$

This approximation means for that no angles will be taken into account for the calculations of the moment on the beams resulting from the connecting the buoys. This means that forces perpendicular on the beam apply a moment and the forces in line with the beam do not apply any moment on the beam. It further means that no horizontal displacement of the buoys are taken into account. This will limit the number of buoys that can be placed in line. For the goal of the research, the horizontal displacement is less relevant as it is assumed that it will not affect the heave response significantly. A further consequences of this approximation and the validity of the small angles be assessed in section 10.4.

6.3. Differential equations for a 4 buoy system

The next step is to analyse a 3D mechanical system. The theory of the multibody dynamics will be applied to a structure existing of four buoys with five connecting beams. Only the relevant components for the vertical response will be included.

6.3.1. Mechanical equations

Figure 6.4 gives a schematic representation of the system. A detailed FBD of every component in this schematic can be found in Figure 6.5. It can be seen that every beam has a local coordinate system (o, p, z) with coinciding z-axis as discussed before. Let's give some specific attention to the naming and the orientations of the moments, forces and axis frames.

- The positive direction of the moments on the beams are always oriented in positive p-direction,
- the A-side of the beam is always in negative o-direction and the B-side is always in a positive direction.
- The hydrodynamic forces are always in a positive direction.
- The o-axis direction is always in the horizontal plane and between $[0 : 120]$ degrees from the x-axis.

- The connecting forces between the beam and the buoy at the B side of the beam are always positively oriented.
- The reaction force is always pointing in the opposite direction.
- The beam is always named based on the two buoys it connects.

This methodology will be used to derive equations for larger systems. Because of the consistency in naming a consistent methodology can be applied to all systems.

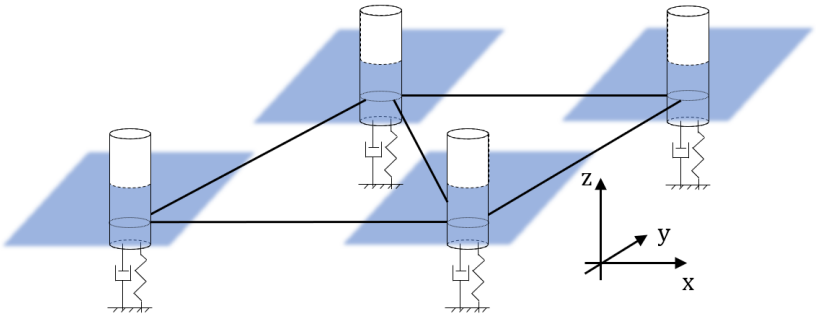

Figure 6.4: Schematising and modelling of a 4 buoy system

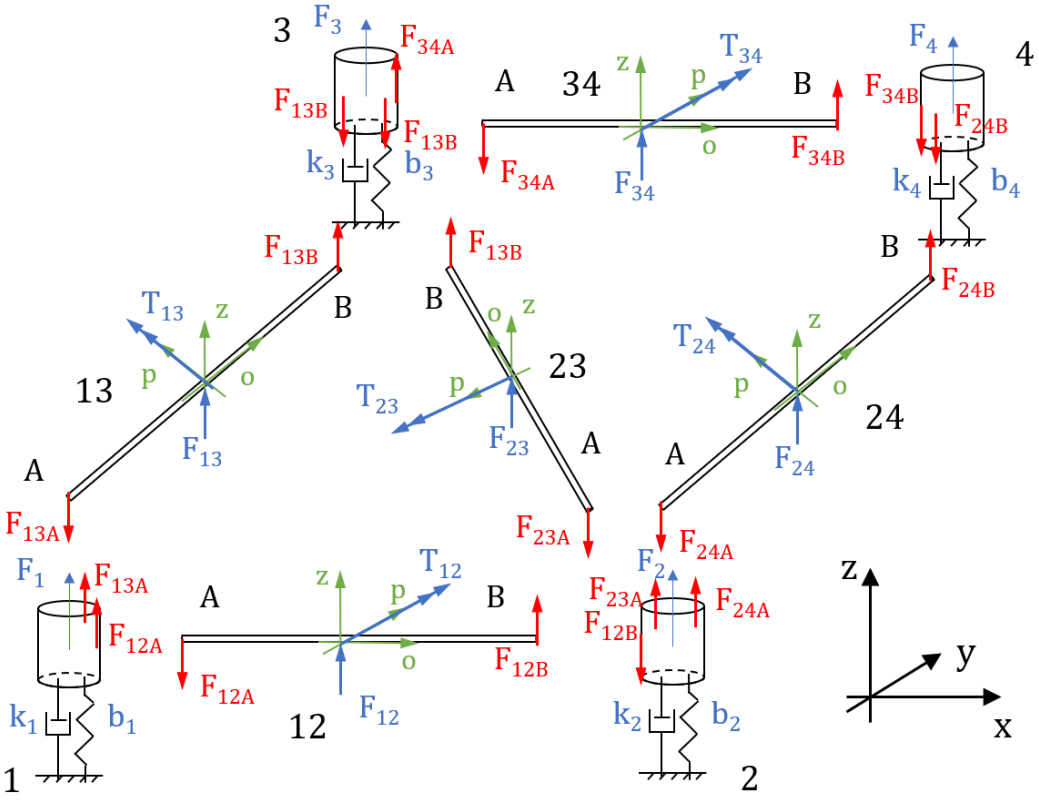

Figure 6.5: FBD of a 4 buoy system
Red: forces of connected elements, blue: buoy hydrodynamic forces, green: local axis system, F: forces, T: Moment, indexes indicate the connected buoys and the location by A and B

The dynamics of the structure is described based on the vertical motion of the buoys. The motion of the beams can be deducted by the motion of the buoys. The FBD in Figure 6.5 only contains the parameters relevant for the heave movement of the buoys. These parameters are the force, damping and stiffness in the vertical direction and the moment on the beam in p-direction. The vertical dynamic equilibrium of the buoys will be discussed first, resulting in four equations (equation 6.5). The forces coming from the connecting beams need to be substituted in these four equations.

$$\text{Buoy 1: } \sum F_z = m\ddot{z} \rightarrow F_{12Az} + F_{13Az} - b_1\dot{z}_1 - k_1 z_1 + F_1 = (m_1 + m_1')\ddot{z}_1 \tag{6.5a}$$

$$\text{Buoy 2: } \sum F_z = m\ddot{z} \rightarrow -F_{12Bz} + F_{23Az} + F_{24Az} - b_2\dot{z}_2 - k_2 z_2 + F_2 = (m_2 + m_2')\ddot{z}_2 \tag{6.5b}$$

$$\text{Buoy 3: } \sum F_z = m\ddot{z} \rightarrow -F_{13Bz} - F_{23Bz} + F_{34Az} - b_3\dot{z}_3 - k_3 z_3 + F_3 = (m_3 + m_3')\ddot{z}_3 \tag{6.5c}$$

$$\text{Buoy 4: } \sum F_z = m\ddot{z} \rightarrow -F_{24Bz} - F_{34Bz} - b_4\dot{z}_4 - k_4 z_4 + F_4 = (m_4 + m_4')\ddot{z}_4 \tag{6.5d}$$

The substitution can be done as follows. First beam 1 2 (read: “beam one, two”) will be analysed. For this beam the dynamic equilibrium in vertical direction and the dynamic equilibrium of the moment in p-direction will be written down, taking into account the previously made assumption: $\sin\alpha = 0$ and that $\cos\alpha = 1$ (section 6.2).

$$\text{Beam 1 2: } \sum F_z = m\ddot{z} \rightarrow -F_{12Az} + F_{12Bz} + F_{12} = m_{12}\ddot{z}_{12} \tag{6.6a}$$

$$\sum T_p = I_p\ddot{\alpha} \rightarrow -(F_{12Az} + F_{12Bz})\frac{L}{2} + T_{12} = I_{12}\ddot{\alpha}_{12} \tag{6.6b}$$

Multiplying equation 6.6b by $\frac{2}{L}$ and adding or subtract this from equation 6.6a. Gives respectively equations 6.7.

$$(6.6b)\cdot\frac{2}{L} + (6.6a) \rightarrow F_{12Az} = \frac{1}{2}F_{12} + \frac{T_{12}}{L} - \frac{1}{2}m_{12}\ddot{z}_{12} - \frac{I_{12}}{L}\ddot{\alpha}_{12} \tag{6.7a}$$

$$(6.6b)\cdot\frac{2}{L} - (6.6a) \rightarrow -F_{12Bz} = \frac{1}{2}F_{12} - \frac{T_{12}}{L} - \frac{1}{2}m_{12}\ddot{z}_{12} + \frac{I_{12}}{L}\ddot{\alpha}_{12} \tag{6.7b}$$

The same can be done for the other 4 beams resulting in the equations 6.8 a & b. Where i represents the lower number buoy physically connected to the beam and j represents the higher number buoy physically connected to the beam. Where $i : 1..3$ and $j : 2..4$ taking into account the topology.

$$F_{ijAz} = \frac{1}{2}F_{ij} + \frac{T_{ij}}{L} - \frac{1}{2}m_{ij}\ddot{z}_{ij} - \frac{I_{ij}}{L}\ddot{\alpha}_{ij} \tag{6.8a}$$

$$-F_{ijBz} = \frac{1}{2}F_{ij} - \frac{T_{ij}}{L} - \frac{1}{2}m_{ij}\ddot{z}_{ij} + \frac{I_{ij}}{L}\ddot{\alpha}_{ij} \tag{6.8b}$$

Equation 6.8 a & b can be substituted in equation 6.5 a & d. This results in 4 large equations describing the motions based on 4 degrees of freedom. The connections of the buoys and beams of the structure result in equations 6.9 a & b. These will be substituted for every connecting beam.

$$z_{ij} = \frac{z_i + z_j}{2} \tag{6.9a}$$

$$\alpha_{ij} = \frac{z_i - z_j}{L} \tag{6.9b}$$

The proposed substitutions based on equation 6.5 result in a linear differential equation that describes the mechanical behaviour of the buoy and beam system. The linear differential equations can be found in equation 6.10.

$$\mathbf{F} = [\mathbf{M}]\ddot{\mathbf{z}} + [\mathbf{B}]\dot{\mathbf{z}} + [\mathbf{K}]\mathbf{z} \tag{6.10a}$$

$$\mathbf{F} = \begin{bmatrix} F_1 + \frac{F_{12}}{2} + \frac{F_{13}}{2} + \frac{T_{12}}{L} + \frac{T_{13}}{L} \\ F_2 + \frac{F_{12}}{2} + \frac{F_{23}}{2} + \frac{F_{24}}{2} - \frac{T_{12}}{L} + \frac{T_{23}}{L} + \frac{T_{24}}{L} \\ F_3 + \frac{F_{13}}{2} + \frac{F_{23}}{2} + \frac{F_{34}}{2} - \frac{T_{13}}{L} - \frac{T_{23}}{L} + \frac{T_{34}}{L} \\ F_4 + \frac{F_{24}}{2} + \frac{F_{34}}{2} - \frac{T_{24}}{L} - \frac{T_{34}}{L} \end{bmatrix} \tag{6.10b}$$

$$[\mathbf{M}] = \begin{bmatrix} m_1 + m_1' + \frac{m_{12}}{4} + \frac{I_{12}}{L^2} + \frac{m_{13}}{4} + \frac{I_{13}}{L^2} & \frac{m_{12}}{4} - \frac{I_{12}}{L^2} & \frac{m_{13}}{4} - \frac{I_{13}}{L^2} & 0 \\ \frac{m_{12}}{4} - \frac{I_{12}}{L^2} & m_2 + m_2' + \frac{m_{12}}{4} + \frac{I_{12}}{L^2} + \frac{m_{23}}{4} + \frac{I_{23}}{L^2} + \frac{m_{24}}{4} + \frac{I_{24}}{L^2} & \frac{m_{23}}{4} - \frac{I_{23}}{L^2} & \frac{m_{24}}{4} - \frac{I_{24}}{L^2} \\ \frac{m_{13}}{4} - \frac{I_{13}}{L^2} & \frac{m_{23}}{4} - \frac{I_{23}}{L^2} & m_3 + m_3' + \frac{m_{13}}{4} + \frac{I_{13}}{L^2} + \frac{m_{23}}{4} + \frac{I_{23}}{L^2} + \frac{m_{34}}{4} + \frac{I_{34}}{L^2} & \frac{m_{34}}{4} - \frac{I_{34}}{L^2} \\ 0 & \frac{m_{24}}{4} - \frac{I_{24}}{L^2} & \frac{m_{34}}{4} - \frac{I_{34}}{L^2} & m_4 + m_4' + \frac{m_{24}}{4} + \frac{I_{24}}{L^2} + \frac{m_{34}}{4} + \frac{I_{34}}{L^2} \end{bmatrix} \tag{6.10c}$$

$$[\mathbf{B}] = \begin{bmatrix} b_1 & 0 & 0 & 0 \\ 0 & b_2 & 0 & 0 \\ 0 & 0 & b_3 & 0 \\ 0 & 0 & 0 & b_4 \end{bmatrix} \tag{6.10d}$$

$$[\mathbf{K}] = \begin{bmatrix} k_1 & 0 & 0 & 0 \\ 0 & k_2 & 0 & 0 \\ 0 & 0 & k_3 & 0 \\ 0 & 0 & 0 & k_4 \end{bmatrix} \tag{6.10e}$$

Equation 6.10a is especially importance. This differential equation will be further constructed over the rest of the thesis. By substituting the hydrodynamic forces and the exact numbers for the different vectors and matrices the complete differential equation will be obtained. Solving this differential equation will give the desired outputs of the model. Still the, so far, unknown hydrodynamic loads need to be substituded.

7

Hydromechanical theory

The loads that are incorporated in the mechanical model of chapter 6 need to be estimated. These loads should be calculated separately and then substituted in the differential equation (equation 6.10). The forces in the z-direction and the moment in local the p-direction on the connecting beams need to be substituted in the differential equation. The loads on the elements depend on the pressure, velocities and accelerations in the fluid. Therefore a suitable wave theory is identified in section 7.1. Next, applicable theories for the estimation of the hydrodynamic loads are selected in section 7.2.
Then the selected theory needs to be applied to the individual elements to obtain the needed loads. First, the theory is applied to the beam elements. The movement of the fluid will induce a first part of the load, and the movement of the structure will induce a second part of the loads. These two parts will be separated in section 7.3. After the separation, the calculations for all individual elements that contribute to the load will be explained. Lastly, the loads on the buoy elements will be calculated in section 7.4.

7.1. Wave theory

In the scope on page 31 it was stated that the response would be examined for regular waves. For the first estimation of the feasibility of the construction, it will be sufficient to take into account regular waves. Chakrabarti [4] discusses wave theories and their application. It is not the aim to check if the construction can survive the most extreme conditions. However, the aim is finding relations between the response of the construction in regular waves and the design parameters of the construction. Where the response is directly related to the feasibility. A wavelength and an amplitude will define these regular waves.
According to Chakrabarti [4], the Airy wave theory (i.e. linear wave theory) is appropriate to simulate sea states up to the one-year storms, swells and long term statistics. For this reason, it is concluded that Airy wave theory, is the appropriate option. The Airy wave theory does not take into account the splash zones or are above the still water surface, and asymmetry (non-perfect sinus shaped) profile of the wave. The aim is to develop a structure in offshore conditions. Therefore the deepwater equation of the Airy wave theory will be used. This means that the wave can be described by wave height and wave period. These two parameters give information on the wave steepness, wavelength, velocities and accelerations in the fluid, etc.

7.1.1. Variation in offshore wave characteristics

The waves described by the Airy wave theory depends on the wave height and wave period. The overall goal of the research is to find a feasible concept. This means that it survives in realistic offshore conditions. Thus it is desirable to assess the structure on realistic wave amplitudes and frequencies, within the limits of Airy wave theory. It should be noted that in the case of a linear system, the wave amplitude will be linear with respect to the response. In that case, the amplitude is less relevant in the simulation. The relevant amplitudes and wavelengths for the assessment depend on two factors. First, there is the realism of the wave in offshore conditions. Second, the relative dimensions of the structure with respect to the wavelength should be taken into account. Short waves relative to the structure size

will not influence the construction. In really long waves the structure most probably moves completely with the waves.
A more general approach is taken, and a specific spectrum is not yet incorporated. In the book of Journée et al. [19], a table from Bales is presented that is also adopted by the 17th ITTC (1984) [19, p5-51]. This indicates on the probability and a relation between the sea state, wave height and modal wave period (Table 7.1).

Table 7.1: "Open Ocean Annual Sea State Occurrences" [19]

Sea state	Probability of the Sea State (%)	Significant wave height		Modal Wave Period	
		range	mean	Range	Most probable
0 - 1	0	0.0 - 0.1	0.05		
2	7.2	0.1 - 0.5	0.3	3.3 - 12.8	7.5
3	22.4	0.5 - 1.25	0.88	5.0 - 14.8	7.5
4	28.7	1.25 - 2.5	1.88	6.1 - 15.2	8.8
5	15.5	2.5 - 4	3.25	9.8 - 16.2	9.7
6	18.7	4 - 6	5	11.8 - 18.5	12.4
7	6.1	6 - 9	7.5	14.2 - 18.6	15
8	1.2	9 - 14	11.5	14.2 - 18.6	16.4
8+	< 0.05	> 14	> 14	18.0 - 23.7	20

For this thesis, the simulation range on wave characteristics can be based on Table 7.1. The wave period should at least be varied between 3 seconds and 15 seconds. This corresponds with a wavelength of 15 to 350 meters and an angular frequency of 0.42 to 2.09 rad/s which includes 90 % of the sea states indicated in Table 7.1. It is not yet the aim to test the concept on the most severe condition (sea state 7 or higher). Neither can the Airy wave theory describe these conditions. The table also demonstrates a clear relationship between the significant wave height and the most probable wave period. Although the significant wave height is not the same as the maximum wave height, the relationship can be used to indicate a relevant wave height. The table also confirms the small angle approximation that was introduced in section 6.2 on page 49.
As the focus is on the heave response of the structure, the waves with a wavelength of multiple times, the total structure length could be left out of consideration for answering the research question. The construction will move with the wave, certainly within the Airy wave theory. Significantly shorter waves than the individual structural elements should have no significant influence on the response of the structure. Those extreme positions are interesting for verification purposes.

7.2. Selection of theory for estimation of hydrodynamic loads

The structure and the hydrodynamic environment as described with the Airy wave theory will interact and will on one side result in loads on the structure and will result in a change within the water on the other side.

7.2.1. General principles of hydrodynamics and selection of theory

It is a common assumption that hydrodynamic loads can be calculated by superposition of the loads on structural elements in multiple directions. On each element, the force can be calculated by integrating the pressure over the wetted surface. The hydrodynamic loads can be split into three parts: The"[1] Froude-Krylov force: pressure effects due to undisturbed incident waves; [2] Hydrodynamic mass 'added mass and potential damping force: pressure effects due to relative acceleration and velocity between water particles and structural components in an ideal fluid; [3] viscous drag force: pressure effect due to relative velocity between water particles and structural components" [6, p.220].
Literature makes a distinction between hydrodynamic transparent structures and hydrodynamic compact structures. The first group of structures has a small dimension relative to wavelength and are said to have minimal influence on the wave. In this case, it is assumed that the effect of the construction on the wave can be discarded. Structures that are larger with respect to wavelength will disturb and pos-

sibly reflect the incoming wave. For the hydrodynamic transparent cylindrical structures, the Morison equation is applied, and for hydrodynamic compact structures (linear) diffraction theory is used. Figure 7.1 shows this relation. [4, 6]
The general framework that is visualised in Figure 7.1. With on the vertical axis the Keulegan-Carpenter (number) (KC)-number (or the relative wave height) calculated by equation 7.2. The higher the KC-number, the higher the contribution of the viscous damping component. In the horizontal axis relative structure size. [4, 6]

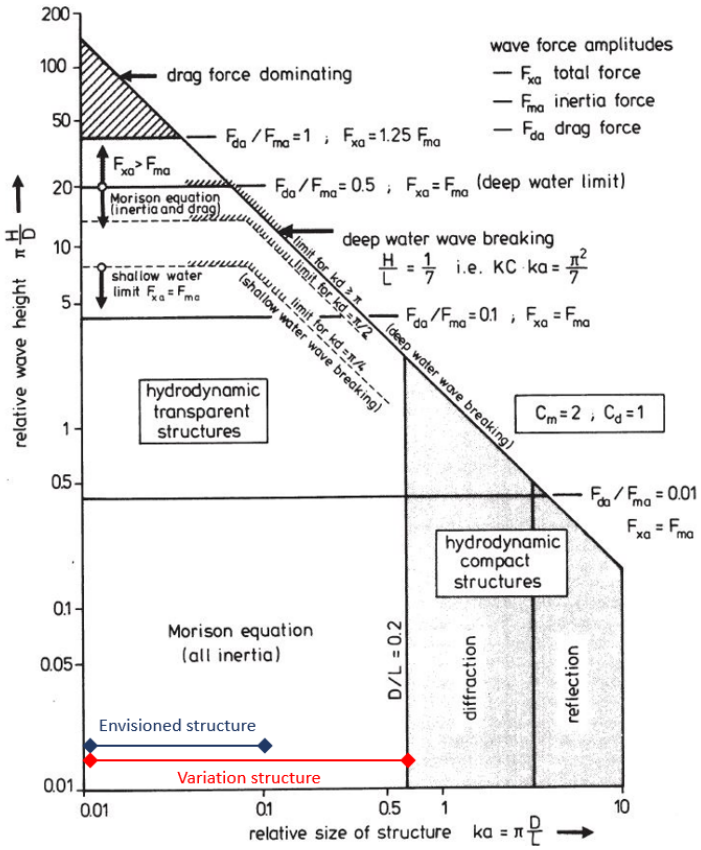

Figure 7.1: Modelling methods selection graph for hydrodynamic (circular) structures [6]. In red the relative structure size for the envisioned variations to find the design parameters and in blue, the envisioned buoy and beam structure as described in section 5.3

It needs to be determined if the buoy and beams structure can be considered a hydrodynamic transparent structure. This can be determined with the following approach. First, the diffraction parameter (equation 7.1) is introduced. The diffraction parameter, also called the relative size of the construction, indicates if diffraction theory needs to be applied. In other words, if the diffraction parameter is larger than $\frac{\pi}{5}$, then the construction is considered hydrodynamic compact. [4, 6] Therefore, the maximum structure sizes that will be simulated, will be divided by the smallest wavelengths. These relative structure sizes will be used to select the appropriate theory.

$$\text{Diffraction parameter or relative structure size:}\frac{\pi D}{\lambda} \tag{7.1}$$

$$KC=\frac{u_a T}{D}=\frac{\zeta_a \omega \frac{2\pi}{\omega}}{D}=\frac{2\zeta\pi}{D} \tag{7.2}$$

As indicated on beforehand, the aim is estimating the influence of the main parameter (and its ratios), on the heave response of a buoy and beam structure. When the most extreme positions (largest wave with the smallest construction and smallest wave with the largest construction) are considered the position in Figure 7.1 can be indicated.

In section 5.3 an envisioning of the structure was done. There it was said on page 38 “that the sides of the triangle are in the range of 10 to 40 meters and buoys of a diameter of 1.5 meters and a draft of 5 meters.” This was only a first indication. Taking a diameter of 1.5 meters for the buoys and 0.75 meters for the beams as a first indication with the shortest wavelength of 15m would result in a relative structure size of $\pi/10$ to $\pi/20$. To find relations between the design parameters and the response multiple dimensions of the buoys and beams will be simulated. Diameters in the range of 0.5 to 9 meters could be thought off. With a wavelength of 15 meters, these dimensions would results in a relative structure size from $\pi/30$ to $3\pi/5$. The two ranges of structure sizes are indicated in Figure 7.1. The relative structure size indicated on the x-axis in Figure 7.1 shows that this extreme combination is on the border area. The border area between the application of diffraction and the application of Morison is indicated on $D/L = 0.2$ with D the diameter and λ the wavelength. Slightly going over this border, when simulating higher frequencies, would only cause a small error. When simulating significant larger relative structure sizes diffraction theory is needed and the outcomes of the modelling without diffraction will have no relevance. This result in the conclusion that the structure can efficiently be modelled with the Morison equation.

7.3. Morison equation

In this section, the Morison equation will be introduced. First, the most standard case of the Morison equation will be disused i.e. the Morison equation for a fixed vertical cylinder. Then the adapted equation for a cylinder with random orientation will be discussed. This incorporates loads for a cylinder moving that is moving in the water.
Initially, the Morison equation was presented for the force on a vertical cylinder segment in waves in Morison et al. [28]. The equation is used to calculate the perpendicular force on a vertical cylinder segment. In which u is the vertical component of the fluid velocity. This equation can be found in equation 7.3.

$$d\vec{F} = \underbrace{\rho\frac{\pi D^2}{4}dz\dot{u}}_{\text{Froude-Krylov}} + \underbrace{C_a\rho\frac{\pi D^2}{4}dz\dot{u}}_{\text{hydrodynamic mass}} + \underbrace{C_D\frac{\rho}{2}Ddz\,|u|\,u}_{\text{viscous drag}} \tag{7.3}$$

The equation contains an inertia term (or Froude-Krylov and hydrodynamic mass term) that is depending on the accelerations and it contains a damping term (or viscous drag term) that is depending on the velocity. Figure 7.1 on page 57 indicates on the vertical axis the relevance of the inertia and damping parts within the Morison equation. KC is an indication of the proportion of the damping and the inertia contribution to the force calculated by the Morison equation. Based on the vertical axis, a structure with a small relative structure size allows the Morison equation to calculate the accelerations and velocities at the centre line and extrapolate these values over the diameter of the cylinder.
In this section, an alternative Morison equation will be presented for the randomly oriented cylinder that is vibrating in the fluid in section 7.3.1. This will result in terms that are either depending on the fluid or the fluid movement. All different terms will be integrated separately to obtain the relevant moment and force components as indicated in section 7.3.5. Lastly this proposed integration is executed in section 7.3.6.

7.3.1. Morison equation for random orientation in waves

The beams of the buoy and beam structure move through the water and the elements have different orientations. The Morison equation for the force on a randomly oriented cylinder can be found in equation 7.4. With equation 7.4 the force on a segment with length ds can be calculated. The general framework is presented in literature in: Chakrabarti et al. [3], Clauss et al. [6, p.255].

$$d\vec{F}_N = \underbrace{\rho\frac{\pi D^2}{4}\dot{\vec{v}}_N ds}_{\text{Froude-Krylov force}} + \underbrace{C_a\rho\frac{\pi D^2}{4}\dot{\vec{u}}_{RN}ds}_{\text{Hydrodynamic mass force}} + \underbrace{C_d\frac{\rho}{2}D\,|\vec{u}_{RN}|\,\vec{u}_{RN}ds}_{\text{Viscous drag force}} \tag{7.4}$$

In equation 7.4: D indicates the diameter of the cylinder, $\vec{v}_N$ indicates the velocity of the fluid perpendicular to the cylinder centre line, C_a and C_d are respectively the added mass and damping coefficients, $\vec{u}_{RN}$ indicates the relative velocity of the fluid perpendicular to the cylinder centre line and ds indicates the segment length of the cylinder over which the force is calculated.
This equation is presented in three parts: the Froude-Krylov part, the hydrodynamic mass part and the

viscous drag part. The Froude-Krylov term is the force arising from the acceleration of the fluid in an undistributed incoming wave and can be calculated with the acceleration in the fluid. The hydrodynamic mass forces use the relative acceleration to calculate the force. The relative acceleration is the fluid acceleration seen from the moving cylinder. The viscous drag depends on the relative velocity of the structure. This part is in nonlinear as the velocity is multiplied with the absolute value of the velocity. The linearized equation will be discussed later when discussing the viscous drag force.
To know the total perpendicular force on the full cylinder the force needs to be integrated over its full length. The same method can be used to examine the moment on a cylinder. By integrating $\vec{r} \times d\vec{F}_N$, with r the distance between a fixed point and the cylinder section, the moment is obtained. The desire is to obtain the relevant forces and moments for the movement of the structure as defined in chapter 6. Therefore the forces, added masses and damping terms for the movement of a horizontal beam in the z-direction are obtained. For the rotation of the beams, the same is done but now for the rotation in the local p-direction.

7.3.2. Froude-Krylov part

For the calculation of the Froude-Krylov term, the acceleration of the fluid is projected on a plane perpendicular to the centre line of the cylinder (equation 7.5).

$$\vec{v}_N = \vec{e}_t \times \left(\vec{v} \times \vec{e}_t\right) \tag{7.5}$$

The unit vector $\vec{e}_t$ indicates the orientation of the cylinder centre line. The accelerations $\left(\dot{\vec{v}}\right)$ and the velocities $(\vec{v})$ of the fluid are expressed with the Airy wave theory.

7.3.3. Splitting the hydrodynamic mass part

The hydrodynamic mass part is dependent on the relative perpendicular acceleration of the fluid. This can be calculated by projecting the relative acceleration on a plane, perpendicular to the centre line of the cylinder as indicated in equation 7.6.

$$\dot{\vec{u}}_{RN} = \vec{e}_t \times \left(\dot{\vec{u}}_R \times \vec{e}_t\right) \tag{7.6}$$

The relative acceleration ($\dot{\vec{u}}_R$) is obtained by subtracting the acceleration of the structure from acceleration in the fluid.

$$\dot{\vec{u}}_R = \dot{\vec{v}} - \dot{\vec{u}}_c \tag{7.7}$$

When this is substituted in the full equation two parts can be identified in equation 7.8.

$$\begin{aligned} d\vec{F}_{HM} &= C_a \rho \frac{\pi D^2}{4}\left[\vec{e}_t \times \left(\left(\dot{\vec{v}} - \dot{\vec{u}}_c\right) \times \vec{e}_t\right)\right] ds \\ &= C_a \rho \frac{\pi D^2}{4}\left[\vec{e}_t \times \left(\dot{\vec{v}} \times \vec{e}_t\right)\right] ds - C_a \rho \frac{\pi D^2}{4}\left[\vec{e}_t \times \left(\dot{\vec{u}}_c \times \vec{e}_t\right)\right] ds \\ &= C_a \rho \frac{\pi D^2}{4} \dot{\vec{v}}_N ds - C_a \rho \frac{\pi D^2}{4} \dot{\vec{u}}_{cN} ds \end{aligned} \tag{7.8}$$

The first part is only dependent on the acceleration of the fluid within the wave and has large similarities with the previously explained Froude-Krylov part. The second part is only dependent on the acceleration of the structure and is therefore an added mass term.

7.3.4. Linearising and splitting the viscous drag part

The viscous drag force is calculated based on the velocities of the particles in the wave and the velocity of structure. Equation 7.9 introduces the linearised version of the viscous damping. The process of linearisation is based on equivalent energy and is explained in Appendix B.3, or can be found in Clauss et al. [6]. The linearised version makes use of the amplitude of the perpendicular velocity of the fluid (u_{RNa}). To calculate u_{RNa}, the velocity expressions in the fluid of the Airy wave theory and the velocity of the construction are used. As the velocity of the construction is initially unknown this term should be

iterated. The calculation of u_{RNa} will be discussed later (section 7.3.6) and the implementation of the iteration will be discussed in chapter 9.

$$d\vec{F}_{VD} = \frac{8}{3\pi} C_d \frac{\rho}{2} D\, u_{RNa} \vec{u}_{RN} ds \tag{7.9}$$

The relative velocity $\vec{u}_{RN}$ is calculated in a similar fashion as the relative acceleration for the hydrodynamic mass force in equation 7.6. First the components perpendicular to the cylinder centre line are calculated by equation 7.10. The relative velocity ($\vec{u}_R$) is calculated with equation 7.11.

$$\vec{u}_{RN} = \vec{e}_t \times (\vec{u}_R \times \vec{e}_t) \tag{7.10}$$

$$\vec{u}_R = \vec{v} - \vec{u}_c \tag{7.11}$$

By substituting equation 7.11 and equation 7.10 in equation 7.9, equation 7.12 is obtained.

$$\begin{aligned} d\vec{F}_{VD} &= \frac{8}{3\pi} C_d \frac{\rho}{2} D\, u_{RNa} \left[\vec{e}_t \times ((\vec{v} - \vec{u}_c) \times \vec{e}_t)\right] ds \\ &= \frac{8}{3\pi} C_d \frac{\rho}{2} D\, u_{RNa} \left[\vec{e}_t \times (\vec{v} \times \vec{e}_t)\right] ds - \frac{8}{3\pi} C_d \frac{\rho}{2} D\, u_{RNa} \left[\vec{e}_t \times (\vec{u}_c \times \vec{e}_t)\right] ds \\ &= \frac{8}{3\pi} C_d \frac{\rho}{2} D\, u_{RNa} \vec{v}_N ds - \frac{8}{3\pi} C_d \frac{\rho}{2} D\, u_{RNa} \vec{u}_{cN} ds \end{aligned} \tag{7.12}$$

This splits equation 7.9 in two independent terms: one term based on the fluid velocity and one term based on the structure velocity.

7.3.5. Total Morison equation

The previous steps are combined in equation 7.13. Each term is named differently.

$$d\vec{F}_N = \underbrace{(1 + C_a)\, \rho \frac{\pi D^2}{4} \dot{\vec{v}}_N ds}_{d\vec{F}_{N,FK,HM,\zeta}} \underbrace{- C_a \rho \frac{\pi D^2}{4} \dot{\vec{u}}_{cN} ds}_{d\vec{F}_{N,HM,c}} + \underbrace{\frac{8}{3\pi} C_d \frac{\rho}{2} D\, u_{RNa} \vec{v}_N ds}_{d\vec{F}_{N,VD,\zeta}} \underbrace{- \frac{8}{3\pi} C_d \frac{\rho}{2} D\, u_{RNa} \vec{u}_{cN} ds}_{d\vec{F}_{N,VD,c}} \tag{7.13}$$

The first term is a combination of the Froude-Krylov term and part of the hydrodynamic mass force. The first term only depends on the wave indicated by the subscript ζ. The second term contains the second part of the hydrodynamic mass and is fully dependent on the structure movement, indicated by the subscript c. This is called the added mass term. The third term is the viscous drag term dependent on the velocities of the fluid in the waves. The last part is the damping term dependent on the velocity of the elements in a fluid.
To obtain the full force and moment on a cylinder the Morison equation must be integrated over the length of the cylinder. This can be done making use of equation 7.14 a & b.

$$\vec{F}_M = \int_0^L \frac{d\vec{F}_N}{ds} ds \tag{7.14a}$$

$$\vec{T}_M = \int_0^L \left(\vec{r} \times \frac{d\vec{F}_N}{ds} \right) ds \tag{7.14b}$$

Integrating the different terms of equation 7.13 results in equation 7.15 and equation 7.16.

$$\vec{F}_M = \int_0^L \frac{d\vec{F}_{N,FK,HM,\zeta}}{ds} - \frac{d\vec{F}_{N,HM,c}}{ds} + \frac{d\vec{F}_{N,VD,\zeta}}{ds} - \frac{d\vec{F}_{N,VD,c}}{ds} ds \tag{7.15a}$$

$$\vec{F}_M = \vec{F}_{FK,HM,\zeta} - \vec{F}_{HM,c} + \vec{F}_{VD,\zeta} - \vec{F}_{VD,c} \tag{7.15b}$$

$$\vec{T}_M = \int_0^L \left(\vec{r} \times \frac{d\vec{F}_{N,FK,HM,\zeta}}{ds} \right) - \left(\vec{r} \times \frac{d\vec{F}_{N,HM,c}}{ds} \right) + \left(\vec{r} \times \frac{d\vec{F}_{N,VD,\zeta}}{ds} \right) - \left(\vec{r} \times \frac{d\vec{F}_{N,VD,c}}{ds} \right) ds \tag{7.16a}$$

$$\vec{T}_M = \vec{T}_{FK,HM,\zeta} - \vec{T}_{HM,c} + \vec{F}_{VD,\zeta} - \vec{T}_{VD,c} \tag{7.16b}$$

This results in a method to obtain all forces and moments on the beams. Now it is needed to obtain the exact method to calculate the individual terms.

7.3.6. Calculation of the Morison terms

The individual terms indicated in equation 7.15 and equation 7.16 will be integrated to obtain the forces in the z-direction and the moment in p-direction. Next the added mass term and added moment of inertia are deducted based on the same equations for the relevant directions. Then the same is done for the viscous drag terms.

Froude-Krylov and hydrodynamic mass force

Substituting equation 7.5 results in the integral of equation 7.15 results in equation 7.17.

$$\vec{F}_{FKHM,\zeta} = \int_0^L (1 + C_a)\rho \frac{\pi D^2}{4} \left[\vec{e}_t \times \left(\vec{v} \times \vec{e}_t\right)\right] ds \tag{7.17}$$

Making use of the Airy wave theory explained in Appendix B.1 the accelerations in the fluid can be substituted. The tangent unit vector $\vec{e_t}$ can be calculated based on the positions of the outer points of the cylinder.

Froude-Krylov and hydrodynamic mass torque

For the buoy and beam structure the moment is calculated for a cylinder in the horizontal plane. The aim is to obtain the moment in p-direction. Therefore the moment is calculated by integrating the distance in o-direction times the z-component of the Morison force. With the p-, o- and z-direction as defined in Figure 6.1. This results in equation 7.18. In which the distance in o-direction to the middle point is defined as $(\vec{r})_o$ (see Figure 6.2a).

$$T_{FKHM,\zeta,p} = \int_0^L (\vec{r})_o \times \left((1 + C_a)\rho \frac{\pi D^2}{4} \left[\vec{e}_t \times \left(\vec{v} \times \vec{e}_t\right)\right]\right)_z ds \tag{7.18}$$

Added mass

The added mass can be obtained by integrating equation 7.13 as shown in equation 7.19.

$$\vec{F}_{HM,c} = \int_0^L C_a \rho \frac{\pi D^2}{4} \left[\vec{e}_t \times \left(\vec{u}_c \times \vec{e}_t\right)\right] ds \tag{7.19}$$

First equation 7.20 is substituted in equation 7.19 resulting in equation 7.21. The point of reference for accelerations and the angular acceleration is taken in the middle of the cylinder.

$$\vec{u}_c = \vec{u}_T + \vec{\ddot{\alpha}} \times \vec{r}_s \tag{7.20}$$

$$\vec{F}_{HM,c} = \int_0^L C_a \rho \frac{\pi D^2}{4} \left[\vec{e}_t \times \left(\left[\vec{\ddot{u}}_T + \vec{\ddot{\alpha}} \times \vec{r}_s\right] \times \vec{e}_t\right)\right] ds \tag{7.21}$$

From equation 7.21 it can be concluded that $\vec{\ddot{\alpha}}$ will not contribute to the force as it is part of the solution of the integral. This follows the logic as the point of reference is in the middle so rotation does not result in a force.

The z-component of the result of the integration of equation 7.21 is given in equation 7.22.

$$F_{HM,c,z} = \frac{C_a D^2 \pi \rho L \left(e_{tx}^2 + e_{ty}^2\right)}{4} \left(\vec{\ddot{u}}_T\right)_z = m'_z \ddot{z}_T \tag{7.22}$$

The solution of the integral generates the opportunity to introduce an added mass term (m'_z) for the acceleration in z-direction. All motion dependent terms contain $\left(e_{tx}^2 + e_{ty}^2\right)$ for a motion in z-direction. As horizontal beams are considered this equals one. the added mass term m' contains the volume of the beam times the added mass coefficient.

$$m'_z = \frac{C_a D^2 \pi \rho L}{4} \tag{7.23}$$

Moment of inertia caused by added mass

A similar equation as shown in 7.19 must be integrated. The force should be multiplied with the distance to the middle and integrated over its length.

$$T_{HM,c,o} = \int_0^L (\vec{r})_o \times \left(C_a \rho \frac{\pi D^2}{4} \left[\vec{e}_t \times \left(\left[\vec{\ddot{u}}_T + \vec{\ddot{\alpha}} \times \vec{r}_s\right] \times \vec{e}_t\right)\right]\right)_z ds \tag{7.24}$$

When solving this integral the translation will not result in any moment. For that reason, it will not appear in the outcome of the integral. Equation 7.25 only contains the inertia by cause of the added mass in local p-direction of the beam as indicated in Figure 6.1.

$$T_{HM,c,p} = \frac{\pi D^2 C_a L^3 \rho}{48} \left(\vec{\ddot{\alpha}}\right)_p = I'_p \ddot{\alpha}_p \tag{7.25}$$

Now the added inertia term I'_p for a beam in the horizontal plane is introduced for rotation around the local o-axis. This is exactly the moment of inertia of the added mass term as defined in equation 7.23. The moment of inertia of a rod is calculated by: $I = \frac{m' L^2}{12}$.

$$I'_p = \frac{\pi D^2 C_a L^3 \rho}{48} \tag{7.26}$$

Amplitude of relative velocity

Because of the linearisation of the viscous drag term the amplitude of the relative velocity (u_{RNa}) is introduced in equation 7.13. Equation 7.27 till equation 7.30 are used to calculate u_{RNa}.

$$u_{RNa} = |\vec{u}_{RN}| \tag{7.27}$$

$$\vec{u}_{RN} = \vec{e}_t \times (\vec{u}_R \times \vec{e}_t) \tag{7.28}$$

$$\vec{u}_R = \vec{v} - \vec{u}_c \tag{7.29}$$

As the velocity amplitude varies over the beam length one average value over the length will be taken into account. The structure is assumed to only displace in z-direction. Therefore the displacement ($\vec{u}_c$) only has a z-component. The movement over the beam is not constant over its length as it consists out of a translation and rotation motion. Consequently equation 7.30 is expressed in the response of the two outer parts of the beam.

$$u_{c,z} = \vec{Z}_1 \frac{L - s}{L} + \vec{Z}_2 \frac{s}{L} \tag{7.30}$$

The magnitude of the velocity vector varies both over time as over the length of the beam. Therefore the magnitude of the velocity should be iterated. The average of the real component of the velocity will be taken over the length of the beam per time increment and then the maximum velocity over the time will be taken. By only taking the real part into account and varying over the time the relative phase angle between the velocities and the velocity of the construction is taken into account.

Viscous drag force matrix

The viscous drag part needs to be integrated over the length. Before this can be done the term needs to be linearised. The linearisation is explained in Appendix B.3 for a vertical cylinder. Here the just obtained u_{RNa} term is applied. For a cylinder with random orientation the same approach can be used. Substituting equation 7.28 in equation 7.13 results in the integral shown in equation 7.31.

$$\vec{F}_{VD,\zeta} = \int_0^L \frac{8}{3\pi} C_d \, \frac{\rho}{2} \, D \, u_{RNa} \, [\vec{e}_t \times (\vec{v} \times \vec{e}_t)] \, ds \tag{7.31}$$

Again only the z-component is taken into account as the response of the structure in z-direction is desired.

Viscous drag moment matrix

Calculating the moment is largely similar as previously applied sequences.

$$T_{VD,\zeta,p} = \int_0^L (\vec{r})_o \times \left(\frac{8}{3\pi} C_d \, \frac{\rho}{2} \, D \, u_{RNa} \, [\vec{e}_t \times (\vec{v} \times \vec{e}_t)] \right)_z \, ds \tag{7.32}$$

For the buoy and beam structure only the p-component of the moment is relevant. The p-component is calculated by multiplying the distance in o-direction with the force component in z-direction for cylinders in the horizontal plane.

Viscous drag damping force matrix
A similar sequence of steps should be taken to find the damping and the angular damping of the structure. The forces are calculated by substituting equation 7.28 and equation 7.33 in equation 7.13. It results in equation 7.34.

$$\vec{u}_C = \vec{u}_T + \vec{\dot{\alpha}} \times \vec{r}_s \tag{7.33}$$

$$\vec{F}_{VD,c} = \int_0^L \frac{8}{3\pi} C_d \frac{\rho}{2} D u_{RNa} \left[\vec{e}_t \times \left(\left[\vec{u}_T + \vec{\dot{\alpha}} \times \vec{r}_s\right] \times \vec{e}_t\right)\right] ds \tag{7.34}$$

Here again the angular velocity will not play any role in the damping as result of translation. When the integral is solved the $\vec{\dot{\alpha}}$ term is not part of the solution. The force in z-direction that is obtained by the integral is found in equation 7.35. A damping term b'_z is introduced in equation 7.36.

$$F_{VD,c,z} = \frac{8}{3\pi} C_d \frac{\rho}{2} D u_{RNa} L \left(\vec{u}_T\right)_z = b'_z \dot{z}_T \tag{7.35}$$

$$b'_z = \frac{8}{3\pi} C_d \frac{\rho}{2} D u_{RNa} L \tag{7.36}$$

Viscous drag damping moment matrix
Lastly, the damping resulting form the angular velocity should be obtained. Equation 7.28 and equation 7.33 are substituted in equation 7.13.

$$\vec{T}_{VD,c} = \int_0^L (\vec{r})_o \times \left(\frac{8}{3\pi} C_d \frac{\rho}{2} D u_{RNa} \left[\vec{e}_t \times \left(\left[\vec{u}_T + \vec{\dot{\alpha}} \times \vec{r}_s\right] \times \vec{e}_t\right)\right]\right)_z ds \tag{7.37}$$

Here again the translation velocity will not play any role in the angular damping. When the integral is solved the $\vec{u_T}$ term disappears. The moment in p-direction that is obtained by the integral is found in 7.38. Here again the damping as result of rotation and the damping as result of translation have the same relation as the added mass: $B'_p = \frac{b'_z L^2}{12}$.

$$T_{VD,c,p} = \frac{8}{3\pi} C_d \frac{\rho}{2} D u_{RNa} \frac{L^3}{12} \left(\vec{\ddot{\alpha}}\right)_p = B'_p \dot{\alpha}_p \tag{7.38}$$

$$B'_p = \frac{8}{3\pi} C_d \frac{\rho}{2} D u_{RNa} \frac{L^3}{12} \tag{7.39}$$

All external forces relevant for the heave response of the beam structure are now derived.

7.4. Hydrodynamics of a heaving buoy

The buoy will experience a hydrodynamic upwards force ($\mathbf{F}_{buoy}$ in equation 8.1b), added mass ("m'_i" in equation 9.2), damping ("b_i" in equation 6.10) and a hydrodynamic stiffness. The hydrodynamic stiffness does not vary with the position of the buoy. This means that the buoy has an endless hight above the water i.e. that stiffness is not lost at a certain point of submergence. These elements must be calculated.

7.4.1. Vertical force on a having buoy

$\mathbf{F}_{buoy}$ is the dynamic force in the vertical direction on the bottom of the buoy. This force can be calculated with the Froude-Krylov part of the Morison equation. The hydrostatic force is equal but in the opposite direction of the gravitation force and consequently cancels out. The dynamic part can be rewritten with the Bernoulli equation to equation 7.40 [6]. The potential based on Airy wave theory can be found in equation B.4 of Appendix B.1 is substituted to obtain the force.

$$\vec{F} = -\int_{(S)} p\vec{n} dS = \rho \int_{(S)} \dot{\Phi}\vec{n} dS \tag{7.40}$$

Because of the relative small buoy-diameter - wavelength proportion (i.e. hydrodynamic transparent structure) it is reasonable to assume that the pressure variation over the bottom surface of the buoy

will be limited. Therefore, the pressure will not be integrated over the whole surface. Alternatively, the pressure in the centre of the buoy will be calculated and multiplied with the area of the bottom surface of the buoy.

$$F_{buoy,i} = \rho\, \zeta_a g e^{kz} e^{-ikx} \frac{\pi D^2}{4} e^{i\omega t} \tag{7.41}$$

7.4.2. Added mass heaving buoy

The added mass is derived from Figure 7.2. The method is copied from [6, p.281]. α needs to be calculated, this result in a value for C_a which is it used to calculate the added mass (m_{c33} in the Figure 7.2 or m' in this report).

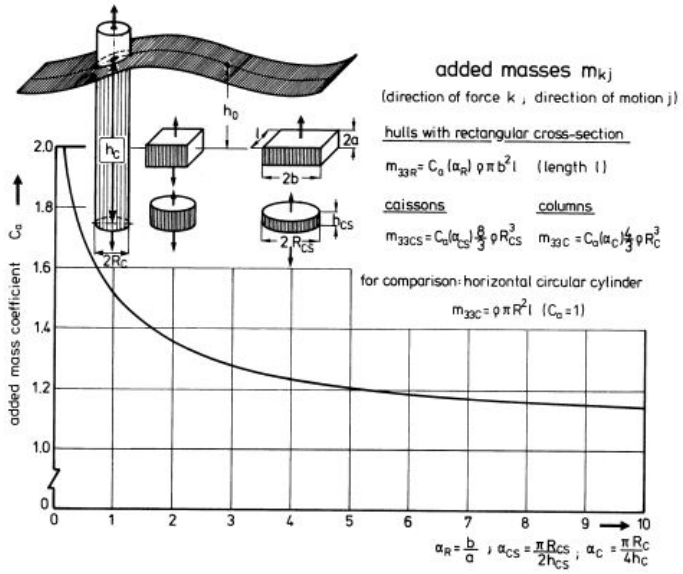

Figure 7.2: “Added masses of vertically oscillating components of offshore structures” [6]

$$\alpha = \frac{\pi}{4}\frac{R}{h} \tag{7.42a}$$

$$m' = C_a(\alpha)\frac{4}{3}\rho R^3 \tag{7.42b}$$

7.4.3. Damping of a heaving buoy

For the damping, there is no such straight forward method found in the literature. The damping could be calculated with for example potential theory. For this step of the design process, there is no need for high accuracy. Also, not all details are known for an accurate estimation of the damping. Higher accuracy will also mean longer calculation time.

Therefore an alternative way is chosen. The damping will be chosen as a percentage of the critical damping of the buoy. The ratio or percentage is called the damping ratio. The damping can in this way be varied for different buoy shapes or the construction above the water. Determining the percentage of the critical damping will be done by analysing tests. One test was executed for this thesis and one was obtained from an online lecture. The analysis and the specific tests can be found in Appendix B.2.

$$b_{cr} = 2\sqrt{km} = 2\sqrt{S\rho g \quad ST\rho} = 2\rho S\sqrt{gT} \tag{7.43}$$

The critical damping (c_{cr}) is depending on the hydrostatic stiffness, the mass and added mass. Because of the cylindrical shape of the buoy, this can be rewritten. Found from the experiments in Appendix B.2 it is shown that the damping is around 0.05% and 1% of the critical damping. For the model, 0.5% will be applied. The damping for the heaving buoy is relatively low it is most probably insignificant compared to the damping of the other component of the FPV structure. If it is shown later that the heave

damping of the buoys is significant the approach of critical damping should be reassessed.
The implementation in the code is as straight forward as the implementation of the masses and stiffness matrices of the buoy.
Now all hydrodynamic loads on the system elements are known; they can be implemented in the mechanical equations from chapter 6.

8

Substitution and solution of the differential equation

So far, the mechanical equations of the system and the hydrodynamic forces on the separate elements were determined. First, a differential equation for the mechanical system was obtained in chapter 6. Then, the hydrodynamic forces on randomly oriented cylinders in waves were examined, both for the forces perpendicular on the centre line in section 7.3 (with Morison for the beams) and the forces in line with the centre line in section 7.4 (with Froude-Krylov for the buoys). These two parts are now combined in chapter 8. Furthermore, a method to find the response, eigenmodes and eigenfrequencies is presented in section 8.2. Just like in chapter 6 this is executed for the four buoys system.
There are two options to describe the response of a system. A first option is a time-domain approach. Thus, the response will be simulated and represented over time. This option can incorporate nonlinear effects when present in the system. These calculations are complex and time-consuming calculations. The second option is a frequency domain analysis. Here the calculations (of the responses) are done over a varying harmonic frequency. The advantage of the frequency domain is that the calculations are time-efficient. But the downside is that it can only describe the behaviour of linear systems. Some nonlinear systems can be approximated by a linear system. This linearisations will decrease the accuracy of the result but will highly speed up the calculation and simulation process. In this thesis the differential equation obtained and all elements of the differential equation are linear. Parts that were initially nonlinear are linearised as calculation speed is preferred over accuracy. Therefore, the calculations will be executed in a frequency domain.
To obtain the desired responses for the analysis the following steps are undertaken. The substitution of the hydrodynamic loads in the differential equation is executed in section 8.1. The obtained differential equation is solved in section 8.2. Next some additional responses are derived based on the solution of the differential equation is section 8.3.

8.1. Substitution of hydrodynamic forces in differential equation

In section 6.3, the differential equation 6.10a was found. Equation 6.10a describes the response of the buoy elements of the structure in heave direction. The matrices $[\mathbf{M}]$, $[\mathbf{B}]$ and $[\mathbf{K}]$ contain the hydrodynamic mass, the hydrodynamic damping and the hydrodynamic stiffness of the buoys as indicated in equation 6.10 on page 53.

$$\mathbf{F} = [\mathbf{M}]\ddot{\boldsymbol{z}} + [\mathbf{B}]\dot{\boldsymbol{z}} + [\mathbf{K}]\boldsymbol{z} \tag{6.10a}$$

All hydrodynamic loads i.e. forces, damping, added masses on the beams are now within the force vector as shown in equation 8.1a. These hydrodynamic loads can now be substituted. To organise the substitution the force vector as presented in equation 6.10b on page 52 is subdivided as presented in 8.1a. The vector $\vec{1}_4$ indicates a vector of length 4 where every entry contains the value 1.

$$\mathbf{F} = \mathbf{F}_{buoy} + \left[[\mathbf{F}_M] + \frac{[\mathbf{T}_M]}{L}\right]\vec{1}_4 \tag{8.1a}$$

$$\mathbf{F}_{buoy} = \begin{bmatrix} F_1 \\ F_2 \\ F_3 \\ F_4 \end{bmatrix} \tag{8.1b}$$

$$[\mathbf{F}_M] = \begin{bmatrix} 0 & \frac{F_{12}}{2} & \frac{F_{13}}{2} & 0 \\ \frac{F_{12}}{2} & 0 & \frac{F_{23}}{2} & \frac{F_{24}}{2} \\ \frac{F_{13}}{2} & \frac{F_{23}}{2} & 0 & \frac{F_{34}}{2} \\ 0 & \frac{F_{24}}{2} & \frac{F_{34}}{2} & 0 \end{bmatrix} \tag{8.1c}$$

$$\frac{[\mathbf{T}_M]}{L} = \begin{bmatrix} 0 & \frac{T_{12}}{L} & \frac{T_{13}}{L} & 0 \\ -\frac{T_{12}}{L} & 0 & \frac{T_{23}}{L} & \frac{T_{24}}{L} \\ -\frac{T_{13}}{L} & -\frac{T_{23}}{L} & 0 & \frac{T_{34}}{L} \\ 0 & -\frac{T_{24}}{L} & -\frac{T_{34}}{L} & 0 \end{bmatrix} \tag{8.1d}$$

The inputs of vector $\mathbf{F}_{buoy}$ are obtained based on section 7.4. For the other matrices the conclusions on the Morison equation for a random oriented cylinder as discussed in section 7.3.1 and resulted in equation 7.15 and equation 7.16 should be substituted.

$$\vec{F}_M = \vec{F}_{FK,HM,\zeta} - \vec{F}_{HM,c} + \vec{F}_{VD,\zeta} - \vec{F}_{VD,c} \tag{7.15}$$

$$\vec{T}_M = \vec{T}_{FK,HM,\zeta} - \vec{T}_{HM,c} + \vec{F}_{VD,\zeta} - \vec{T}_{VD,c} \tag{7.16}$$

Equation 7.15 and equation 7.16 indicate a force in three directions. For the heave response only the force in heave direction on all elements and the moment in the local p-direction on the beams are needed. For simplicity the indexes z and p are not further written as this would lead to an overkill of indexes and therefore confusion. For the following instances only forces and moments in these directions are described.
The added mass and damping related terms are substituted (m'_{ij}-, b'_{ij}-, I'_{ij}-, B'_{ij} in equation 7.22, 7.25, 7.35 and 7.38) in equation 7.15 and equation 7.16. This results in equation 8.3 and equation 8.4. The index i and j indicate a buoy number on the end of a connecting beam.

$$F_{ij} = F_{FK,HM,\zeta,ij} - m'_{ij}\ddot{z}_{ij} + F_{VD,\zeta,ij} - b'_{ij}\dot{z}_{ij} \tag{8.3a}$$

$$F_{ij} = F_{FK,HM,\zeta,ij} - m'_{ij}\frac{1}{2}\left(\ddot{z}_i + \ddot{z}_j\right) + F_{VD,\zeta,ij} - b'_{ij}\frac{1}{2}\left(\dot{z}_i + \dot{z}_j\right) \tag{8.3b}$$

$$\frac{T_{ij}}{L} = \frac{T_{FK,HM,\zeta,ij}}{L} - I'_{ij}\ddot{\alpha}_{ij} + \frac{T_{VD,\zeta,ij}}{L} - B'_{ij}\dot{\alpha}_{ij} \tag{8.4a}$$

$$\frac{T_{ij}}{L} = \frac{T_{FK,HM,\zeta,ij}}{L} - I'_{ij}\frac{1}{L}\left(\ddot{z}_i - \ddot{z}_j\right) + \frac{T_{VD,\zeta,ij}}{L} - B'_{ij}\frac{1}{L}\left(\dot{z}_i - \dot{z}_j\right) \tag{8.4b}$$

Equation 8.3 and equation 8.4 describe the force and the moment on one beam elements and can be substituted in equation 8.1c and equation 8.1d. The added mass terms and the damping terms are dependent on the acceleration and the velocity of the neighbouring buoys as indicated in equation 6.9. These acceleration and velocity terms are replaced in one vector.

$$z_{ij} = \frac{z_i + z_j}{2} \tag{6.9a}$$

$$\alpha_{ij} = \frac{z_i - z_j}{L} \tag{6.9b}$$

It can be noticed that in equation 8.7a the division by the length is only valid when all lengths are equal. When this would not be the case, the division should be executed with a point wise division (⊘).

$$[\mathbf{F}_M]\,\vec{1}_4 = \left[\mathbf{F}_{FK,HM,\zeta}\right]\vec{1}_4 + \left[\mathbf{F}_{VD,\zeta}\right]\vec{1}_4 - [\mathbf{m}']\,\ddot{\boldsymbol{z}} - [\mathbf{b}']\,\dot{\boldsymbol{z}} \tag{8.6a}$$

$$\left[\mathbf{F}_{FK,HM,\zeta}\right]\vec{1}_4 = \frac{1}{2}\begin{bmatrix} 0 & F_{12,FK,HM,\zeta} & F_{13,FK,HM,\zeta} & 0 \\ F_{12,FK,HM,\zeta} & 0 & F_{23,FK,HM,\zeta} & F_{24,FK,HM,\zeta} \\ F_{13,FK,HM,\zeta} & F_{23,FK,HM,\zeta} & 0 & F_{34,FK,HM,\zeta} \\ 0 & F_{24,FK,HM,\zeta} & F_{34,FK,HM,\zeta} & 0 \end{bmatrix}\vec{1}_4 \tag{8.6b}$$

$$\left[\mathbf{F}_{VD,\zeta}\right]\vec{1}_4 = \frac{1}{2}\begin{bmatrix} 0 & F_{12,VD,\zeta} & F_{13,VD,\zeta} & 0 \\ F_{12,VD,\zeta} & 0 & F_{23,VD,\zeta} & F_{24,VD,\zeta} \\ F_{13,VD,\zeta} & F_{23,VD,\zeta} & 0 & F_{34,VD,\zeta} \\ 0 & F_{24,VD,\zeta} & F_{34,VD,\zeta} & 0 \end{bmatrix}\vec{1}_4 \tag{8.6c}$$

$$[\mathbf{m}'] = \frac{1}{4}\begin{bmatrix} m'_{12}+m'_{13} & m'_{12} & m'_{13} & 0 \\ m'_{12} & m'_{12}+m'_{23}+m'_{24} & m'_{23} & m'_{24} \\ m'_{13} & m'_{23} & m'_{13}+m'_{23}+m'_{34} & m'_{34} \\ 0 & m'_{24} & m'_{34} & m'_{24}+m'_{34} \end{bmatrix} \tag{8.6d}$$

$$[\mathbf{b}'] = \frac{1}{4}\begin{bmatrix} b'_{12}+b'_{13} & b'_{12} & b'_{13} & 0 \\ b'_{12} & b'_{12}+b'_{23}+b'_{24} & b'_{23} & b'_{24} \\ b'_{13} & b'_{23} & b'_{13}+b'_{23}+b'_{34} & b'_{34} \\ 0 & b'_{24} & b'_{34} & b'_{24}+b'_{34} \end{bmatrix} \tag{8.6e}$$

$$\frac{[\mathbf{T}_M]}{L}\vec{1}_4 = \frac{\left[\mathbf{T}_{FK,HM,\zeta}\right]}{L}\vec{1}_4 + \frac{\left[\mathbf{T}_{VD,\zeta}\right]}{L}\vec{1}_4 - \frac{[\mathbf{I}']}{L}\ddot{\boldsymbol{z}} - \frac{[\mathbf{B}']}{L}\dot{\boldsymbol{z}} \tag{8.7a}$$

$$\frac{\left[\mathbf{T}_{FK,HM,\zeta}\right]}{L}\vec{1}_4 = \frac{1}{L}\begin{bmatrix} 0 & T_{12,FK,HM,\zeta} & T_{13,FK,HM,\zeta} & 0 \\ T_{12,FK,HM,\zeta} & 0 & T_{23,FK,HM,\zeta} & T_{24,FK,HM,\zeta} \\ T_{13,FK,HM,\zeta} & T_{23,FK,HM,\zeta} & 0 & T_{34,FK,HM,\zeta} \\ 0 & T_{24,FK,HM,\zeta} & T_{34,FK,HM,\zeta} & 0 \end{bmatrix}\vec{1}_4 \tag{8.7b}$$

$$\frac{\left[\mathbf{T}_{VD,\zeta}\right]}{L}\vec{1}_4 = \frac{1}{L}\begin{bmatrix} 0 & T_{12,VD,\zeta} & T_{13,VD,\zeta} & 0 \\ T_{12,VD,\zeta} & 0 & T_{23,VD,\zeta} & T_{24,VD,\zeta} \\ T_{13,VD,\zeta} & T_{23,VD,\zeta} & 0 & T_{34,VD,\zeta} \\ 0 & T_{24,VD,\zeta} & T_{34,VD,\zeta} & 0 \end{bmatrix}\vec{1}_4 \tag{8.7c}$$

$$\frac{[\mathbf{I}']}{L} = \frac{1}{L^2}\begin{bmatrix} I'_{12}+I'_{13} & -I'_{12} & -I'_{13} & 0 \\ -I'_{12} & I'_{12}+I'_{23}+I'_{24} & -I'_{23} & -I'_{24} \\ -I'_{13} & -I'_{23} & I'_{13}+I'_{23}+I'_{34} & -I'_{34} \\ 0 & -I'_{24} & -I'_{34} & I'_{24}+I'_{34} \end{bmatrix} \tag{8.7d}$$

$$\frac{[\mathbf{B}']}{L} = \frac{1}{L^2}\begin{bmatrix} B'_{12}+B'_{13} & -B'_{12} & -B'_{13} & 0 \\ -B'_{12} & B'_{12}+B'_{23}+B'_{24} & -B'_{23} & -B'_{24} \\ -B'_{13} & -B'_{23} & B'_{13}+B'_{23}+B'_{34} & -B'_{34} \\ 0 & -B'_{24} & -B'_{34} & B'_{24}+B'_{34} \end{bmatrix} \tag{8.7e}$$

Substituting equation 8.6a and equation 8.7a in equation 6.10a and replacing all acceleration, velocity and position dependent terms on the right side of the equation and keeping all motion independent terms on the left side of the equation, results in equation 8.8.

$$\mathbf{F}_{buoy} + \left(\left[\mathbf{F}_{FK,HM,\zeta}\right] + \left[\mathbf{F}_{VD,\zeta}\right] + \frac{\left[\mathbf{T}_{FK,HM,\zeta}\right]}{L} + \frac{\left[\mathbf{T}_{VD,\zeta}\right]}{L}\right)\vec{1}_4 = \left([\mathbf{M}] + [\mathbf{m}'] + \frac{[\mathbf{I}']}{L}\right)\ddot{\boldsymbol{z}} + \left([\mathbf{B}] + [\mathbf{b}'] + \frac{[\mathbf{B}']}{L}\right)\dot{\boldsymbol{z}} + [\mathbf{K}]\boldsymbol{z} \tag{8.8}$$

Equation 8.8 is a fully defined differential equation that describes the heave motion of the beam and buoy structure. It should be pointed out that the differential equation is fully linear as indicated in the introduction of this chapter. The heave motion of the construction is described by the motion of the buoys. The number of buoys determines the number of degrees of freedom of the system.

8.2. Solving differential equation

The two main results from the differential equation that are desired in this thesis are the frequency response and the eigenfrequencies of the system, as these describe the most critical response. These can be found by solving the differential equation. First, the solution method for the eigenmodes and eigenfrequencies will be explained, then the method for obtaining the frequency response is discussed. The eigenfrequencies and eigenmodes can be calculated by rewriting the differential equation as an eigenvalue problem. The damping and excitation force are excluded when solving the eigenvalue problem as seen in equation 8.9. An eigenvalue problem is obtained by substituting equation 8.10 resulting in equation 8.11b. In equation 8.10 the system response is indicated with A. Equation 8.11b can be solved with $\omega^2 = \lambda$. Where the eigenvalues are obtained, the square of the eigenfrequencies and the eigenvectors represent the corresponding eigenmodes.

$$\left([\mathbf{M}] + [\mathbf{m}'] + \frac{[\mathbf{I}']}{L}\right)\ddot{\boldsymbol{z}} + [\mathbf{K}]\boldsymbol{z} = 0 \tag{8.9}$$

$$z = Ze^{i\omega t} \tag{8.10}$$

$$[\mathbf{K}]\mathbf{Z} - \omega^2\left([\mathbf{M}] + [\mathbf{m}'] + \frac{[\mathbf{I}']}{L}\right)\mathbf{Z} = 0 \tag{8.11a}$$

$$\left[\left([\mathbf{M}] + [\mathbf{m}'] + \frac{[\mathbf{I}']}{L}\right)^{-1}[\mathbf{K}] - \omega^2[\mathbf{I_n}]\right]\mathbf{Z} = 0 \tag{8.11b}$$

Furthermore, the frequency response, indicated by A, should be obtained. To obtain the frequency response the following steps can be taken. First the previously used equation 8.10 will be substitute in equation 6.10 this results in equation 8.13. This can now be solved as shown in equation 8.14.

$$\mathbf{F} = [\mathbf{M}]\ddot{\boldsymbol{z}} + [\mathbf{B}]\dot{\boldsymbol{z}} + [\mathbf{K}]\boldsymbol{z} \tag{8.12}$$

$$\mathbf{F} = -\omega^2[\mathbf{M}]\mathbf{Z} + i\omega[\mathbf{B}]\mathbf{Z} + [\mathbf{K}]\mathbf{Z} \tag{8.13}$$

$$\mathbf{Z} = \mathbf{F} \cdot \left[-\omega^2[\mathbf{M}] + i\omega[\mathbf{B}] + [\mathbf{K}]\right]^{-1} \tag{8.14}$$

The response for every buoy can be obtained for varying values of ω. Since the differential equation is fully linear, a fixed wave amplitude is used to obtain the $\mathbf{F}$ vector. These solution methods for the eigenfrequencies, eigenmodes and frequency response result in the following results for the 4 buoy system as shown in Figure 8.1.

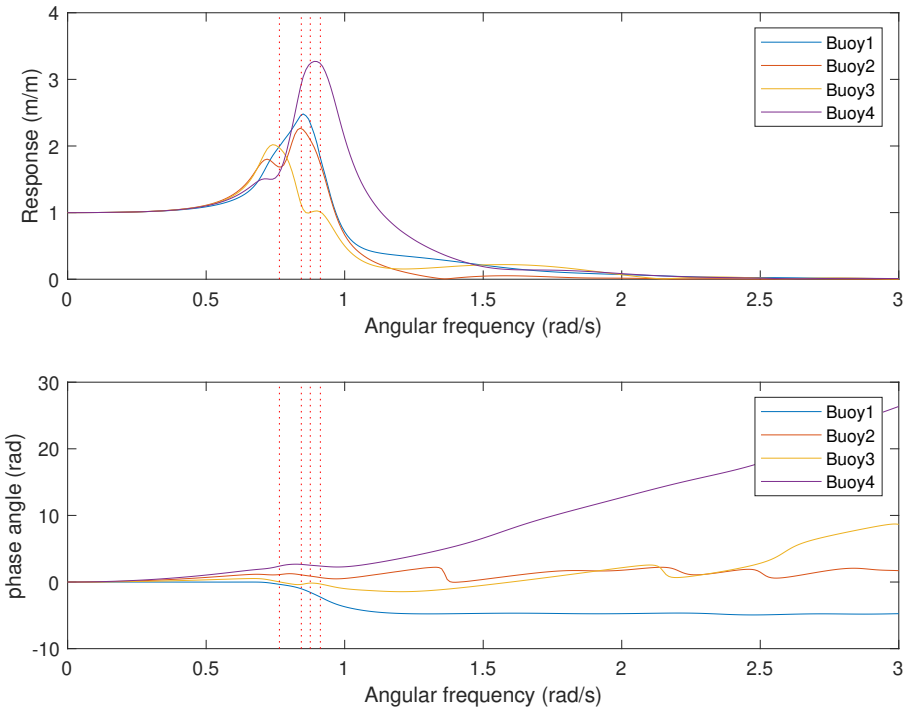

Figure 8.1: Example of a response of a four buoy system (a more in depth analysis will follow in chapter 10 and chapter 11, then items such as dimensions and orientation will be discussed.)

8.3. Theoretical derivations for the analysis

To analyse the structure and the most critical response of the structure, some small steps are still necessary. The most critical response of the system was indicated to be the heave motion. This heave motion determines the relative wave height of the structure. The relative wave height gives an indication on the needed distance between the still water surface and the bottom of the triangle PV-panel platforms considering regular waves and a linear system. Another interesting parameter is the dissipated damping energy per element over one period of the system.

8.3.1. Relative wave height

The relative wave height at the buoys can be calculated by subtracting the wave height from the response of the structure as indicated in equation 8.15. The relative wave height does not take into account the free board of the construction nor the air gap between the still water surface and the triangle platforms of the buoy and beam structure. The magnitude of the complex vector indicates the minimally needed air gap considering a linear system and regular waves.

$$\left|z_i - \zeta e^{-ix_i k}\right| \tag{8.15}$$

The relative wave height will differ over the triangle platform. So far only regular waves are considered and the platform is considered to be fully flat and rigid. Therefore, the maximum relative wave height will appear at the sides of the triangle platforms. Consequently only the sides of the platform needs to be studied. The response of the sides of the platform are a linear combination of the response of the two related buoys. The maximum relative wave height over the length can be calculated as indicated in equation 8.16. s expresses the length and is varied from zero to one in hundred equal steps.

$$Max_{\mathrm{s}}\left(\left|z_i(1-s) + z_j s - \zeta e^{-i\left(x_i(1-s)+x_j s\right)k}\right|\right) \text{ with s:}[0-1] \tag{8.16}$$

By taking the maximum values of the magnitude over the wave length, the most extreme situation is considered and indicates the needed airgap.

8.3.2. Energy dissipation by damping

In the system damping is caused by translation of the buoys and the beams and by the rotation of the beams. For both the dissipating damping energy is calculated by integrating the power over one period. The power is calculated by multiplying the force times the velocity. The force is determined by multiplying the damping coefficient by velocity. The velocity is calculated by the derivation of the response over the time. In case of damping caused by a rotation, the damping moment is used.

$$\Delta W_{buoy} = \int_{\phi_i}^{\phi_i+T} F\Re(\dot{z}_i)dt = \int_{\phi_i}^{\phi_i+T} b\left(\Re(\dot{z}_i)\right)^2 dt = \int_{\phi_i}^{\phi_i+T} b\left(\Re(i\omega Z_i)\right)^2 dt \tag{8.17}$$

In this section, the damping energy caused by the buoy is calculated. Then damping caused by the translating movement of the beam and lastly the damping caused by the rotational movement caused by the beam is calculated.
When calculating the damping, only the real part of the response over the time is taken into account. The real part of the velocity of the buoy with respect to time is expressed in equation 8.18.

$$\Re(i\omega Z_i e^{i\omega t}) = \Re(i\omega|Z_i|e^{i\omega t}e^{i\phi_i}) = \Re\left(|Z_i|i\omega\left[\cos(\omega t+\phi_i)+i\sin(\omega t+\phi_i)\right]\right) = -\omega|Z_i|\sin(\omega t+\phi_i) \tag{8.18}$$

In equation 8.19 the real part of the velocity is substituted in equation 8.17. Due to the linearity, the starting point of the integration does not matter as long as a full period is taken into account. Therefore, the phase angle is disregarded. The integral of a $\sin^2(t)$ over one period equals that period divided by two times the amplitude. $T = \frac{2\pi}{\omega}$ obtains the dissipated damping energy.

$$\Delta W_{buoy} = \int_{\phi_i}^{\phi_i+T} b_i\left(-\omega|Z_i|\sin(\omega t+\phi_i)\right)^2 dt = \int_0^T b_i\omega^2|Z_i|^2\sin^2(\omega t)dt = b_i\omega^2|Z_i|^2\frac{T}{2} = b_i\pi\omega|Z_i|^2 \tag{8.19}$$

The damping, as result of the beams' translating movement, can be calculated with the response of the two outer buoys. As defined before (equation 6.9b), the response is the average of the response of the two outer buoys. This average again has a magnitude and a phase angle. The real part is used to calculate the dampings energy.

$$\begin{aligned}\Re(i\omega Z_{ij}e^{i\omega t}) &= \Re\left(i\omega\frac{Z_i+Z_j}{2}e^{i\omega t}\right)\\ &= \Re\left(|Z_{ij}|i\omega\left[\cos(\omega t+\phi_{ij})+i\sin(\omega t+\phi_{ij})\right]\right) = -\omega|Z_{ij}|\sin(\omega t+\phi_{ij})\end{aligned} \tag{8.20}$$

Now the damping can be calculated similar to equation 8.19 resulting in equation 8.21.

$$\Delta W_{beam} = b_{ij}\pi\omega\left|\frac{Z_i+Z_j}{2}\right|^2 \tag{8.21}$$

Computing the damping as result of a rotational movement is slightly different as the moment times the angular velocity is integrated over one period. Therefor, the angular velocity needs to be determined. This is again based on the constraints that were set in equation 6.9a.

$$\begin{aligned}\Re(\dot{\alpha_{ij}}) = \Re(i\omega\alpha_{ij}e^{i\omega t}) &= \Re\left(i\omega\frac{Z_i-Z_j}{L}e^{i\omega t}\right)\\ &= \Re\left(|\alpha_{ij}|i\omega\left[\cos(\omega t+\phi_{ij})+i\sin(\omega t+\phi_{ij})\right]\right) = -\omega|\alpha_{ij}|\sin(\omega t+\phi_{ij})\end{aligned} \tag{8.22}$$

Based on the previously used methodology, the dissipated damping energy for the rotation of the beam can be calculated.

$$\Delta W = \int_{\phi_i}^{\phi_i+T} M_{ij}\left(\Re(\dot{\alpha_{ij}})\right)dt = \int_{\phi_i}^{\phi_i+T} B_{ij}\left(\Re(\dot{\alpha_{ij}})\right)^2 dt = B_{ij}\pi\omega\left|\frac{Z_i-Z_j}{L}\right|^2 \tag{8.23}$$

This results in three equations to compute the dissipated damping energy for the buoy and beam structure's elements.

9

Implementation

Chapter 6 and chapter 7 explained the theory to obtain the frequency response of a four buoy system. In chapter 8 a fully linear differential equation was obtained for a four buoy system. As result of the linearity, the frequency response can be obtained in a frequency domain. Therefore, the frequency dependent parts of the differential equation will be obtained for the desired frequencies.
In chapter 4, it was argued that other topologies and variations must be assessed. The desired input and output variables in section 5.4.1 further defined the aims of the calculation tool that is developed. In this chapter, the method to derive the differential equations of the four buoy structure is extrapolated to assess variations of the layout (section 9.1). Additionally, the implementation and coding of the hydrodynamic loads on the individual elements is discussed in section 9.2. The basic code can be found in Appendix D so results can be reproduced for engineering or educational purposes. Therefore, the theory explained in chapter 6, chapter 7 and chapter 8 will be used. This is all combined in a calculation tool or program written in MATLAB. The general composition and additional functions in the MATLAB code are explained in section 9.3.
Figure 9.1 indicates the program layout. It reads from top to bottom. The inputs are defined at the top. Based on these inputs, one vector and three matrices of the differential equation, i.e. equation of motion, are composed. The individual matrix entries are calculated by functions that include the hydrodynamic calculation. These functions are the red, purple, green and black boxes. The matrices are then substituted in the equation of motion, and the differential equation is solved to obtain the frequency response, eigenmodes and eigenfrequencies. The right side of the figure indicates the iterative process with a dotted line. This calculates all components that are indicated with an asterisk (*). This loop is executed until the calculation tool obtains a certain accuracy.

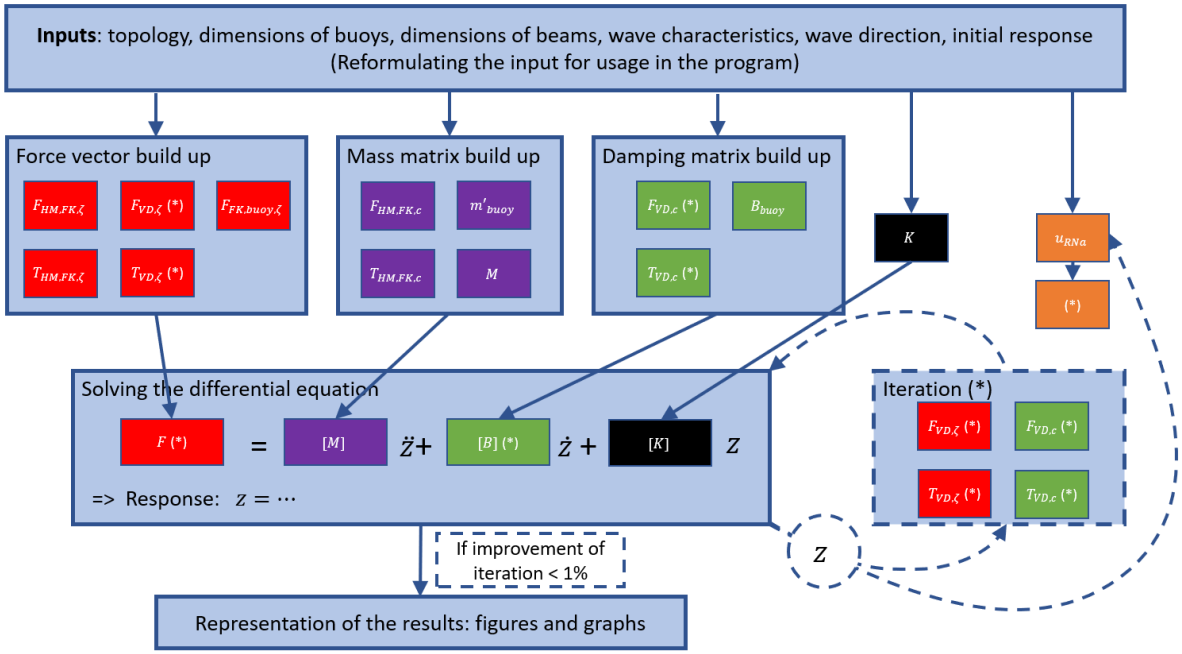

Figure 9.1: Program layout
Red: force contributions, Purple: mass contributions, Green: damping contributions, Black: stiffness contributions. (*) indicate an iterative process dependent on u_{RNa}

Additionally to the inputs indicated in Figure 9.1, a wave amplitude of 1 meter, frequency range, added mass and damping coefficients, the gravitational acceleration and the density of seawater are used throughout the program.

9.1. Matrix build-up for an arbitrary topology

A full differential equation for a four buoy structure was obtained and shown in equation 8.8 on page 69. The matrices in this differential equation are shown in equation 6.10 on page 53 and in equation 8.6a and 8.7a on page 68. When analysing the obtained matrices, a logic and a system are found in relation to the topology matrix as shown in equation 9.1. The goal is to generalise the used method so that the differential equation of a structure can be obtained based on the topology matrix. The topology matrix describes which buoys are connected by a beam.

$$\begin{array}{c} \\ 1 \\ 2 \\ 3 \\ 4 \end{array} \begin{array}{c} \begin{array}{cccc} 1 & 2 & 3 & 4 \end{array} \\ \begin{pmatrix} . & \mathbf{1} & 1 & \mathbf{0} \\ \mathbf{-1} & . & 1 & 1 \\ -1 & -1 & . & 1 \\ \mathbf{0} & -1 & -1 & . \end{pmatrix} \end{array} \tag{9.1}$$

The topology matrix in equation 9.1 can be interpreted as follows. All buoys are numbered as indicated above and on the left side of the matrix in equation 9.1. The bold written "**1**" in equation 9.1 indicates that buoy 1 and buoy 2 are connected. On the other hand, the bolt "**0**" indicates that buoy 1 and 4 are not connected. No entries have been indicated on the diagonal of the matrix. In the program, the diagonal terms are all 1, these are replaced by zero's when needed for the build of the matrices. The lower triangle of the connections is decided to have negative numbers. The negative numbers will turn out useful when composing the matrices that contain terms coming from bending moments on the beams.
Based on this topology matrix, an interconnections matrix and corresponding matrices with the positions and responses can be generated. This only rearranges the predefined information that was stated at the program input. This is necessary for the creation of the matrix. The exact working principle of this rearrangement will be presented later.

9.1.1. Matrix generation

The matrix build-up will be explained based on the part of the mass matrix. To find a methodology, the mass matrix [$\mathbf{M}$], found in equation 9.2, will be analysed (recalled from equation 6.10c). Parts of the methods used to build up the mass matrix will be used to build up the other matrices. Based on this found logic, a methodology explained in different steps and a block diagram is build up. This is then reformulated in a code. Lastly, the similarities with other matrices are presented.
The matrix is first reformulated in a summation of different matrices in equation 9.2.

$$[\mathbf{M}] = \underbrace{\begin{bmatrix} m_1+m_1' & 0 & 0 & 0 \\ 0 & m_2+m_2' & 0 & 0 \\ 0 & 0 & m_3+m_3' & 0 \\ 0 & 0 & 0 & m_4+m_4' \end{bmatrix}}_{\text{Part A}} + \underbrace{\begin{bmatrix} 0 & \frac{m_{12}}{4} & \frac{m_{13}}{4} & 0 \\ \frac{m_{12}}{4} & 0 & \frac{m_{23}}{4} & \frac{m_{24}}{4} \\ \frac{m_{13}}{4} & \frac{m_{23}}{4} & 0 & \frac{m_{34}}{4} \\ 0 & \frac{m_{24}}{4} & \frac{m_{34}}{4} & 0 \end{bmatrix}}_{\text{Part B:}}$$

$$+ \underbrace{\begin{bmatrix} 0 & -\frac{I_{12}}{L^2} & -\frac{I_{13}}{L^2} & 0 \\ -\frac{I_{12}}{L^2} & 0 & -\frac{I_{23}}{L^2} & -\frac{I_{24}}{L^2} \\ -\frac{I_{13}}{L^2} & -\frac{I_{23}}{L^2} & 0 & -\frac{I_{34}}{L^2} \\ 0 & -\frac{I_{24}}{L^2} & -\frac{I_{34}}{L^2} & 0 \end{bmatrix}}_{\text{Part C}} + \text{Diag}\left(\underbrace{\begin{bmatrix} \frac{m_{12}}{4}+\frac{I_{12}}{L^2}+\frac{m_{13}}{4}+\frac{I_{13}}{L^2} & & & \\ & \frac{m_{12}}{4}+\frac{I_{12}}{L^2}+\frac{m_{23}}{4}+\frac{I_{23}}{L^2}+\frac{m_{24}}{4}+\frac{I_{24}}{L^2} & & \\ & & \frac{m_{13}}{4}+\frac{I_{13}}{L^2}+\frac{m_{23}}{4}+\frac{I_{23}}{L^2}+\frac{m_{34}}{4}+\frac{I_{34}}{L^2} & \\ & & & \frac{m_{24}}{4}+\frac{I_{24}}{L^2}+\frac{m_{34}}{4}+\frac{I_{34}}{L^2} \end{bmatrix}}_{\text{Part D}} \right) \quad (9.2)$$

In equation 9.2 four different parts are identified. The following logic can be recognised.

- Part A is a diagonal matrix that contains the masses of the buoys and the added masses of the coresponding buoys.
- Part B is a matrix that contains all the masses of the beams divided by 4. It is directly related to the interconnecting beams, and therefore it has entries on the same position as the topology matrix.
- Part C is a matrix containing all moments of inertia of the connecting beams divided by the square of the lengths of these beams. This has entries on the same position as the topology matrix. In this case, all entries are negative.
- Part D is a diagonal matrix. Every element on the diagonal is the summation or subtraction of row elements that are obtained from the matrices in part C and part B. When the matrix that will be summed over a row that contains elements related to a rotation (I, T or B') these it should multiplied with -1 so the minus disappears.

This knowledge can now be used to build the mass matrix for other topologies. The matrix is an (n x n) matrix where n equals the number of buoys and consequently the degrees of freedom. In the code (Listing 9.1) the following steps are undertaken. These steps are also visualised in Figure 9.2.

- Part A: A diagonal matrix is build up. For every diagonal element, the mass of the buoy is calculated based on the water displacement. The function AddemassFK.m calculates the added mass per buoy.
- Part B (**): The dimensions of the beam elements and topology matrix are used to calculate the different entries of the matrix. These are divided by four. All entries are positive.
- Part C (**): The same method is used, but now the moment of inertia is calculated. This is divided by the length of the beam squared. All entries are negative. The matrix elements are negative when it is related to a rotation: I, B' or T and are positive when they contain elements related to translation: F, m'_{ij} or b'_{ij}.
- Part D: This part is simply derived from part B and C as indicated before. The summation of the rows of part C is subtracted from the summation of the rows of part B. In case of terms that are related to translation (m'_{ij} or b'_{ij}), these two parts are added up. This results in all positive terms. The obtained terms are placed on the diagonal of the matrix.

- (**): When building up matrices with the Morison terms an additional sequence is executed indicated with (**). In the complete mass matrix, the parts $[\mathbf{m}']$ and $\frac{[\mathbf{I}']}{L}$ are determined with the use of Morison. The sequence to build up these matrices is explained in Figure 9.3. In Listing 9.2 the exact implementation in the code for such a sequence can be found.

  – The entries of the upper triangle are calculated in a for loop over the different connecting beam. This is done making use of the rearranged inputs per connecting beam. This rearrangement is explained later in section 9.3.1.

  – The upper triangle is transpose and then added to the matrix resulting in the full matrix.

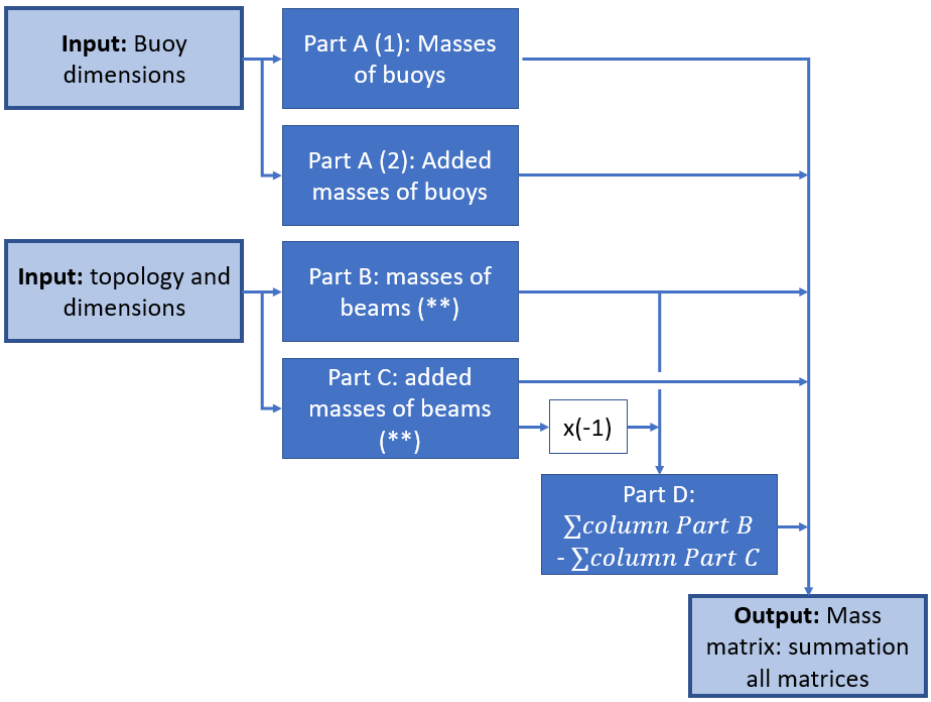

Figure 9.2: Block diagram on the build-up of the mass matrix

Listing 9.1: First part of BuildupMassMatrix.m code which builds up the mass matrix of the system

```
%% Masses and added masses from buoys (Part A)
Mbuoy=rho*pi*(DiameterBuoy.^2)/4.*abs(Z);                    %Vector of masses of the buoys
Mbuoyadded=AddedmassFK(abs(Z),DiameterBuoy);                 %Vector of added masses of the buoys
M1a_buoy=diag(Mbuoy+Mbuoyadded);                             %Summation and make diagonal matrix

%% Masses and moment of inertia's from beams (Part B and part C)
M1b_beam_dv4=pi*rho.*(DiameterBeam.^2/4).*LengthBeam/4;      %Mass matrix of beams

M1c=-1/12.*pi*rho.*(DiameterBeam.^2/4).*LengthBeam;          %Moment of inertia
%% Diagonal entries (Part D)
M1d=diag(sum(M1b_beam_dv4));                                 %Summation of rows mass matrix

M1e=diag(sum(-M1c));                                         %Summation of rows inertia matrix times -1

M1=M1a_buoy+M1b_beam_dv4+M1c+M1d+M1e;                        %Total mass matrix excluding Morison
    contribution
```

Input	Connecting buoy		Pos 1			Pos 2			(Resp 1)	(Resp 2)	Diameter
Beam 1	Buoy 1	Buoy 2	x_1	y_1	z_1	x_2	y_2	z_2	R_1	R_2	D_{12}
Beam 2	Buoy 1	Buoy 3	x_1	y_1	z_1	x_3	y_3	z_3	R_1	R_3	D_{13}
Beam n	.	.	.	.	.	.	.	.	.	.	.

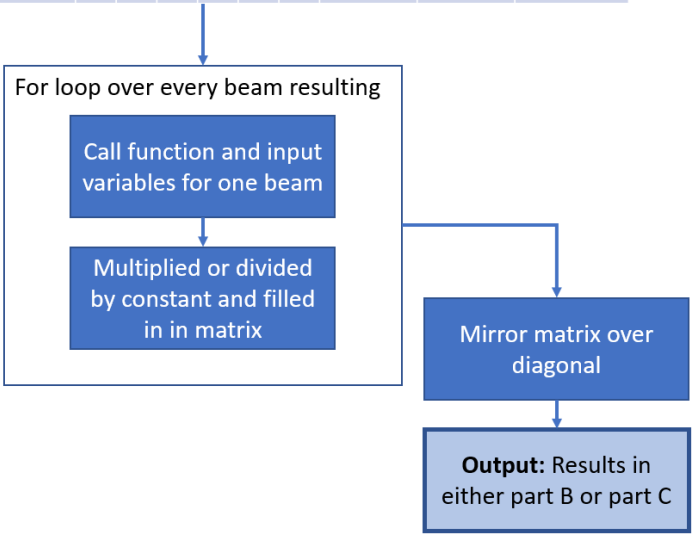

Figure 9.3: (**) Block diagram on the build-up of a matrix with Morison

Listing 9.2: (**) Second part of BuildupMassMatrix.m code which is applied to the Morison contributions to the mass matrix

```
%% Build up of added mass from Morison
M2=zeros(DimSystem,DimSystem);                          %initialising a zero matrix for the added masses
M3=zeros(DimSystem,DimSystem);

for n=1:size(BuoyCon,1)
    % the for loop calculates the values per connecting beam.
    M2a=MorisonAddedHM(Pos1(n,:),Pos2(n,:),DiameterBeam(BuoyCon(n,1),BuoyCon(n,2)));
    M2(BuoyCon(n,1),BuoyCon(n,2),:)=1/4*M2a;            %first the added mass is calculated for one connecting beam,
    % then they are divided by four and placed on the right position based
    % on the connecting buoys (making use of the connection matrix that is
    % based on the topology matrix.

    M3a=MorisonAddedHMTorque(Pos1(n,:),Pos2(n,:),DiameterBeam(BuoyCon(n,1),BuoyCon(n,2)));
    M3(BuoyCon(n,1),BuoyCon(n,2),:)=M3a/LengthBeam(BuoyCon(n,1),BuoyCon(n,2))^2;
    % the same sequence is not executed for the moment of inertia due to
    % added mass.
end
    % the four loop only results in a matrix with the top triangle filled
M2=M2+permute(M2,[2 1 3]);                              % the matrix is mirrored over its diagonal
M2_sum=sum(M2,2);                                       % the rows are summed
M2_diag=diag(M2_sum);
M2_tot=M2+M2_diag;                                      % and are added to the matrix

M3=M3+permute(M3,[2 1 3]);                              % the same is done for the moment inertia part of the mass matrix
M3_sum=-sum(M3,2);
M3_diag=diag(M3_sum);
M3_tot=M3+M3_diag;
```

This method results in the full mass matrix, as indicated in equation 6.10a. Similar methods are used for the other matrices indicated in equation 8.8. The main difference is that the calculation of the individual terms indicated with (**) in Figure 9.2 is sometimes calculated as indicated in Figure 9.3 and Listing 9.2. The implementation of this sequence for $[\mathbf{m}']$ and $\frac{[\mathbf{I}']}{L}$ is shown.

In Table 9.1, an overview of the implementation method of the different matrices is given. It shows with which method the matrix is build-up. Additionally, a reference to Appendix D indicates where the corresponding code can be found. All terms marked with (**) make use of the sequence stated in 9.3. In the second row, the build-up of the mass matrix is included. Based on the build-up of the mass

matrix, the method of the other matrices can be determined. For example, the added mass matrix $[m']$ is build up by utilising the topology matrix and the function that calculates the added mass. Then a summation of all elements in the individual rows is executed. The result is substituted on the diagonal. "-X$^{(1)}$" indicates that the dedicated part of the matrix needs to be multiplied with minus one.

Table 9.1: Overview of the different methods to build up the matrix and vector. The columns show which particular method is used by referring back to the explanation of the mass matrix build up. $^{(1)}$ indicates that the obtained diagonal matrix needs to be multiplied with -1.

	Script name in Appendix D	Diagonal elements related to buoys	Topology matrix related to beams	Sum of rows of toplogy matrix
$[\mathbf{M}]$	BuildupMassMatrix.m	Part A: $[m_i + m_i']$	Part B & D: $\frac{[m_{ij}]}{4}, -\frac{[I_{ij}]}{L^2}$	Part C: $\frac{[m_{ij}]}{4}, \frac{[I_{ij}]}{L^2}$ $^{(1)}$
$[\mathbf{F}_{buoy}]$	BuildupForceVector.m	X		
$[\mathbf{F}_{FK,HM,\zeta}]$	BuildupForceVector.m		X (*)	
$[\mathbf{F}_{VD,\zeta}]$	BuildupForceVector.m		X (*)	
$\frac{[\mathbf{T}_{FK,HM,\zeta}]}{L}$	BuildupForceVector.m		X (*)	
$\frac{[\mathbf{T}_{VD,\zeta}]}{L}$	BuildupForceVector.m		X (*)	
$[\mathbf{m}']$	BuildupMassMatrix.m		X (*)	X
$\frac{[\mathbf{I}']}{L}$	BuildupMassMatrix.m		-X$^{(1)}$ (*)	-X$^{(1)}$
$[\mathbf{B}]$	BuildupDampingsMatrix.m	X		
$[\mathbf{b}']$	BuildupDampingsMatrix.m		X (*)	X
$\frac{[\mathbf{B}']}{L}$	BuildupDampingsMatrix.m		-X$^{(1)}$ (*)	-X$^{(1)}$
$[\mathbf{K}]$	BuildupStiffnessMatrix.m	X		

With this method, all matrices needed for the differential equation can be build-up for any arbitrary triangle buoy and beam structure.

9.2. Implementation of the hydrodynamic loads

The obtained formulas in chapter 7 are now implemented in the code. As indicated in Figure 9.1, the calculation of some entries of the matrix are done in isolated functions. The code that builds up the matrices calls the function based on the needed variables as was indicated in Figure 9.3. Then the dedicated function calculates the entries.
The implementation of these separate parts will be presented in this section. First, the implementation of the force contribution resulting from the wave will be presented in section 9.2.1. Then the added mass and damping functions will be shown 9.2.2. For these parts, the amplitude of the relative velocity over the beam is used. The implementation the amplitude of the relative velocity is presented in 9.2.3. Lastly, the calculation of the heave force, the added mass and the damping related to the buoy will be presented. For all cases, repetition in the explanation is avoided. One example will be presented, and the similarities and differences with the other cases will be explained.

9.2.1. Implementation of the wave dependent terms

The $\vec{F}_{FK,HM,\zeta}$ term will be presented in detail then the similarities and differences with $\vec{F}_{VD,\zeta}$, $\vec{T}_{FK,HM,\zeta}$ and $\vec{F}_{VD,\zeta}$ will be presented.
In section 7.3.6 equation 7.17 is derived and recalled. The implementation is done making use of the symbolic toolbox for the integration over the length of the beam. The code is found in Listing 9.3 and is schematised in Figure 9.4. First, the accelerations, as defined in the Airy wave theory, are defined in the code. This can be seen in Figure 9.4. Then the projection on a plane perpendicular to the centre

line is executed making use of the tangent unit vector $\vec{e_t}$.

$$\vec{F}_{FKHM,\zeta} = \int_0^L (1 + C_a)\rho \frac{\pi D^2}{4} \left[\vec{e}_t \times \left(\vec{v} \times \vec{e}_t\right)\right] ds \tag{7.17}$$

The tangent unit vector can be calculated base on the positions of these outer points (A & B) as shown in equation 9.3. These are the positions of the buoys at both ends of the beam.

$$\vec{e_t} = \begin{bmatrix} e_{tx} \\ e_{ty} \\ e_{tz} \end{bmatrix} = \frac{1}{L} \begin{bmatrix} x_B - x_A \\ y_B - y_A \\ z_B - z_A \end{bmatrix} \tag{9.3}$$

When substituting equation 9.4, the force in the z-direction can be obtained by integration over s. s is a coordinate over the beam length and is indicated in Figure 6.1.

$$\begin{aligned} x &= x_A + s \cdot e_{tx} \\ y &= y_A + s \cdot e_{ty} \\ z &= z_A + s \cdot e_{tz} \end{aligned} \tag{9.4}$$

The obtained formula is integrated over the length of the beam from 0 to L. This result is multiplied with the constants indicated in equation 7.17 ($f(C_a, \pi, D, \rho)$). For every desired frequency, the frequency and the wavenumber are substituted in the z-component of the force. The result in one vector, containing all z-components for the desired frequencies. This is then outputted to the matrix build-up script.

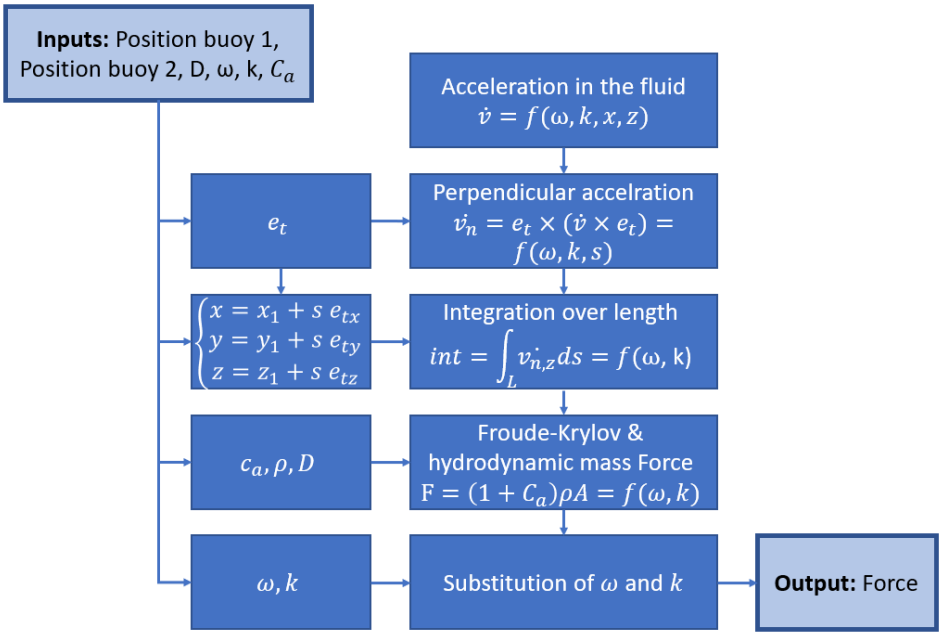

Figure 9.4: Block diagram on the implementation of the Froude-Krylov and hydrodynamic mass force

Listing 9.3: MorisonFKHM function which calculates the Froude-Krylov and Hydrodynamic mass force.

```
1  function [Force] = MorisonFKHM(Pos1,Pos2,D)
2  % Written by Andreas Feys for graduation process
3  % Summary of this function
4  %   Inported globals:  rho, k, ampletude, omega and c_a
5  %   Pos1: position of one end of on end of the cylinder (x, y, z)'
6  %   Pos2 position other end of cylinder,
7  %   D; diameter of cylinder,
8  %   Force: output the force vector in vertical direction per given omega
9  % All units are in meter, newton, rad/s
10 % The time varying part (exp(i*omega*t)) is not included
11
12 global rho k Ampletude omega c_a
13
```

```
syms s x y z a a_n t Omega K
% s, coordinate along cylinder axis
% x y z global coordinate system
% e_t unit vector along cylinder axis with coordinates ex ey ez in global
% system
% a particle acceleration in fluid
% t time
% Omega, angular frequegncy
% K wavenumber

a = [1j*Ampletude .* Omega^2 .* exp(K .* z) .* exp(-1j .* K .* x);...   %definition of acceleration in
     fluid by Airy wave theory without time varying part
     0;...
    - Ampletude .* Omega^2 .* exp(K .* z) .* exp(-1j .* K .* x)];

L=norm(Pos2-Pos1);       %calculation of beam length
e_t=(Pos2-Pos1)/L;       %calculation of tanguent unit vector

a_n=cross(e_t,cross(a,e_t));    %perpendicular acceleration

a_n=subs(a_n, [x, y, z], [Pos1(1)+s.*e_t(1), Pos1(2)+s.*e_t(2), Pos1(3)+s.*e_t(3)]);    %substitution
     before acceleration

a_n_int=int(a_n,s,0,L);    %integration of equiation

F_n_FK=(1+c_a)*rho*pi*D^2/4*a_n_int;    %calculation of total force

Force=zeros(1,length(omega));
for v = 1:length(omega)
    Force(v)=eval(subs(F_n_FK(3),[Omega, K],[omega(v), k(v)]));      % substitution of omega and k of
         symbolic toolbox for all desired omega's
end

end
```

A similar process is executed for $\vec{F}_{VD,\zeta}$, $\vec{T}_{FK,HM,\zeta}$ and $\vec{T}_{VD,\zeta}$. For the viscous damping force and moment, the velocity as defined by the Airy wave theory is used in stead of the acceleration. As result of the linearisation in these terms another script that calculates u_{RNa} is used. The implementation for the calculation of the u_{RNa} will be explained later in section 9.2.3.
The moment is calculated by multiplying the z-component of the perpendicular acceleration with the arm in local o-direction. This is a simplification that results from the assumption that the beams will only experience small angles. For the other terms, the same procedure is used.
Table 9.2 indicates which function calculates which part of the force.

Table 9.2: Reference to Appendix D where the code for the specific Morison contributions are indicated.

$\vec{F}_{FK,HM,\zeta}$	MorisonFKHM.m
$\vec{F}_{VD,\zeta}$	MorisonFKRMTorque.m
$\vec{T}_{FK,HM,\zeta}$	MorisonVD.m
$\vec{F}_{VD,\zeta}$	MorisonVDTorque.m

9.2.2. Implementation of the added mass and damping terms

The difference with the previous explained function is that the outcome of the integration is implemented directly. Therefore, the function only fills in the input values in a fixed and predefined formula, so no integration is executed. This is indicated in Figure 9.5 and Listing 9.4. The added mass and damping terms that need to be calculated coming from equation 8.8 are: m', I', b' and B'. The system will be explained based on the added mass term m'. The similarities and differences with the other parts will be presented. Equation 7.23 is recalled.

$$m'_z = \frac{C_a D^2 \pi \rho L}{4} \tag{7.23}$$

The positions of the connected buoys are imported in the function. From these positions, the length of the beam is calculated. Based on this information the added mass can be calculated.

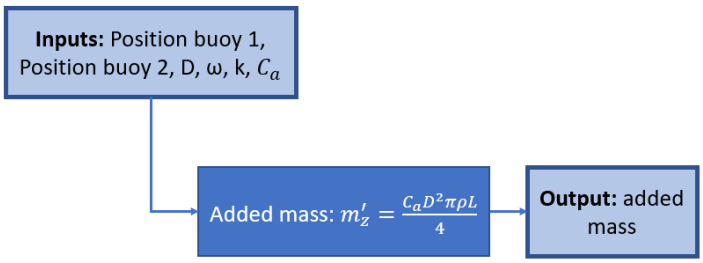

Figure 9.5: Block diagram implementation of added mass with Morison

Listing 9.4: MorisonAddedHM function, code that calculates the added mass part coming from the Morison equation.

```
function [addedmass] = MorisonAddedHM(Pos1,Pos2,D)
% Written by Andreas Feys for graduation process
% Summary of this function
%   Imported globals: rho and c_a
%   Pos1: position of one end of on end of the cylinder (x, y, z)'
%   Pos2 position other end of cylinder,
%   D; diameter of cylinder,
%   addedmass: output the force vector in vertical direction per given omega
% All units are in meter, newton, rad/s
% The time varying part is not included

global rho c_a
L=norm(Pos2-Pos1);
e_t=(Pos2-Pos1)/L;

addedmass=c_a * rho * pi * D ^ 2 * L * (e_t(1) ^ 2 + e_t(2) ^ 2) / 4;
end
```

The same is done for the other terms. For the calculation of the damping terms, u_{RNa} is used which is explained subsequently. The exact implementation in the code can be found according to Table 9.3 in Appendix D.

Table 9.3: Reference to the code in Appendix D, where the code for the specific Morison contributions are indicated

m'	MorisonAddedFKHM.m
I'	MorisonAdddedFKRMTorque.m
b'	MorisonAddedVD.m
B'	MorisonAddedVDTorque.m

9.2.3. Calculation of the magnitude of the relative velocity

As said on page 62, equations were proposed to calculate the magnitude of the relative velocity (u_{RNa}) over the beam length. Therefore, an iterative process has been used, which is indicated in Figure 9.6a. The velocity vector that is calculated is illustrated by the red vector in Figure 9.6b.

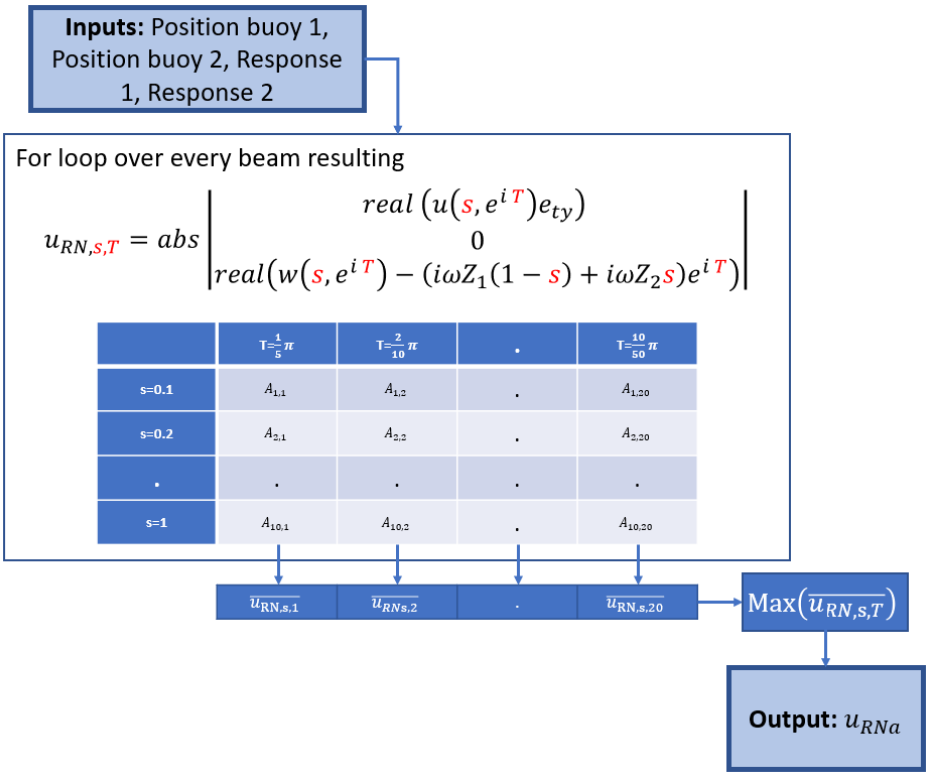

(a) Block diagram on the iteration of the magnitude of the relative velocity

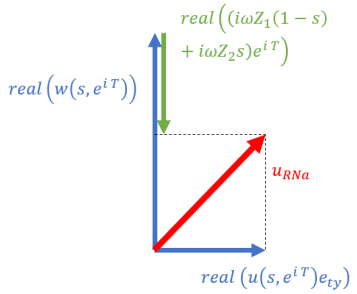

(b) Vector diagram for the calculation of the relative perpendicular velocity

Figure 9.6: Calculation of the magnitude of the relative velocity

In the function programmed in MATLAB, the position and the response of the end of the beam is imported. In a for loop, a matrix is built that calculates the velocity amplitude of the real part on ten different positions at ten time steps on one period. When the for loop is executed, the average is taken over the length of the beam for every time step. Of these averages, the maximum is selected. The maximum should indicate the amplitude over time.
This is implemented in the code as indicated in Listing 9.5. The full function can be found in Appendix D Listing D.10.

Listing 9.5: part from MorisonMagentudeUra.m code to calculate the relative magnitude of the relative velocity.

```
24      for S=1:length(s)
25          for TT=1:length(T)
26              urn1a(S,TT,:)= reshape(sqrt(real(1j * Ampletude * omega .* exp(k * Pos1(3)) .* exp(-1j * k * (
                    s(S) * L * e_t(1) + Pos1(1))) * exp( 1j * T(TT)) - 1j * Resp1 * ( 1 - s(S) ) .* omega *
                    exp( 1j * T(TT)) -  1j *  s(S) * Resp2 .* omega * exp( 1j *T(TT))).^2 +real(Ampletude *
                    omega .* exp(k * Pos1(3)) .* exp(-1j * k * (s(S) * L * e_t(1) + Pos1(1))) * exp( 1j * T(
                    TT))).^2),[1,1,length(omega)]);
27          end
28      end
29      urn1b=reshape(max(mean(urn1a,1),[],2),[1,length(omega)]);
30      end
```

The subdivision of the beam in ten steps was based on a convergence study. This conversion study was executed by comparing different results obtained with difference division numbers to the result of obtained with a division number of hundred. A division number of hundred means that the velocity was checked on hundred different locations on the beam and on hundred time steps within one wave period. The convergent study was based on an arbitrary beam with a length of 27 meter which has an angle of 45°on the wave propagating direction and assessed over a frequency range of 0 to 3 rad/s. Figure 9.7a shows that with a division number of ten, an accuracy of more then two percent is obtain with this example.

$$\text{Error compared to division number 100} = \frac{\left|\sum_{n=i}^{n} u_{RNa,m}(\omega_i) - \sum_{n=i}^{n} u_{RNa,100}(\omega_i)\right|}{\sum_{n=i}^{n} u_{RNa,100}(\omega_i)} \tag{9.5}$$

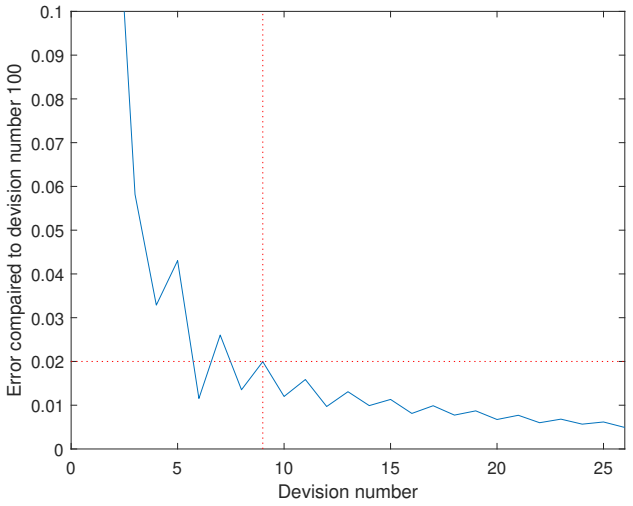

(a) Convergence over division number

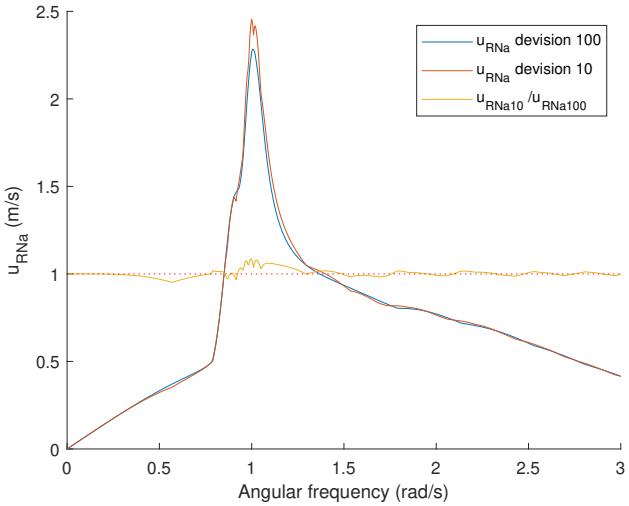

(b) Comparison between division number 10 and 100

Figure 9.7: Convergence study for the calculation of the magnitude of the relative velocity

9.2.4. Implementation of the hydrodynamic loads on the heaving buoys

The hydrodynamic loads on the buoy has three different parts. First, there is the force on the buoy. Then the added mass needs to be determined and lastly the damping needs to be calculated.
The heave force on the buoy is determined by making use of equation 7.41. This equation is substituted in the matrix build-up script, as indicated. Thus, no separate function is written. The time-dependent part $e^{i\omega t}$ is excluded from the code.

$$F_{buoy,i} = \rho\, \zeta_a g e^{kz} e^{-ikx} \frac{\pi D^2}{4} e^{i\omega t} \tag{7.41}$$

Function (addedmassFK.m) calculates the added mass of a heaving buoy. This is implemented in the code, as shown in Listing 9.6. The values for α are obtained with the equation indicated on the horizontal axis of Figure 7.2 [6, p.281]. The data of Figure 7.2 on page 64 was inserted using 15 points on the curve. The values of the horizontal axis were inputted in one column, and the values on the vertical axis in a second column. Based on this data, the value on the vertical axis of the graph was found by interpolation. Then the added mass was calculated using equation 9.6. The function, as indicated in Listing 9.6, outputs the added masses of the buoys.

$$m_i' = C_a \frac{4}{3} \rho \left(\frac{D}{2}\right)^3 \tag{9.6}$$

Listing 9.6: AddemassFK function for a heaving buoy

```
function [MaddedFK] = AddedmassFK(Draft,D)
% Written by Andreas Feys for graduation process
%   Summary of this function
%   returns added masses for column based on graph in Clauss et al based on
%   draft and diameter.
%   Draft: column vector containing the draft for the different buoys
%   D: column vector containing the diameter of different buoys
%   MaddedFK: added mass in kg for the heave motion of the buoy

global rho %global water density

R=D/2;
alpha=pi/4*R.*(Draft.^-1);                                  % input for the graph (x axis)
alphaclauss=[0 0.2 0.5 1 1.5 2 2.5 3 4 5 6 7 8 9 10]';      % Values on x axis of graph
Caclauss=[2 2 1.7 1.52 1.42 1.35 1.32 1.28 1.25 1.21 1.18 1.16 1.15 1.145 1.14]';   %values of y-axis of
    graph
```

```
16 Ca = interp1(alphaclauss,Caclauss,alpha,'spline'); %output of the graph (y axis)
       based on interpolation
17 MaddedFK=4/3*rho.*Ca.*(R.^3); % added mass calculation based
       on Ca
18 end
```

The damping was calculated as discussed in section 7.4.3. There, a simple equation based on the calculation of the critical damping was proposed (equation B.2). This formula is written out in the script BuildupDampingsMatrix.m and multiplied with the percentage of the critical damping.

```
6 %% Damping due to buoys determined with critical damping
7 Kbuoy=pi*rho*g.*(DiameterBuoy.^2)/4;
8 bBuoy=percentCritDamp*2*sqrt(Kbuoy.*Mbuoy); %calculation damping based on critical
       damping taking into account the hardcoded stiffness and mass
9 B1=diag(bBuoy);
```

9.3. Program layout and additional functions

Multiple parts of the program were presented. In the introduction of this chapter, the layout of the program was illustrated in Figure 9.1. The same sequence indicated in the layout will be followed to elaborate on the program. First, the inputs needed in the calculation tool will be introduced. Some of these inputs are reformulated or are recalculated (section 9.3.1). The force vector, the mass, damping, and stiffness matrix are build up. This is then used to solve the differential equation leading to a response. With the response, the damping terms in the equation are iterated.
This sequence of calling the different scripts is fixed in Run.m, which can be seen in Appendix D. Firstly, the inputs are loaded. After which the respectively mass, damping, stiffness and force matrix or vector are build up. The response is obtained from the differential equation. Then the outcome is used for recalculating the damping and force as these are dependent on the amplitude of the relative velocity (u_{RNa}). This iterates the response of the structure based on the changing linearised damping.

9.3.1. Inputs

Initially some basic constants are defined in the program. These constants are defined in Table 9.4. The frequency range cam be changed depending on the region of interest. These inputs (except of the critical damping ratio) are defined globally over the program and are therefore available over all functions and scripts.

Table 9.4: Inputs and constants in the code

ρ	1025	kg/m^3
g	9.81	m/s^2
ζ	1	m
ω	$0-3(7)$	rad/s
k	$\frac{\omega^2}{g}$	hz
C_a	1	[\]
C_d	1.2	[\]
Critical damping ratio	0.005	[\]

In Table 9.4 the added mass and the dampingscoefficient of the Morison equation, indicated as C_a and C_d respectively. These were chosen based on Clauss et al. [6, p.264].
Based on the desired variations of the structure identified in section 5.4.1 on page 46 the inputs seen in Table 9.5 are identified.

Table 9.5: Input variables for variation of the calculation tool

Inputs	**MATLAB name**	**Description**
Topology matrix	C	Indicates the topology of the structure by the topology matrix
Beam length	BeamLength	Indicates the beam length of all beams
Beam diameter	BeamDiameter	Indicates the beam diameter
Beam depth	BeamDepth	Indicates the depth of all beams
Buoy diameter	BuoyDiameter	Indicate the diameter of all buoys
Buoy draft	BuoyDraft	Indicates the buoy draft of all buoys
X position buoys	Xini	Indicates the x position of all buoys
Y position buoys	Yini	Indicates the y position of all buoys
Z position buoys	Zini	Indicates the z position of all buoys
Rotation angle structure	alpha	The structure is described based on x,y and z positions of the buoys. These can be rotated around the z-axis indicated by angle alpha
Initial response	InitialResp	Indicates the initial response of the structure used for the start of the iteration

These inputs can still be overwritten if it is desired to simulate varying dimensions over the different construction elements such as buoy diameter or buoy draft. To use the inputs in the program, they are rewritten resulting in the following items shown in Table 9.6. The coordinates of the buoys are rewritten based on the rotation angle indicated with alpha. In this way the construction can change orientation in respect to the wave direction. This means that in the calculations the wave propagating direction always follows the x-axis and the orientation of the construction can be set.

Table 9.6: Rewritten and recalculated inputs

Inputs	**Matlab name**	**Discription**
X position buoys	X	X position after rotation
Y position buoys	Y	Y position after rotation
Z position buoys	Z	Z position after rotation
Diameter buoy vector	DiameterBuoy	The buoy diameter placed in a vector
Length beam matrix	LengthBeam	Matrix containing the lengths of the beams taking into account the topology
Diameter beam matrix	DiameterBeam	Matrix containing the diameters of the beams taking into account the topology
Depth beam matrix	DepthBeam	Matrix containing the depth of the beams taking into account the topology
Depth beam vector	DepthBeamVec	Vector with beam depth (same information as previous)
Connected buoy matrix	BuoyCon	Matrix containing on every row the numbers of two connecting buoys
Position buoy A matrix	Pos1	Position of the buoy at the A side of the beam for every beam
Position buoy B matrix	Pos2	Position of the buoy at the B side of the beam for every beam
Response of connected buoys	Resp_BuoyCon	A matrix with two rows containing the response of previous iteration
Triangle matrix	TriangleMatrix	Based on the topology matrix a matrix is composed where very row contains the buoys that form one triangle

The connected buoy matrix has one row per connecting beam. On every row, the two buoy numbers

that are on each side are inserted. Based on this information the coordinates of the different buoys are reorganised. This information is now used to calculate different matrix entries. An example of an interconnection matrix can be found in equation 9.7. Similar matrices are obtained containing the position in x, y, and z-direction and the response of the specific buoy. The exact code can be found in Listing 9.7.

$$\text{Connections: } \begin{bmatrix} 1 & 2 \\ 1 & 3 \\ 2 & 3 \\ 2 & 4 \\ 3 & 4 \end{bmatrix}; \quad \text{Position buoy A: } \begin{bmatrix} x_1 & y_1 & z_1 \\ x_1 & y_1 & z_1 \\ x_2 & y_2 & z_2 \\ x_2 & y_2 & z_2 \\ x_3 & y_3 & z_3 \end{bmatrix}; \quad \text{Position buoy B: } \begin{bmatrix} x_2 & y_2 & z_2 \\ x_3 & y_3 & z_3 \\ x_3 & y_3 & z_3 \\ x_4 & y_4 & z_4 \\ x_4 & y_4 & z_4 \end{bmatrix};$$

$$\text{Response buoy A: } \begin{bmatrix} Z_1 \\ Z_1 \\ Z_2 \\ Z_2 \\ Z_3 \end{bmatrix}; \quad \text{Response buoy B: } \begin{bmatrix} Z_2 \\ Z_3 \\ Z_3 \\ Z_4 \\ Z_4 \end{bmatrix} \tag{9.7}$$

Listing 9.7: Connections.m code

```
function [Combinaties,Pos1,Pos2,Responcecombinatie] = Connections(Topology,X,Y,DeptConnection,Responces)
% Function: Converts the topology to a matrix with every row two values of
% the X, Y, Response for a beam.
% inputs: X and Y location of the buoys. Z: vector of the depth of the beams
% Response of the system of previous iteration, topology matrix of the system.

ddd=triu(Topology,1);% positive triangle without diagonal

I_inds = find(ddd); % find indices of non zero items
[row,col] = ind2sub(size(Topology),I_inds); %convert indices to coordinates resulting in a matrix with on
    every row two buoys that are directly connected. This is used to rearrange the position information
    of all connect buoys

Combinaties = [row col];
Xcom=X(Combinaties)';
Ycom=Y(Combinaties)';
Zcom=DeptConnection(Combinaties)';

Responcecombinatie=zeros([size(Combinaties) length(Responces)]); % The same reorganisation is done for the
     response

    for n=1:size(Combinaties,1)
        Responcecombinatie(n,1,:)=Responces(Combinaties(n,1),:);
        Responcecombinatie(n,2,:)=Responces(Combinaties(n,2),:);
    end

Pos1=[Xcom(:,1) Ycom(:,1) Zcom(:,1)]; % combining these coordinates for positions used in Morison
     calculations
Pos2=[Xcom(:,2) Ycom(:,2) Zcom(:,1)];
end
```

Lastly, the the triangles in the construction are found based on the triangle matrix. Based on graph theory the triangles in the construction are recognised and listed by Listing 9.8.

Listing 9.8: Part from count_triangle.m code to find triangles based on topology matrix.

```
N_nodes = size(G.Nodes,1);  % with G the graph indicating the topology
TL = [];
for i = 1:N_nodes %iterate over all nodes

    % find neighbors N2 of point under investigation N1
    N2 = G.neighbors(i);

    % find neighbors N3 of N2
    for j=1:length(N2)
        N3 = G.neighbors(N2(j));
        N3 = N3(N3~=i); %remove N1 from list
        overlaps = intersect(N3,G.neighbors(i)); %check if N3 was also a neighbor of N1.
        % add triangles to list (multiple may be added at the same time)
        N_overlaps = length(overlaps);
        mat = repmat([i N2(j)],[N_overlaps 1]);
        mat2 = [mat overlaps];
        TL = [TL;mat2];
    end
end
```

```
TL2 = sort(TL,2); %sort horizontally from low node number to high
T = unique(TL2,'rows'); %remove double entries
```

9.3.2. Obtaining the response of the structure

Now that all the matrices are build up the solution method for the differential equation must be implemented. The eigenmodes and eigenfrequencies are obtained after which the frequency response is calculated in a for loop. The code can be found in Listing 9.9.

Listing 9.9: Calculations.m script

```
%% Calculations:
% solving the differential equation
 global omega
% obtaining the eigenmodes and the eigenfrequencies
 [Evecs,Evals]=eig(K,M);
omega1=sqrt(Evals);
Evecnorm=Evecs.*(max(abs(Evecs),[],1).^-1);

% obtaining the frequency response per frequency
Qc=zeros(DimSystem,length(omega));

 for a=1:length(omega)
     Zdyn=-M*(omega(a)).^2+1j*B(:,:,a).*omega(a)+K;
     Qc(:,a)=Zdyn\F(:,a);
 end

Qa=abs(Qc);
Qtheta=angle(Qc);
```

9.3.3. Iteration

To obtain the response, an iterative process based on the calculations of u_{RNa} (see section 9.2.3) is implemented. The iteration process is continued till the criteria shown in equation 9.8 is met. Equation 9.8 calculates the difference of summation of absolute value of the response over all frequencies (m) and buoys (n) of this iteration is within one percent of that of the previous iteration.

$$\frac{a_n - a_{n-1}}{a_n} \leq 0.01 \text{ for } a = \sum_{n=i}^{n} \sum_{j=0}^{m} \left| Resp(\omega_j)_i \right| \tag{9.8}$$

Iterating the solution based on previous found result does not lead to an conversion. This can be seen in Figure 9.8. The thick line shows the response based on an alternative method with ten iterations, which is verified later in this thesis and therefore is believed to be accurate. The thinner lines show ten steps of iterations (a to j) based on the response found in previous iteration.

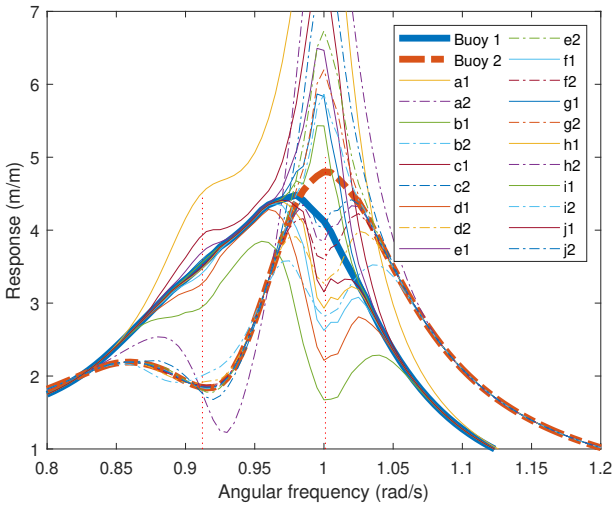

Figure 9.8: Iteration based on previously found response, thin lines indicate iteration steps thick line indicates final solution.

The response next to the eigenfrequencies (indicated with the vertical lines) converges after one or two iterations. For the lower eigenfrequency, it can be seen that convergence is reached after 6 iterations. For the second eigenfrequency convergence is not found. By analysing the process that lead to Figure 9.8, it can be noted that the damping is over- and underestimated in an alternating way.
By using a linear combination of the last two obtained responses (Z), a converging solution is achieved. An optimisation was executed to find an appropriate linear combination. The value of A in equation 9.9 indicates the ratio of the linear combination. For the first iterations, the initial response is used. This initial response was arbitrarily set on “1” for all frequencies.

$$Z = A \quad Z_{n-2} + (A - 1) \quad Z_{n-1} \tag{9.9}$$

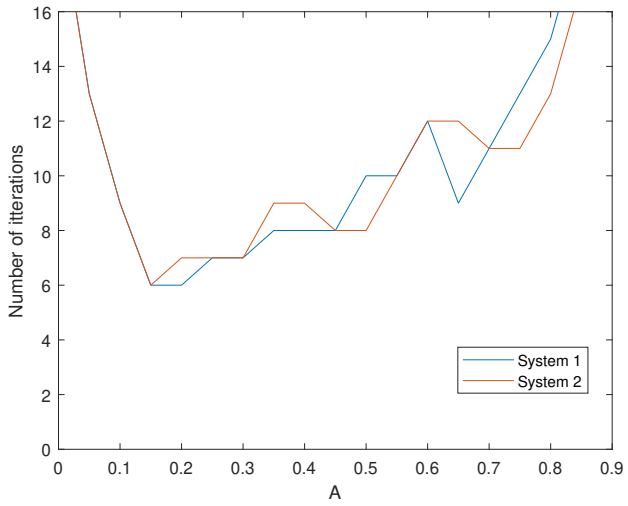

Figure 9.9: Number of iterations needed to obtain the desired accuracy depending on the ratio of previously obtained solutions.

A is varied with steps of 0.05. A equals 0.15 works best as can be seen in Figure 9.9. Two structures were varied. Firstly, a two buoy structure with a beam of 27-meters length and 1-meter diameter, which is oriented 45 degrees on the wave propagating direction. Second, a two buoy structure where the beam is oriented in the wave propagating direction with a length of 20 meters and a diameter of 1 meter.
This systematic is implemented in Listing D.1 in Appendix D. This results in a fully implemented code as it was theoretically described in chapter 6, 7 and 8 and was visualised in Figure 9.1.
The code can be found in Appendix D. With this code the variations indicated in section 5.4.1 can be simulated in the calculation tool. Before this is done, it needs to be shown that the implementation of theory was executed correctly.

10

Verification

First the implementation of the mechanical system will be verified then the individual functions and methods related to hydrodynamics and mechanics will be verified (section 10.1 and section 10.2). Next, a system will be composed to verify the total program in section 10.3. This will be done starting with one buoy and building up to a five buoys system. Lastly the small angle approximation is tested based on a five buoys inline system in section 10.4.

10.1. Verification of the matrices in the differential equation

The methodology identified to compose the differential equation as shown in section 9.1 should be verified. This section will verify the methodology for the matrix build-up will be verified. The verification of the total program will be done at the end of this chapter (section 10.3). The verification will be done by excluding the hydrodynamic forces that were derived in chapter 7. This simplification is valid as the hydrodynamic matrices are obtained via substitution in these matrices, therefore the methodology to compose the matrices is still tested.
The verification of the matrix build-up will be done in two steps. First, the matrices of a larger structure of six buoys will be build based on the method explained in section 9.1. Then the differential equations for three individual buoys of the six buoys system are derived with the same method as indicated in chapter 6. This will lead to the verification of the method. Second, an inline structure of five buoys will be analysed. The frequency response, eigenfrequencies and eigenmodes of the inline structure based on the methodology will be compared with a separately derived hardcoded system for the same structure.

10.1.1. Six buoys structure

Figure 10.1 displays the system that will be used for verification. The matrix build-up is based on the forces indicated in Figure 6.1 and 6.2a on respectively page 48 and page 49 of chapter 6. By substituting the values indicated in Table 10.1 the entries as indicated in chapter 6 can be derived. To verify if these matrices are correct the differential equations for buoy 1, 2 and 3 will be derived manually.

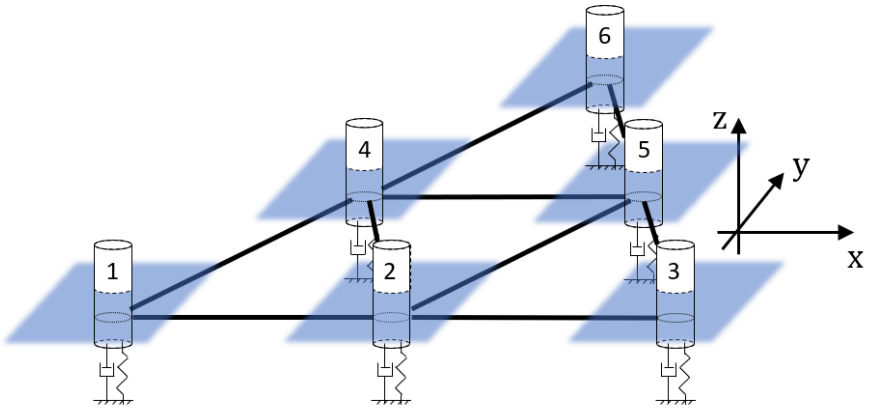

Figure 10.1: Visualisation of structure consisting of six buoys

Table 10.1: Substitution for the verification of the matrix build-up.

$\mathbf{F}_{i,buoy}$	$\mathbf{F}_{i,buoy}$
$\mathbf{F}_{ij,FK,HM,\zeta}$	$\mathbf{F}_{ij}$
$\mathbf{F}_{ijVD,\zeta}$	0
$\frac{\mathbf{T}_{ij,FK,HM,\zeta}}{L}$	$\frac{\mathbf{T}_{ij}}{L}$
$\frac{\mathbf{T}_{ij,VD,\zeta}}{L}$	0
$\mathbf{m}'_{ij}$	0
$\frac{\mathbf{I}'_{ij}}{L}$	0
$\mathbf{B}_i$	$\mathbf{B}_i$
$\mathbf{b}'_{ij}$	0
$\frac{\mathbf{B}'_{ij}}{L}$	0
$\mathbf{K}_i$	$\mathbf{K}_i$

First the topology matrix C of the structure is created based on Figure 10.1.

$$C = \begin{array}{c} \\ 1 \\ 2 \\ 3 \\ 4 \\ 5 \\ 6 \end{array} \begin{array}{c} \begin{array}{cccccc} 1 & 2 & 3 & 4 & 5 & 6 \end{array} \\ \begin{pmatrix} . & 1 & 0 & 1 & 0 & 0 \\ -1 & . & 1 & 1 & 1 & 0 \\ 0 & -1 & . & 0 & 1 & 0 \\ -1 & -1 & 0 & . & 1 & 1 \\ 0 & -1 & -1 & -1 & . & 1 \\ 0 & 0 & 0 & -1 & -1 & . \end{pmatrix} \end{array} \tag{10.1}$$

Using the methodology explained in section 9.1 and the proposed substitution the following differential equation is obtained.

$$\mathbf{F}_{buoy} + \left[[\mathbf{F}_M] + \frac{[\mathbf{T}_M]}{L} \right] \vec{1}_6 = ([\mathbf{M_A}] + [\mathbf{M_B}] + [\mathbf{M_C}] + [\mathbf{M_D}])\, \ddot{\boldsymbol{z}} + [\mathbf{B}]\dot{\boldsymbol{z}} + [\mathbf{K}]\boldsymbol{z} \tag{10.2a}$$

$$\mathbf{F}_{buoy} = \begin{bmatrix} F_1 \\ F_2 \\ F_3 \\ F_4 \\ F_5 \\ F_6 \end{bmatrix} \tag{10.2b}$$

$$[\mathbf{F}_M] = \begin{bmatrix} 0 & \frac{F_{12}}{2} & 0 & \frac{F_{14}}{2} & 0 & 0 \\ \frac{F_{12}}{2} & 0 & \frac{F_{23}}{2} & \frac{F_{24}}{2} & \frac{F_{25}}{2} & 0 \\ 0 & \frac{F_{23}}{2} & 0 & 0 & \frac{F_{35}}{2} & 0 \\ \frac{F_{14}}{2} & \frac{F_{24}}{2} & 0 & 0 & \frac{F_{45}}{2} & \frac{F_{46}}{2} \\ 0 & \frac{F_{25}}{2} & \frac{F_{35}}{2} & \frac{F_{45}}{2} & 0 & \frac{F_{56}}{2} \\ 0 & 0 & 0 & \frac{F_{46}}{2} & \frac{F_{56}}{2} & 0 \end{bmatrix} \tag{10.2c}$$

$$\frac{[\mathbf{T}_M]}{L} = \begin{bmatrix} 0 & \frac{T_{12}}{L} & 0 & \frac{T_{14}}{L} & 0 & 0 \\ -\frac{T_{12}}{L} & 0 & \frac{T_{23}}{L} & \frac{T_{24}}{L} & \frac{T_{25}}{L} & 0 \\ 0 & -\frac{T_{23}}{L} & 0 & 0 & \frac{T_{35}}{L} & 0 \\ -\frac{T_{14}}{L} & -\frac{T_{24}}{L} & 0 & 0 & \frac{T_{45}}{L} & \frac{T_{46}}{L} \\ 0 & -\frac{T_{25}}{L} & -\frac{T_{35}}{L} & -\frac{T_{45}}{L} & 0 & \frac{T_{56}}{L} \\ 0 & 0 & 0 & -\frac{T_{46}}{L} & -\frac{T_{56}}{L} & 0 \end{bmatrix} \tag{10.2d}$$

$$[\mathbf{M_A}] = \begin{bmatrix} m_1 + m_1' & 0 & 0 & 0 & 0 & 0 \\ 0 & m_2 + m_2' & 0 & 0 & 0 & 0 \\ 0 & 0 & m_3 + m_3' & 0 & 0 & 0 \\ 0 & 0 & 0 & m_4 + m_4' & 0 & 0 \\ 0 & 0 & 0 & 0 & m_5 + m_5' & 0 \\ 0 & 0 & 0 & 0 & 0 & m_6 + m_6' \end{bmatrix} \tag{10.2e}$$

$$[\mathbf{M_B}] = \begin{bmatrix} 0 & \frac{m_{12}}{4} & 0 & \frac{m_{14}}{4} & 0 & 0 \\ \frac{m_{12}}{4} & 0 & \frac{m_{23}}{4} & \frac{m_{24}}{4} & \frac{m_{25}}{4} & 0 \\ 0 & \frac{m_{23}}{4} & 0 & 0 & \frac{m_{35}}{4} & 0 \\ \frac{m_{14}}{4} & \frac{m_{24}}{4} & 0 & 0 & \frac{m_{45}}{4} & \frac{m_{46}}{4} \\ 0 & \frac{m_{25}}{4} & \frac{m_{35}}{4} & \frac{m_{45}}{4} & 0 & \frac{m_{56}}{4} \\ 0 & 0 & 0 & \frac{m_{46}}{4} & \frac{m_{56}}{4} & 0 \end{bmatrix} \tag{10.2f}$$

$$[\mathbf{M_C}] = \begin{bmatrix} 0 & -\frac{I_{12}}{L^2} & 0 & -\frac{I_{14}}{L^2} & 0 & 0 \\ -\frac{I_{12}}{L^2} & 0 & -\frac{I_{23}}{L^2} & -\frac{I_{24}}{L^2} & -\frac{I_{25}}{L^2} & 0 \\ 0 & -\frac{I_{23}}{L^2} & 0 & 0 & -\frac{I_{35}}{L^2} & 0 \\ -\frac{I_{14}}{L^2} & -\frac{I_{24}}{L^2} & 0 & 0 & -\frac{I_{45}}{L^2} & -\frac{I_{46}}{L^2} \\ 0 & -\frac{I_{25}}{L^2} & -\frac{I_{35}}{L^2} & -\frac{I_{45}}{L^2} & 0 & -\frac{I_{56}}{L^2} \\ 0 & 0 & 0 & -\frac{I_{46}}{L^2} & -\frac{I_{56}}{L^2} & 0 \end{bmatrix} \tag{10.2g}$$

$$[\mathbf{M_D}] = \text{Diag}\left(\begin{bmatrix} \frac{m_{12}}{4} + \frac{m_{14}}{4} + \frac{I_{12}}{L^2} + \frac{I_{14}}{L^2} \\ \frac{m_{12}}{4} + \frac{m_{23}}{4} + \frac{m_{24}}{4} + \frac{m_{25}}{4} + \frac{I_{12}}{L^2} + \frac{I_{23}}{L^2} + \frac{I_{24}}{L^2} + \frac{I_{25}}{L^2} \\ \frac{m_{23}}{4} + \frac{m_{35}}{4} + \frac{I_{23}}{L^2} + \frac{I_{35}}{L^2} \\ \frac{m_{14}}{4} + \frac{m_{24}}{4} + \frac{m_{45}}{4} + \frac{m_{46}}{4} + \frac{I_{14}}{L^2} + \frac{I_{24}}{L^2} + \frac{I_{45}}{L^2} + \frac{I_{46}}{L^2} \\ \frac{m_{25}}{4} + \frac{m_{35}}{4} + \frac{m_{45}}{4} + \frac{m_{56}}{4} + \frac{I_{25}}{L^2} + \frac{I_{35}}{L^2} + \frac{I_{45}}{L^2} + \frac{I_{56}}{L^2} \\ \frac{m_{46}}{4} + \frac{m_{56}}{4} + \frac{I_{46}}{L^2} + \frac{I_{56}}{L^2} \end{bmatrix}\right) \tag{10.2h}$$

$$[\mathbf{B}] = \begin{bmatrix} b_1 & 0 & 0 & 0 & 0 & 0 \\ 0 & b_2 & 0 & 0 & 0 & 0 \\ 0 & 0 & b_3 & 0 & 0 & 0 \\ 0 & 0 & 0 & b_4 & 0 & 0 \\ 0 & 0 & 0 & 0 & b_5 & 0 \\ 0 & 0 & 0 & 0 & 0 & b_6 \end{bmatrix} \tag{10.2i}$$

$$[\mathbf{K}] = \begin{bmatrix} k_1 & 0 & 0 & 0 & 0 & 0 \\ 0 & k_2 & 0 & 0 & 0 & 0 \\ 0 & 0 & k_3 & 0 & 0 & 0 \\ 0 & 0 & 0 & k_4 & 0 & 0 \\ 0 & 0 & 0 & 0 & k_5 & 0 \\ 0 & 0 & 0 & 0 & 0 & k_6 \end{bmatrix} \tag{10.2j}$$

Now the differential equations for buoy 1, 2 and 3 will be derived with Newton Euler mechanics as was done in chapter 6. Buoy 1 of the four buoys structure has the same connections as buoy 1 of the six buoys structure. The difference is that buoy 3 in the four buoys structure is named buoy 4 in the six buoys structure. When this is taken into account it can be seen that the first line of equation 6.10a on page 52 and the first line of equation 10.2 are identical.

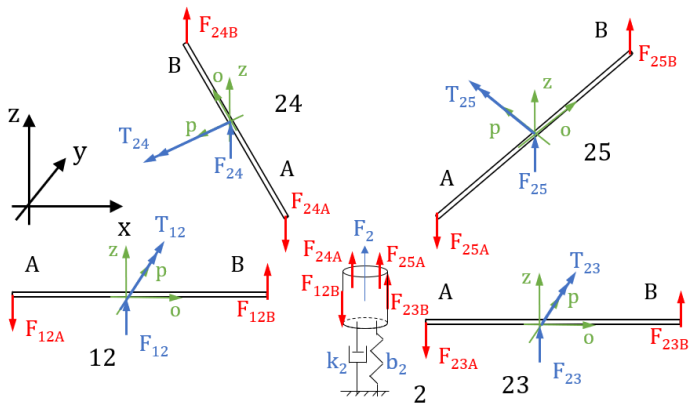

(a) Free Body Diagram (FBD) of buoy number 2 of a six buoys structure

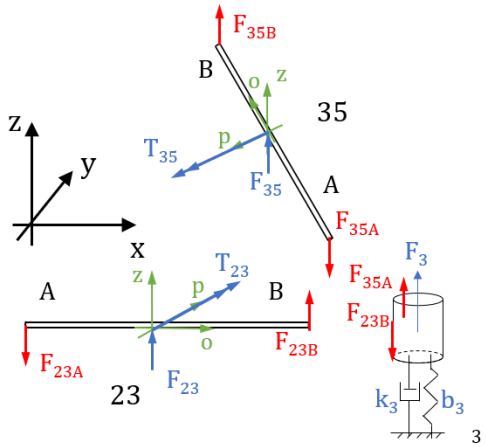

(b) FBD of buoy number 3 of a six buoys structure

Figure 10.2: FBD of six buoys structure

Buoy number 2 and 3 of the six buoys system have no similarities with one of the buoys of the previously discussed structure. The same system to name the different forces is used as explained on page 50. The free body diagrams are shown in Figure 10.2a and Figure 10.2b. First the force balance in vertical direction is calculated in equation 10.3a and equation 10.3b.

$$\text{Buoy 2: } \sum F_z = m\ddot{z} \rightarrow -F_{12Bz} + F_{23Az} + F_{24Az} + F_{25Az} - b_2\dot{z}_2 - k_2 z_2 + F_2 = (m_2 + m_2')\ddot{z}_2 \tag{10.3a}$$

$$\text{Buoy 3: } \sum F_z = m\ddot{z} \rightarrow -F_{23Bz} + F_{35Az} - b_3\dot{z}_3 - k_3 z_3 + F_3 = (m_3 + m_3')\ddot{z}_3 \tag{10.3b}$$

Then equation 6.8a and equation 6.8b are used to substituted in equation 10.3a and equation 10.3b. “i” and “j” are the buoy numbers (at the end of the beam) where $i < j$.

$$F_{ijAz} = \frac{1}{2}F_{ij} + \frac{T_{ij}}{L} - \frac{1}{2}m_{ij}\ddot{z}_{ij} - \frac{I_{ij}}{L}\ddot{\alpha}_{ij} \tag{6.8a}$$

$$-F_{ijBz} = \frac{1}{2}F_{ij} - \frac{T_{ij}}{L} - \frac{1}{2}m_{ij}\ddot{z}_{ij} + \frac{I_{ij}}{L}\ddot{\alpha}_{ij} \tag{6.8b}$$

This results in equation 10.5 and equation 10.6.

$$F_2 + \frac{F_{12}}{2} + \frac{F_{23}}{2} + \frac{F_{24}}{2} + \frac{F_{25}}{2} - \frac{T_{12}}{L} + \frac{T_{23}}{L} + \frac{T_{24}}{L} + \frac{T_{25}}{L}$$
$$= (m_2 + m_2')\ddot{z_2} + \frac{m_{12}}{4}\ddot{z_1} + \left(\frac{m_{12}}{4} + \frac{m_{23}}{4} + \frac{m_{24}}{4} + \frac{m_{25}}{4}\right)\ddot{z_2} + \frac{m_{23}}{4}\ddot{z_3} + \frac{m_{24}}{4}\ddot{z_4} + \frac{m_{25}}{4}\ddot{z_5}$$
$$- \frac{I_{12}}{L^2}\ddot{z_1} + \left(\frac{I_{12}}{L^2} + \frac{I_{23}}{L^2} + \frac{I_{24}}{L^2} + \frac{I_{25}}{L^2}\right)\ddot{z_2} - \frac{I_{23}}{L^2}\ddot{z_3} - \frac{I_{24}}{L^2}\ddot{z_4} - \frac{I_{25}}{L^2}\ddot{z_5} + b_2\dot{z_2} + k_2 z_2 \quad (10.5)$$

$$F_3 + \frac{F_{23}}{2} + \frac{F_{35}}{2} - \frac{T_{23}}{L} + \frac{T_{35}}{L}$$
$$= (m_3 + m_3')\ddot{z_3} + \frac{m_{23}}{4}\ddot{z_2} + \left(\frac{m_{23}}{4} + \frac{m_{35}}{4}\right)\ddot{z_3} + \frac{m_{35}}{4}\ddot{z_5}$$
$$- \frac{I_{23}}{L^2}\ddot{z_2} + \left(\frac{I_{23}}{L^2} + \frac{I_{35}}{L^2}\right)\ddot{z_3} - \frac{I_{35}}{L^2}\ddot{z_5} + b_3\dot{z_3} + k_3 z_3 \quad (10.6)$$

It can be seen that this results in the same equations that can be found on line 2 and 3 of equation 10.2. This demonstrates that the method to build up the matrices works correctly.

10.1.2. Five buoys in line structure

Now that the system has proven some redundancy for building up the matrices and vectors for a four buoys and six buoys structure an additional verification step is executed. The five buoys in line structure that is simulated is visualised in figure 10.3. First the system can be build up with the method that was identified in section 9.1. Because this is a simpler structure it can also be calculated by hand. The matrices of the differential equation of the structure derived by hand were hardcoded. For both ways of implementation, the response, eigenmodes and eigenfrequencies can be calculated. It should be noted that this verification step does not include any hydrodynamics. The values in Table 10.2 are arbitrarily chosen and substituted in the equations. The response and the eigenmodes are found based on the method explained in section 8.2.

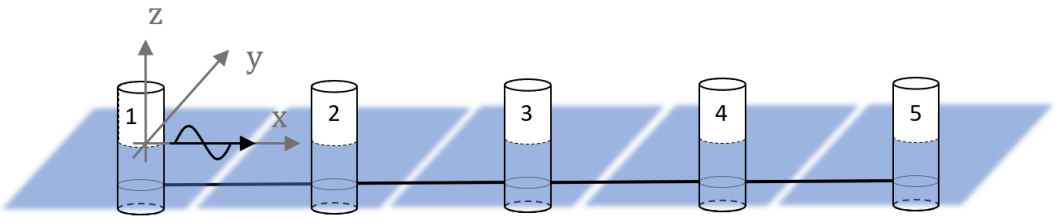

Figure 10.3: Visualisation of the five buoys inline system.

Table 10.2: Values used for inline verification step

L_{beam}	15 m
m_{buoy}	1 kg
m_{beam}	1 kg
b_{buoy}	0.15 kg/s
k_{buoy}	20 N/m
F_{buoy}	10 N
F_{beam}	10 N

The response of both structure and the eigenfrequencies can be found in Figure 10.4a and in Figure 10.4b for respectively the structure that was hardcoded and the structure build up with the topology matrix. It can clearly be seen that the response is identical and that the eigenfrequencies coincide. The same is done for the eigenmodes as can be seen in Figure 10.5a and Figure 10.5b.

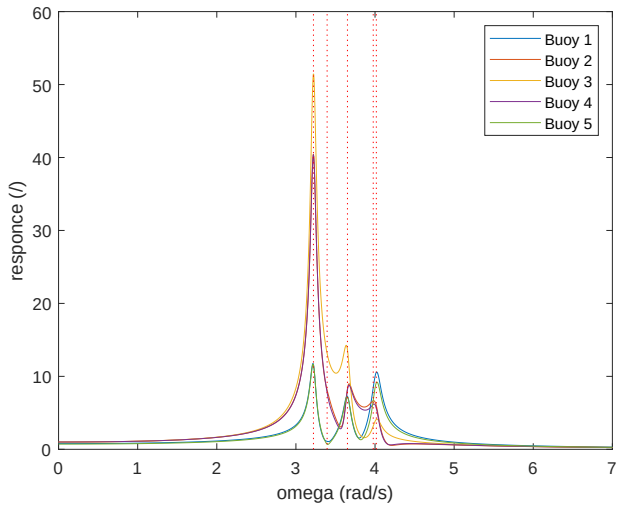

(a) Response of a five buoys inline structure hardcoded

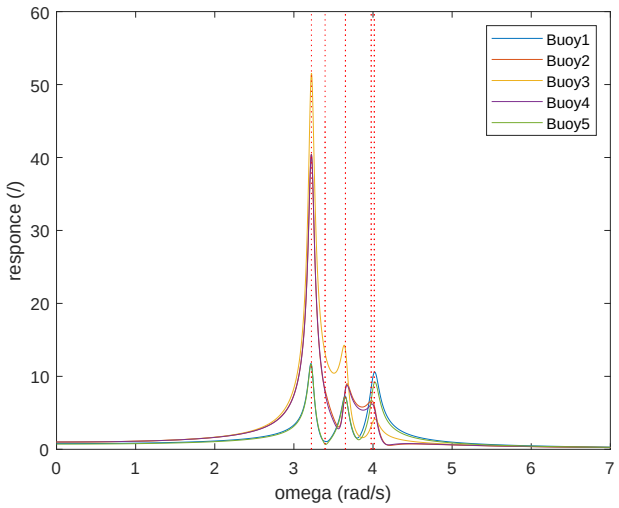

(b) Response of a five buoys inline structure based on methodology

Figure 10.4: Response of a five buoys inline structure

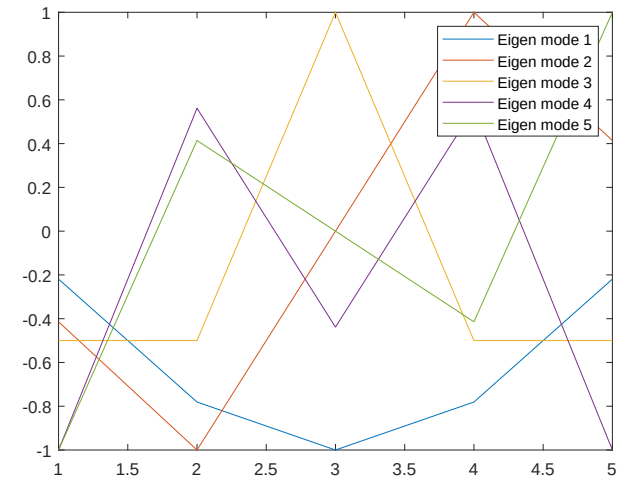

(a) Eigen modes of a five buoys inline structure hardcoded

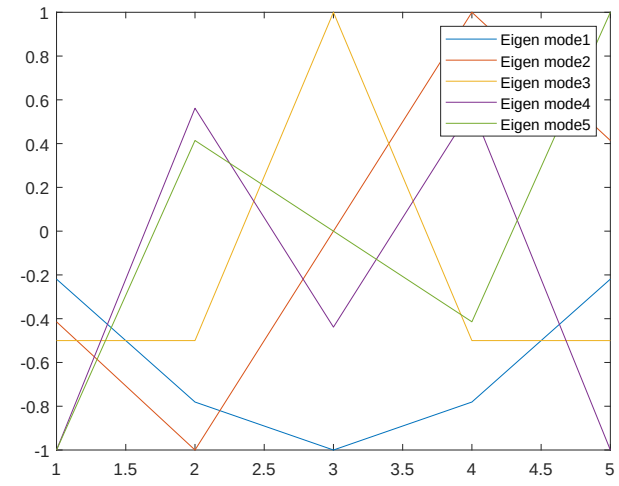

(b) Response of a five buoys inline structure based on methodology

Figure 10.5: Eigen modes of a five buoys inline structure

This demonstrates that the method to build up the matrices works correctly. Next, the hydrodynamics that were substituted in the mechanical equations needs to be verified before the complete system can be verified.

10.2. Verification of the hydrodynamic loads

In this section the verification is done for the individual forces and the moments of equation 7.15 and equation 7.16, which is recalled here. To show the procedure the verification for $\vec{F}_{FK,HM,\zeta}$ and for $\vec{F}_{HM,c}$ is written out in this section. For the other parts, an outcome of the verification is shown in Appendix

C.1. The exact steps of the verification in the Appendix are not discussed as the method used is highly similar. The calculations that were executed in the verification process in Maple can be found in Appendix C.1. The force was calculated by MATLAB and Maple in x, y and z-direction. This helps to improve confidence in the verification. For the moments only the moment in p-direction was verified as this is the only part that is relevant for the heave response of the structure.

$$\vec{F}_M = \int_0^L \frac{d\vec{F}_{N,FK,HM,\zeta}}{ds} - \frac{d\vec{F}_{N,HM,c}}{ds} + \frac{d\vec{F}_{N,VD,\zeta}}{ds} - \frac{d\vec{F}_{N,VD,c}}{ds} ds \tag{7.15a}$$

$$\vec{F}_M = \vec{F}_{FK,HM,\zeta} - \vec{F}_{HM,c} + \vec{F}_{VD,\zeta} - \vec{F}_{VD,c} \tag{7.15b}$$

$$\vec{T}_M = \int_0^L \left(\vec{r} \times \frac{d\vec{F}_{N,FK,HM,\zeta}}{ds}\right) - \left(\vec{r} \times \frac{d\vec{F}_{N,HM,c}}{ds}\right) + \left(\vec{r} \times \frac{d\vec{F}_{N,VD,\zeta}}{ds}\right) - \left(\vec{r} \times \frac{d\vec{F}_{N,VD,c}}{ds}\right) ds \tag{7.16a}$$

$$\vec{T}_M = \vec{T}_{FK,HM,\zeta} - \vec{T}_{HM,c} + \vec{F}_{VD,\zeta} - \vec{T}_{VD,c} \tag{7.16b}$$

10.2.1. Verification of Froude-Krylov and hydrodynamic mass force

Base on the code discussed in section 9.2, the forces for different orientations can be obtained. To verify if the implementation is correct, the result of the calculation tool is compared to the result from alternative calculations made in Maple. The verification of the Froude-Krylov and hydrodynamic mass force is indicated in Table 10.3 on page 96. For every verification step a discussion and explanation is added in the table. The first two columns of the table contain the coordinates of two outer positions of the cylinder. The third column gives the resulting length of the cylinder. The fourth and the fifth column contain respectively the MATLAB output and the output of the verification method. Lastly, there is a reference to the calculation in Maple in Appendix B where the calculation for verification is executed.

$$F_z = (1 + C_a)\rho \frac{\pi D^2}{4} \vec{v}_N ds \tag{10.9}$$

$$\frac{\partial w}{\partial t} = -\zeta_a \omega^2 e^{kz}\, e^{-ikx} \cdot [e^{i\omega t}] \tag{10.10}$$

Next a variation in wave and diameter is made to further verify the outputs (Table 10.4 on page 97). The same logic as applied before can be recognised. On the verification's steps taken in Table 10.10 and Table 10.3 it can be concluded that the coding calculate the force correctly. Additionally, in Appendix C.1 the same steps were executed for the other force components. The same methodology and conclusions are applied. Therefore it is demonstrated that the implementation works correctly.

10.2.2. Verification of the added mass term

The added mass equals the mass of the displaced volume of the cylinder times an added mass constant as can be seen in equation 7.23. The added mass term resulting from the rotation (I') seen in equation 7.26 can also be derived by calculating the moment of inertia of the added mass $\left(I = \frac{m'L^2}{12}\right)$. The damping term does not have such a straight forward method, but a clear logic between equation 7.36 and equation B.20 can be found. The equation for the damping resulting from rotation can also be obtained with $B'_p = \frac{b'_z L^2}{12}$. This increases the confidence in the found equations.
The implementation of the added mass and damping terms is verified by comparing the result of MATLAB with the result by simple equations for a beam located between (0,0,0) and (-10,-10,0) with a diameter of 1 meter. For the damping terms u_{RNa} is needed, for now the value of 1 is substituted. The results are shown in Table 10.5 on page 97.

Table 10.3: Verification of Froude-Krylov and hydrodynamic mass force

ω=1.5; ζ=1; c_a=1; λ=27.5; D=0.1;					
Pos 1	Pos 2	Length	MATLAB (N)	Verification (N)	Reference
(0,0,0)	(-0.1,0,0)	0.1	0.0000 + 0.0000i 0.0000 + 0.0000i **-3.6223** - 0.0415i	**-3.62**	Appendix C.2 part 1.2.A equation 2.2.1.2
A segment of 0.1 meter located at the axis origin is simulated where the centre line of the cylinder is oriented along the x-axis. The force can be calculate by using equation 10.9 and substituting the acceleration of equation 10.10 as defined by the Airy wave theory. The magnitudes of both calculation methods are the same. In the verification the orientation is not included. As result of the orientation of the segment and the orientation of the acceleration in the fluid it can be concluded that the force vector should be real and in the negative z-direction. This matches the found result in MATLAB.					
(0,0,0)	(0,-0.1,0)	0.1	0.0000 + **3.6226i** 0.0000 + 0.0000i **-3.6226** +0.0000i		Appendix C.2 part 1.2.A equation 2.2.1.2
(0,0,0)	(0,0,-0.1)	0.1	0.0000 + 3.5814i 0.0000 + 0.0000i 0.0000 + 0.0000i		Appendix C.2 part 1.2.A equation 2.2.1.2
The length and position of the segments is identical as the previously discussed situation. Only the orientation is now in y and z-direction. Therefore the magnitude of the force is identical. The orientation of the forces matches with what can be expected from the Airy wave theory.					
(0,0,0)	λ,0,0)	λ	**0** **0** **0.6993 * 1.0e-06**	**0**	
A segment with the length equal to the wavelength is simulated. The segment is oriented in the wave propagating direction. The magnitude of the force should therefor be zero.					
(0,0,0)	(-10,-10,-10)	$10\sqrt{3}$	**-38.29+149.37i** **97.28 - 6.90i** **-58.99 - 142.47i**	**-38.26+149.29i** **97.28 - 6.897i** **-58.96 - 142.39i**	Appendix C.2 part 1.2.B equation 2.2.2.1
$(\frac{\lambda}{4}, \frac{\lambda}{4}, 0)$	$(\frac{\lambda}{4} - 10, \frac{\lambda}{4} - 10, -10)$	$10\sqrt{3}$	**149.37 + 38.29i** **-6.90 - 97.28i** **-142.47+58.99i**	**149.4 +37.67i** **-7.28 - 97.20i** **-142.2+59.53i**	Appendix C.2 part 1.2.B equation 2.2.2.2
For this more complex orientation an alternative derivation is done in Maple (see reference to Appendix C.1). The values obtained in with both methods should be the same. In the second situation the cylinder is moved one fourth of a wave length in the direction of the propagating wave. Therefore the magnitude of the complex parts and the magnitude the real parts of the force should be switched.					

Table 10.4: Verification of Froude-Krylov and hydrodynamic mass force (2)

ω=0.5; ζ=5; c_a=1; λ=247; D=1					
Pos 1	Pos 2	Length	MATLAB	Verification	Reference
(0,0,0)	(-0.1,0,0)	0.1	0.0000 + 0.0000i 0.0000 + 0.0000i -201.26 - 0.26i	**-201.2**	Appendix C.2 part 1.2.B equation 2.2.1.3
(0,0,0)	(-10,-10,-10)	$10\sqrt{3}$	**7664 + 21552i** **11399 - 8909i** **-19062 - 12644i**	**7659 + 21541i** **11392 - 8904i** **-19052 - 12637i**	Appendix C.2 part 1.2.B equation 2.2.2.3
(0,0,0)	$(-\frac{\sqrt{3}}{2}27, \frac{\sqrt{3}}{2}27, 0)$	27	**-6480 + 26111i** **-6480 + 26111i** **-52221 - 12961i**	**-6477+26097i** **-6477+26097i** **-52195-12954i**	Appendix C.2 part 1.2.B equation 2.2.2.4

Table 10.5: Verification of added mass and damping implementation

	MATLAB outcome	Manual calculation
m'	11385 kg	$\frac{C_a D^2 \pi \rho L}{4} = 11385$ kg
I'	189750 kgm^2	$I' = \frac{m' L^2}{12} = 189750\ kgm^2$
b'	6152 kg/s	$\frac{8}{3\pi} C_d \frac{\rho}{2} D u_{RNa} L = 6152$ kg/s
B'	102540 kgm^2/s	$B' = \frac{b' L^2}{12} = 102540\ kgm^2/s$

10.2.3. Verification of the hydrodynamic loads on a buoy

The implementation of the vertical hydrodynamic loads on a vertical cylinder are discussed in section 9.2.4. These methods need to be verified to prove its accuracy. The method for the calculation and the implementation of the Froude-Krylov force, the added mass and damping will be verified.
The added mass term will be verified by checking the outcome of the function with hand calculations that are both based on the same method. This will be done for 5 different situations as indicated in Table 10.6. The calculations are done for cylinders with the same displacement but varying diameter. In the last column of Table 10.6 the difference between the result of the MATLAB function and the manual calculations. This indicates a trustworthy result.

Table 10.6: Verification of added mass of a heaving buoy for different dimensions

D (m)	**Volume (m^3)**	**Draft (m)**	α	**C_a**	**m' (kg) Manual**	**m' (kg) MATLAB**	**Difference**
5	6	0.31	6.43	1.18	25198	24994	1%
4	6	0.48	5.26	1.2	13120	13838	5%
3	6	0.85	2.22	1.37	6319	6657	5%
2	6	1.91	0.66	1.75	2392	2447	2%
1	6	7.64	0.08	2	342	347	2%
3	53.0	7.5	0.25	1.95	8994	9337	4%

For the verification of the damping term two steps should be made. First, the calculation of the critical damping needs to be checked. Second, the realism of the percentage of the critical damping should be assessed. The first part will be done here. The second part will be assessed in next section. For this verification a percentage of 0.5% is taken into account. As can be seen in Table 10.7.

Table 10.7: Verification of the damping on a heaving buoy

D (m)	Volume (m^3)	Draft (m)	Mass (kg)	Stiffness (n/m)	b (kg/s) Manual	b (kg/s) MATLAB	Difference
5	6	0.306	6150	197434	348	348	0%
4	6	0.477	6150	126358	279	279	0%
3	6	0.849	6150	71076	209	209	0%
2	6	1.910	6150	31589	139	139	0%
1	6	7.639	6150	7897	70	70	0%

10.2.4. Verification of the magnitude of velocity

In the verification of the damping forces a fixed value was taken for u_{RNa} to simplify the verification procedure. Therefore the verification of the magnitude of the relative velocity is executed hereafter. When creating the function in MATLAB this was done step wise. Figure 9.6b is recalled for clarity on the steps that are taken.

1. The first step takes into account the average response of the two buoys and only the vertical movement of the beam.

2. Next the difference in response of the two ends of the beams was taken into account and assessed on ten equally distributed places on the beam. The result of this step is indicated with $u_{RNa}*$ in Table 10.8.

3. Lastly the horizontal velocity of the fluid was taken into account. Therefore the method discussed in section 9.2.3 on page 9.2.3 was used.

This helped to create confident in the code. As the build up of the tool proved to follow the logic. Still a step wise verification for beams with a relative simple orientation is executed.

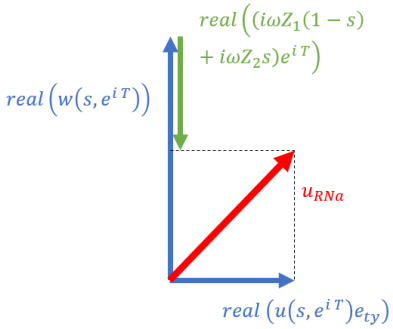

Figure 9.6b: Vector diagram for the calculation of the relative perpendicular velocity

Table 10.8: Verification of the magnitude of velocity indicating the position and response. Additionally the simplified relative velocity, the maximum velocity and the average maximum velocity are shown.

	ω=1 rad/s; ζ=1 m ; λ=61.63 m						
	Pos 1	**Pos 2**	**Resp 1**	**Resp 2**	$\mathbf{u_{RNa}}*$	**max**	$\mathbf{u_{RNa}}$
1	(0,0,0)	(0,0.1,0)	0	0	1	1	1
2	(0,0,0)	(0,0.1,0)	1	1	0	1	1
3	(0,0,0)	(0,0.1,0)	-1	-1	2	2	2
4	(0,0,0)	(0,0.1,0)	1j	1j	1.39	1.61	1.61
5	(0,0,0)	(0,0.1,0)	-1j	-1j	1.39	1.61	1.61
6	(0,0,0)	(0,0.1,0)	-1j	1j	1	1.61	1.17
7	(0,0,0)	(λ,0,0)	1	1	0.91	2	0.91
8	(0,0,0)	(0,λ,0)	1	1	1	1	1

Table 10.8 indicates the steps that are taken. For all rows a rather simple and short beam is chosen. Only the last part indicates a beam length that equals the wave length. The first four columns indicate the location and the response of the cylinder. The fifth column indicates the outcome form the function when the motion of the fluid in horizontal direction is eliminated (u in Figure 9.6b). The sixth column indicates the maximum velocity obtained over the beam length and over time. The last column indicates the outcome of the function as implemented in the code.
The following conclusions can be drawn from Table 10.8. The verification is mainly based on logic thinking and by comparing the build up stages of the derivation. The numbers refer back to Table 10.8.

1. Considering a fixed beam the wave amplitude times the angular frequency is given by the function.
2. When a beam follows the wave in vertical direction, there is only relative velocity in horizontal direction that equals the wave amplitude times the angular frequency. The simplified calculation method (u_{RNa}*) indicates no amplitude as the fluid velocity in horizontal direction is not taken into account.
3. The structure velocity is in anti phase with respect to the wave velocity and therefore results in an amplitude of 2.
4. When the construction moves with a phase angle of 90 degrees a value a bit bigger then $\sqrt{2}$ is obtained.
5. The same logic as previous point holds also for this case.
6. When considering a fixed beam over its beam length the average velocity should be 1. Then this beam is moving with the fluid in vertical direction it should be slightly lower. (Be aware of the orientation difference)
7. The same beam is now oriented in y-direction. Consequently, the value obtained should be the same as the second step of the iteration.

The function is hereby tested in a select number of situations and has shown to return the correct value.

10.3. Verification of total system

To verify the total system the structure will be build up in several steps. First, a single buoy will be analysed. Then two independent buoys will be analysed, the hydrodynamic loads will be build up step wise. Then the system will be scaled up to a three and five buoys system. In this build up it can be assessed if the obtained response follows a logic pattern.

10.3.1. Response of a heaving buoy

The most simplified layout of the system exists of one buoy. In section 10.2.3 all separate loads involved in the heaving buoy were verified. This is now combined to obtain the response of a heaving buoy. As the calculation tool is not made to test one individual buoy parts of the program are exactly copied

and reconfigured to obtain the response of one buoy. As a verification step some variations on the characteristics of the buoy have been executed.
A buoy with a diameter of 3 meters, a draft of 9 meters (Table 10.10) and a critical damping ratio of 0.005 is taken as starting point of the variation. The buoy is located in to origin (0,0,0). The draft (Z), the diameter (D) and the critical damping ration (CR) are respectively varied from the starting point. For these specific variations the eigenfrequency will be calculated in a simplified way as indicated in equation 10.11.

$$\omega_n = \sqrt{\frac{K}{m + m'}} \tag{10.11}$$

In Figure 10.6 the result can be seen and the following remarks can be made. The initial buoy is each time indicated with the bolt black line.

- The variation of the buoy draft is shown in Figure 10.6a and Figure 10.6d. An estimation of the eigenfrequency is made with equation 10.11 and this is compared with the results of the code that was obtained by an eigenvalue solution and indicated in Table 10.11. For this calculation the added mass was estimated to be 9.3 metric tons with the method indicated in section 7.4.2.

Table 10.9: Eigenfrequencies of a buoy related to the draft

Draft	Estimated eigenfrequency based on equation 10.11	Obtained eigenfrequency
15	0.78	0.78
11	0.89	0.89
9	0.98	0.98
7	1.09	1.09
5	1.25	1.25
3	1.51	1.54

  The obtained eigenfrequencies of the third column of Table 10.9 are indicated with the red dotted line in the Figure 10.6. Both calculations are give in highly similar results.

- By varying the diameter in Figure 10.6b and Figure 10.6e are obtained. Only the added mass has an influences on the eigenfrequency because the stiffness and the mass of the displaced water have the same proportion. The proportion of the added mass in respect to the total mass (added and actual mass) is respectively 27%, 19%, 13%, 4.6% and 2.3%. Therefore the variation of the eigenfrequency is small and reduces over the variations.

- From Figure 10.6c and 10.6f the effect of the chosen damping ratio can be seen. Comparing the response with a damping ration of 0.005 with graphs found in [18] an damping ratio of 0.005 is a reasonable choice. As similar frequency responses were seen in the simulations shown in Journée and Massie [18].

- In Figure 10.6a and Figure 10.6b it can be seen that the damping is related to the mass and the spring stiffness of the system. As the mass of the buoy increases with the draft or the diameter or when the stiffness increases by an increase of diameter the damping peak turns out to be lower.

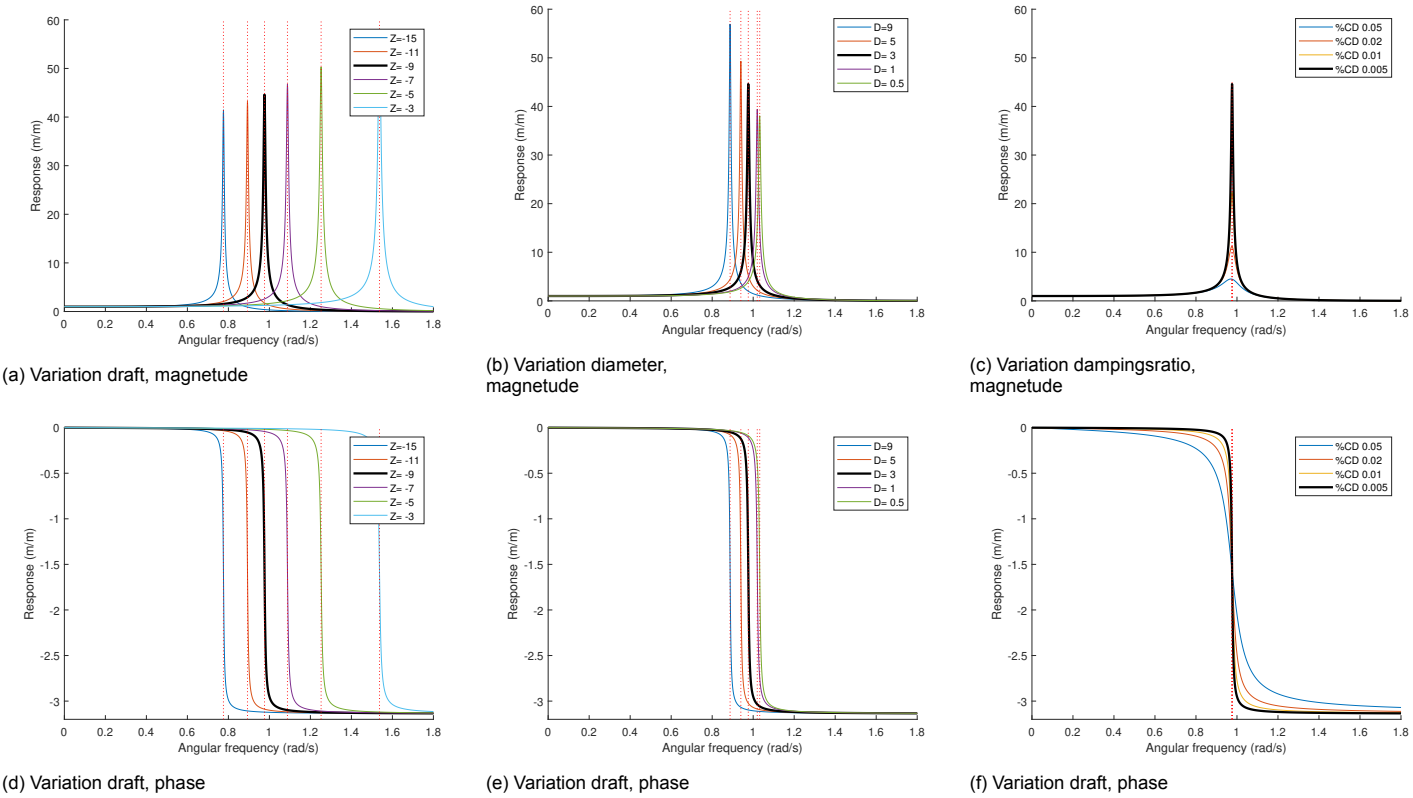

(a) Variation draft, magnetude

(b) Variation diameter, magnetude

(c) Variation dampingsratio, magnetude

(d) Variation draft, phase

(e) Variation draft, phase

(f) Variation draft, phase

Figure 10.6: Frequency response of a heaving buoy for varying characteristics where the doted lines indicated the eigenfrequencies.

10.3.2. Two buoy system

The next step is to simulate two buoys that are connected with one beam. First, two independent buoys will be simulated. Then a system where the two buoys are connected with a beam. Both systems have the same displacement. The extra water displacement of the submerged beam will be compensated by reducing the draft of the buoys. The Morison contributions indicated in differential equation 8.8 will first be excluded and then they will be added step wise to the solution. The first buoy is located at the origin. The second buoy is located at $x = 27\frac{\sqrt{2}}{2}$m and $y = 27\frac{\sqrt{2}}{2}$m giving an overall length of 27 meters. This system is visualised in Figure 10.7 and the dimensions are indicated in table 10.10.

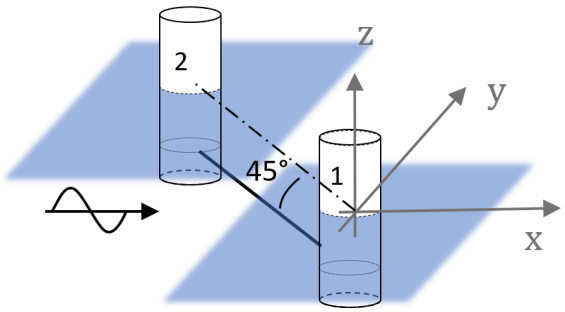

Figure 10.7: Visualisation of the two buoy system

Table 10.10: Dimensions of the two buoy systems

	Unconnected system	Connected system
Diameter buoy (m)	3	3
Draft buoy (m)	9	7.5
Position buoy 1	(0, 0, 0)	(0, 0, 0)
Position buoy 2	$(27\frac{\sqrt{2}}{2}, 27\frac{\sqrt{2}}{2}, 0)$	$(27\frac{\sqrt{2}}{2}, 27\frac{\sqrt{2}}{2}, 0)$
Diameter beam (m)	0	1
Length beam (m)	0	27
Draft centre line beam (m)	0	2
Volume total system (m^3)	127	127
Mass total system (metric ton)	130	130

Comparing a one and a two buoy system

First two buoys are simulated that have the same dimensions as in the previous section. The simulation of two independent buoys is indicated with the black line in Figure 10.8a. The frequency response does not depend on the position. Only the phase depends on the location (Figure 10.8c). Then a second system of two connected buoys is simulated. This connected system has a beam in between the two buoys. The hydrodynamic loads on the beam due to the hydrodynamic environment are not yet incorporated. Only the mass and the buoyancy is taken into account in Figure 10.8a and Figure 10.8c. Secondary, the moment of inertia of the beam is added, indicated with the red line in Figure 10.8d and Figure 10.8b.
For the two buoy system the eigenfrequencies were obtained with the eigenvalue method explained in section 8.2 by the calculation tool. The eigenvectors indicated two corresponding eigenmodes. The first eigenmode corresponds with a heave motion of the buoys where both buoys move in phase. The second eigenmode indicates that the buoys move with opposite phase. This corresponds with a pitch movement. In Figure 10.8c and Figure 10.8d the phase difference at the second frequency is approximately π this also indicates the pitch motion.

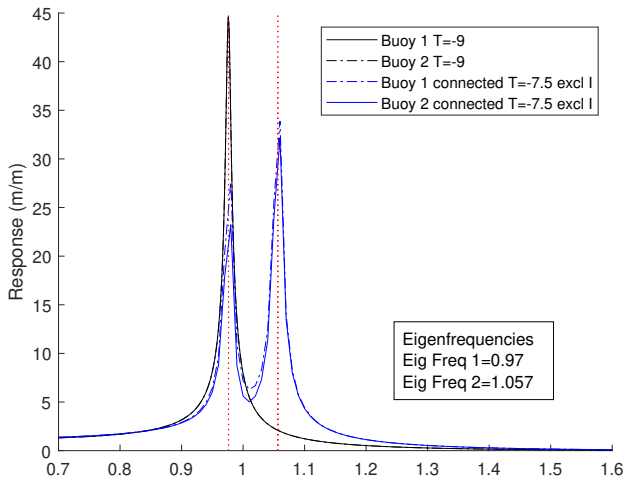

(a) Difference in response due to connecting of two buoys: Frequency response

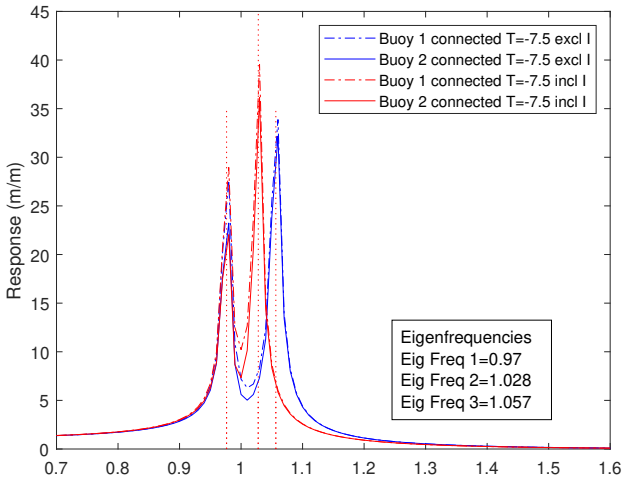

(b) Difference in response due to incorporation of moment of inertia: Frequency response

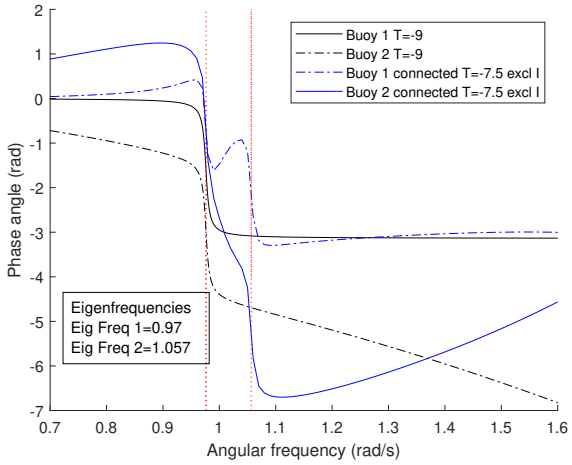

(c) Difference in response due to connecting of two buoys: Phase angle

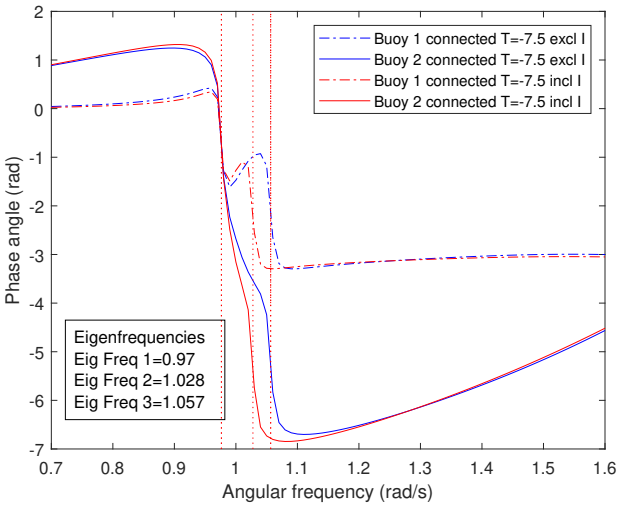

(d) Difference in response due to incorporation of moment of inertia: Phase angle

Figure 10.8: Analysis of two buoys, unconnected (black), connected excl moment of inertia (blue), connected incl moment of inertia (red).

In Figure 10.8a it can be seen that the lowest of the two eigenfrequencies of the connected buoys (i.e. the eigenfrequency corresponding with the coupled eigenmode) is exactly the same as the unconnected system. This is because the mass of the system is equal and the diameter of the buoy is equal as the Morison contributions are not yet taken into account. Therefore the added mass of the buoys is equal and the stiffness in heave direction is equal. In Figure 10.8a, the system is simulated excluding the moment of inertia. When the inertia of the connecting beam is added in Figure 10.8b, the second eigenfrequency is lowered because of the addition of the inertia. The system could be compared with a system where the beam is located above the water as no damping and added mass on the connecting beam is taken into account. Still it is assumed that the beam contributes to the buoyancy of the system. As result of the known eigenmode the eigenfrequency can be estimated. In Figure 10.9 only the rotation around point “O” is allowed. This motion will be called the pitch motion of the connecting beam.

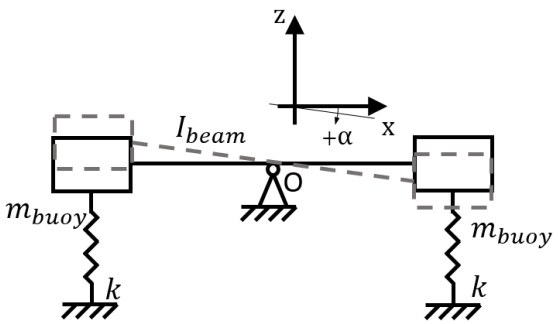

Figure 10.9: FBD indicating pitch motion

For this simplified system in Figure 10.9 the eigenfrequency can be calculated. Based on this figure the moment balance (differential equation) around point “O” is presented in equation 10.12 this will lead to the eigenfrequency when substituting equation 8.10 on page 70.

$$I\ddot{\alpha} = \sum M \tag{10.12}$$

$$I\ddot{\alpha} = -2k\alpha\left(\frac{L_{beam}}{2}\right)^2 \tag{10.13}$$

$$-I\omega^2 A = -2kA\left(\frac{L_{beam}}{2}\right)^2 \tag{10.14}$$

$$\omega^2 = \frac{2k\left(\frac{L_{beam}}{2}\right)^2}{I_{beam} + 2I_{buoy}} = \frac{k\frac{L_{beam}^2}{2}}{\frac{1}{12}m_{beam}L_{beam}^2 + \frac{1}{2}m_{buoy}L_{beam}^2} \tag{10.15}$$

The eigenfrequency that was obtained included the same added mass of 9.3 metric tons as discussed before. This results in an eigenfrequency of 1.0277 rad/s compared to an eigenfrequency of 1.03 rad/s obtained by the MATLAB code and shown in Figure 10.8.

Substitution of the Morison terms in the two buoy system

At this point the terms related to the hydrodynamics of the connecting beam in equation 8.8 need to be substituted in the derivation of the response.

$$\mathbf{F}_{buoy} + \left(\left[\mathbf{F}_{FK,HM,\zeta}\right] + \left[\mathbf{F}_{VD,\zeta}\right] + \frac{\left[\mathbf{T}_{FK,HM,\zeta}\right]}{L} + \frac{\left[\mathbf{T}_{VD,\zeta}\right]}{L}\right)\vec{1}_n = \left([\mathbf{M}] + [\mathbf{m}'] + \frac{[\mathbf{I}']}{L}\right)\ddot{\boldsymbol{z}} + \left([\mathbf{B}] + [\mathbf{b}'] + \frac{[\mathbf{B}']}{L}\right)\dot{\boldsymbol{z}} + [\mathbf{K}]\boldsymbol{z} \tag{8.8}$$

Firstly, the right side of the equation 8.8 will be composed. This will be done stepwise starting with the added mass ($[\mathbf{m}']$). Secondly the left side of equation 8.8 will be taken into account.
The result of these first steps can be found in Figure 10.10. Figure 10.10a indicates in red the outcome as it was given in Figure 10.8b. Therefore the same colour is used. The green line in the Figure 10.10a includes the effect of the added mass ($[\mathbf{m}']$). In Figure 10.10b the same green line is plotted to indicate the difference with the magenta line which include both the added mass and the moment of inertia of the added mass ($[\mathbf{m}']$ and $[\mathbf{I}']$). Consequently the evolution and differences are visualised by using the same colour in the following graph.
By step wise building up the right side of the differential equation the following conclusions can be drawn. The numbers herafter refer to the numbers in brackets in the legend of the figure and the captions of the figures.

1. $\mathbf{F}_{buoy} = ([\mathbf{M}] + [\mathbf{m}'])\,\ddot{\boldsymbol{z}} + [\mathbf{B}]\dot{\boldsymbol{z}} + [\mathbf{K}]\boldsymbol{z}$: Because off the added mass term for translation the first eigenfrequency peak related to the combined heave motion, which is in this case the lower frequency, is shifted to a lower frequency. The eigenfrequency peak related to the pitch motion is unchanged.

2. $\mathbf{F}_{buoy} = \left([\mathbf{M}] + [\mathbf{m}'] + \frac{[\mathbf{I}']}{L}\right)\ddot{\boldsymbol{z}} + [\mathbf{B}]\dot{\boldsymbol{z}} + [\mathbf{K}]\boldsymbol{z}$: The moment of inertia resulting from the added mass of the beam is added to the equation. This results in a shift of the second eigenfrequency peak to a lower frequency.

3. $\mathbf{F}_{buoy} = \left([\mathbf{M}] + [\mathbf{m}'] + \frac{[\mathbf{I}']}{L}\right)\ddot{\boldsymbol{z}} + ([\mathbf{B}] + [\mathbf{b}'])\,\dot{\boldsymbol{z}} + [\mathbf{K}]\boldsymbol{z}$: The damping for translation in z-direction is added. This results in a lower response on the eigenfrequency related to the heave motion.

4. $\mathbf{F}_{buoy} = \left([\mathbf{M}] + [\mathbf{m}'] + \frac{[\mathbf{I}']}{L}\right)\ddot{\boldsymbol{z}} + \left([\mathbf{B}] + [\mathbf{b}'] + \frac{[\mathbf{B}']}{L}\right)\dot{\boldsymbol{z}} + [\mathbf{K}]\boldsymbol{z}$: Lastly the damping for the pitch motion is added. This reduces the response peak at the second eigenfrequency significantly.

The phase difference at the first and the second eigenfrequency still indicate respectively the found eigenmode.

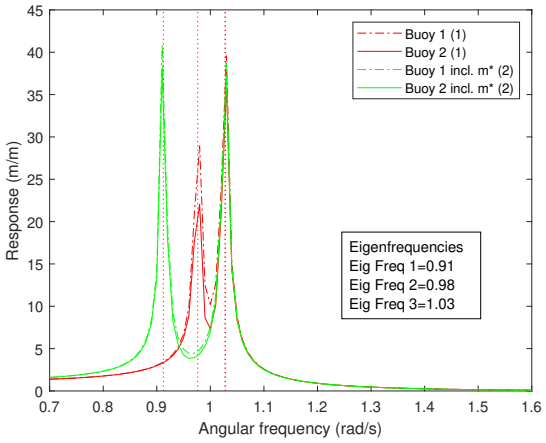

(a) Frequency response excluding and including added mass of the beam (1)

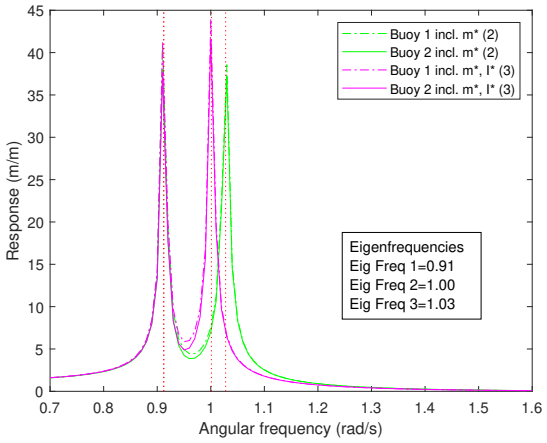

(b) Frequency response excluding and including inertia due to added mass of the beam (2)

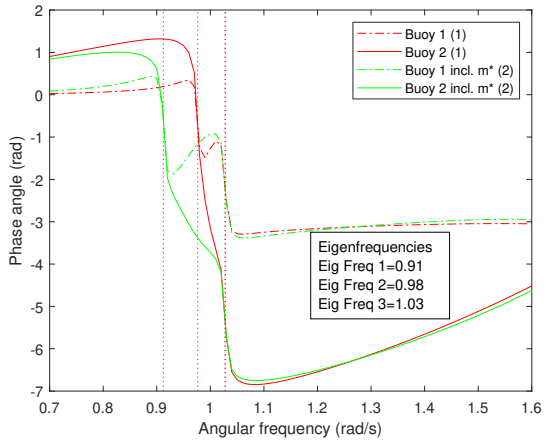

(c) Phase angle excluding and including added mass of the beam (1)

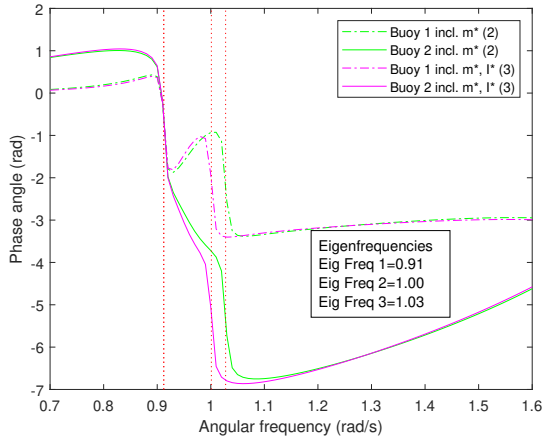

(d) Phase angle excluding and including inertia due to added mass of the beam (2)

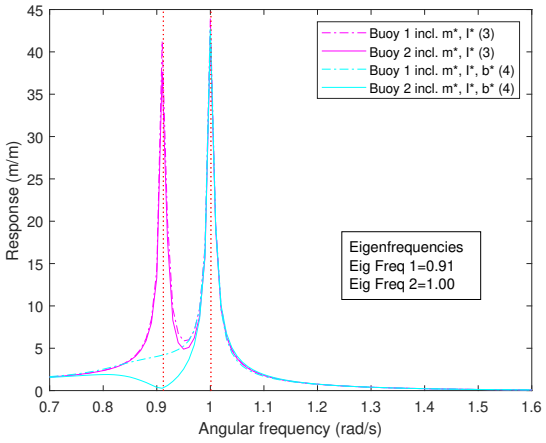

(e) Frequency response excluding and including translation damping on beam (3)

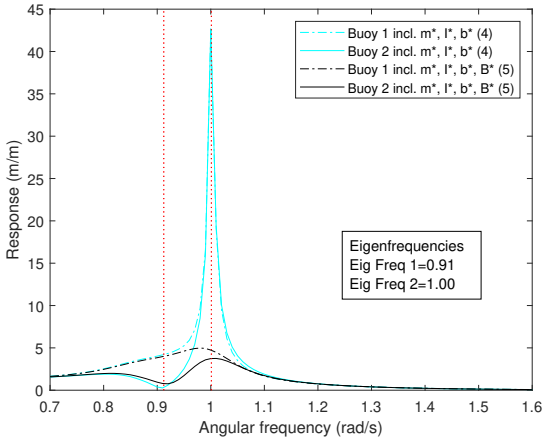

(f) Frequency response excluding and including angular damping on beam (4)

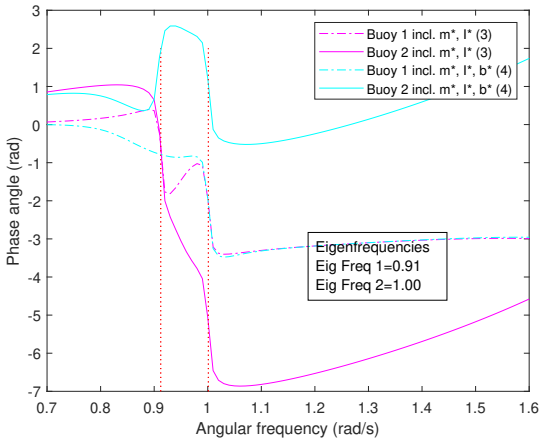

(g) Phase angle excluding and including translation damping on beam (3)

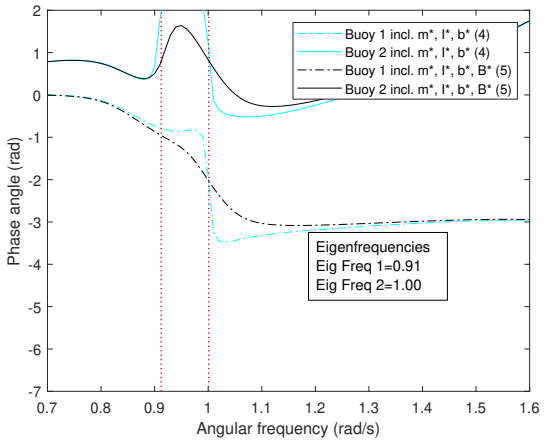

(h) Phase angle excluding and including angular damping on beam (4)

Figure 10.10: Composition of the right side of equation 8.8 for the analysis of a two buoy system.

At this point the response got significantly lower due to the damping. Therefore, in the following figures, the axis limits are changed. For adding the terms of the right side of the differential equation the same sequence is applied.

5. $\mathbf{F}_{buoy} + \left(\left[\mathbf{F}_{FK,HM,\zeta}\right]\right)\vec{1}_2 = \left([\mathbf{M}] + [\mathbf{m}'] + \frac{[\mathbf{I}']}{L}\right)\ddot{\boldsymbol{z}} + \left([\mathbf{B}] + [\mathbf{b}'] + \frac{[\mathbf{B}']}{L}\right)\dot{\boldsymbol{z}} + [\mathbf{K}]\boldsymbol{z}$

6. $\mathbf{F}_{buoy} + \left(\left[\mathbf{F}_{FK,HM,\zeta}\right] + \left[\mathbf{F}_{VD,\zeta}\right]\right)\vec{1}_2 = \left([\mathbf{M}] + [\mathbf{m}'] + \frac{[\mathbf{I}']}{L}\right)\ddot{\boldsymbol{z}} + \left([\mathbf{B}] + [\mathbf{b}'] + \frac{[\mathbf{B}']}{L}\right)\dot{\boldsymbol{z}} + [\mathbf{K}]\boldsymbol{z}$

7. $\mathbf{F}_{buoy} + \left(\left[\mathbf{F}_{FK,HM,\zeta}\right] + \left[\mathbf{F}_{VD,\zeta}\right] + \frac{[\mathbf{T}_{FK,HM,\zeta}]}{L}\right)\vec{1}_2 = \left([\mathbf{M}] + [\mathbf{m}'] + \frac{[\mathbf{I}']}{L}\right)\ddot{\boldsymbol{z}} + \left([\mathbf{B}] + [\mathbf{b}'] + \frac{[\mathbf{B}']}{L}\right)\dot{\boldsymbol{z}} + [\mathbf{K}]\boldsymbol{z}$

8. $\mathbf{F}_{buoy} + \left(\left[\mathbf{F}_{FK,HM,\zeta}\right] + \left[\mathbf{F}_{VD,\zeta}\right] + \frac{[\mathbf{T}_{FK,HM,\zeta}]}{L} + \frac{[\mathbf{T}_{VD,\zeta}]}{L}\right)\vec{1}_2$
$= \left([\mathbf{M}] + [\mathbf{m}'] + \frac{[\mathbf{I}']}{L}\right)\ddot{\boldsymbol{z}} + \left([\mathbf{B}] + [\mathbf{b}'] + \frac{[\mathbf{B}']}{L}\right)\dot{\boldsymbol{z}} + [\mathbf{K}]\boldsymbol{z}$

Adding the forces caused by the wave on the beam only slightly influence the response of the structure. It can be concluded that response is mainly cased by the forces on the buoys.
In general the following items can be conclude. First there is a peak related to the heave motion and a more significant one to the pitch motion for this particular system. At the pitch eigenfrequency it can be seen that the phase difference between the buoys highers to π.

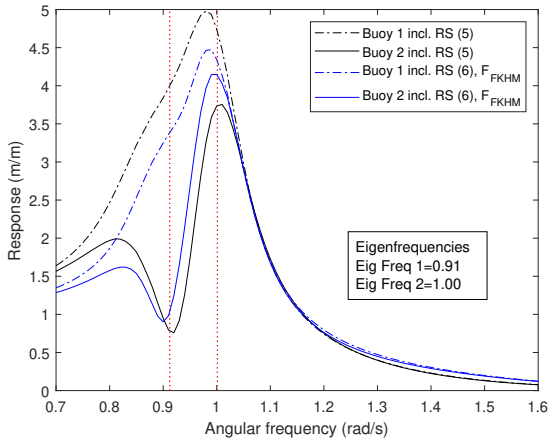

(a) Frequency response excluding and including Froude-Krylov and hydrodynamic mass force (5)

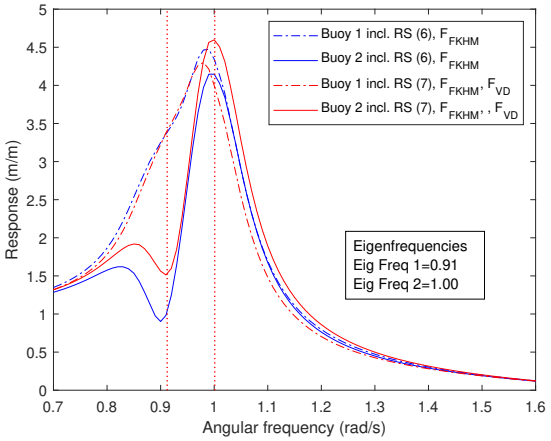

(b) Frequency response excluding and including viscous drag force (6)

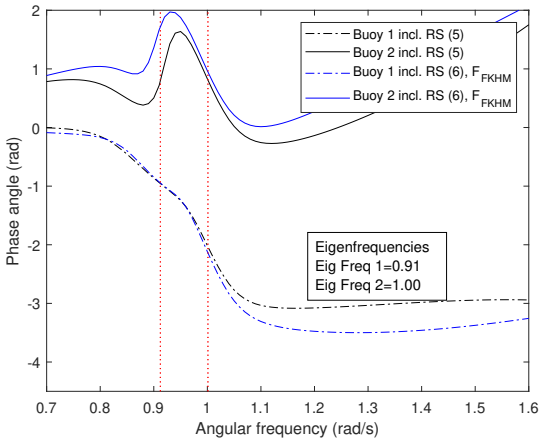

(c) Phase angle excluding and including Froude-Krylov and hydrodynamic mass force (5)

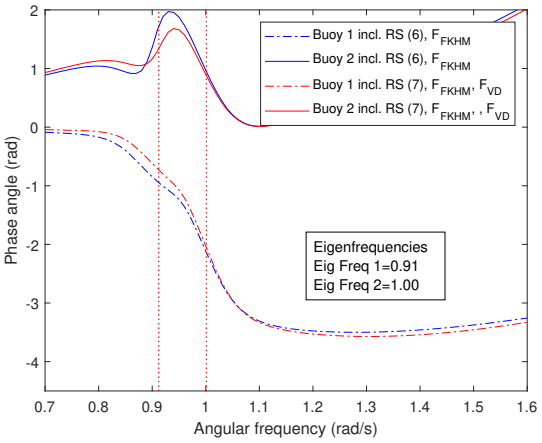

(d) Phase angle excluding and including viscous drag force (6)

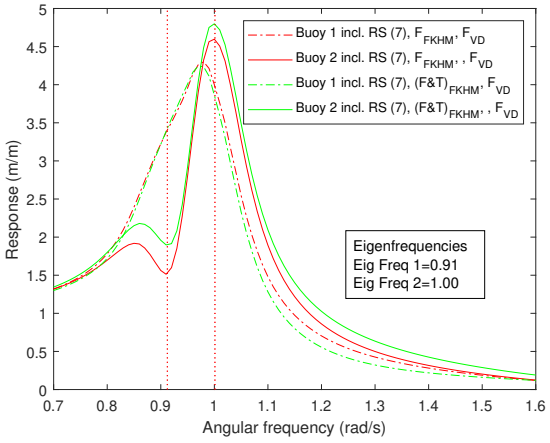

(e) Frequency response excluding and including Froude-Krylov and hydrodynamic mass torque (7)

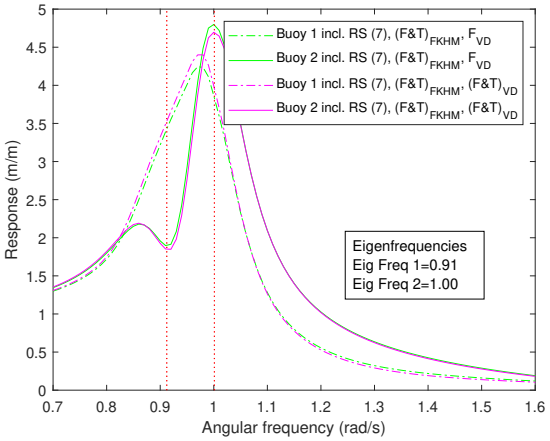

(f) Frequency response excluding and including viscous drag torque (8)

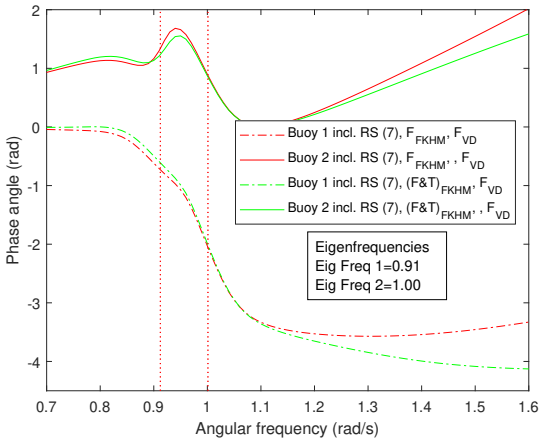

(g) Phase angle excluding and including Froude-Krylov and hydrodynamic mass torque (7)

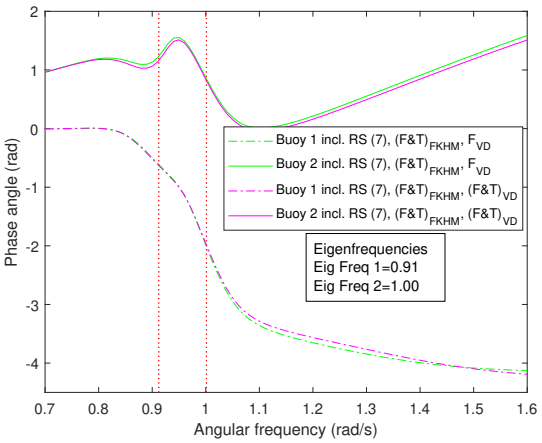

(h) Phase angle excluding and including viscous drag torque (8)

Figure 10.11: Composition of the left side of equation 8.8 for the analysis of a two buoy system.

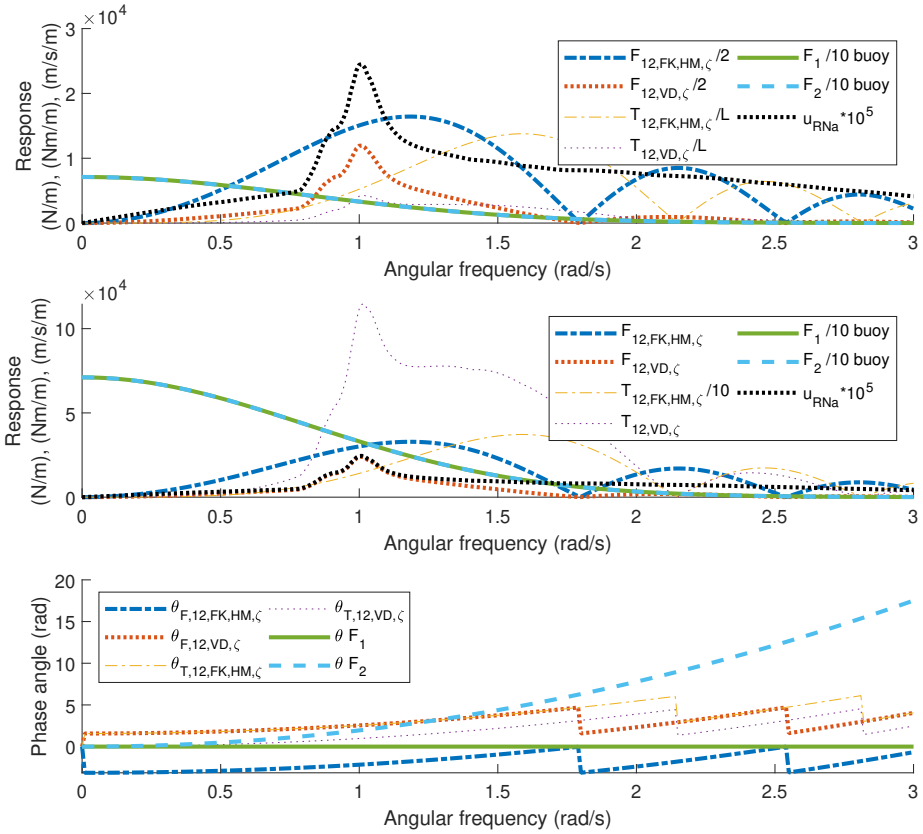

Figure 10.12: Force contribution on the two buoy system, F: force, T: moment, u: velocity

The force contributions that lead to the previously discussed response can be found in Figure 10.12. When building up the force vector equation 10.16 is found for the first entry of the force vector of the differential equation.

$$[\mathbf{F}]_1 = F_1 + \frac{F_{12,FK,HM,\zeta}}{2} + \frac{F_{12,VD,\zeta}}{2} + \frac{T_{12,FK,HM,\zeta}}{L} + \frac{T_{12,VD,\zeta}}{L} \tag{10.16}$$

In the first graph of Figure 10.12 the force contribution that act on the buoys multiplied with the constants as indicated in equation 10.16 can be found. It must be noted that the force on the buoys is also divided by ten in the first and the second graph for the readability of the graph. The second graph of Figure 10.12 indicates the magnitude of the moment and forces on the beam and buoys. Also, the moment due to the Froude-Krylov and Hydrodynamic mass force is divided by ten for the readability of the graph. In both graph $u_{RNa} * 10^5$ is shown. The last graph shown in Figure 10.12 indicate the phase angle of the different forces and moments. The following items could be noticed:

- For lower frequencies the force on the buoys is significantly higher than the force on the cylinders. The force on the buoys as shown in the graph is divided by ten. Therefore it can be concluded that the force on the buoy is a factor 10 bigger in the range of 0.5 to 1 rad/s. This is also the range in which the eigenfrequencies of the system appear. The force magnitude on the buoy depends on the wave number which is inverse proportional with the angular frequency. The magnitude of forces on the beams are dependent on the velocity and acceleration in the fluid which increases over the frequency and depends on the response of the system which decreases over the frequency.

- The other forces are in the same order of magnitude. The forces related to the Froude-Krylov and the hydrodynamic mass force are significantly more important than the viscous drag forces.

- The viscous drag force and moment is strongly related to the magnitude of the velocity term u_{RNa} in the lower frequencies.
- All forces contributions on the beam have the tendency to decrease to zero at certain frequencies. This happens when the beam length projected on the wave propagation direction (the x-axis) equals a number of wave lengths. For the beam that was tested the projected beam length was $\frac{27}{\sqrt{2}} = 19.09$ meter. This corresponds with 1.80 rad/s. This the value can also be seen in the graph. When two wave lengths fit in the projected beam length a frequency of 2.54 rad/s is obtained. At this frequency the Froude-Krylov and Hydordynamic mass force is again zero.
- For the torque contribution it is more complicated to find the frequencies where the torque contribution is minimal. As far as the response plot gives insights the response does not become zero with the accuracy over which the simulation is executed. But this could be a result from the angular frequency steps. Finding the minimum in the following formula would lead to these specific points:

$$min\left(\int_0^T \int_{L/2}^{-L/2} \sin\left(\frac{2\pi}{\lambda}x - \sqrt{\frac{g2\pi}{\lambda}}\right)\left(x - \frac{L}{2}\right)dxdt\right) \text{ with } T = \frac{2\pi}{\omega} \tag{10.17}$$

  The analysis of the equation was not executed in this thesis. The following ratio of the projected beam length and wave length have found to lead to a minimum in the moment. $\frac{L_{proj}}{\lambda}$: 1.43, 2.48, 3.51.
- On higher frequencies all forces tend to decrease to zero. This leads to a lower response as can be seen in the frequency response plots in Figure 10.10.
- In the graph with the phase angles it can be seen that there is a relative phase difference between the Froude-Krylov and the viscous drag forces of $\frac{\pi}{2}$ or $\frac{3\pi}{2}$. Which corresponds with the phase angle between the acceleration and the velocity in the fluid.
- When a force contribution related to the Morison equation passes a minimum there is phase shift noticeable in the force.

In Figure 10.13 the dissipated damping energy of the different elements over one period can be seen. The dissipated damping energy is calculated as was indicated in section 8.3.2.

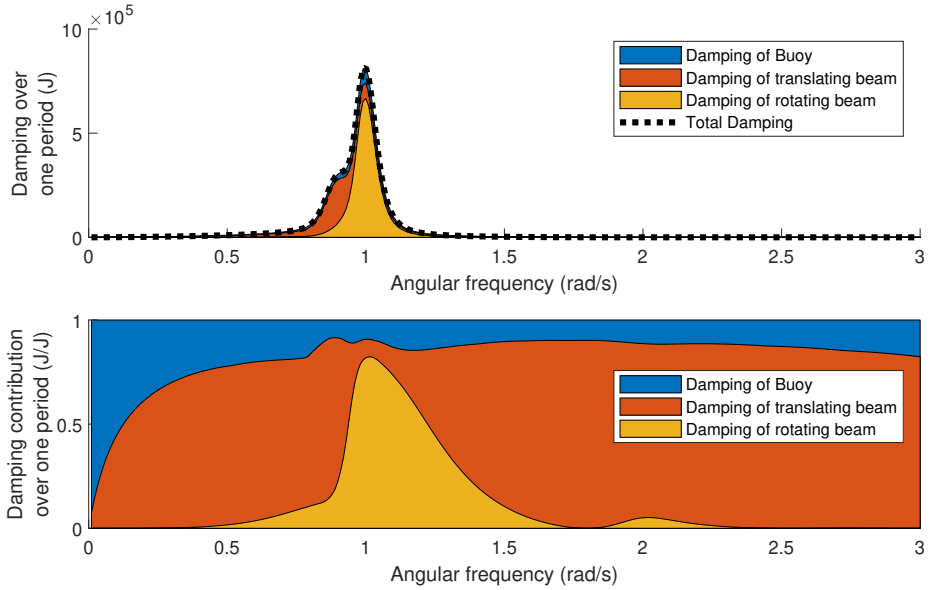

Figure 10.13: Dissipated damping energy on the two buoy system over one period.

The following things can be noticed:

- In the lower frequency range the buoy induces the biggest damping contribution.
- At the eigenfrequency related to the heave motion the dissipated dampings energy related to the translation of the connecting beams increases.
- In the region of the pitch eigenfrequency the damping due to rotation of the beams increases.

The contributions to the mass matrix can be found in Figure 10.14. These are represented in a pie chard as the mass is not dependent on the frequency. First the absolute values of the mass and inertia are displayed respectively in the first and second pie chard. With the differential equation build up as explained in section 9.1 the equation 10.18 is obtained for the first buoy. Based on the constants related to the specific mass contributions the third pie chard of Figure 10.14 is generated.

$$[\mathbf{M}]_1 + [\mathbf{m}]_1 + [\mathbf{I}]'_1 = m_1\ddot{z_1} + m'_1\ddot{z_1} + \left(\frac{m_{12}}{4} + \frac{m'_{12}}{4} + \frac{I_{12}}{L^2} + \frac{I'_{12}}{L^2}\right)\ddot{z_1} + \left(\frac{m_{12}}{4} + \frac{m'_{12}}{4} + \frac{I_{12}}{L^2} + \frac{I'_{12}}{L^2}\right)\ddot{z_2} \tag{10.18}$$

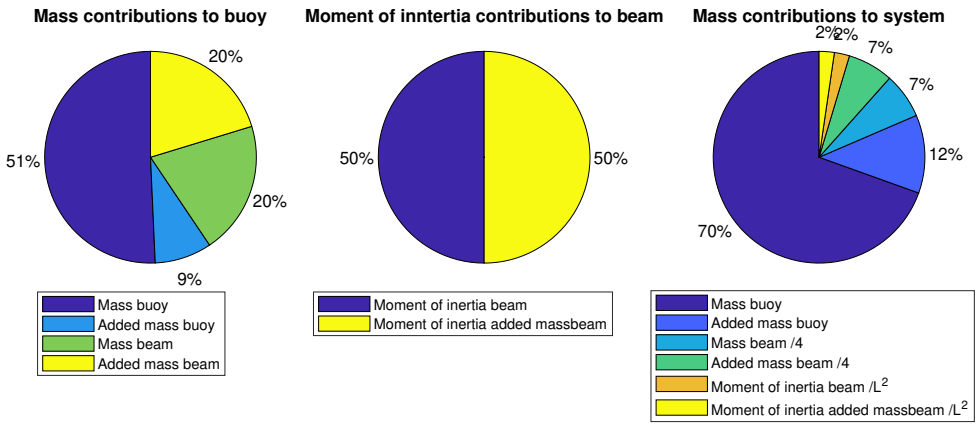

Figure 10.14: Mass contribution on the two buoy system.

10.3.3. Three buoys system

Next a system with three buoys will be simulated. The buoys and beams have the same dimensions as the two buoy system. The coordinates of the buoys can be found in Table 10.11. A visualisation of the system can be seen in Figure 10.15. The beam that connects buoy one and two is exactly the same as the beam of the two buoy system and can therefore be used to compare the results.

Table 10.11: Dimensions of the two buoy systems

	three buoys system
Diameter buoy (m)	3
Draft buoy (m)	7.5
Position buoy 1	(0, 0, 0)
Position buoy 2	$(27\frac{\sqrt{2}}{2}, 27\frac{\sqrt{2}}{2}, 0)$
Position buoy 3	(6.98, 26.08, 0)
Diameter beam (m)	1
Length beam (m)	27
Draft centre line beam (m)	2
Volume total system (m^3)	127
Mass total system (metric ton)	130

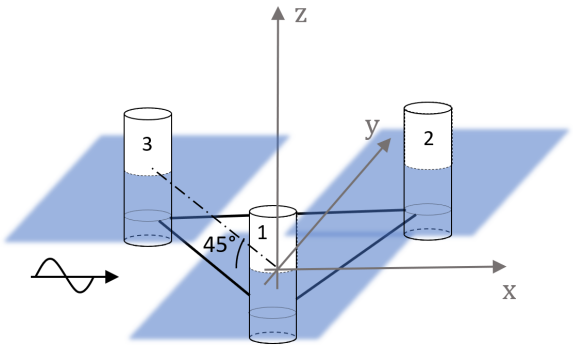

Figure 10.15: Visualisation of the three buoys system

First the eigenmodes and eigenfrequencies were determined and shown in Figure 10.16 and equation 10.19. The first eigenfrequency and eigenmode indicate again a heave motion. The second eigenmode corresponds with a pitch motion where on corner of the triangle moves in opposite direction as the other two corners. In the third eigenmode two corners move in opposite direction where the third corner does not move.

$$\omega_1 = 0.6633 rad/s \begin{bmatrix} 0.5774 \\ 0.5774 \\ 0.5774 \end{bmatrix}, \omega_2 = \omega_3 = 0.8322 rad/s \begin{bmatrix} -0.4082 \\ -0.4082 \\ 0.8165 \end{bmatrix} \& \begin{bmatrix} 0.7071 \\ -0.7071 \\ 0 \end{bmatrix}, \tag{10.19}$$

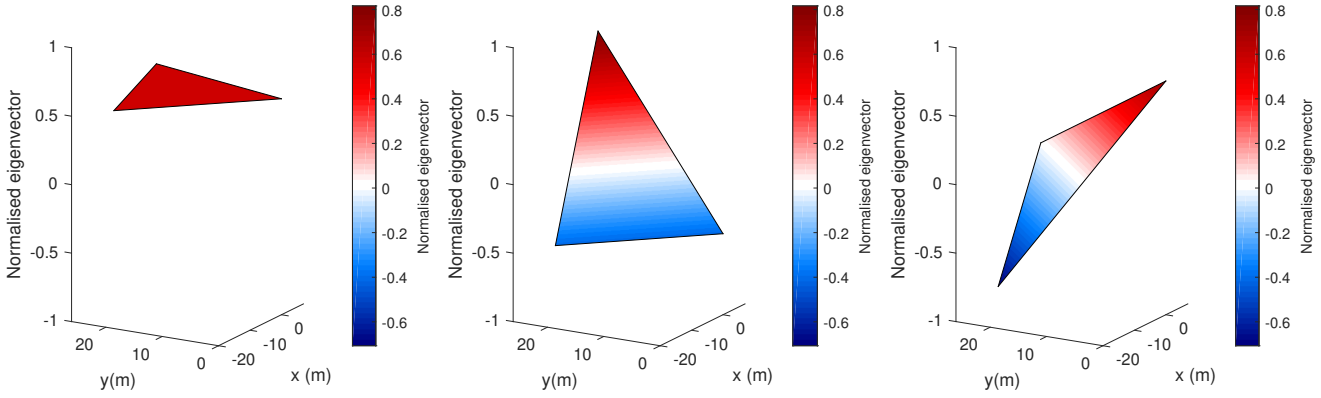

Figure 10.16: Eigenmodes of the three buoys system $\omega_1 = 0.8145$ rad/s, $\omega_2 = \omega_3 = 0.8592$ (1)

The frequency response of the three buoys system can be found in figure 10.17.

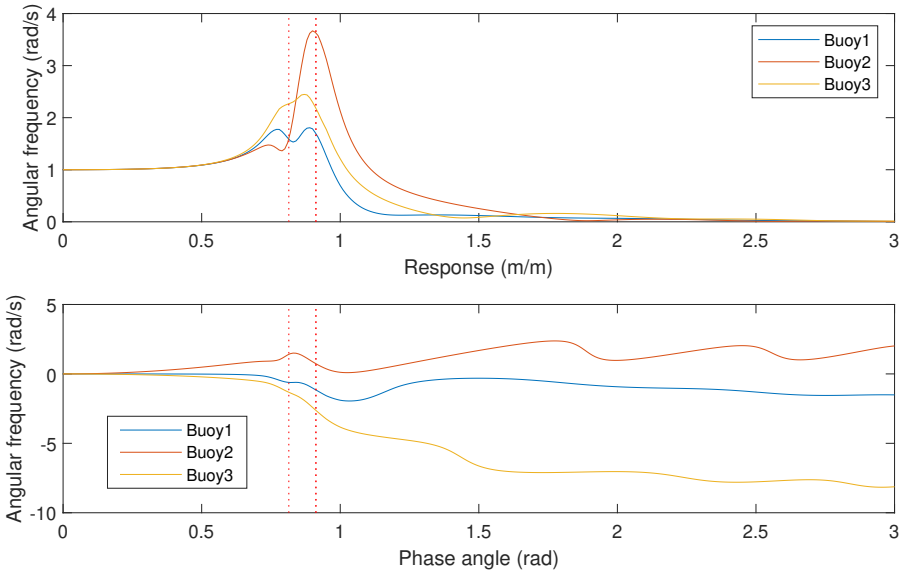

Figure 10.17: Frequency response of the three buoys system

The force contributions on the buoys and the beams are shown in Figure 10.18, Figure 10.19 and Figure 10.20. The results of the two buoy system of section 10.3.2 are indicated in grey. In Figure 10.18 the force and moments due to the Froude-Krylov and hydrodynamic mass terms of the Morison equation are shown. In the first graph the forces as they contribute to the response of the buoy are shown. In the second graph actual value is shown. In the third part the phase angle is shown. As the beam12 has exactly the same orientation and dimensions for the two buoy system and the three buoys system the forces and moment should be identical. When looking at the points where the force curves get zero it can be seen that first $F_{23,FK,HM}$, then $F_{12,FK,HM}$ and lastly $F_{13,FK,HM}$. When the beams are ranged from longest to shortest based on the length projected on the wave propagating direction the same order is seen. This is what can be expected as the force cancels itself out when the wave length equals the beam length projected on the wave propagating direction.

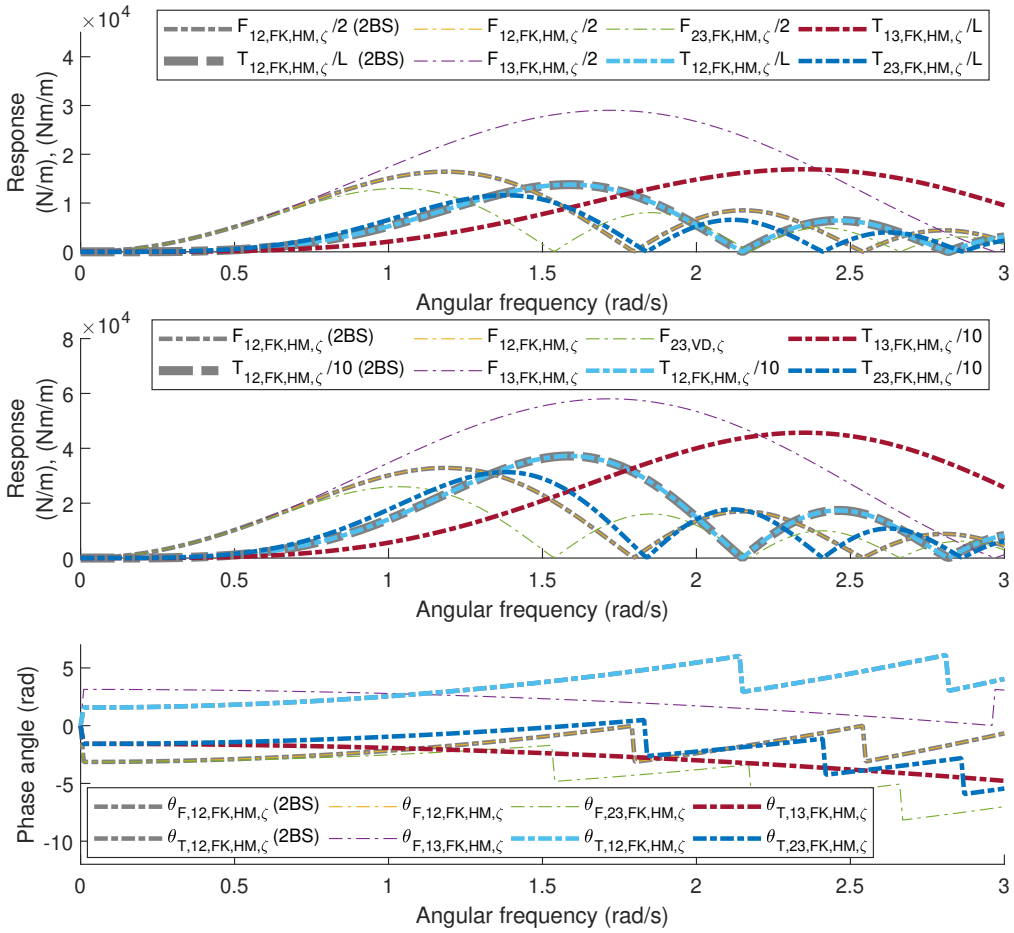

Figure 10.18: Froude-Krylov and hydrodynamic mass forces and moment of the three buoys system in respect to the two buoy system (2BS: grey)

In Figure 10.19 the viscous drag force and moment are shown. The results of the two buoy system are shown in grey. The viscous drag forces is not identical as it is dependent on the relative velocity of the construction in the water. As the response of the three buoys system is slightly lower then the response of the two buoy system the magnitude of the relative velocity should be slightly lower. This can be seen in figure 10.20. As their relative velocity is lower the viscous drag force and torque are slightly lower. The difference in viscous drag force can be seen in Figure 10.19. Here again the beams with the longest projected length on the wave propagating direction tend to go to zero the fastest.

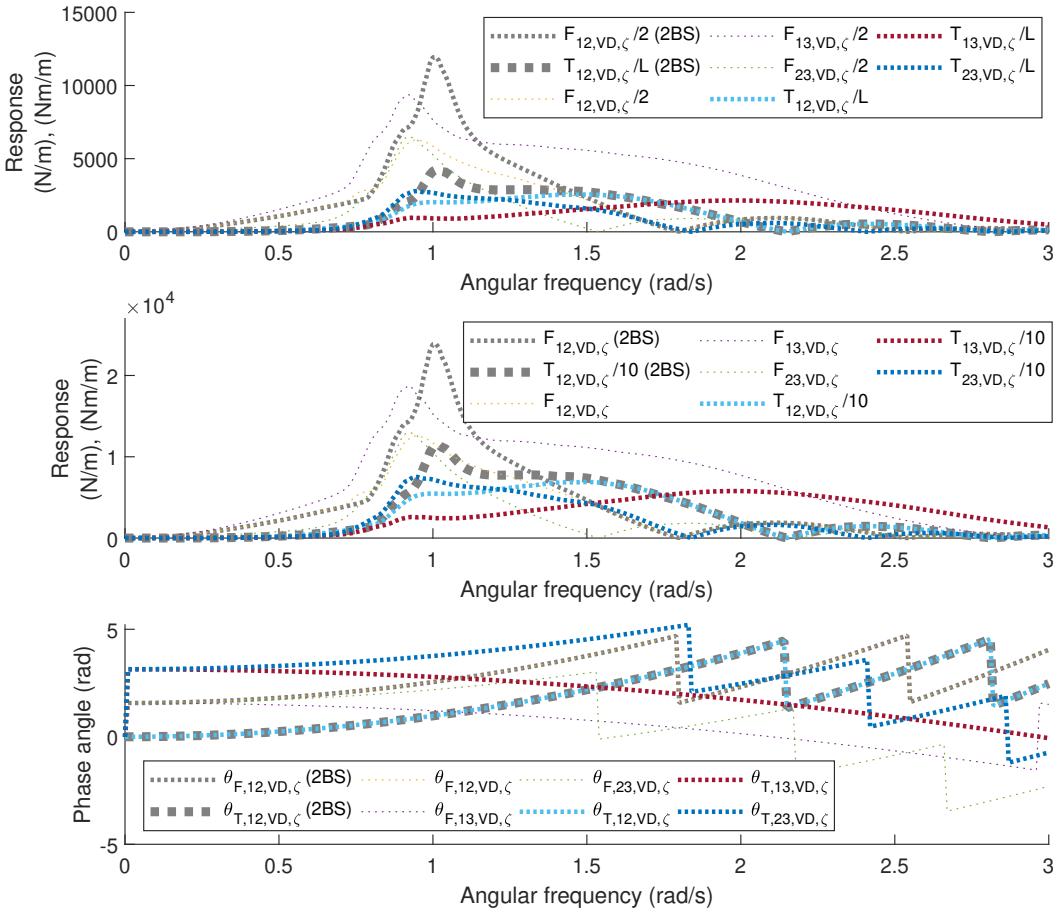

Figure 10.19: Viscous drag forces and moment of the three buoys system in respect to the two buoy system (2BS: grey)

Figure 10.20 indicates the force on the buoy and the relative velocity that is experienced by the beams. As the buoys have the same dimensions the force has the same magnitude. The phase angles of the first buoy is the same and the phase angle of the third buoy diverges down as it is located in negative x-direction.

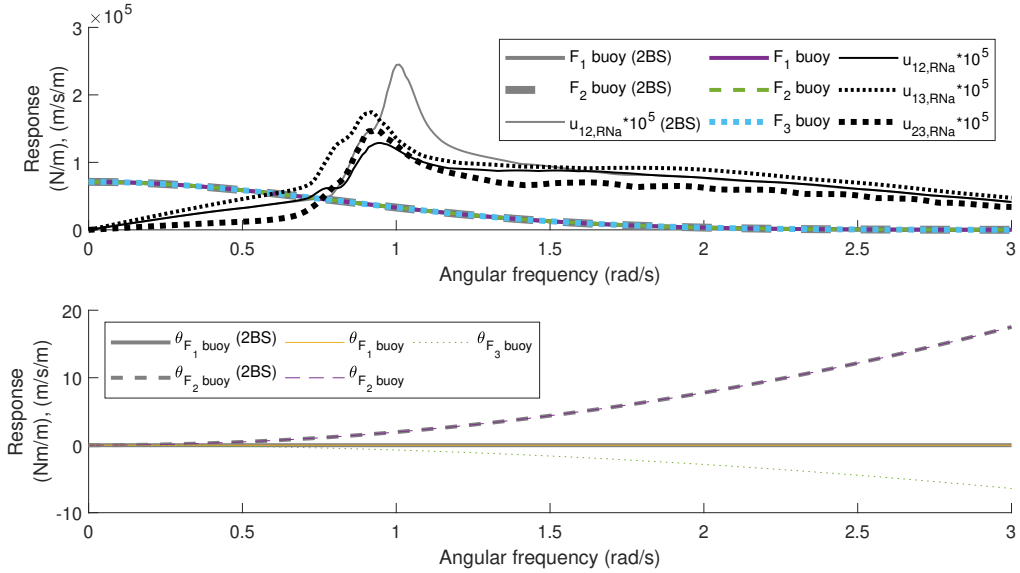

Figure 10.20: Froude-Krylov forces on the buoys and the magnitude of the relative velocity of the three buoys system in respect to the two buoy system (2BS: grey)

Figure 10.21 indicate the dissipated damping energy for translation and rotation of the buoys and the beams of the construction over one period. The rotational damping is more significant then for the two buoy system. This is the result of a relative high number of beams in respect to the number of buoys. Therefore they cause more damping

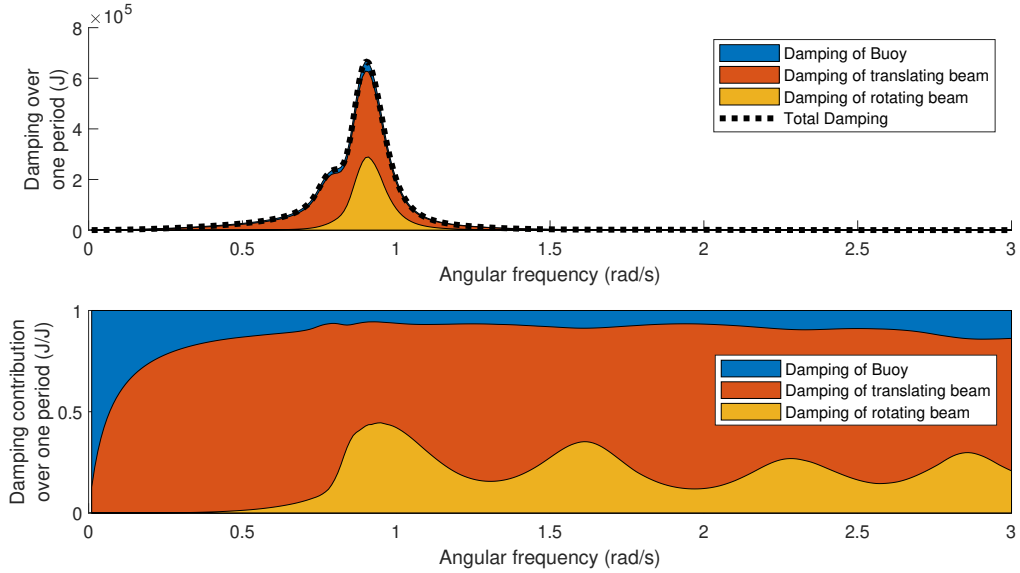

Figure 10.21: Dissipated damping energy on the three buoys system.

10.3.4. Five buoys system

A visualisation of the system can be found in Figure 10.22. Buoy 1, 2 and 4 have the same locations and dimensions as buoys 1, 2 and 3 in the three buoys system. All beams and buoys have the same dimensions throughout the structure and as previous simulations. Due to the orientation the forces magnitude on beam 14 in respect to beam 25 should be the same only the phase angle should be different. The same holds for beams 12, 23 and 45 and for beams 24 and 35.

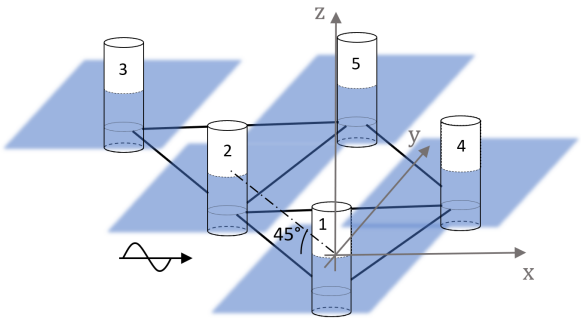

Figure 10.22: Visualisation of the five buoys system

Based on the simulations similar conclusion can be drawn as those that were drawn from the three buoys system. Therefore the detailed analysis can be found in Appendix C.3 on page 174. The conclusions that are relevant for the verification and further analyses are summarised hereafter:

- The first eigenmode indicates a heave motion. The second and third eigenmode indicate a pitch and roll motion.
- The Froude-Krylov and hydrodynamic mass force of the beams with the same location as the three buoys system are identical. The magnitude of the Froude-Krylov and hydrodynamic mass force of the beams with the same orientation is also identical.
- The viscous draft force follows the same trend as seen in the three buoys system but the magnitude is again lower as the response reduces.
- It can be noted that again the response of the system is lower than the three buoys system. Again the relative proportion of beams in respect to buoys did rise. Therefore the damping in the construction has increased.

10.4. Verification of the small angle approximation

With the steps undertaken so far the small angle approximation that was introduced in section 6.2 can be examined. Therefore a five buoys inline system, as indicated in Figure 10.23, is analysed. The angles are indicated in Figure 10.24.

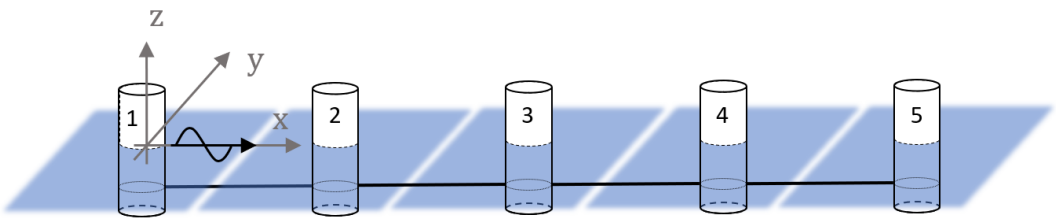

Figure 10.23: Visualisation of the five buoys inline system.

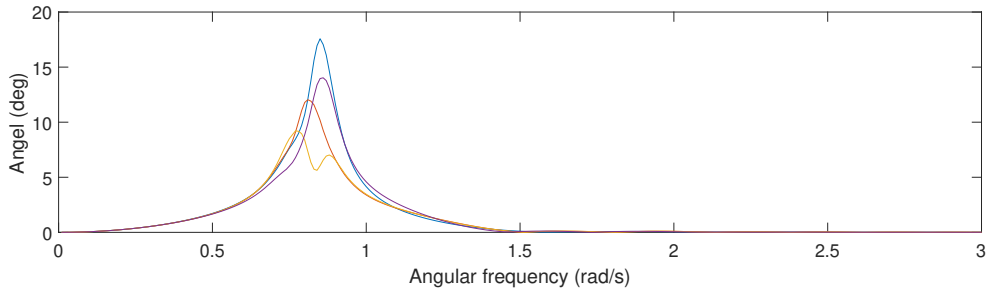

Figure 10.24: Angles appearing in a five buoys inline system

It can be seen that in the range of the eigenfrequencies relatively large angles appear. This means that some caution is needed when interpreting systems with high response. As this is an inline system the ration of beams in respect to buoys is relatively low therefore large responses occur. When larger systems will be simulated this angle will reduce.
It can be concluded that an effective design tool for the estimation of the heave response was developed and verified. The tool makes use of a topology matrix that defines the connections within the structure and makes use of the dimensions of the individual elements to determine the loads. With this information the frequency response of the system can be obtained.

11 Analysis

The research question demands to find a feasible set of design parameters of a buoy and beam structure and to identify the parameters that predominantly minimise the heave response and the relative wave height of the structure. At this point, a calculation tool to obtain the response has been developed and verified. This tool will be used to identify the design parameters that predominantly influence the response in heave direction and the air gap between the triangle platform and the water surface.
When designing the buoy and beam structure for a specific location, the structure's frequency response should be adapted to avoid violent interaction between the triangle platform and the waves. Therefore, two main principles can be applied. In the first place, the system's eigenfrequency should not overlap with the spectrum of the waves. When the response peak overlaps with part of the wave spectrum, resonance will occur. Hence, the eigenfrequencies of the system are ideally higher or lower than the wave spectrum. When lowering the structure's eigenfrequencies with respect to the wave spectrum, the construction will not or only move slightly with the waves. When the eigenfrequencies shift to higher frequencies concerning the wave spectrum, the structure will follow the waves. This means that flexible behaviour will occur.
In chapter 3 multiple flexible designs were discussed. It was believed that a flexible design should be able to change shape to reduce the loads on the structure [36]. Based on this reasoning, the structure needs a high eigenfrequency.
In addition to the avoidance of resonance, the response peaks of the structure should be minimised. A lower response should further reduce the risk of slamming, high loads and violent resonance. The tool developed in this thesis is not ideal for assessing the absolute value of the response peaks due to the linearised viscous damping. The calculation tool underestimates the damping at velocities, i.e. at the eigenfrequency. This results in an overestimation of the response. Still, the response peaks can be compared with respect to each other because the linearisation of the damping results in a proportional equal overestimation of the response.

Design conclusions based on the verification process
Chapter 10 explained the steps that were taken to verify the calculation tool. Based on the verification process, multiple conclusions can already be drawn. As these are relevant for the analysis, these will be summarised here.

- By building up the differential equation in section 10.3.2 on page 101, it could be noted that the damping on the buoy is significantly smaller than the damping on the beam. The resonance peaks strongly decrease when the viscous damping terms of the Morison equation are added to the equation (Figure 10.10e and Figure 10.10f). This finding was confirmed by analysing the energy dissipated of the structural elements, shown in Figure 10.13 and Figure 10.21. Only for low frequencies, the dissipated energy of the damping on the buoys is proportionally bigger. Therefore, the variation of damping on the buoys will not be analysed in this chapter.
- The Froude-Krylov force on the buoys has a significant contribution to the total force acting on the system in the frequency range of the eigenfrequencies. Hence, this force is highly contributing to

the response.

- The first and second eigenfrequencies are, as expected, a heave motion and pitch motion, respectively.

- With an increasing number of buoys, the response decreases. This decline is presumably related to the damping on the beams. When the relative proportion of the number of beams with respect to the number of buoys increases, the damping in the construction increases too. This expansion in damping will lead to lower resonance peaks for larger systems. This conclusion is based on the comparison of Figure 10.11, Figure 10.17 and Figure C.2.

In this chapter, multiple parameters will be varied. With these variations, the influence on both, the eigenfrequency and the response peaks are analysed. The parameters are varied based on a starting design parameter set, as explained in 11.1. The influence of the various design parameters on the relative wave height and the eigenfrequencies will be analysed from section 11.1.1 until section 11.1.3. Next, section 11.1.4 covers conclusions. An alternative and simplified calculation method for the eigenfrequency is suggested in section 11.2. This simplified method is then used to identify additional design parameters.
Based on the relations between the design parameters and the frequency response, four designs are proposed in section 11.3. Two designs are created for a high eigenfrequency, and two for a low eigenfrequency.

11.1. Variation of a five buoys inline system

The design parameters of a system comprising five buoys inline will be varied to find the relations between the frequency response of the system and the design parameters incorporated in the model. This simple system is not realistic as it has no triangle platforms to support the PV-panels. However, such a simple system can serve to identify the influence of the design parameters on the frequency response.
The calculation tool incorporates multiple design parameters, as listed on page 46. The logical hypothesis was that a change in the design parameters will influence both, the amplitude and the frequency of the response peak. The variations will be executed from one specific starting design. Figure 11.1 visualises this starting point. The dimensions of this system can be found in Table 11.1. The variations for the cylinders will be analysed as follows:

1. Variation of the cylinder length with constant diameter. Thereby the mass varies as well.

2. Variation of the cylinder diameter with constant length. Thereby the mass varies as well.

3. Variation of the cylinder diameter and length. The diameter and length are coupled to obtain a constant mass.

4. Variation of additional parameters.

Table 11.1: Dimensions that form the starting point of the variation of the five buoys inline system.

	Standard system
Diameter buoy (m)	4
Draft buoy (m)	7.5
Diameter beam (m)	1
Length beam (m)	27
Draft centre line beam (m)	2

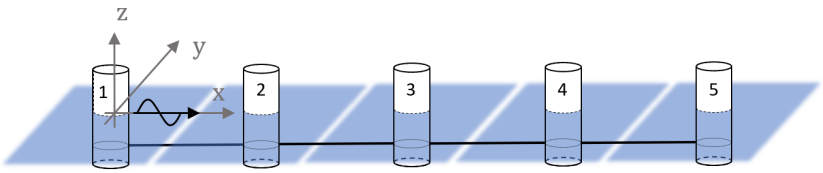

Figure 11.1: Visualisation of the five buoys inline system.

First the dimensions of the buoys will be varied, subsequently the design parameters of the beam are assessed and lastly, the incoming wave angle is varied. The variations do not all account for the required mass to support the PV-panels due to the changing dimensions. The buoys are assumed to provide buoyancy and beams are assumed to be neutrally buoyant. The damping on the buoys is assumed to be 0.5% of the critical damping. A constant diameter determines the stiffness and the mass of the buoys. The incoming wave is always oriented along the x-axis. The graphs in this chapter indicates the two coupled parameters that are varied. The first parameter is displayed on the x-axis, and the second one on the secondary y-axis. Extreme designs with unrealistic proportions are also assessed. This is relevant to indicate the general trend between the response and the dimensions.
The calculation tool obtains the frequency response, the eigenmodes and the corresponding eigenfrequency for every variation. This can be used to calculate multiple parameters in the design. Consequently, the calculation tool can provide much more information than will be used in this chapter. In this chapter, the response peaks of the relative wave height per beam and the eigenfrequencies are assessed. These will be plotted with respect to the varying dimension. The relative wave height is displayed because it was indicated as the most critical response. The black lines in the bottom graphs of the figures show an estimation of the first and second eigenfrequency based on a simplified method. This method and the relevance of the black line in the graph will be explained in section 11.2.

11.1.1. Variation of the buoy dimensions

Figure 11.2 illustrates the following: The mass, indicated with a blue line on the secondary y-axis, grows with an increase of the draft. In the top graph of Figure 11.2 the response peak of the relative wave height is plotted in respect to a varying buoy draft. When varying the buoy draft, the relative wave height does not change extremely. Still, the response follows a positive linear trend with increasing the draft. At significant lower drafts, the relative wave height is remarkably lower. Multiple factors could explain this result. First, this could be the result of increasing amplitude of the Froude-Krylov force at low depths in combination with a significantly lower mass, causing the structure to follow the waves. Second, it could be the result of the increasing eigenfrequency, where the wavelength of the eigenfrequency matches with the length between the buoys.
The bottom graph of Figure 11.2 shows the eigenfrequency. With an increase of the draft, i.e. an increase of mass, the eigenfrequency decreases. Additionally, it can be seen that the eigenfrequencies converge with an increasing draft.

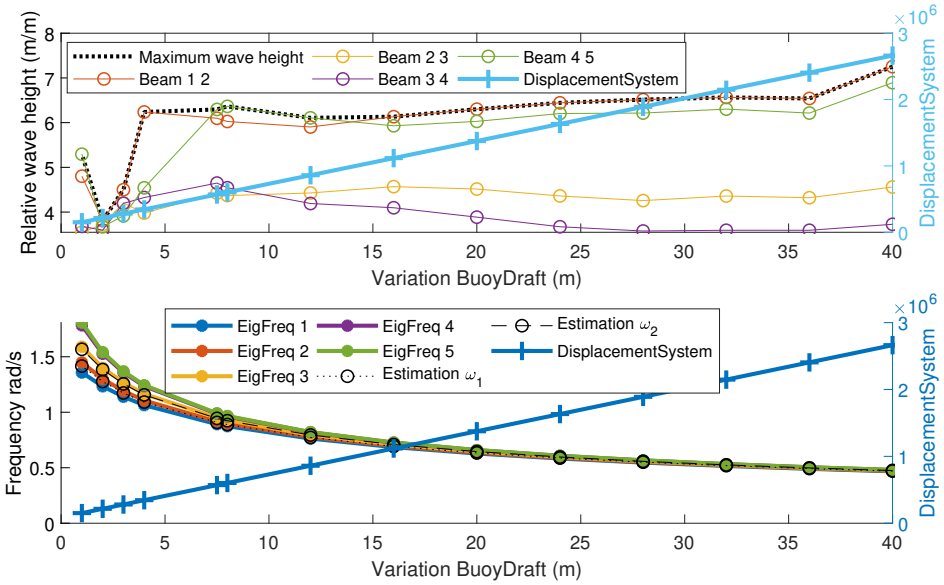

Figure 11.2: Relative wave height of the five buoys inline system and the eigenfrequency with respect to a varying buoy draft. The displacement of the system on the secondary y-axis

An increasing buoy diameter, presented in Figure 11.3, results in a linear upwards trend in the response peaks of the relative wave height. In the second graph, it can be seen that for large diameters the eigenfrequency stabilises. At smaller diameters, the added mass has a relatively larger proportion in the mass. When the added mass becomes insignificant regarding the mass of the buoys, the eigenfrequencies stabilise. This stabilisation is a result of an increase with the same factor of the stiffness and the mass. It can also be seen that the eigenfrequencies converge.

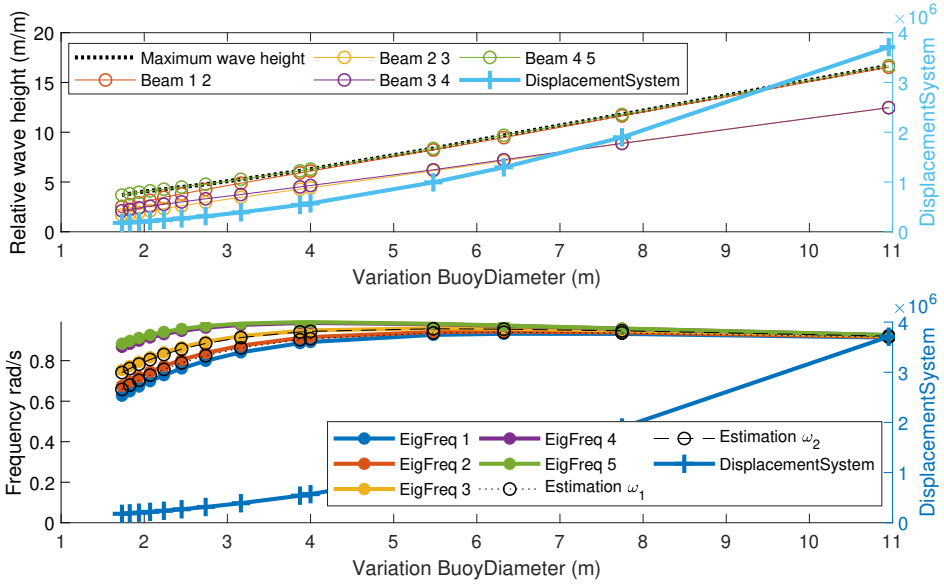

Figure 11.3: Relative wave height of the five buoys inline system and the eigenfrequency for a varying buoy diameter. With the displacement of the system on the secondary y-axis

Figure 11.4 was generated by varying the buoy diameter and compensating the buoy draft so that the water displacement of the system stays the same. The x-axis indicates the buoy diameter, and the secondary y-axis indicates the buoy draft. A maximum in the relative wave height can be seen at a draft of 5.5 meters. The response with smaller diameters and larger draft results in a significantly lower

response. It can be seen that the proportion between the buoy draft and diameter has a significant influence on the eigenfrequency. Consequently, this is a method to influence the eigenfrequency of the system.

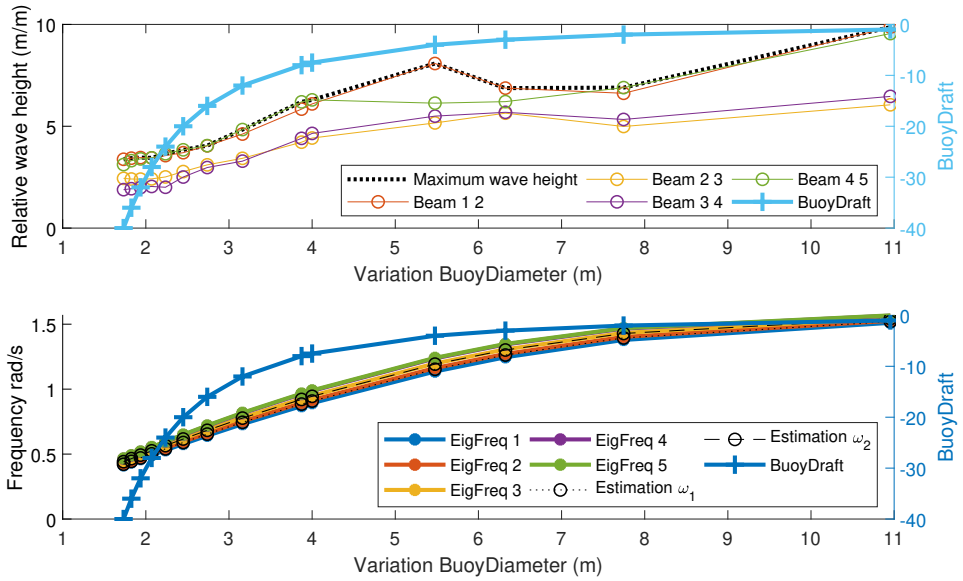

Figure 11.4: Relative wave height of the five buoys inline system and the eigenfrequency with respect to a varying buoy diameter and constant mass of the system. With the reducing buoy draft on the secondary y-axis.

It can be seen in Figure 11.2 and Figure 11.3 that the eigenfrequencies of a heavier system are closer together. When the mass is kept constant, the eigenfrequencies stay at a constant distance from each other.

11.1.2. Variation of beam dimensions

Next, multiple buoy dimensions of the beams tested. First, Figure 11.5 shows the variation of the beam length. Over the increasing beam length, the displacements increases, and the diameter of the beams is kept constant. The maximum response over the system decreases significantly between a beam length of 40 and 60 meters. Nevertheless, the eigenfrequencies reduce and diverge slightly over an increasing beam length.

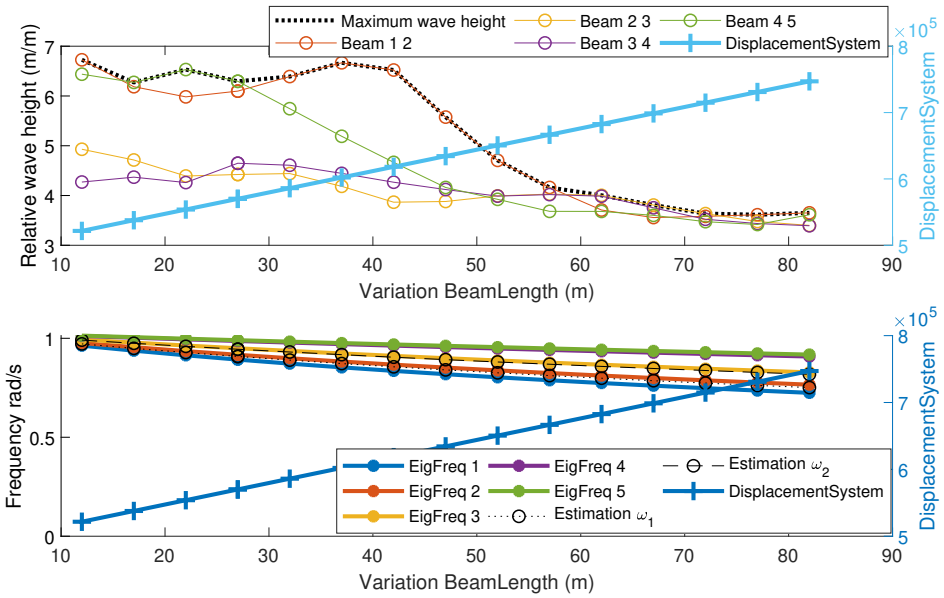

Figure 11.5: Relative wave height of the five buoys inline system and the eigenfrequency with respect to a varying beam length. With the displacement of the system on the secondary y-axis

Next the beam diameter is varied in Figure 11.6. As the beam length is kept constant, the mass increases with the beam diameter. A clear but marginal downwards trend is visible in the response peaks of the relative wave height. Also here the eigenfrequencies are close together but diverge slightly over an increasing beam diameter.

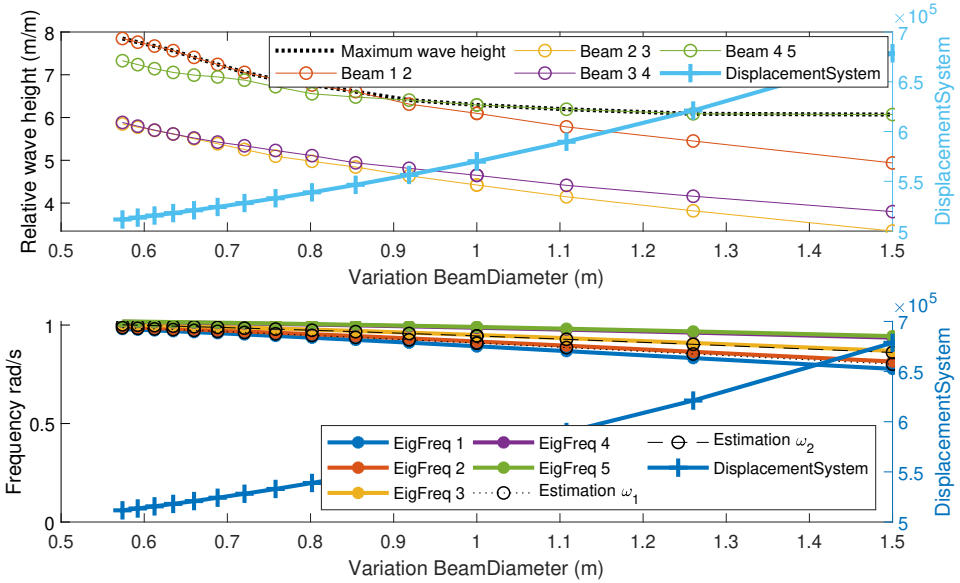

Figure 11.6: Relative wave height of the five buoys inline system and the eigenfrequency for a varying beam diameter. With the displacement of the system on the secondary y-axis

Figure 11.7 is obtained by varying the beam length and compensating the beam diameter so that the volume of the beam stays constant. The relative wave height varies over the different beam length with a significantly lower point around 55 to 75 meters. The second graph of Figure 11.7 shows that the eigenfrequency stays constant over the different beam length and beam diameter.

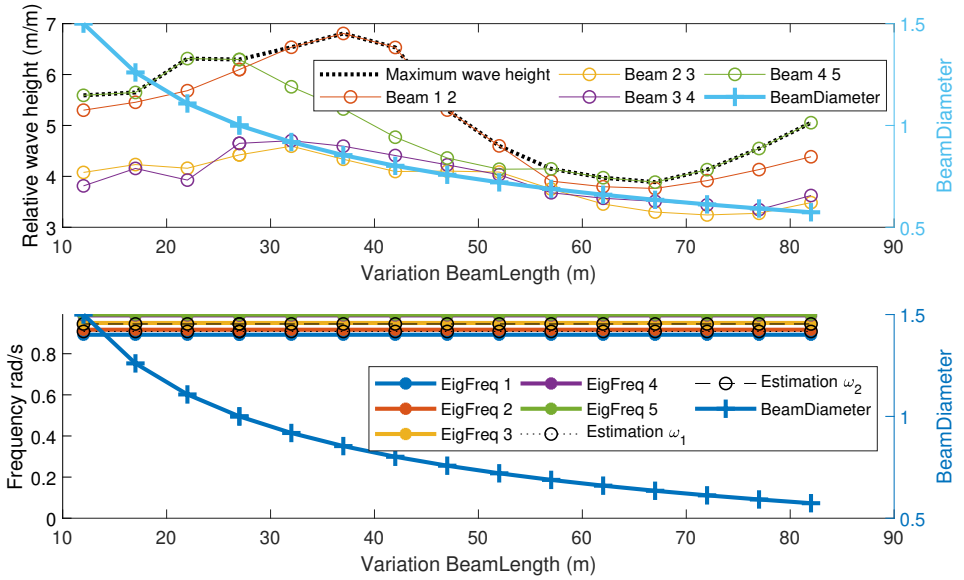

Figure 11.7: Relative wave height of the five buoys inline system and the eigenfrequency for a varying beam length and constant mass of the system. With the reducing beam diameter on the secondary y-axis.

In Figure 11.8 it can be seen that varying the depth at which the beam is installed does not significantly influence the relative wave height. When the beam is mounted closer to the surface, the structure moves more with the waves. Therefore the relative wave height reduces. The same was seen with a decreasing buoy draft, i.e. the bottom of the buoy closer to the surface. The eigenfrequency is not influenced by the depth of the beam as both, the stiffness and the mass do not change.

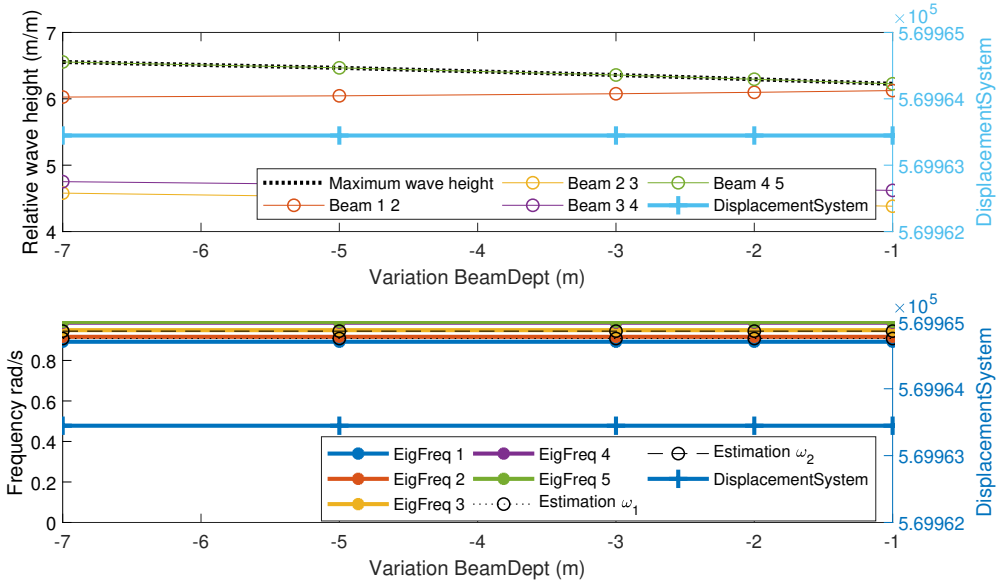

Figure 11.8: Relative wave height of the five buoys inline system and the eigenfrequency for a varying beam depth.

11.1.3. Variation of incoming wave angle

When analysing the change in incoming wave direction with respect to the structure orientation, Figure 11.9 is obtained. $\alpha = 0°$ means that the incoming wave is inline with the beams. It can be seen that for an inline system, the orientation is an important factor in the maximum relative wave height. An inline system where the incoming wave angle is 90 degree on the direction of the beams results in significantly

less response. As could be expected, the system's orientation did not influence the eigenfrequency.

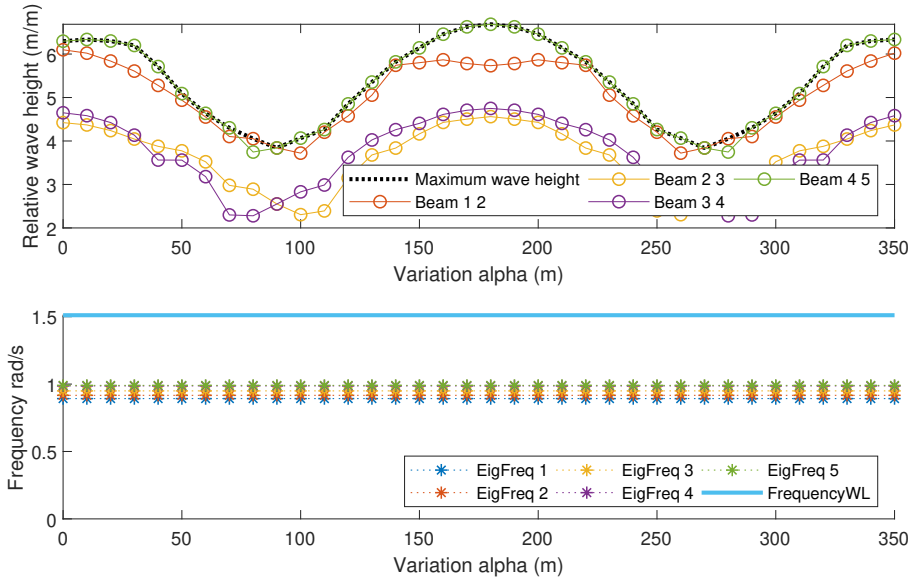

Figure 11.9: Response and relative wave height of the five buoys inline system for a varying incoming wave angle, when the incoming wave is inline with the beams $\alpha = 0°$.

11.1.4. Conclusions based on a five buoys inline system

The shown figures identified multiple trends. The conclusions are grouped here based on the change of eigenfrequencies and those based on the maximum response. By analysing these trends, the feasibility of the currently presented design will be assessed.

Conclusions on the eigenfrequencies

Based on the found eigenfrequencies of the variations, it can be concluded that all eigenfrequencies are close together. In some variation, a slight divergence or convergence is noted on the most extreme positions of the dimensions. The effects of the variation on the eigenfrequencies are summarised in Table 11.2.

Table 11.2: Summary of trends of the eigenfrequencies visible in the variation of a five inline buoy system based on the buoys and beams. (*) Length indicates first the buoy draft (absolute value) and second the beam length. Cte. means that the variable stays constant.

	Diameter	Length (*)	mass	Depth	ω_n
Buoy	Cte	↘	↘	/	Cte, ↗, Divergence
	↗	Cte	↗	/	↗, Cte, Convergence
	↗	↘	Cte	/	↗ ↗
Beam	Cte	↗	↗	Cte	↘/Cte, Divergence
	↗	Cte	↗	Cte	↘/Cte, Divergence
	↗	↘	Cte	Cte	Cte
	Cte	Cte	Cte	↗	Cte

Small changes in eigenfrequencies can be seen in the analysis. Only the draft to diameter ratio of the buoys does influence the eigenfrequency significantly. This means that a variation in the parameters that do not influence the eigenfrequency can be use to optimise other parameters in the design process such as the response peak. Table 7.1 on page 56 indicate that the most of the wave frequencies in the Northern Atlantic are in the range between 0.4 and 2.1 rad/s. With the currently found relations it might not be possible to shift the eigenfrequency away from the frequencies present in the wave spectrum. As the largest range of eigenfrequencies is found in Figure 11.4 and range from 0.5 to 1.5

rad/s. Consequently, more opportunities to optimise the eigenfrequencies need to be found as it does not influence the eigenfrequency sufficient.

Conclusions on the response peaks

First, it is seen that the relative wave height reduces if the bottom of the elements are closer to the surface. Due to the relatively higher amplitude of the loads, the structure moves more with the waves. Contrary, an increasing buoy diameter does increase the relative wave height. This relation confirmed the finding of chapter 10 that the Froude-Krylov force has relatively a substantial contribution to the force in the region of the eigenfrequencies. A second clear trend indicates that with a beam length longer then 50 meters the relative wave height reduces significantly and that an increasing beam diameter decreases the relative wave height slightly. A relation between the beam length and the wavelength of the eigenfrequency could be a path for further research. The obtained absolute values need some caution as they could be related to the specific start case defined at the beginning of this chapter. Still, the buoy draft, the buoy diameter, the beam length and the total mass of the system can be used to minimise the response.

The trends found between the dimensions and the response height require more variations to be further iterated from other starting points. It might be possible that the discovered trends are only applicable for designs that are similar to the starting point of the variations; For example the beam length is fixed on 27 meters for almost all variations. A starting point with another beam length will interfere differently with the wavelength.

The response of the system is significantly higher than what is acceptable in the range of the wave spectrum. A realistic amplification factor should be at least lower than two and preferably close to one, in the perspective of the writer of this thesis. An amplification factor of two would indicate that the relative wave height would be double the wave height. Therefore, the previously mentioned desire to avoid an eigenfrequency that overlaps with the wave spectrum is even more important to avoid high resonance. From chapter 10 it was concluded that a larger system with a higher number of beams relative to the number of buoys has a significantly lower response. A more realistic design where the structure forms triangles instead of an inline design implies that the relative number of beams in respect to the number of buoys increases. Consequently, a larger system is simulated in Figure 11.10. A five buoys system is simulated and shown in the top graph, and on the bottom, a hexagon nineteen buoy system is simulated (for the layout see Figure 11.13). The structural elements have, for both cases, the dimensions indicated in Table 11.1. A clear difference in response peak can be noted. The nineteen buoy system has 42 beams. A higher beam to buoy proportion results in higher damping.

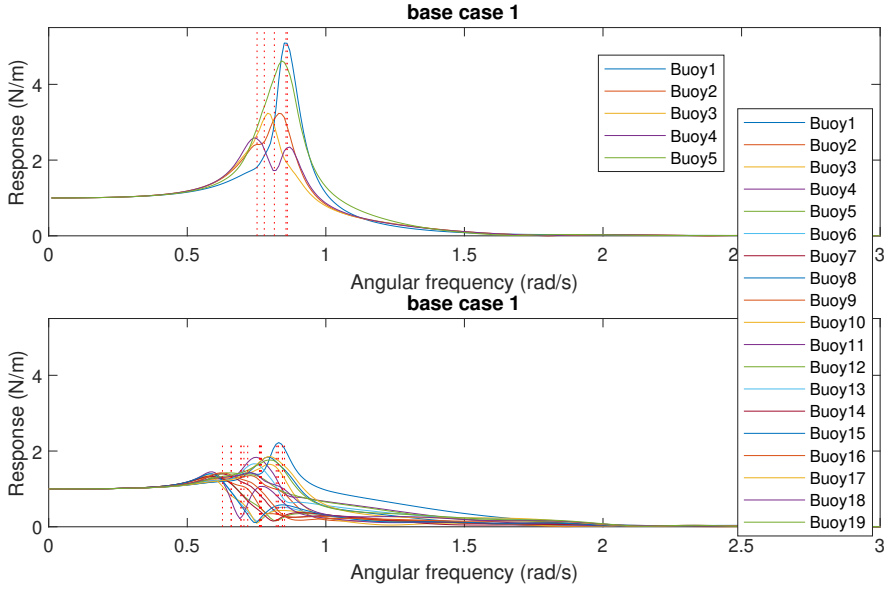

Figure 11.10: The top graph shows the response of the base case five buoys inline system of the analysis. The bottom graph shows the frequency response of a nineteen buoy hexagon system where the individual elements have the same dimensions as the five buoys inline system.

11.2. Identification of additional design parameters

In the previous section, it was concluded that additional design parameters to influence the eigenfrequency should be identified. In order to do so, a simplified method to find the eigenfrequencies will be presented. This method will be verified with the simulation presented so far in this chapter. With this method, the relations between the design parameters and the eigenfrequency should become more apparent, and additional design parameters should be found.

11.2.1. Simplified method to estimate the first two eigenfrequencies

The stiffness of a particular eigenmode and the mass distribution of the system influence the eigenfrequency. It must be noted that within the current design parameters, it is difficult to independently influence the mass or the moment of inertia without changing the stiffness with a similar proportion. To further influence the eigenfrequencies, the stiffness and the mass need to be uncoupled. The implementation of this uncoupling in the model will be discussed in the following chapter as recommendations for future work. For now, an alternative method is introduced.

To sum up, the eigenfrequencies of the system are relatively close together. The eigenfrequencies follow the same trend over the variation. It is known that the first eigenfrequency is a heave motion and the second eigenfrequency is always a pitch or roll motion. Knowing this, the previously found trends in the eigenfrequencies can be determined. For the verification of the calculation tool, the first and second eigenfrequency of a two buoy system was calculated based on the stiffness, as shown on page 100 till page 104.

The eigenfrequency of the heave motion can be found as follows. The first eigenfrequency is calculated in a simplified manner, as indicated in equation 10.11.

$$\omega_n = \sqrt{\frac{\sum K}{\sum m + \sum m'}} \tag{10.11}$$

Equation 10.11 can be rewritten in terms that were varied in the buoy and beam structure. This is done in equation 11.1. The summation is executed over all buoys, which are indicated with subscript "i", and over all beams, indicated with "j". The summation of all water crossing surfaces is summed and multiplied with the density and the gravitational force of the water. And the mass of the total displaced water is calculated to find the total weight of the system.

$$\omega_n = \sqrt{\frac{\sum A_{i,buoy}\rho g}{\sum\left(m_{i,buoy} + m'_{i,buoy}\right) + \sum\left(m_{j,beam} + m'_{j,beam}\right)}} \tag{11.1}$$

Next, the masses and the stiffness of the individual elements are rewritten by substituting the design parameters. This directly indicates the dimensions of the buoys and beams and their influence on the first eigenfrequency, which can be seen in equation 11.2.

$$\omega_n = \sqrt{\frac{\sum \frac{\pi D_{i,buoy}^2}{4}\rho g}{\sum\left(\frac{\pi D_{i,buoy}^2}{4}T_i\rho + m'_{i,buoy}\right) + \sum\left(\frac{\pi D_{j,beam}^2}{4}L_j\rho(1+C_a)\right)}} \tag{11.2}$$

The same can be done for the pitch motion. The eigenfrequency can be calculated based on equation 10.12.

$$I_{tot}\ddot{\alpha} = \sum M \tag{10.12}$$

On page 103 equation 10.12 was introduced to find the second eigenfrequency of the two buoy system. The moment of inertia is expressed by the mass of the individual elements. This moment of inertia is calculated around the geometrical centre of the construction and the moment is calculated with the stiffness of the buoys. Here r_i and r_j indicated the distance of the middle of the cylinder to the middle point of the construction. Therefore, r_i and r_j are directly related to the beam length.

$$\left(\sum\left[\left(m_{i,buoy} + m'_{i,buoy}\right)r_i^2\right] + \sum I_{j,beam}(1+C_a) + \sum\left(m_{j,beam}(1+C_a)r_j^2\right)\right)\ddot{\alpha} = -\sum\left(K\left(\frac{r_i}{2}\right)^2 g\right)\alpha \tag{11.3}$$

Now the masses and the moments of inertia are further substituted in the equation. Hereby the influence of the dimensions of the buoy and beam elements become visible.

$$\left(\sum\left[\left(\frac{\pi D_{i,buoy}^2}{4}T_i\rho + m'_{i,buoy}\right)r_i^2\right] + \sum\frac{L_{j,beam}^2 m_{j,beam}(1+C_a)}{12} + \sum\left[\frac{\pi D_{j,beam}^2}{4}L_j\rho(1+C_a)r_j^2\right]\right)\ddot{\alpha} = -\sum\left(\frac{\pi D_i^2}{4}\rho\left(\frac{r_i}{2}\right)^2\right)\alpha \quad (11.4)$$

The differential equation is solved to find the eigenfrequency where only the positive answer is taken into account. To further indicate that r_i and r_j are related to the beam length the following substitution is executed: $r_i = r_i' L$ and $r_j = r_j' L$.

$$\omega_n = \sqrt{\frac{\sum\left(\frac{\pi D_i^2}{4}\rho\left(\frac{r_i' L_j}{2}\right)^2\right)g}{\sum\left[\left(\frac{\pi D_{i,buoy}^2}{4}T_i\rho + m'_{i,buoy}\right)(r_i' L_j)^2\right] + \sum\frac{L_j^3\frac{\pi D_{j,beam}^2}{4}\rho(1+C_a)}{12} + \sum\left(\frac{\pi D_{j,beam}^2}{4}L_j\rho(1+C_a)(r_j' L_j)^2\right)}} \quad (11.5)$$

To mutually test, the accuracy of this simplified method and to further verify the calculation tool, the eigenfrequencies of the systems in this chapter are calculated. This resulted in the black lines in Figures 11.2 until 11.8. A high accuracy is reached with this method. However, this technique can now be used to identify and quantify other design parameters. With equation 11.2 and equation 11.5 the same basic relations between the dimensions and the impact on the eigenfrequency can be found as indicated in Table 11.2.

11.2.2. Finding additional design parameters

Additional design parameters that could influence the eigenfrequency will be tested based on the simplified method. Based on equations 11.2 and 11.5 some suggestions for other design parameters can be indicated.

Reduction of the water surface

The first and most obvious method would be to uncouple the mass of the buoy and the hydrostatic stiffness of the buoy by two separate diameters. Hereby the numerator and denominator of equation 11.2 and equation 11.5 can be influenced independently. Therefore, the mass and the stiffness in the equations are incorporated in a slightly different way. The stiffness is calculated with a diameter "d" at the water surface and the mass is determined by that same diameter, and height of both parts as indicated in Figure 11.11.

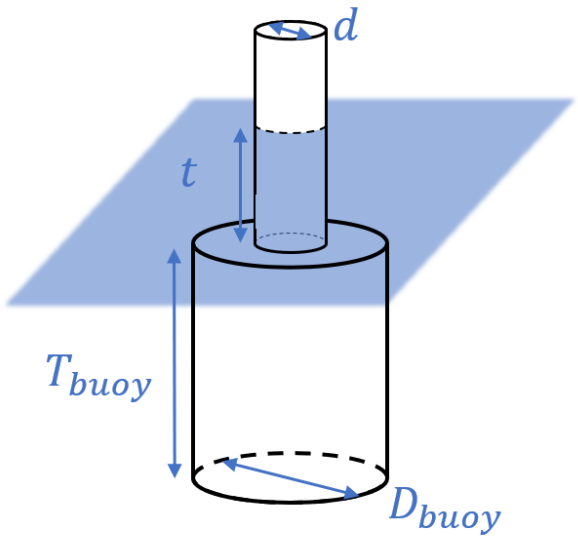

Figure 11.11: Visualisation of the uncoupling of the water displacement and hydrostatic stiffness of the buoy.

The introduction of the additional diameter in the system is incorporated in equation 11.6 and 11.7. The added mass due to the top and the bottom surface of the larger diameter cylinder is indicated by $m"_{i,buoy}$, i.e. $(m"_{i,buoy} = m'_{i,buoy,bottom} + m'_{i,buoy,rim})$.

$$\omega_n = \sqrt{\frac{\sum \frac{\pi d_{i,buoy}^2}{4}\rho g}{\sum\left(\frac{\pi D_{i,buoy}^2}{4}T_i\rho + \frac{\pi d_{i,buoy}^2}{4}t_i\rho + m'_{i,buoy}\right) + \sum\left(\frac{\pi D_{j,beam}^2}{4}L_j\rho(1+C_a)\rho\right)}} \tag{11.6}$$

$$\omega_n = \sqrt{\frac{\sum\left(\frac{\pi d_i^2}{4}\rho\left(\frac{r'_i L_j}{2}\right)^2\right)g}{\sum\left[\left(\frac{\pi D_{i,buoy}^2}{4}T_i\rho + \frac{\pi d_{i,buoy}^2}{4}t_i\rho + m'_{i,buoy}\right)(r'_i L_j)^2\right] + \sum\frac{L_j^3\frac{\pi D_{j,beam}^2}{4}(1+C_a)\rho}{12} + \sum\left(\frac{\pi D_{j,beam}^2}{4}L_j(1+C_a)\rho(r'_j L_j)^2\right)}} \tag{11.7}$$

Based on this equation, an additional analysis on different dimensions of the five buoys inline system can be executed. This is executed in Figure 11.11. The same base case, as indicated in Table 11.1, is used. To incorporate this system in the calculation tool, the force on the top surface and the extra added mass should be incorporated. This will be formulated as a recommendation in the next chapter.

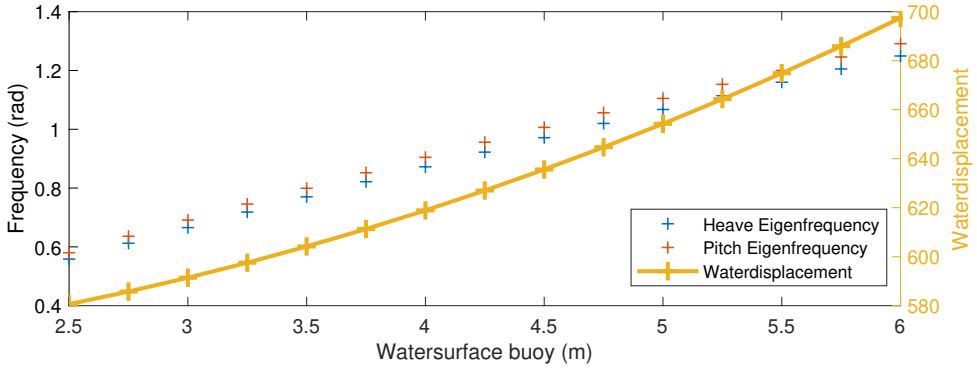

Figure 11.12: Eigenfrequencies when reducing the water surface of the buoy including the effect of the reduction of water displacement.

This extra design parameter largely influences the behaviour of the system and is therefore highly relevant.

Estimation of the weight

In this thesis it was assumed that the beams do not contribute to the buoyancy of the system, i.e. they are neutrally buoyant. This is be seen in section 5.3.2. The mass of the beam still influences the dynamic behaviour. To reduce the mass of the system, it might be necessary to let the beams contribute to the buoyancy of the system. This will also reduce the required size of the buoys. Consequently, it impacts the dynamic behaviour of the system.
The beams contributed to the buoyancy, this means that the dimensions of the buoys can be reduced. The analysis showed that a reduction of buoy diameter leads to a decrease of the eigenfrequency and that a decrease of draft leads to an increase of eigenfrequency. This means that there is extra room for variations. The mass estimation shown in section 5.3.2 needs to be updated for this. The calculation tool can stay unchanged. As the displaced water volume equals the total mass of the system and is a good approximation for the mass distribution.

11.3. Optimising eigenfrequency of the buoy and beam structure

The aim is to find suitable dimensions for the buoy and beam structure. Two main strategies are defined. Firstly, the aim should be that the response peak and the wave spectrum do not overlap. Therefore the eigenfrequencies should be higher or lower than the wave spectrum. Secondly, the response peaks of the structure should be minimised.
Form the verification in chapter 10 it was concluded that the proportion of beams with respect to the number of buoys should be maximised in order to reduce the response peak. In the variation of the incoming wave angle, it was concluded that the orientation of the structure influences the response peaks. Consequently, a 19 buoy hexagon system is proposed in Figure 11.13. This layout maximises the number of beams and maximises the number of triangle platforms over the number of buoys. The change in incoming wave angle will not lead to large changes in the response as the system approaches point symmetry around the centre. Furthermore, it provides a surface for a large quantity of PV-panels which influences the profit aspect of the TBL-assessment, as discussed in chapter 2.

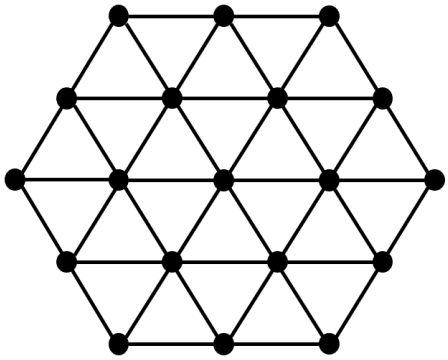

Figure 11.13: Visualisation of the layout of a 19 buoy hexagon system

In section 7.1.1, a wave spectrum was introduced. It was concluded that the main part of the waves is within the range of 0.42 to 2.09 rad/s. Based on the trends found in Table 11.2 and the additional trends found in section 11.2.2, the design parameters can be used to obtain a design with a high or low eigenfrequency.
The four designs indicated in Table 11.3 will be analysed in the calculation tool. Design one and two should result in a high eigenfrequency, and design three and four should result in a low eigenfrequency. The dimensions of the design are based on the effect of the design parameters on the eigenfrequency. A new weight and buoyancy estimation will be executed to incorporate the buoyancy generated by the beams.

Table 11.3: Dimensions, total mass and buoyancy of the four suggested designs for an 19 buoy system.

	Design	1	2	3	4
Buoy	Total draft (m)	5	7	10	15
	Reduced diameter (m)	7.5	5.5	1.5	1
	Diameter (m)	7.5	5.5	2.5	2
Beam	Length (m)	20	25	40	50
	Diameter (m)	1	1.5	1.75	3
	Depth (m)	1	1.5	7	8
	Total mass (1000 kg)	4358	4666	9054	12984
	Total water displacement (1000 kg)	4978	5141	11184	16133

The weight of one platform is calculated based on the length between the interconnecting beams. This method is explained in section 5.3.2 on page 41. Then the weight of the beams and buoys are estimated. Hence the surface is calculated and multiplied with a plate thickness of four centimetres. This volume is multiplied with the density of steel (7850 kg/m^3) to obtain the mass. The total mass of the structure is obtained in equation 11.8 by assuming that every buoy has to carry two full triangle platforms and three full beams. This calculation method again assumes that the buoys at the side of the platforms should be ballasted as they support fewer platforms then the buoys in the middle of the structure. Less ballast will be needed with respect to the system where the beams do not contribute to the buoyancy, as shown in section 5.3.2.

$$\text{Total Mass} = 19 \times (3 \times \text{Mass Beam} + 2 \times \text{Mass Platform} + \text{Mass buoy}) \tag{11.8}$$

The water displacement of the structure is calculated by the volume of the buoys times the number of buoys (19) and the volume of the beams times the number of beams (42). The weight and the water displacement of the total system is shown in Table 11.3. As can be seen, the mass and displacement can be balanced out by adding water ballast to the system. The displacement is higher than the buoyancy. Therefore they are realistic and can be used to assess the feasibility of the system.
Currently, the calculation tool is not set up to calculate the frequency response of the system because the added mass, damping and forces, as result of the extra rim on the buoy, are not taken into account. This leads to an unrealistic response of the structure. Still, the eigenvalue problem, as explained in section 8.2, can be used to obtain an estimation of the eigenfrequencies of the 19 buoy system. Hence, the hydrostatic stiffness of the buoys is incorporated as follows. The stiffness matrix, as introduced in equation 6.10 on page 53 and implemented as indicated in Table 9.1, is overwritten with another stiffness matrix that was obtained with the reduced diameter. This results in the eigenfrequencies indicated in Figure 11.14.

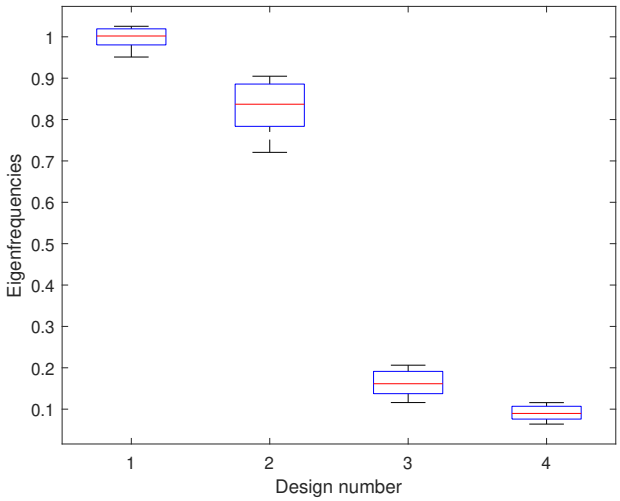

Figure 11.14: Distribution of the eigenfrequencies represented in a box plot. These eigenfrequencies correspond with the designs indicated in Table 11.3

It can be concluded from the eigenfrequencies of design one and two, shown in Figure 11.14, that it will not result in a realistic system. The eigenfrequencies are in the range of most wave spectra. Therefore, it will not support any activity that needs a stable basis. By reassessing the mass estimation to obtain a lower mass of the system, a further increase of the eigenfrequency could be obtained. Still, this will not be significant in the perspective of the author of this thesis. On the other hand, the eigenfrequencies of design three and four are significantly lower than most of the waves indicated in Table 7.1. Furthermore, these larger designs could have a smaller response as the response decreased with a larger beam length and with an increasing beam diameter. As a result of the larger beam length, a higher filling rate (surface filled with PV-panels divided by the total used surface of the system) could be achieved. This higher filling rate would result in a better performance of the profitability indicated by the TBL-assessment.
Finally, the conclusion of this chapter is that the diameter to draft ratio is the main criteria for the design of a buoy and beam structure. More specifically, the water cross-section with respect to the water displacement has a big influence on the eigenfrequency. A small diameter with respect to the draft leads to a realistic design concerning the eigenfrequency. The low eigenfrequency means that the system does not move much with the waves. The buoy and beam structure has in all cases a relatively small water plane area. Therefore the stiffness is rather small regarding the displaced mass, which automatically leads to a relatively low eigenfrequency. This high mass does mean that more material is needed than in a system with high eigenfrequencies. Although the eigenfrequency is in a realistic range, the responses obtained in this chapter are high and need further research to estimate the absolute value. Furthermore, the response peak needs to be further minimised. Still more research and further development on the calculation tool need to be executed to obtain the frequency response.

12

Discussion and recommendations

This chapter firstly assesses the limitations, the assumptions and the simplifications of the calculation tool. The assumptions and the consequences of these assumptions on the results are discussed in section 12.1. In the current calculation tool, additional improvements can be made. The validity and accuracy of the calculation tool could be further refined, and more information than is currently used can be analysed. These improvements and further simulations will be proposed in section 12.2. Lastly, the design parameters and the feasibility of the system will be discussed in a broader context in section 12.3. This discussion will suggest further design steps on the path to a possible feasible buoy and beam structure.

12.1. Limitations of the calculation tool

In the calculation tool simplifications and assumptions were incorporated as shown in chapter 6 and chapter 7. The simplifications and assumptions impact the outcome of the calculation tool. These consequences will be assessed in this section. First, the assumptions in the mechanical analysis will be evaluated then the assumption in the hydrodynamic modelling will be evaluated.

12.1.1. Mechanical

The main assumptions that were made are the small-angle approximation and the incorporation of the triangle platforms.

Small angle approximation

In section 6.2, the small-angle approximation was introduced. The validity of the small-angle approximation was verified in section 10.4. In some situations, such as structures with shorter beam lengths, the angles become relatively large in the resonance peak. In this extreme case, this assumption is broken. This can be seen in Figure 12.1. This violation only occurs when a high response occurs. The structure should be optimised for a realistic design, i.e. for a relatively low response. In these cases, the approximation of small angles will not be violated, and therefore the assumption is valid.

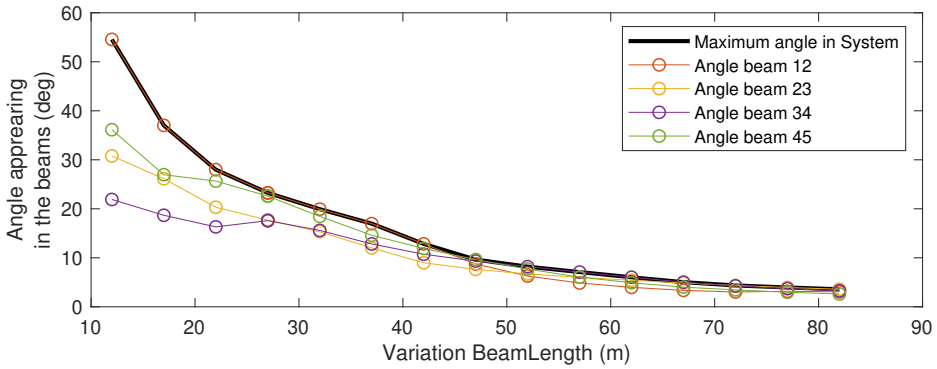

Figure 12.1: Maximum angles of the buoys relative to the horizontal plane of a five buoy inline system in respect with a changing beam length

The assumption of small angles also implies that no horizontal displacement of the buoys is taken into account. Even with small angles, a small horizontal displacement will appear. Based on the response of the structure and the beam length, the horizontal displacement is calculated, for the system that formed the starting point of the variations as presented in section 11.1. In the top part of Figure 12.2, the maximum horizontal difference in distance between two neighbouring buoys can be seen. In the bottom graph, the displacement relative to the first buoy can be seen for the standard situation shown in Table 11.1. The effect of these displacements on the structure should be further researched.

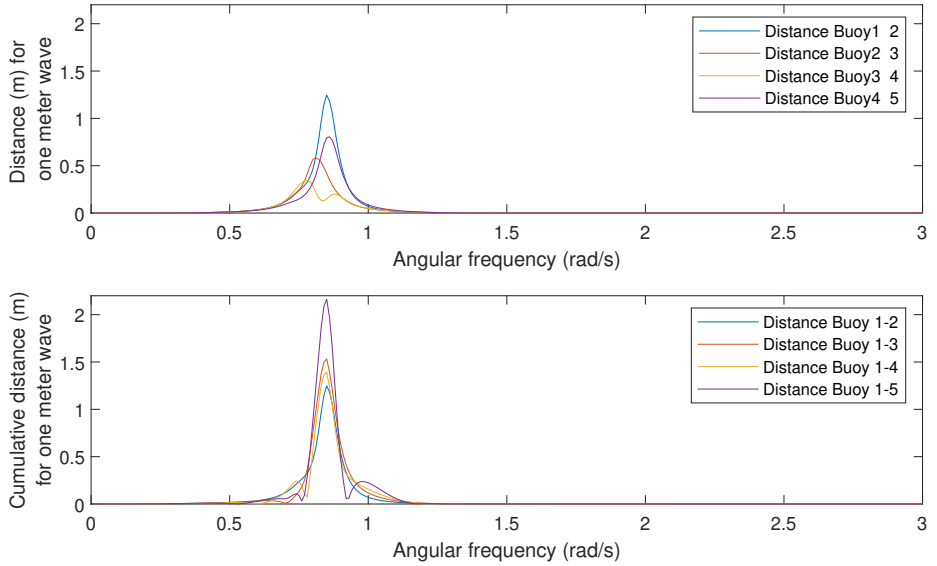

Figure 12.2: Horizontal displacement of a five buoy inline system with a beam length of 27 as shown in Table 11.1 in respect with the original position based on the vertical response of the buoys.

Incorporation of the triangle platforms in the calculation tool

In the proposed calculation tool, the mass of the triangle platforms was not directly included. In section 5.3.2, an estimation of the weight in the function of the beam length was proposed. This estimation determines the required water displacement of the buoys, assuming that the beams are neutrally buoyant and therefore, they do not support the platforms. Then the mass of the displaced water of the submerged elements, i.e. the buoys and the beams, is determined by the dimensions of the cylinder times the water density. This mass, together with the added mass, is incorporated in the mechanical model. This way of incorporating the triangle platforms' mass means that the weight of the platform is assumed to be fully concentrated in the buoys. This overestimates the moment of inertia of the platform and consequently overestimates the eigenfrequency. Chapter 11 concluded that it could be benefi-

cial to obtain high eigenfrequencies if the beams also provide buoyancy. During the calculation of the eigenfrequency, the mass and mass distribution was calculated based on the volume of the displaced water. The damping caused by the moving triangle platforms is left out of the model but could also be incorporated. The intention of incorporating the damping of the platform in the linear damping of the buoys was described in section 5.4. So far, this intention was not executed. For high velocities, this damping could be relevant. Further research is needed to incorporate this effect.

12.1.2. Hydromechanical

On the hydromechanical aspect, multiple simplifications are introduced. First, it is assumed that the structure size was smaller than one-fifth of the wavelength. This allowed assessing the loads with the Morison equation. As this calculation tool serves as a first assessment, the damping was linearised. This lead to an overestimation of the response peak.

Hydromechanical transparent structure and wave theory

In chapter 7, the structure was predicted to be hydromechanical transparent. In the analysis in chapter 11 design parameters were varied, and the response over a frequency range was assessed. There are three approaches to assess if the simulated systems are hydrodynamic transparent. (1) Based on the frequency range maximum diameter can be set, (2) based on the maximum dimensions a maximum frequency can be set or (3) based on the region of interest the requirements can be checked. In this region of interest, the requirements must be met, though small errors could be allowed. Based on the eigenfrequency range, a maximal relevant structure size could be identified. The appropriate structure size is the diameter of the cylinders. The frequency range of zero to three radians per second was based on Table 7.1. With a frequency of three radians per second structures with structural elements of maximum 1.36 meter could be assessed. Assessing slightly bigger structural elements would only lead to small errors and can, therefore, be justified. The accuracy would decrease when simulating too big diameters. The dimensions of the structure that were assessed in the analysis in section 10.6 varied between 0.57m and 9m. These dimensions would imply that the structure can be assessed up to a maximum frequency of 4.65 rad/s and 1.17 rad/s, respectively. For these large diameters, the maximum frequency is relatively low. As said before, analysing a slightly larger relative structure size would only cause small errors. Additionally, these large dimensions were mainly simulated to assess the general trends of the structure size on the response. These extreme proportions in the dimensions, such as diameter to draft ratio, are unrealistic in the vision of the author of this thesis. The main point of interest, in the analysis, is the behaviour of the structure in the range of the eigenfrequencies. The eigenfrequency influences the feasibility of the design. The eigenfrequencies range from 0.3 rad/s to 1.6 rad/s in the analysis. These frequencies correspond to a maximum structure size of 137 meters to 4.86 meters, respectively. This means that only for the two largest variations and for design one and two of the shown in Table 11.3 the buoy diameter causes small errors by not taking into account the diffraction according to Figure 7.1. For the structures analysed in section 11.3 only the added mass coming from the Morison equation is incorporated to obtain the eigenfrequency. Consequently, the possible error is minimised. The same reasoning for the relative structure size could also be applied to the motion of the structure, according to this author. When the structure moves with an amplitude larger then one-fifth of the structure size, diffraction becomes relevant. In the analysis, significant responses are seen. The response should be minimised, and result in a lower response than one-fifth of the wavelength. Therefore the calculation tool is valid. It can be concluded that most of the designs that were tested in section 10.6 are hydrodynamic structures. Only for more extremes in frequencies and dimensions, small errors can occur due to omission of diffraction.

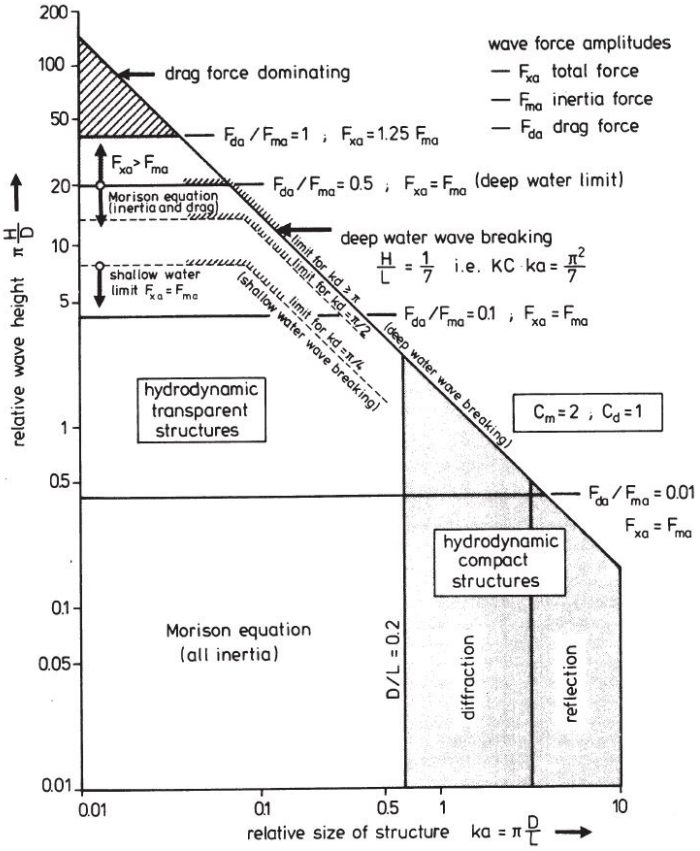

Figure 7.1: Modelling methods selection graph for hydrodynamic (circular) structures [6].

Morison and Froude-Krylov

The classification of the structure as a hydromechanical transparent structure makes that the Morison equation was selected to assess the loads on the cylinders. For the vertical force on the buoys, the Froude-Krylov force was used. This is a part of the Morison equation. Just before, it was discussed that the response should be minimal to obtain a realistic system and an accurate result where diffraction is irrelevant. Here it becomes apparent why this is necessary. The loads are calculated based on acceleration, velocity and pressure in the fluid. These loads are calculated on an exact and fixed location. For the beams, the centre of the cylinder in still water conditions is taken, and for the buoys, the position of the centre of the bottom surface in still water conditions is taken. In this specific location, the hydrodynamic characteristics such as acceleration, velocity and pressure are determined to assess the load. As a result of the small relative structure size and modest response, this specific position gives a sufficiently accurate answer. Consequently, it is necessary that the displacements also stay within the range of one-fifth of the wavelength.

Linearisation of damping and damping on buoys

The physical phenomena modelled in the calculation tool were fully linearised, as mentioned at the beginning of this section. First, the damping of the viscous drag term in the Morison equations was linearised, and second, the simplified linear assessment of the damping on the buoys was incorporated. These approximations are probably part of the explanation of the relatively high response peaks. The relative wave height as defined on the y-axis in Figure 7.1 indicates the proportion of inertia force with respect with the damping force perpendicular on a cylinder depending on the wave height and the diameter. For a relative wave height of “20” in deep water, the inertia force equals double the damping force, and for a relative wave height, $\pm$ 40 the inertia force equals the damping force. The more significant the proportion of the damping, the more impact the linearisation gets. ”$\pi H/D < 20$ the maximum value of horizontal force corresponds to the maximum inertia force. Drag effects are only relevant for larger values of $\pi H/D$, and dominate at values greater than 40” according to Clauss et al. [6]. In the in-between region, it is acceptable to linearise the drag force. The response of the system is

normalised by the wave height. Therefore, the response is where possible indicated in meter per meter (m/m). In other cases, the response is indicated per meter wave height. This does not mean that the KC-number or relative wave height should be based on a one-meter wave. In Table 12.1 the relative wave height is calculated based on two extreme and one average wave heights based on Table 7.1 and based on the variation of the beam diameter in section 11. This analysis assumes a fixed construction in a wave. When the construction moves in antiphase, the KC-number will increase. Only in the most extreme case of Table 12.1 a too high relative wave height is found. This extreme case of 0.57 meter over a length of 27 meters is structurally unrealistic.

Table 12.1: Different relative wave heights over a realistic spectrum based on Table 7.1 and on the beam diameters analysed in chapter 11.

	Diameter (m)		
Wave height (m)	0.57	1	1.5
1	5.51	3.14	2.09
5	27.6	15.7	10.5
10	55.1	31.4	20.9

As discussed in section 7.4, a linear approach was suggested based on a percentage of the critical damping. This method was based on two experiments. Therefore, it needs further research. Tarik and Sander [53] discusses an alternative and improved way for incorporating the damping.

12.2. Recommendations on the calculation tool

The calculation tool was composed to obtain the heave response of a buoy and beam structure. With this tool, some calculations were performed. In this chapter further improvements on the calculation tool, and additional simulations, analyses and calculations that might be interesting for the hydrodynamic behaviour will be suggested.

- Section 11.2.2 indicated that the calculation tool should also be able to simulate the behaviour of a system with a reduced buoy diameter at the water surface. The effect of the reduced diameter on the eigenfrequency was already estimated in section 11.2.2. Still, the force, added mass and damping due to the change of diameter should be incorporated in the model to obtain the full frequency response.
- The response peaks need to be assessed more in detail as they highly influence the feasibility of the structure. Most probably this must be done separately to take into account the nonlinear damping.
- The system presented in Table 12.2 should be used to create a new starting point for further iteration. The newly found relation can then help to further understand the relations between the response and to iterate the construction. Also, with the suggestions incorporated in this section, better insight can be generated.
  For now, the response peaks and relation with the dimensions were not used as an input for the proposed dimensions in Table 12.2. Because, there is, so far, no proof that the trends that were found for the response peaks are also applicable when another starting point for the variations were chosen. Consequently, more variations need to be checked from different starting points or specifically starting from the designs proposed in Table 12.2.
- The program, at this moment, does need a rather long calculation time. There are multiple opportunities to improve the computational cost of the calculation tool. The first and most important factor would be to remove the `eval()`-function out of the Morison functions that are used to create the force vector. In this function, the integral is calculated for every frequency and every iteration. The `eval()`-function in MATLAB is a computationally expensive function and can be replaced by the direct solution of the integral. Only for the case where the beam is oriented in y-direction an if statement could avoid a division by zero.
- The tool, as presented in this thesis, can assess multiple responses. So far, the relative wave height is used as this was indicated as the most critical response. This response is derived from

the response of the structure. The individual force contributions used to calculate the response can be checked separately, and the forces on the hinges can be calculated with equations used in chapter 6. Furthermore, all aspects that depend on the response can be determined, i.e. forces between the elements. These responses can be used to give a first estimation of the forces on the hinges. These forces on the hinges highly influence the feasibility of the buoy and beam concept.

- As discussed in section 12.1, the mass and mass distribution of the triangle platforms can be improved. First, the estimation of the mass of the platforms should be improved. Second, the mass distribution of the structural elements should be changed. The mass is currently incorporated with the mass of the displaced system. This simplification could be improved with the mass and mass distribution of the individual elements.

- The calculation tool uses multiple times the Morison equation to calculate the forces on the cylinders. This equation can also be used to calculate the forces in the horizontal plane. Before this can be done, multiple steps need to be undertaken before the horizontal forces could be approximated. It is valuable to know these forces in order to further estimate the forces in the hinges, the mooring and on the individual elements.

- A design procedure needs to be developed. A suggestion based on the current calculation tool for a possible procedure is described hereafter: First, the desired beam length could be identified. With this beam length, an appropriate draft to diameter, or still waterplane area to displacement proportion, of the buoys could be obtained by iteration. Next, the diameter and height of the beam could be optimised. This will result in a design that could be used for further optimisation.

- All simulations that were done for the analysis in chapter 11 assume constant dimensions over the construction. There is no reason to apply this further. It should be possible to change the draft, diameter and depth of the buoys and beams over the construction. It should even be possible to slit a triangle on specific locations in smaller triangles. The changes of dimensions over the constructions would make it possible to influence specific eigenfrequencies and eigenmodes. Additionally, it could influence the response peak of individual buoys.

- The desired topology of the structure needs further research. A nineteen buoy or larger system in a hexagon shape seems promising as a result of its symmetry, but other or more complex topologies could be interesting.

- On page 44 it was indicated that the triangle platforms and the hinges were not taken into account. This simplification assumed that the hinges do not incorporate any damping, mass or stiffness. This could be reconsidered. Adding damping or stiffness to the hinges will lead to different frequency responses. Still, the technical feasibility of these more complicated hinges remains questionable.

In this thesis, a validation of the build model is missing. Before the results of the model can be fully trusted, a system should be tested in real life to determine the accuracy of the presented calculation tool. The validation could indicate if the assumption to discard diffraction is fully valid when multiple buoys heave in the proximity of each other. The principles used in the calculation tool such as the Morison equation and the Froude-Krylov force on the buoys are well-established theory. Still, a validation step would indicate to what extent these principles are fully applicable in the simulation of a buoy and beam structure.

12.3. Discussion on a feasible design

Based on the conclusions of the analysis in section 5.4.1 four designs shown in Table 11.3 were identified and proposed in section 11.3. The outcomes indicated that a system with low eigenfrequency is favourable to avoid interference with the wave spectrum. Therefore the two designs depicted in Table 12.2 were suggested to obtain a low eigenfrequency. The tends that were found in the response peaks were not used to obtain the design. Still the same tends to obtain a modes response and a low eigenfrequency are complimentary.

Table 12.2: Possible dimensions, total mass and buoyancy of the suggested designs for a 19 buoy system.

	Design	3	4
Buoy	Total draft (m)	10	15
	Reduced diameter (m)	1.5	1
	Diameter (m)	2.5	2
Beam	Length (m)	40	50
	Diameter (m)	1.75	3
	Depth (m)	7	8
	Total mass (1000 kg)	9054	12984
	Total water displacement (1000 kg)	11184	16133

When designing, all aspects discussed in chapter 2 must be taken into account. The heave response and the relative wave height of the system have a significant impact on the feasibility of the system. Therefore, these factors where considered the main points of interest in this thesis. Secondary other aspects should be taken into account, as a buoy and beam system for offshore solar should meet all requirements to become feasible. When reassessing the parameters based on the outcomes of the Triple Bottom Line (TBL)-assessment the following can be noted. First, the diameter is probably rather small. This would mean that an accurate weight estimation of the system needs to be made to obtain the design draft. Also, over time additional weight can accumulate on the construction. This additional weight will reduce the air gap and increase the draft. The same holds for maintenance where people and equipment need to be brought on board. It also generates only limited redundancy in case one of the cylinders loses its buoyancy. The possible loss of buoyancy advocate for a larger buoy diameter and sufficient air gap. If the diameter is increased for one of these reasons, the mass should be reduced to maintain the low eigenfrequency. The beam draft should be investigated further. It might be more efficient to have a slightly larger diameter if the beam does not interact with the water surface in waves. The depth to which the reduced diameter continues needs to be determined based on the response in the specific spectrum of the desired location. A considerable beam length is suggested. This beam length implies that significant bending moments will appear in both the triangle platforms and the connecting beams. It will be a structural and technical challenge to design and produce platforms in this size. Due to the large overhang, the material cost could become high. It also means that the forces on the hinges would be substantial. The advantage of the long beams is that the filling rate of the PV-panels is probably higher. Next, it was suggested that the system has a hexagon layout with 19 buoys. This system will behave rather constant over varying incoming wave angles. Most locations will not have an evenly distributed wave field over the incoming wave angles. The topology and the variation of the dimensions in the system could be optimised for this incoming wave angle. Lastly, the buoy and beam structure still needs to be developed in a broader context. Multiple requirements were indicated with the TBL-assessment in chapter 2. In this thesis, the main focus point was the heave response and the relative wave height as this was identified as most critical. At this point, the main conclusions are based on the eigenfrequency of the frequency response, whereby the critical heave response is avoided by shifting the eigenfrequency to a lower frequency and out of the wave spectrum. The response of the tested structures appears to be rather high. If this resonance can be avoided, a realistic design could be obtained on the matter of heave response. As this appears to be possible, it can be concluded that on the matter of possible interaction between the waves and the platforms a feasible system could be obtained. It is now necessary to again oversee the larger picture and identify the potential of the concept. Additional pitfalls and critical responses must be identified and analysed. Special attention should go to the forces in the hinges, the response in the horizontal direction in respect of the mooring. Moreover the second order effect such as folding of the structure should be a point of concern. In the larger picture, the ecological impact and economic feasibility of Offshore Floating PV (OFPV) in general and for the buoy and beam structure desire more research to unlock the potential.

13

Conclusion

At the beginning of this thesis, offshore floating energy was identified as a promising energy solution to answer the increasing demand for sustainable energy. Multiple concepts for Offshore Floating PV support structures were proposed in literature or by the industry. Currently, these solutions are in concept or testing phase. Due to the requirements coming from the complex environment, the feasibility of all concepts is still debatable. Therefore, the research goal was to develop a new design for an OFPV support structure and, in addition, demonstrate its feasibility.

Proposing the buoy and beam structure and the identification of the most critical response
A brainstorm and selection based on predefined requirements led to the proposition of the buoy and beam structure. The buoy and beam structure is a structure in which submerged beams are mounted between floating buoys. These beams form a triangle grid. The top of the buoys support triangle platforms. These platforms have the same dimensions as the triangles created by the beams. Every corner of a triangle platform is connected to one buoy. All connections between the buoys, beams and platforms are hinged. This composition creates a flexible structure that can move with the waves and therefore mitigates the external loads coming from the environment. In respect to other concepts this concept has a rather modest waterplane area.
The flexibility in combination with the relatively small waterplane area should work as an advantage to mitigate the external loads. As a result of the relatively small waterplane area, the forces on the hinges should stay modest and a reasonable response should be obtained.
Many pitfalls for the feasibility of the concept were identified. The heave response is seen as the most critical response. High heave responses would imply that the platforms and the PV-panels will experience slamming by the waves leading to damage. Hence, the heave response is modelled.

Description of the chosen modelling method
The heave response of a buoy and beam structure is modelled to give a first estimation on the feasibility. Only regular waves were taken into account. The damping resulting from the movement of the triangle platform trough the air is not taken into account. The mass and mass distribution of the system is estimated with the mass of the displaced water. This simplification means that the submerged part of the construction determines the mass distribution. The buoy and beam elements are approximated by cylinders. The masses and interconnections of the individual cylinders are described by a differential equation. To obtain a feasible structure, the response of the structure should be modest and thereby only small angles in the beams could appear for a realistic design. Therefore the differential equation is based on the assumption of small angular displacements of the beams.
The structure was identified as a hydrodynamic transparent structure which means that the diffraction can be neglected. The relevant hydrodynamic loads for the heave response are obtained with the Airy wave theory. The loads on the beams are obtained with the Morison equation. The vertical loads on the cylinders are estimated with the Froude-Krylov. In the model, all damping terms could be linearised. The damping on the buoys was modelled as a percentage of the critical damping. The obtained linear differential equation is solved in a frequency domain to find the frequency response, eigenfrequencies

and eigenmodes.
This differential equation is implemented in a calculation tool in MATLAB. The individual building blocks of the program are first verified and the total code is verified by stepwise connecting the building blocks. Simplified systems are modelled for verification. The developed calculation tool makes it possible to obtain the frequency response by inserting (1) the topology matrix, which fixes the number of buoys and beams and the interconnection, and (2) inserting the main dimensions of the buoys and the beams.

Identification of the design parameters and proposition of a design direction for further development

With this calculation tool, variations in the dimensions of the buoys and beams for a five buoys inline system were executed. A specific starting design was chosen. The relations, between the changing dimensions on the one hand and on the other hand the eigenfrequency and the maximum response, are analysed. The following conclusions were made on the found eigenfrequencies. Firstly, it was noted that the eigenfrequencies are always within the same range. Secondly, it was shown that the first and second eigenfrequency could be calculated with a simplified method. Thirdly, it was seen that an increasing buoy diameter to mass ratio, has a strong positive linear coloration, with the eigenfrequency, i.e. a higher stiffens to mass ratio of the system results in a higher eigenfrequency. Furthermore, it was shown that the eigenfrequency could even be more reduced by lowering the buoy diameter around the water surface. Next, the executed variations indicate that an increasing beam length has a moderate negative linear correlation with the eigenfrequency.
Based on the outcome of the analysis a nineteen buoys hexagon system was suggested and analysed. A hexagon system is beneficial for multiple reasons. First, a hexagon system has a high number of triangle platforms in respect to the number of buoys which is determines for the number of solar panels. Second, it was concluded that the response is lower as a result of the high number of beams that cause damping. Thirdly, a hexagon system should have minimal change in response with a change in incoming wave angles.
Four different nineteen buoys hexagon designs were proposed and modelled. Based on the previously found relations, the response of two designs for high eigenfrequencies, and two designs for low eigenfrequencies were obtained. The eigenfrequencies should not overlap with the wave spectrum and should, therefore, the eigenfrequency should be higher or lower. A high eigenfrequency results in a structure that moves flexibly with the waves. A low eigenfrequency would mean that the structure does not move with the waves. Based on the simulation of the nineteen-buoy system, it was concluded that within the set of design parameters, a buoy and beam structure that has a sufficiently high eigenfrequency, with respect to the wave spectrum, was not found. Contrary, it was concluded that it should be possible to design a system with a low eigenfrequency resulting in a system that will only slightly move with the waves.
In the analysis of the five buoys inline system, it was seen that a relatively long beam length, a large beam diameter, a small buoy diameter and an appropriate incoming wave angle result in a lower response for a five buoy inline system. It was not tested if these trends are identical when a variation would have been executed, starting from another starting point.
Consequently, some additional iterations and research are needed. For the variations executed in this thesis, unfeasible high responses were obtained. Still, the requirements to obtain a low eigenfrequency and a modest response match. Consequently it should be possible to design a structure that has modest response in a realistic wave spectrum.
However, some additional steps on the research of the heave response and the relative wave height are needed to further identify the feasibility in respect to the heave response. The two main points of improvement of the calculation tool are firstly the modelling and implementation of reduced buoy diameter at the water surface to obtain an even low eigenfrequency. And secondly, the improvement of the modelling of the damping on the different elements so that the response peaks can be estimated with higher accuracy as the response peaks profoundly influence the feasibility.
It is concluded that violent and extreme heave responses and resonance can be avoided by a set of design parameters that result in an eigenfrequency which is sufficiently lower than the wave spectrum. Therefore, a feasible system could be obtained with respect to the heave response. A suggestion for the design parameters that should result in a feasible eigenfrequencies of system can be obtained with the relations shown by this thesis. The thesis provide and presented a simple but efficient design tool that can estimate the frequency response and RAO for a set of design parameters. It would be inter-

esting to validate the theory and the implementation of the theory with model test. This would indicate to what extend the used assumptions are fully valid.
Still, some further iterations in a slightly improved calculation tool must be executed to determine the precise dimensions of a feasible design. Together with this next iteration, a possible location with corresponding wave spectrum should be identified so that location and response can be matched. The obtained dimensions should be assessed in the perspective of the feasibility of the total system. Additional critical responses need to be researched, such as forces in the hinges and response in the horizontal direction to design the hinges and the mooring system. Next to the technical aspects, the human, ecological and economic aspects and feasibility needs to be researched for all Offshore Floating PV systems to unlock the potential of offshore solar energy.

Abbreviations

List of Acronyms

AHP	Analytic Hierarchy Process
PV	Photo Voltaic
FPV	Floating Photo Voltaic
IFPV	Inland Floating PV
OFPV	Offshore Floating PV
KC	Keulegan-Carpenter (number)
TBL	Triple Bottom Line
FBD	Free Body Diagram

Nomenclature

Greek and other symbols

α	Angle with x-axis, angle with horisontal plane
$\ddot{}$	Second derivative to time
$\dot{\Phi}$	Velocity potential
$\dot{}$	First derivative to time
λ	Wavelength
ω	Angular frequency
ω_n	Eigenfrequency
ϕ	Phase angle
$\Re$	Real part of number
ρ	Density water
ρ_{st}	Density steel
σ	Tensile strength
Θ	Phase angle
ζ	Wave amplitude
(*)	Indication of the dependency on the relative velocity and therefore the need for itteration

Latin symbols

$[\mathbf{B}]$	Damping matrix
$[\mathbf{K}]$	Stiffness matrix
$[\mathbf{M}]$	Mass matrix
$\ddot{z}, \ddot{y}, \ddot{z}$	Respectively acceleration in $x-$, $y-$, $z-$ direction
$\dot{u}_T$	Velocity as result of translation
$\dot{u}_{RN}$, u_{RN}	Relative perpendicular acceleration, relative perpendicular velocity
$\dot{z}, \dot{y}, \dot{z}$	Respectively velocity in $x-$, $y-$, $z-$ direction
$[\mathbf{I_n}]$	(n x n) unit matrix
$\mathbf{b}'$	Damping matrix due to translation coming from the Morison equation
$\mathbf{B}$	Damping matrix due to rotation coming from the Morison equation
$\mathbf{F}$	Force vector
$\mathbf{I}'$	Inertia matrix due to added mass coming form the Morison equation
$\mathbf{K}$	Stiffness matrix
$\mathbf{m}'$	Added mass matrix coming from the Morison equation
$\mathbf{T}$	Torque matrix
$\boldsymbol{z}$	Vector containing z-positions
$\vec{1}_n$	A (n x 1) vector with every entry equal to one
$\vec{e}_t$	tangent unit vector

B	With
b	Linear damping
B'	Damping due to rotation of the beam
b'	Damping due to translation of the beam
b_{cr}	Critical damping
C_a	Added mass coefficient
C_d	Drag coefficient
F	Force
H	Height
I	Moment of inertia
i	Complex number
I'	Moment of inertia of added mass
k	Linear spring stiffness
L	Beam length, i.e. distance between two buoys, i.e. platform side
m	Mass
m'	Added mass
o, p, q	alternative axis system where o is in the direction of the beam centre line
r	Position vector for bending moment or torque
r_s	Distance to centre
T	Bending moment or torque
t	Thickness
u, v, w	Fluid velocity in x-, y-, z-direction
u_c, $\dot{u}_c$	Acceleration of construction
u_{RN}, u_{RN}	Magnitude of the relative velocity
V	Volume
W	Work
z, y, z	Respectively $x-$, $y-$, $z-$ position
C	Topology matrix
D	Diameter
g	Acceleration due to gravity g=9.81 m/s^2
k	Wavenumber, spring stiffness
KC	Keulegan–Carpenter
R	Radius
S	Surface
s	Integration constant for Morison equation
T	Draft, Period
T	Translation
u, $\dot{u}$	Velocity, acceleration
Z	Response

Subscripts

ζ	Due to the wave
A, B	Indicating respectively of the A or B end of beam
e	External
G	Gravity
HD	Hydrodynamic
HS	Hydro static
ij	Item related to the connecting beam between buoy i and j
o, p, q	Respectively $o-$, $p-$, $q-$component
x, y, z	Respectively x-, y-, z-component
a	Ampletude
c	construction
FK	Froude-Krylov
FKHM	Froude-Krylov hydrodynamic mass
HM	Hydrodynamic mass
M	Morison
N	Normal direction
R	Relative
VD	Viscous drag

Bibliography

[1] D. O. Akinyele and R. K. Rayudu. Review of energy storage technologies for sustainable power networks. *Sustainable Energy Technologies and Assessments*, 8:74–91, 2014. ISSN 22131388. doi: 10.1016/j.seta.2014.07.004.

[2] Aniket. How much does an average solar panel weigh? https://ecotality.com/solar-panel-weights/, 08 2019. (Accessed on 04/26/2020).

[3] S. K. Chakrabarti, W. A. Tarn, and A. L. Wolbert. Wave forces on a randomly oriented tube. *Proceedings of the Annual Offshore Technology Conference*, 1975-May:433–441, 1975. ISSN 01603663. doi: 10.4043/2190-ms.

[4] Subrata Chakrabarti. Elsevier, 2005. ISBN 978-0-08-044381-2. URL https://app.knovel.com/hotlink/toc/id:kpHOEV0001/handbook-offshore-engineering/handbook-offshore-engineering.

[5] Young Kwan Choi. A study on power generation analysis of floating PV system considering environmental impact. *International Journal of Software Engineering and its Applications*, 8(1):75–84, 2014. ISSN 17389984. doi: 10.14257/ijseia.2014.8.1.07. URL http://dx.doi.org/10.14257/ijseia.2014.8.1.07.

[6] Günther Clauss, Eike Lehmann, and Carsten Östergaard. *Offshore structures: volume I: conceptual design and hydromechanics*. Springer-Verslag, 1992. ISBN 3-540-19709-5.

[7] C. Diendorfer, M. Haider, and M. Lauermann. Performance analysis of offshore solar power plants. In *Energy Procedia*, volume 49, pages 2462–2471. Elsevier, jan 2013. ISBN 1876-6102. doi: 10.1016/j.egypro.2014.03.261. URL https://www.sciencedirect.com/science/article/pii/S1876610214007152.

[8] Ekrullia. Ocean waves in grayscale photography · free stock photo. https://www.pexels.com/photo/ocean-waves-in-grayscale-photography-4035587/, 03 2020.

[9] Environment European Commission| Energy, Climate change. 2050 long-term strategy | climate action. https://ec.europa.eu/clima/policies/strategies/2050_en, . (Accessed on 01/30/2020).

[10] Environment European Commission| Energy, Climate change. 2030 climate & energy framework | climate action. https://ec.europa.eu/clima/policies/strategies/2030_en, . (Accessed on 01/30/2020).

[11] Carlos Ferrer-Gisbert, José J. Ferrán-Gozálvez, Miguel Redón-Santafé, Pablo Ferrer-Gisbert, Francisco J. Sánchez-Romero, and Juan Bautista Torregrosa-Soler. A new photovoltaic floating cover system for water reservoirs. *Renewable Energy*, 60:63–70, dec 2013. ISSN 09601481. doi: 10.1016/j.renene.2013.04.007. URL https://www.sciencedirect.com/science/article/pii/S0960148113002231.

[12] Flevoland. Omroep flevoland - nieuws - d66 wil zonne-eiland op ijsselmeer. https://www.omroepflevoland.nl/nieuws/170820/d66-wil-zonne-eiland-op-ijsselmeer, 08 2019. (Accessed on 01/31/2020).

[13] Jonathan A. Foley, Ruth DeFries, Gregory P. Asner, Carol Barford, Gordon Bonan, Stephen R. Carpenter, F. Stuart Chapin, Michael T. Coe, Gretchen C. Daily, Holly K. Gibbs, Joseph H. Helkowski, Tracey Holloway, Erica A. Howard, Christopher J. Kucharik, Chad Monfreda, Jonathan A. Patz, I. Colin Prentice, Navin Ramankutty, and Peter K. Snyder. Global consequences of land use. *Science*, 309(5734):570–574, 2005. ISSN 0036-8075. doi: 10.1126/science.1111772. URL https://science.sciencemag.org/content/309/5734/570.

[14] Wiep Folkerts, Wilfried van Sark, Corry de Keizer, Wijnand van Hooff, and Menno van den Donker. ROADMAP PV Systemen en Toepassingen. page 50, 2017. URL https://www.uu.nl/sites/default/files/roadmap-pv-systemen-en-toepassingen-final.pdf.

[15] Reinout Heijungs, Gjalt Huppes, and Jeroen B. Guinée. Life cycle assessment and sustainability analysis of products, materials and technologies. Toward a scientific framework for sustainability life cycle analysis. *Polymer Degradation and Stability*, 95(3):422–428, mar 2010. ISSN 01413910. doi: 10.1016/j.polymdegradstab.2009.11.010.

[16] Paraic Higgins and Aoife M. Foley. Review of offshore wind power development in the United Kingdom. In *12th International Conference on Environment and Electrical Engineering, EEEIC 2013*, pages 589–593, 2013. ISBN 9781467330589. doi: 10.1109/EEEIC.2013.6549584.

[17] Janette Hogerwaard, Ibrahim Dincer, Greg F. Naterer, and Bruce D. Patterson. Solar methanol synthesis by clean hydrogen production from seawater on offshore artificial islands. *International Journal of Energy Research*, 43(11):5687–5700, jul 2019. ISSN 1099114X. doi: 10.1002/er.4627. URL https://onlinelibrary.wiley.com/doi/abs/10.1002/er.4627.

[18] J. M. J. Journée and W. W. Massie. Wave forces on slender cylinders. *Offshore Hydromechanics*, (January), 2001.

[19] J M J Journée, W W Massie, and R H M Huijsmans. OFFSHORE HYDROMECHANICS Third Edition (2015) Based on Original Lecture Notes (2000). 2015.

[20] Ehsanul Kabir, Pawan Kumar, Sandeep Kumar, Adedeji A. Adelodun, and Ki Hyun Kim. Solar energy: Potential and future prospects, 2018. ISSN 18790690.

[21] Austin Kana. Design tools: Analytic hierarchy process (ah, March 2018.

[22] DNV KEMA. SUNdy , a floating solar field concept. Technical Report Dc. URL www.dnvkema.com/SUNdy.

[23] Trygve Kristiansen and Petter Borvik. Investigation of an Air-Cushion Supported Solar Island. page V009T13A015, 2018. doi: 10.1115/omae2018-78533.

[24] Daniel A Lashof and Dilip R Ahuja. Relative global warming potentials of greenhouse gas emissions. *Nature*, 344(6266):529–531, 1990.

[25] Salvador Aldret Lee, Diane Allen, and Christopher Wilkins. Patent Application Publication, 2001. URL https://patents.google.com/patent/US20030121768A1/en.

[26] Peng Li. *A Theoretical and Experimental Study of Wave-induced Hydroelastic Response of a Circular Floating Collar*. 2017. ISBN 978-82-326-2223-8. URL https://brage.bibsys.no/xmlui/handle/11250/2436667.

[27] Evonne Miller, Laurie Buys, and Jennifer Summerville. Quantifying the social dimension of triple bottom line: Development of a framework and indicators to assess the social impact of organisations. *International Journal of Business Governance and Ethics*, 3(3):223–237, 2007. ISSN 14779048. doi: 10.1504/IJBGE.2007.014314.

[28] J.R. Morison, J.W. Johnson, and S.A. Schaaf. The Force Exerted by Surface Waves on Piles. *Journal of Petroleum Technology*, 2(05):149–154, 1950. ISSN 0149-2136. doi: 10.2118/950149-g. URL https://www.onepetro.org/download/journal-paper/SPE-950149-G?id=journal-paper{%}2FSPE-950149-G.

[29] Mossmaritime. A Leader In Maritime Technology. URL http://www.mosww.com/pdfs/MossMaritimeGeneralBrochure.pdf.

[30] Ocean of Energy. A world's first: offshore floating solar farm installed at the Dutch North Sea - Oceans of Energy, 2019. URL https://oceansofenergy.blue/2019/12/11/a-worlds-first-offshore-floating-solar-farm-installed-at-the-dutch-north-sea/.

[31] Ocean Sun. Gallery | ocean sun. https://oceansun.no/gallery/, 2018. (Accessed on 01/13/2020).

[32] Ocean Sun. Products | ocean sun. https://oceansun.no/products/, 2018. (Accessed on 08/17/2019).

[33] Megan O'Dea. 25 ridiculous camping fails from real campers just like you. https://thedyrt.com/magazine/lifestyle/ridiculous-camping-fails/, 04 2019. (Accessed on 02/03/2020).

[34] OmroepWest.nl. Tegenstanders willen windmolens in zee voorkomen: 'mensen willen de zon onder zien gaan' - omroep west. https://www.omroepwest.nl/nieuws/3767851/Tegenstanders-willen-windmolens-in-zee-voorkomen-Mensen-willen-de-zon-onder-zien 02 2019. (Accessed on 01/31/2020).

[35] Jules Ortjens. D66 wil drijvende zonnepanelen op het ijsselmeer | trouw. https://www.trouw.nl/duurzaamheid-natuur/d66-wil-drijvende-zonnepanelen-op-het-ijsselmeer~bc266555/, 05 2019. (Accessed on 01/31/2020).

[36] Bruce D Patterson, Frode Mo, Andreas Borgschulte, Magne Hillestad, Fortunat Joos, Trygve Kristiansen, Svein Sunde, and Jeroen A van Bokhoven. Renewable CO 2 recycling and synthetic fuel production in a marine environment. *Proceedings of the National Academy of Sciences*, 116(25):12212–12219, jun 2019. ISSN 0027-8424. doi: 10.1073/pnas.1902335116. URL http://www.ncbi.nlm.nih.gov/pubmed/31160448http://www.pubmedcentral.nih.gov/articlerender.fcgi?artid=PMC6589678.

[37] Bruce D Patterson, Frode Mo, Andreas Borgschulte, Magne Hillestad, Fortunat Joos, Trygve Kristiansen, Svein Sunde, and Jeroen A van Bokhoven. Renewable CO2 recycling and synthetic fuel production in a marine environment. *Proceedings of the National Academy of Sciences of the United States of America*, 116(25):12212–12219, jun 2019. ISSN 10916490. doi: 10.1073/pnas.1902335116. URL http://www.ncbi.nlm.nih.gov/pubmed/31160448http://www.pubmedcentral.nih.gov/articlerender.fcgi?artid=PMC6589678.

[38] Hamid M. Pouran. From collapsed coal mines to floating solar farms, why China's new power stations matter. *Energy Policy*, 123:414–420, dec 2018. ISSN 03014215. doi: 10.1016/j.enpol.2018.09.010. URL https://www.sciencedirect.com/science/article/pii/S0301421518306153.

[39] P.R. Shukla, J. Skea, E. Calvo Buendia, V. Masson-Delmott, H.-O. Pörtner, D. C. Roberts, R. Slade P. Zhai, S. Connors, R. van Diemen, M. Ferrat, E. Haughey, S. Luz, S. Neogi, M. Pathak, J. Petzold, J. Portugal Pereira, P. Vyas, E. Huntley, K. Kissick, M. Belkacemi, J. Malley, and (eds.). IPCC, 2019: Summary for Policymakers. In: Climate Change and Land: an IPCC special report on climate change, desertification, land degradation, sustainable land management, food security, and greenhouse gas fluxes in terrestrial ecosystems. Technical report, 2019.

[40] Alexander PRASCHL, Thomas MIKATS, and Martin PUTSCHEK. EUROPÄISCHE PATENTSCHRIF, nov 2017.

[41] REN21. *Renewbles in Cities - 2019 Global Status Report*. 2019. ISBN 9783981891140. URL https://wedocs.unep.org/bitstream/handle/20.500.11822/28496/REN2019.pdf?sequence=1{&}isAllowed=y{%}0Ahttp://www.ren21.net/cities/wp-content/uploads/2019/05/REC-GSR-Low-Res.pdf.

[42] Rijksoverheid. Duurzame energie | rijksoverheid.nl. https://www.rijksoverheid.nl/onderwerpen/duurzame-energie. (Accessed on 01/30/2020).

[43] Alok Sahu, Neha Yadav, and K. Sudhakar. Floating photovoltaic power plant: A review. *Renewable and Sustainable Energy Reviews*, 66:815–824, dec 2016. ISSN 1364-0321. doi: 10.1016/J.RSER.2016.08.051. URL https://www-sciencedirect-com.tudelft.idm.oclc.org/science/article/pii/S1364032116304841?{_}rdoc=1{&}{_}fmt=high{&}{_}origin=gateway{&}{_}docanchor={&}md5=b8429449ccfc9c30159a5f9aeaa92ffb{&}ccp=y.

[44] Alok Sahu, Neha Yadav, and K. Sudhakar. Floating photovoltaic power plant: A review, dec 2016. ISSN 18790690. URL https://www-sciencedirect-com.tudelft.idm.oclc.org/science/article/pii/S1364032116304841?{_}rdoc=1{&}{_}fmt=high{&}{_}origin=gateway{&}{_}docanchor={&}md5=b8429449ccfc9c30159a5f9aeaa92ffb{&}ccp=y.

[45] UNFCCC secretariat (UN Climate Change). The paris agreement | unfccc. https://unfccc.int/process-and-meetings/the-paris-agreement/the-paris-agreement, October 2018. (Accessed on 08/15/2019).

[46] Timothy F Slaper. The Triple Bottom Line: What Is It and How Does It Work? The Triple Bottom Line Defined. *Indiana Business Review*, 86(1):4–8, 2011. URL http://www.ibrc.indiana.edu/ibr/2011/spring/article2.html.

[47] Chintan Solanki, Garlapati Nagababu, and Surendra Singh Kachhwaha. Assessment of offshore solar energy along the coast of India. In *Energy Procedia*, volume 138, pages 530–535. Elsevier, oct 2017. ISBN 1111111111. doi: 10.1016/j.egypro.2017.10.240. URL https://www.sciencedirect.com/science/article/pii/S1876610217351901.

[48] Sungevity. Zonnepanelen plat dak: dit is wat je móet weten | sungevity. https://www.sungevity.nl/zonnepanelen/plat-dak. (Accessed on 04/26/2020).

[49] SunMetrix. Is my roof suitable for solar panels (and what is the weight of a solar panel)? – sunmetrix. https://sunmetrix.com/is-my-roof-suitable-for-solar-panels-and-what-is-the-weight-of-a-solar-panel/, 07 2013. (Accessed on 04/26/2020).

[50] Surfer Today. Paddling is history: Meet surfing's floating dock. https://www.surfertoday.com/surfing/paddling-is-history-meet-surfings-floating-dock, 06 2017. (Accessed on 02/03/2020).

[51] Swimsol. Floating solar technology at sea - solarsea™. roof solar for islands. https://swimsol.com/, 2019. (Accessed on 03/18/2019).

[52] M. E. Taboada, L. Cáceres, T. A. Graber, H. R. Galleguillos, L. F. Cabeza, and R. Rojas. Solar water heating system and photovoltaic floating cover to reduce evaporation: Experimental results and modeling. *Renewable Energy*, 105:601–615, may 2017. ISSN 18790682. doi: 10.1016/j.renene.2016.12.094. URL https://www.sciencedirect.com/science/article/pii/S0960148116311636.

[53] Sabuncu Tarik and Calisal Sander. *Hydrodynamic coefficients for vertical circular cylinders at finite depth*. 1981.

[54] Lanka Thabrew, Debra Perrone, Alexandra Ewing, Mark Abkowitz, and George Hornberger. Using triple bottom line metrics and multi-criteria methodology in corporate settings. *Journal of Environmental Planning and Management*, 61(1):49–63, jan 2018. ISSN 13600559. doi: 10.1080/09640568.2017.1289900.

[55] Kim Trapani. FLEXIBLE FLOATING THIN FILM PHOTOVOLTAIC (PV) ARRAY CONCEPT FOR MARINE AND LACUSTRINE ENVIRONMENTS by Kim Trapani Thesis submitted in partial fulfilment of the requirements for the degree of Doctor of Philosophy (PhD) in Natural Resources Engineering. 2014.

[56] Kim Trapani and Dean L. Millar. Proposing offshore photovoltaic (PV) technology to the energy mix of the Maltese islands. *Energy Conversion and Management*, 67:18–26, 2013. ISSN 01968904. doi: 10.1016/j.enconman.2012.10.022. URL http://dx.doi.org/10.1016/j.enconman.2012.10.022.

[57] Kim Trapani and Dean L. Millar. The thin film flexible floating PV (T3F-PV) array: The concept and development of the prototype. *Renewable Energy*, 71:43–50, nov 2014. ISSN 09601481. doi: 10.1016/j.renene.2014.05.007. URL https://www.sciencedirect.com/science/article/pii/S0960148114002584?via{%}3Dihub.

[58] Kim Trapani and Miguel Redõn Santafé. A review of floating photovoltaic installations: 2007-2013, apr 2015. ISSN 10535888. URL http://doi.wiley.com/10.1002/pip.2466.

[59] United Nations| Department of Economic and Social Affairs. 68% of the world population projected to live in urban areas by 2050, says un. https://www.un.org/development/desa/en/news/population/2018-revision-of-world-urbanization-prospects.html, 05 2018. (Accessed on 01/04/2020).

[60] Edwin van Gastel. Solar Magazine - Oceans of Energy verdubbelt aantal zonnepanelen van drijvend zonnepark op Noordzee, 2020. URL https://solarmagazine.nl/nieuws-zonne-energie/i20453/oceans-of-energy-verdubbelt-aantal-zonnepanelen-van-drijvend-zonnepark-op-noordz

[61] William Otto & Olaf Waals. Oceanopolis, March 2019.

[62] Thomas Wiedmann and John Barrett. A review of the ecological footprint indicator-perceptions and methods, 2010. ISSN 20711050.

[63] Wikimedia Commons. Water lily, 2005. URL https://commons.wikimedia.org/wiki/File:Water_lily_leafs_on_pond.jpg. File: Water lily leafs on pond.jpg, original author: NASA.

[64] World Bank. Where Sun Meets Water: Floating Solar Market. *World Bank Group, ESMAP and SERIS*, 1(2):1–131, 2019. URL www.worldbank.org.

[65] World Bank, ESMAP, and SERIS. Where Sun Meets Water : Floating Solar Market Report - Executive Summary. pages 1–24, 2018. URL www.worldbank.orghttp://documents.worldbank.org/curated/en/579941540407455831/Where-Sun-Meets-Water-Floating-Solar-Market-Report-Executive-Summary.

[66] World Bank Group, ESMAP, and SERIS. Where Sun Meets Water: Floating Solar Handbook for Practitioners. Technical report, 2019. URL www.worldbank.org.

[67] Ueda Yuzuru, Sakurai Tsurugi, Tatebe Shinya, Itoh Akihiro, and Kurokawa Kosuke. PERFORMANCE ANALYSIS OF PV SYSTEMS ON THE WATER. *Solar Energy*, (September):5–8, 2008. URL https://www.researchgate.net/publication/281325437{_}Performance{_}analysis{_}of{_}PV{_}systems{_}on{_}the{_}water.

A

AHP decision process

To select a concept for further research, the AHP method was used. The selection is executed in two steps. First, a prioritisation on the requirements is made, and then this is used for the selection of the concept.

A.1. Pairwise comparison of criteria

The requirements are pairwise compared. For example, development cost over material cost is given 0.8, meaning that development cost is slightly more important. This is done for all requirements. Additionally, the matrix obtained is made cardinal-consistent and is solved as an eigenvalue problem. The normalised principal eigenvector associated with the dominant eigenvalue indicates the prioritisation of the requirements. The eigenvalues are normalised to obtain the percentages, which is resulting in the values indicated in Table 5.1 on page 37.

	Development costs	Material costs	Production and installation costs	Operation and maintenance costs	Decomissioning and recycling costs	Survive in Waves	Survive in wind	Survive in curent	Biofouling	Ageing	Development time	Safety
Development costs	1.00	0.80	0.80	0.60	0.80	0.35	0.35	0.35	0.90	0.60	0.30	0.60
Material costs	1.25	1.00	1.00	0.75	1.00	0.44	0.44	0.44	1.13	0.75	0.38	0.75
Production and installation costs	1.25	1.00	1.00	0.75	1.00	0.44	0.44	0.44	1.13	0.75	0.38	0.75
Operation and maintenance costs	1.67	1.33	1.33	1.00	1.33	0.58	0.58	0.58	1.50	1.00	0.50	1.00
Decomissioning and recycling costs	1.25	1.00	1.00	0.75	1.00	0.44	0.44	0.44	1.13	0.75	0.38	0.75
Survive in Waves	2.86	2.29	2.29	1.71	2.29	1.00	1.00	1.00	2.57	1.71	0.86	1.71
Survive in wind	2.86	2.29	2.29	1.71	2.29	1.00	1.00	1.00	2.57	1.71	0.86	1.71
Survive in curent	2.86	2.29	2.29	1.71	2.29	1.00	1.00	1.00	2.57	1.71	0.86	1.71
Biofouling	1.11	0.89	0.89	0.67	0.89	0.39	0.39	0.39	1.00	0.67	0.33	0.67
Ageing	1.67	1.33	1.33	1.00	1.33	0.58	0.58	0.58	1.50	1.00	0.50	1.00
Development time	3.33	2.67	2.67	2.00	2.67	1.17	1.17	1.17	3.00	2.00	1.00	2.00
Safety	1.67	1.33	1.33	1.00	1.33	0.58	0.58	0.58	1.50	1.00	0.50	1.00

Figure A.1: AHP input for the requirements

A.2. Concept selection

This can now be used for a further selection of the concepts. Based on every requirement, the concepts are compared as can be seen in Figure A.2. Again all these matrices are made cardinal-consistent. Then the principal eigenvectors were obtained.

	Buoy and beam	Flexible connected	Moss Maritime	Oceans of Energy	Buoy and beam	Flexible connected	Moss Maritime	Oceans of Energy	Buoy and beam	Flexible connected	Moss Maritime	Oceans of Energy	Buoy and beam	Flexible connected	Moss Maritime	Oceans of Energy
	Development costs				**Material costs**				**Survive in wind**				**Survive in curent**			
Buoy and beam	1.0	3.0	0.9	0.7	1.0	3.0	1.1	0.8	1.0	0.8	1.0	0.7	1.0	0.5	1.0	1.0
Flexible connected pontoons	0.3	1.0	0.3	0.2	0.3	1.0	0.4	0.3	1.3	1.0	1.3	0.9	2.0	1.0	2.0	2.0
Moss Maritime	1.1	3.3	1.0	0.8	0.9	2.7	1.0	0.7	1.0	0.8	1.0	0.7	1.0	0.5	1.0	1.0
Oceans of Energy	1.4	4.3	1.3	1.0	1.3	3.8	1.4	1.0	1.4	1.1	1.4	1.0	1.0	0.5	1.0	1.0
	costs				**maintenance costs**				**Biofouling**				**Ageing**			
Buoy and beam	1.0	0.9	0.7	0.7	1.0	3.0	1.0	2.0	1.0	3.0	1.0	3.0	1.0	0.2	2.0	2.0
Flexible connected pontoons	1.1	1.0	0.8	0.8	0.3	1.0	0.3	0.7	0.3	1.0	0.3	1.0	5.0	1.0	10.0	10.0
Moss Maritime	1.4	1.3	1.0	1.0	1.0	3.0	1.0	2.0	1.0	3.0	1.0	3.0	0.5	0.1	1.0	1.0
Oceans of Energy	1.4	1.3	1.0	1.0	0.5	1.5	0.5	1.0	0.3	1.0	0.3	1.0	0.5	0.1	1.0	1.0
	recycling costs				**Survive in Waves**				**Development time**				**Safety**			
Buoy and beam	1.0	1.0	1.0	1.0	1.0	4.0	1.2	2.5	1.0	5.0	0.8	0.7	1.0	3.0	1.0	3.0
Flexible connected pontoons	1.0	1.0	1.0	1.0	0.3	1.0	0.3	0.6	0.2	1.0	0.2	0.1	0.3	1.0	0.3	1.0
Moss Maritime	1.0	1.0	1.0	1.0	0.8	3.3	1.0	2.1	1.3	6.3	1.0	0.9	1.0	3.0	1.0	3.0
Oceans of Energy	1.0	1.0	1.0	1.0	0.4	1.6	0.5	1.0	1.4	7.1	1.1	1.0	0.3	1.0	0.3	1.0

Figure A.2: AHP input for the concept

To obtain the total result seen in Table 5.2 on page 37, a matrix was created by combining all concept eigenvectors in a matrix and multiplying this matrix with the requirements weightings normalised eigenvector.

B

Appendix on basic ydrodynamics

B.1. Airy wave theory

The Airy wave theory was selected. In which the amplitude ζ is small relative to the wave length and waterdepth. Airy wave theory is developed by Laplace and Airy and is base on the Laplace differential equation B.1 and the linearised boundary conditions of the seabed (equation B.2) and the water surface (equation B.3).

$$\frac{\partial^2 \Phi}{\partial x^2} = \frac{\partial^2 \Phi}{\partial z^2} = 0 \tag{B.1}$$

$$w = \frac{\partial \Phi}{\partial x} = 0 \quad at \quad z = -d \tag{B.2}$$

$$\frac{\partial \zeta}{\partial t} - \frac{\partial \Phi}{\partial} = 0 \tag{B.3a}$$

$$\frac{\partial \Phi}{\partial t} + g\zeta = 0 \quad at \quad z = \zeta = 0 \tag{B.3b}$$

Using Laplace equation and the boundary conditions have some implications. The fluid is assumed incompressible and homogeneous in the continuity equation. From the continuity equation the Laplace equation is obtained. The use of these theories imply that an irrational and inviscous fluid is assumed. Additionally Airy wave theory is only applicable for waves with a small amplitude relative to wave length. From the Laplace equations and the boundary conditions a velocity potential for deep water is derived (equation B.4). This potential can be used to determine the velocities, accelerations and pressure in the fluid.

$$\Phi = i\,\zeta_a \frac{g}{\omega} e^{kz} e^{-ikx} e^{i\omega t} \tag{B.4}$$

This results in the following equations for the speed and acceleration in both the x and z direction.

$$u = \frac{\partial \Phi}{\partial x} = \zeta_a \omega e^{kz}\, e^{-ikx} \cdot [e^{i\omega t}] \tag{B.5}$$

$$\frac{\partial u}{\partial t} = \frac{\partial^2 \Phi}{\partial x \partial t} = i\zeta_a \omega^2 e^{kz}\, e^{-ikx} \cdot [e^{i\omega t}] \tag{B.6}$$

$$w = \frac{\partial \Phi}{\partial z} = i\,\zeta_a \omega e^{kz}\, e^{-ikx} \cdot [e^{i\omega t}] \tag{B.7}$$

$$\frac{\partial w}{\partial t} = \frac{\partial^2 \Phi}{\partial z \partial t} = -\zeta_a \omega^2 e^{kz}\, e^{-ikx} \cdot [e^{i\omega t}] \tag{B.8}$$

To obtain the equation for the pressure the linearised Bernoulli equation is used:

$$p = -\rho \frac{\partial \Phi}{\partial t} - \rho g z = \rho\,\zeta_a g e^{kz} e^{-ikx} e^{i\omega t} - \rho g z \tag{B.9}$$

These velocity, acceleration an pressure will operate as the input to calculate the hydrodynamic forces on the system.

B.2. The estimation of a damping coefficient from experiments

Two test with heaving cylinders were analysed. The first test was executed and recorded by Peter Naaijen for educational purposes. It was executed with high accuracy and dedicated equipment. The

second test was a free floating tube. Table B.1 was made based on the hereafter following equations.

Table B.1: Damping of heaving buoy

	Test 1	Test 2
Diameter	0.2	0.11
Draft	0.42	0.313575
natural frequency	4.5	5.09
mass	13.19469	2.98
added mass	2	0.61
Critical damping	1287.67	36.5889
damping	0.5	0.368232
damping ratio	0.04%	1.01%
Logaritmic decrament	0.00244	0.063237
surface	0.031416	0.009503

$$c_{cr} = 2\sqrt{km} \tag{B.10}$$

$$\omega_n = \sqrt{\frac{K}{m+a}} \tag{B.11}$$

$$\delta = \frac{1}{n} ln \frac{x(t)}{x(t+nT)} \tag{B.12}$$

$$\zeta = \frac{1}{\sqrt{1+(\frac{2\pi}{\delta})^2}} \tag{B.13}$$

B.3. Linearisation of the damping term in Morison

The forces acting on the system will be calculated with the Morison equation. The difficulty of this is the nonlinear damping term that is present in the equation. For that reason the damping will be linearised. The linearisation will be done making use of an equivalent energy assumption. Meaning that the energy (dissipation) over one period of the non-linear system is equal to the energy (dissipation) over one period of the linear system.

$$\frac{Energy}{T} = \frac{1}{T}\int_0^T F_m u dt => \frac{1}{T}\int_0^T b^{\{eq\}} dz u\, u dt = \frac{1}{T}\int_0^T \frac{\rho}{2} C_D D dz\, |u|\, u \cdot u dt \tag{B.14}$$

inserting:

$$u = -\zeta\omega\, \sin(\omega t + \epsilon) \tag{B.15}$$

results in:

$$\frac{1}{T}\int_0^T b^{\{eq\}}\, dz\, \zeta^2\omega^2 \sin^2(\omega t+\epsilon)\, dt = \frac{1}{T}\int_0^T \frac{\rho}{2} C_D D dz\, |\zeta\omega\, \sin(\omega t+\epsilon)|\, \zeta^2\omega^2\, \sin^2(\omega t+\epsilon)\, dt \tag{B.16}$$

The following result can be obtained.

$$\frac{1}{2}\, b^{\{eq\}}\, \zeta^2\omega^2 = \frac{\int_0^T 1/2\, \rho\, C_D D\, |\zeta\, \omega\, \sin(\omega t+\epsilon)|\, \zeta^2\omega^2\, (\sin(\omega t+\epsilon))^2\, \mathrm{d}t}{T} \tag{B.17}$$

$$=> b^{\{eq\}} = \frac{\rho\, C_D D\, \int_0^T |\zeta\, \omega\, \sin(\omega t+\epsilon)|\, (\sin(\omega t+\epsilon))^2\, \mathrm{d}t}{T} \tag{B.18}$$

Now the integral over the absolute value should be solved by splitting the integral over the negative and positive part within $|\zeta\, \omega\, \sin(\omega t+\epsilon)|$.

$$b^{\{eq\}} = \frac{\rho\, C\_DD\, \int_0^{T/2} \zeta\omega\, (\sin(\omega t+\epsilon))^3\, \mathrm{d}t}{T} - \frac{\rho\, C\_DD\, \int_{T/2}^{T} \zeta\omega\, (\sin(\omega t+\epsilon))^3\, \mathrm{d}t}{T} \tag{B.19}$$

Integrating the right hand side of the equation separately for its positive and negative part within the absolute and solving it for $b^{\{eq\}}$ results in the following expression:

$$b^{\{eq\}} = \frac{4\rho\, C_D\, D\ |u - \dot{x}|_a}{3\pi} \tag{B.20}$$

To find the amplitude of the relative movement of the structure: $|u - \dot{x}|_a$ some iteration is necessary. This equivalent damping results in the following adapted Morison equation:

$$dF_M = \rho\, dV\, \dot{u} + \rho\, c_m\, dV\, \dot{u} - \rho\, c_m\, dV\, \ddot{x} + b^{\{eq\}}(u - \dot{x})\, dl \tag{B.21}$$

With dl indicating a segment corresponding with the same orientation as the cnetre line of the construction.
As seen in formula B.21 the damping depends on the relative velocity of the fluid to the moving structure. In that way the linearised damping obtained so far for a non moving structure could also be used for a moving structure. So it is fair to assume that:

$$\frac{1}{2}\rho\, C_D\, D\, dl(u - \dot{x})\, |u - \dot{x}|_a \approx b^{\{eq\}}(u - \dot{x})\, dl \tag{B.22}$$

It could appear that this linearisation forgets the $2ab$ term in the solution of $(a + b)^2$. As taking the absolute value means the same as taking the magnitude of vector $u - v$ it is actually a scalar vector product.

C

Verification

C.1. Verification of Morison terms

Verification of Froude-Krylov and hydrodynamic mass torque

Table C.1: Verification of Froude-Krylov and hydrodynamic mass torque

ω=1.5; ζ=1; c_a=1; λ=27.5; D=0.1;					
Pos 1	Pos 2	Length	MATLAB	Verification	Reference
(0,0,0)	(-10,0,0)	10	-551.9 + 249.12i	-551.6+249.0i	Appendix C.2 part 1.4 equation 2.4.1
(0,0,0)	(0,-10,0)	10	0	0	
(0,0,0)	(WL,0,0)	WL	0 + 4326.9i	42.88+4324i	Appendix C.2 part 1.4 equation 2.4.3
$(\frac{WL}{4}, 0, 0)$	$(\frac{5\,WL}{4}, 0, 0)$	WL	4326.9 + 0i	-4324-21.44i	Appendix C.2 part 1.4 equation 2.4.4
(0,0,0)	(-10,-10,0)	$10\sqrt{2}$	-1103.8 + 498.2i	-1103+498.0i	Appendix C.2 part 1.4 equation 2.4.5

Table C.2: Verification of Froude-Krylov and hydrodynamic mass torque (2)

ω=0.5; ζ=5; C_a=1; λ=247; D=1					
Pos 1	Pos 2	Length	MATLAB	Verification	Reference
(0,0,0)	(-10,0,0)	10	-542.3 + 4232i	-542.0+4230i	Appendix C.2 part 1.4 equation 2.4.6
(0,0,0)	(-10,-10,0)	$10\sqrt{2}$	-1084.5 + 8465.1i	-1084+8461i	Appendix C.2 part 1.4 equation 2.4.7
(0,0,0)	$(-\frac{\sqrt{2}}{2}27, \frac{\sqrt{2}}{2}27, 0)$	27	-14244 + 57394i	-14237+57365i	Appendix C.2 part 1.4 equation 2.4.8

Verification of viscous drag force

Table C.3: Verification of viscous drag force

ω=1.5; ζ=1; C_d=1; λ=27.5; D=0.1; u_{RNa}=$\sqrt{2}, \zeta$, u_c=0					
Pos 1	Pos 2	Length	MATLAB	Verification	Reference
(0,0,0)	(-0.1,0,0)	0.1	0.0000 + 0.0000i 0.0000 + 0.0000i -0.1058 + 9.2274i	**9.233i**	Appendix C.2 part 2.3 equation 3.3.2
(0,0,0)	(0,-0.1,0)	0.1	9.2282 + 0.0000i 0.0000 + 0.0000i 0.0000 + 9.2282i		Appendix C.2 part 2.3 equation 3.3.2
(0,0,0)	(0,0,-0.1)	0.1	9.1232 0 0		Appendix C.2 part 2.3 equation 3.3.2
(0,0,0)	(WL,0,0)	WL	0 + 0i 0 + 0i 0 - 0.1781i * e-05	0	
(0,0,0)	(-10,-10,-10)	$10\sqrt{3}$	**380.49 + 97.53i -17.58 - 247.80i -362.91 + 150.27i**	**380.68 + 97.58i -17.58 - 247.9i -362.1 + 150.3i**	Appendix C.2 part 2.3 equation 3.3.3
$(\frac{WL}{4}, \frac{WL}{4}, 0)$	$(\frac{WL}{4} - 10, \frac{WL}{4} - 10, -10)$	$10\sqrt{3}$	**97.53 - 380.49i -247.80 + 17.58i 150.27 + 362.91i**	**95.69-381.2i -247.9+18.82i 152.1+362.3i**	Appendix C.2 part 2.3 equation 3.3.4

Table C.4: Verification of viscous drag force (2)

ω=0.5; ζ=5; C_a=1; λ=247; D=1; u_{RNa}=$\sqrt{2}\zeta$, u_c=0					
Pos 1	Pos 2	Length	MATLAB	Verification	Reference
(0,0,0)	(-0.1,0,0)	0.1	0.0000 + 0.0000i 0.0000 + 0.0000i -0.98 + 76.90i	76.94i	Appendix C.2 part 2.3 equation 3.3.5
(0,0,0)	(-10,-10,-10)	$10\sqrt{3}$	82352 - 29283i -34040 - 43554i -48312 + 72837i	82393 - 29297i -34057 - 43576i -48336 + 72874i	Appendix C.2 part 2.3 equation 3.3.6
(0,0,0)	$(-\frac{\sqrt{2}}{2}27, \frac{\sqrt{2}}{2}27, 0)$	27	99770 + 24760i 99770 + 24760i -49520 + 199540i	99821+24774i 99821+24774i -49548+199641i	Appendix C.2 part 2.3 equation 3.3.7

Verification of viscous drag torque

Table C.5: Verification of viscous drag torque

ω=1.5; ζ=1; C_d=1; λ=27.5; D=0.1; u_{RNa}=$\sqrt{2}\zeta$, u_c=0					
Pos 1	Pos 2	Length	MATLAB	Verification	Reference
(0,0,0)	(-10,0,0)	10	634.60 + 1405.9i	634.9+1406i	Appendix C.2 part 2.5 equation 3.5.1
(0,0,0)	(0,-10,0)	10	0	0	
(0,0,0)	(WL,0,0)	WL	11022 + 2.4 e-05i	11027-109.3i	Appendix C.2 part 2.5 equation 3.5.2
$(\frac{WL}{4}, 0, 0)$	$(\frac{5\,WL}{4}, 0, 0)$	WL	3.02e-05 - 11022i	-164.0 - 11026i	Appendix C.2 part 2.5 equation 3.5.3
(0,0,0)	(-10,-10,0)	$10\sqrt{2}$	1269.2 + 2811.8i	1270 + 2813i	Appendix C.2 part 2.5 equation 3.5.4

Table C.6: Verification of viscous drag torque (2)

ω=0.5; ζ=5; C_a=1; λ=247; D=1; u_{RNa}=$sqrt(2)\zeta$, u_c=0					
Pos 1	Pos 2	Length	MATLAB	Verification	Reference
(0,0,0)	(-10,0,0)	10	16173 + 2072i	16181 + 2073i	Appendix C.2 part 2.5 equation 3.5.5
(0,0,0)	(-10,-10,0)	$10\sqrt{2}$	32346 + 4144i	32362 + 4146i	Appendix C.2 part 2.5 equation 3.5.6
(0,0,0)	$(-\frac{\sqrt{2}}{2}27, \frac{\sqrt{2}}{2}27, 0)$	27	219310 + 54429	219418 + 54457i	Appendix C.2 part C.2 part 2.5 equation 3.5.7

C.2. Verification of the Morison terms (maple code)

see next page

Maple script for verification

This appendix is is generated in Maple 2018 by Andreas Feys for his master Thesis. It explains the application of the Morison equation for the calculation of the force on a cylinder with random orientation. These calculations contain an exact solution on the integration of the forces in vertical direction. The maple language will be transfered to MATLAB language.

u and w indicate velocities, when a "_d" is indicated this means the derivitive with respect to time. Other subscripts indicated in the formulas comming from clauss et al are represeted with "_" and the same letters as indicated in the coppy pasted formulas. The beams have a local axis frame (o,p,z) with o-axis in the direction of the beam and the z-axis the vertical direction. From time to timp multiplications of two parts are indicated by attaching the two parts with an underscore

For the calculation of the force on a random oriented beam the following formula is used as difined in Clauss et al

$$\mathrm{d}\mathbf{F}_N = \underbrace{\rho \frac{\pi D^2}{4}\,\mathrm{d}s\,\frac{\partial \boldsymbol{v}_N}{\partial t}}_{\text{Froude–Krylov force}} + \underbrace{C_a \rho \frac{\pi D^2}{4}\,\mathrm{d}s\,\frac{\partial \mathbf{u}_{RN}}{\partial t}}_{\text{Hydrodynamic mass force}} + \underbrace{C_d \frac{\rho}{2} D\,\mathrm{d}s\,|\mathbf{u}_{RN}|\mathbf{u}_{RN}}_{\text{Viscous drag force}},$$

It consists of three parts. Each part will be calculated individualy

0. Maple toolbox, Airy wave theory and tanguent vector

The velocity of the water (u, 0, w) and the unit vector for the orientation of the beam: e_t

```
> restart;
> with(LinearAlgebra)
```

[&x, Add, Adjoint, BackwardSubstitute, BandMatrix, Basis, BezoutMatrix, BidiagonalForm, BilinearForm, CARE, CharacteristicMatrix, CharacteristicPolynomial, Column, ColumnDimension, ColumnOperation, ColumnSpace, CompanionMatrix, CompressedSparseForm, ConditionNumber, ConstantMatrix, ConstantVector, Copy, CreatePermutation, CrossProduct, DARE, DeleteColumn, DeleteRow, Determinant, Diagonal, DiagonalMatrix, Dimension, Dimensions, DotProduct, EigenConditionNumbers, Eigenvalues, Eigenvectors, Equal, ForwardSubstitute, FrobeniusForm, FromCompressedSparseForm, FromSplitForm, GaussianElimination, GenerateEquations, GenerateMatrix, Generic, GetResultDataType, GetResultShape, GivensRotationMatrix, GramSchmidt, HankelMatrix, HermiteForm, HermitianTranspose, HessenbergForm, HilbertMatrix, HouseholderMatrix, IdentityMatrix, IntersectionBasis, IsDefinite, IsOrthogonal, IsSimilar, IsUnitary, JordanBlockMatrix, JordanForm, KroneckerProduct, LA_Main, LUDecomposition, LeastSquares, LinearSolve, LyapunovSolve, Map, Map2, MatrixAdd, MatrixExponential, MatrixFunction, MatrixInverse, MatrixMatrixMultiply, MatrixNorm, MatrixPower, MatrixScalarMultiply, MatrixVectorMultiply, MinimalPolynomial, Minor, Modular, Multiply, NoUserValue, Norm, Normalize, NullSpace, OuterProductMatrix, Permanent, Pivot, PopovForm, ProjectionMatrix, QRDecomposition, RandomMatrix, RandomVector, Rank, RationalCanonicalForm, ReducedRowEchelonForm, Row, RowDimension, RowOperation, RowSpace, ScalarMatrix, ScalarMultiply, ScalarVector, SchurForm, SingularValues, SmithForm, SplitForm, StronglyConnectedBlocks, SubMatrix, SubVector, SumBasis, SylvesterMatrix, SylvesterSolve, ToeplitzMatrix, Trace, Transpose, TridiagonalForm, UnitVector, VandermondeMatrix, VectorAdd, VectorAngle, VectorMatrixMultiply, VectorNorm, VectorScalarMultiply, ZeroMatrix, ZeroVector, Zip] **(1.1)**

```
> u := ζ·omega·exp(k·z)·exp(-I·k·x)·exp(I·omega·t);
```

$$u := \zeta\,\omega\,e^{kz}\,e^{-\mathrm{I}kx}\,e^{\mathrm{I}\omega t} \quad \textbf{(1.2)}$$

```
> w := I·ζ·omega·exp(k·z)·exp(-I·k·x)·exp(I·omega·t);
```

$$w := \mathrm{I}\,\zeta\,\omega\,e^{kz}\,e^{-\mathrm{I}kx}\,e^{\mathrm{I}\omega t} \quad \textbf{(1.3)}$$

```
> v := Vector([u, 0, w]);
```

$$v := \begin{bmatrix} \zeta\,\omega\,e^{kz}\,e^{-\mathrm{I}kx}\,e^{\mathrm{I}\omega t} \\ 0 \\ \mathrm{I}\,\zeta\,\omega\,e^{kz}\,e^{-\mathrm{I}kx}\,e^{\mathrm{I}\omega t} \end{bmatrix} \quad \textbf{(1.4)}$$

```
> v_d := diff(v, t);
```

$$v\_d := \begin{bmatrix} \mathrm{I}\,\zeta\,\omega^2\,e^{kz}\,e^{-\mathrm{I}kx}\,e^{\mathrm{I}\omega t} \\ 0 \\ -\zeta\,\omega^2\,e^{kz}\,e^{-\mathrm{I}kx}\,e^{\mathrm{I}\omega t} \end{bmatrix} \quad \textbf{(1.5)}$$

```
> e_t := Vector([e_tx, e_ty, e_tz]);
```

$$e\_t := \begin{bmatrix} e\_tx \\ e\_ty \\ e\_tz \end{bmatrix} \quad \textbf{(1.6)}$$

```
> Omega := Vector([0, Omega_p·exp(I·omega·t), 0]); r_s := Vector([r_so, 0, 0]); Omega_x_rs := simplify(CrossProduct(Omega, r_s));
```

$$\Omega := \begin{bmatrix} 0 \\ Omega\_p\,e^{\mathrm{I}\omega t} \\ 0 \end{bmatrix}$$

$$r\_s := \begin{bmatrix} r\_so \\ 0 \\ 0 \end{bmatrix}$$

$$Omega\_x\_rs := \begin{bmatrix} 0 \\ 0 \\ -Omega\_p\, e^{I\omega t}\, r\_so \end{bmatrix} \quad (1.7)$$

> $u\_c := Vector([0, 0, c\_z \cdot \exp(I \cdot \text{omega} \cdot t)]) + Omega\_x\_rs;$

$$u\_c := \begin{bmatrix} 0 \\ 0 \\ c\_z\, e^{I\omega t} - Omega\_p\, e^{I\omega t}\, r\_so \end{bmatrix} \quad (1.8)$$

> $Omega\_d := Vector([0, Omega\_d\_p \cdot \exp(I \cdot \text{omega} \cdot t), 0]);\ Omega\_d\_x\_rs := simplify(CrossProduct(Omega\_d, r\_s));$

$$Omega\_d := \begin{bmatrix} 0 \\ Omega\_d\_p\, e^{I\omega t} \\ 0 \end{bmatrix}$$

$$Omega\_d\_x\_rs := \begin{bmatrix} 0 \\ 0 \\ -Omega\_d\_p\, e^{I\omega t}\, r\_so \end{bmatrix} \quad (1.9)$$

> $u\_dc := Vector([0, 0, c\_dz \cdot \exp(I \cdot \text{omega} \cdot t)]) + Omega\_d\_x\_rs;$

$$u\_dc := \begin{bmatrix} 0 \\ 0 \\ c\_dz\, e^{I\omega t} - Omega\_d\_p\, e^{I\omega t}\, r\_so \end{bmatrix} \quad (1.10)$$

1. Froude-Krylov & hydrodynamic mass part due to wave

1.1 Froude-Krylov & hydrodynamic mass force due to waves

1.2 Verification matlab based on Froude-Krylov & hydrodynamic mass force due to waves

1.3 Froude-Krylov & hydrodynamic mass torque due to waves for horizontal orientation

1.4 Verification matlab based on Froude-Krylov & hydrodynamic mass torque due to waves

> $simplify\left(subs\left(\left[c\_a = 1, D = 0.1, rho = 1025, L = 10, \zeta = 1, \omega = 1.5, k = \frac{1.5^2}{9.81}, pi = 3.14, x\_1 = 0, z\_1 = 0, e\_tx = -1, e\_ty = 0, e\_tz = 0\right], M\_sperpendicular\_FKHM\_horizontal\right)\right);$

$$-551.6173152 + 248.9932689\, I \quad (2.4.1)$$

> $WL := 9.84\left(\frac{2 \cdot 3.1419}{1.5^2}\right);$

$$WL := 27.48115200 \quad (2.4.2)$$

> $simplify\left(subs\left(\left[c\_a = 1, D = 0.1, rho = 1025, L = WL, \zeta = 1, \omega = 1.5, k = \frac{1.5^2}{9.81}, pi = 3.14, x\_1 = 0, z\_1 = 0, e\_tx = 1, e\_ty = 0, e\_tz = 0\right], M\_sperpendicular\_FKHM\_horizontal\right)\right);$

$$42.87948309 + 4324.303204\, I \quad (2.4.3)$$

> $simplify\left(subs\left(\left[c\_a = 1, D = 0.1, rho = 1025, L = WL, \zeta = 1, \omega = 1.5, k = \frac{1.5^2}{9.81}, pi = 3.14, x\_1 = \frac{WL}{4}, z\_1 = 0, e\_tx = -1, e\_ty = 0, e\_tz = 0\right], M\_sperpendicular\_FKHM\_horizontal\right)\right);$

$$-4324.462647 - 21.44000384\, I \quad (2.4.4)$$

> $simplify\left(subs\left(\left[c\_a = 1, D = 0.1, rho = 1025, L = \text{sqrt}(2) \cdot 10, \zeta = 1, \omega = 1.5, k = \frac{1.5^2}{9.81}, pi = 3.14, x\_1 = 0, z\_1 = 0, e\_tx = \frac{-1}{\text{sqrt}(2)}, e\_ty = \frac{-1}{\text{sqrt}(2)}, e\_tz = 0\right], M\_sperpendicular\_FKHM\_horizontal\right)\right);$

$$-1103.234631 + 497.9865380\, I \quad (2.4.5)$$

> $simplify\left(subs\left(\left[c\_a = 1, D = 1, rho = 1025, L = 10, \zeta = 5, \omega = 0.5, k = \frac{0.5^2}{9.81}, pi = 3.14, x\_1 = 0, z\_1 = 0, e\_tx = -1, e\_ty = 0, e\_tz = 0\right], M\_sperpendicular\_FKHM\_horizontal\right)\right);$

$$-541.9794183 + 4230.413299\, I \quad (2.4.6)$$

> $simplify\left(subs\left(\left[c\_a=1, D=1, rho=1025, L=sqrt(2)\cdot 10, \zeta=5, \omega=0.5, k=\frac{0.5^2}{9.81}, pi=3.14, x\_1=0, z\_1=0, e\_tx=\frac{-1}{sqrt(2)}, e\_ty=\frac{-1}{sqrt(2)}, e\_tz=0\right], M\_sperpendicular\_FKHM\_horizontal\right)\right);$

$$-1083.959766 + 8460.826596\,I \tag{2.4.7}$$

> $simplify\left(subs\left(\left[c\_a=1, D=1, rho=1025, L=27, \zeta=5, \omega=0.5, k=\frac{0.5^2}{9.81}, pi=3.14, x\_1=0, z\_1=0, e\_tx=\frac{-1}{sqrt(2)}, e\_ty=\frac{+1}{sqrt(2)}, e\_tz=0\right], M\_sperpendicular\_FKHM\_horizontal\right)\right);$

$$-14237.20982 + 57365.06724\,I \tag{2.4.8}$$

2. Viscous drag part due to wave

2.1 Ampletude

As the assumption is made that the construction will only move in vertical direction only this angular velocity (arround the local p-axis) is taken into account. for the distance vector only the distance till the middel is taken into account in the direction of the local p-axis. This results in a movement only in the z direction. this matches with what was expected.

> $u\_c;$

$$\begin{bmatrix} 0 \\ 0 \\ c\_z\,e^{I\omega t} - Omega\_p\,e^{I\omega t}\,r\_so \end{bmatrix} \tag{3.1.1}$$

So the relative velocity is calculated: $\mathbf{u_R} = \boldsymbol{v} - \mathbf{u_c}$, , with v the perviously defined velocity in the fluid

> $u\_R := v - u\_c;$

$$u\_R := \begin{bmatrix} \zeta\,\omega\,e^{kz}\,e^{-Ikx}\,e^{I\omega t} \\ 0 \\ I\,\zeta\,\omega\,e^{kz}\,e^{-Ikx}\,e^{I\omega t} - c\_z\,e^{I\omega t} + Omega\_p\,e^{I\omega t}\,r\_so \end{bmatrix} \tag{3.1.2}$$

Then the velocity is decomposed in perpendicular direction to the cylinder centre line $\mathbf{u_{RN}} = \mathbf{e_t} \times (\mathbf{u_R} \times \mathbf{e_t})$,

> $u\_RN := simplify(CrossProduct(e\_t, CrossProduct(u\_R, e\_t)));$

$$u\_RN := \begin{bmatrix} -\left(I\,e\_tx\,e\_tz - e\_ty^2 - e\_tz^2\right)\zeta\,\omega\,e^{(z-Ix)k+I\omega t} - e^{I\omega t}\,e\_tx\,e\_tz\,(Omega\_p\,r\_so - c\_z) \\ -\left((e\_tx + I\,e\_tz)\,\zeta\,\omega\,e^{-k(Ix-z)} + e\_tz\,(Omega\_p\,r\_so - c\_z)\right)e^{I\omega t}\,e\_ty \\ \zeta\,\omega\left(I\,e\_tx^2 + I\,e\_ty^2 - e\_tx\,e\_tz\right)e^{(z-Ix)k+I\omega t} + e^{I\omega t}\left(e\_tx^2 + e\_ty^2\right)(Omega\_p\,r\_so - c\_z) \end{bmatrix} \tag{3.1.3}$$

To find the linearised drag force the ampletude of the relative perpendicular velocity need to be calculated.

$$d\mathbf{F_d} = C_{dl}\,\frac{\rho}{2}\,D\,ds\cdot\mathbf{u_{RN}} = \frac{8}{3\pi}\,C_d\cdot\frac{\rho}{2}\,D\,ds\cdot u_{RNa}\mathbf{u_{RN}},$$

> $u\_RN\_a := simplify\left(abs\left(\sqrt{\left(\frac{u\_RN(1,1)}{exp(I\,omega\,t)}\right)^2 + \left(\frac{u\_RN(2,1)}{exp(I\,omega\,t)}\right)^2 + \left(\frac{u\_RN(3,1)}{exp(I\,omega\,t)}\right)^2}\right)\right)$

$$u\_RN\_a := \sqrt{2}\left(\left|\left(-\zeta\,(Omega\_p\,r\_so - c\_z)\,\omega\,(I\,e\_tx^2 + I\,e\_ty^2 - e\_tx\,e\_tz)\,e^{-k(Ix-z)} + \zeta^2\,\omega^2\left(I\,e\_tx\,e\_tz + \frac{e\_tx^2}{2} - \frac{e\_tz^2}{2}\right)e^{-2k(Ix-z)} - \frac{\left(e\_tx^2 + e\_ty^2\right)(Omega\_p\,r\_so - c\_z)^2}{2}\right)\left(e\_tx^2 + e\_ty^2 + e\_tz^2\right)\right|\right)^{1/2} \tag{3.1.4}$$

2.2 Viscous drag Force

> $v;$

$$\begin{bmatrix} \zeta\,\omega\,e^{kz}\,e^{-Ikx}\,e^{I\omega t} \\ 0 \\ I\,\zeta\,\omega\,e^{kz}\,e^{-Ikx}\,e^{I\omega t} \end{bmatrix} \tag{3.2.1}$$

> $v\_RN := simplify(CrossProduct(e\_t, CrossProduct(v, e\_t)));$

$$v\_RN := \begin{bmatrix} -\left(I\,e\_tx\,e\_tz - e\_ty^2 - e\_tz^2\right)\zeta\,\omega\,e^{(z-Ix)k+I\omega t} \\ -e^{(z-Ix)k+I\omega t}\,\zeta\,e\_ty\,\omega\,(e\_tx + I\,e\_tz) \\ \zeta\,\omega\left(I\,e\_tx^2 + I\,e\_ty^2 - e\_tx\,e\_tz\right)e^{(z-Ix)k+I\omega t} \end{bmatrix} \tag{3.2.2}$$

> $v\_RN := simplify(subs(z = z\_1 + s\cdot e\_tz, subs(x = x\_1 + s\cdot e\_tx, v\_RN)));$

$$v\_RN := \begin{bmatrix} -\left(\mathrm{I}\, e\_tx\, e\_tz - e\_ty^2 - e\_tz^2\right)\zeta\,\omega\, e^{((-\mathrm{I}e\_tx+e\_tz)\,s-\mathrm{I}x\_1+z\_1)\,k+\mathrm{I}\omega t} \\ -e^{((-\mathrm{I}e\_tx+e\_tz)\,s-\mathrm{I}x\_1+z\_1)\,k+\mathrm{I}\omega t}\,\zeta\, e\_ty\,\omega\,(e\_tx+\mathrm{I}\,e\_tz) \\ \zeta\,\omega\left(\mathrm{I}\, e\_tx^2+\mathrm{I}\, e\_ty^2-e\_tx\, e\_tz\right) e^{((-\mathrm{I}e\_tx+e\_tz)\,s-\mathrm{I}x\_1+z\_1)\,k+\mathrm{I}\omega t} \end{bmatrix} \tag{3.2.3}$$

> $v\_RN\_ds := simplify\left(Vector\left(\left[\int_0^L \frac{v\_RN(1,1)}{\exp(I\,\mathrm{omega}\,t)}\,ds, \int_0^L \frac{v\_RN(2,1)}{\exp(I\,\mathrm{omega}\,t)}\,ds, \int_0^L \frac{v\_RN(3,1)}{\exp(I\,\mathrm{omega}\,t)}\,ds\right]\right)\right);$

$$v\_RN\_ds := \begin{bmatrix} \frac{\omega\,\zeta\left(\mathrm{I}\, e\_tx\, e\_tz - e\_ty^2 - e\_tz^2\right)\left(e^{-k((\mathrm{I}e\_tx-e\_tz)\,L+\mathrm{I}x\_1-z\_1)}-e^{-k(\mathrm{I}x\_1-z\_1)}\right)}{(\mathrm{I}\,e\_tx-e\_tz)\,k} \\ \frac{(e\_tx+\mathrm{I}\,e\_tz)\,\zeta\, e\_ty\,\omega\left(e^{-k((\mathrm{I}e\_tx-e\_tz)\,L+\mathrm{I}x\_1-z\_1)}-e^{-k(\mathrm{I}x\_1-z\_1)}\right)}{(\mathrm{I}\,e\_tx-e\_tz)\,k} \\ \frac{\left(\mathrm{I}\, e\_tx^2+\mathrm{I}\, e\_ty^2-e\_tx\, e\_tz\right)\zeta\,\omega\left(e^{-k(\mathrm{I}x\_1-z\_1)}-e^{-k((\mathrm{I}e\_tx-e\_tz)\,L+\mathrm{I}x\_1-z\_1)}\right)}{(\mathrm{I}\,e\_tx-e\_tz)\,k} \end{bmatrix} \tag{3.2.4}$$

> $F\_n\_VD := simplify\left(\frac{8}{3\cdot \mathrm{pi}}\, c\_dl\cdot\, \frac{\mathrm{rho}}{2}\, \mathrm{D}\, u\_RN\_A\cdot\sim v\_RN\_ds\right);$

$$F\_n\_VD := \begin{bmatrix} -\frac{4\, c\_dl\,\rho\,\mathrm{D}\, u\_RN\_A\,\omega\,\zeta\left(\mathrm{I}\, e\_tx\, e\_tz - e\_ty^2 - e\_tz^2\right)\left(e^{-k(\mathrm{I}x\_1-z\_1)}-e^{-k((\mathrm{I}e\_tx-e\_tz)\,L+\mathrm{I}x\_1-z\_1)}\right)}{3\,\pi\,(\mathrm{I}\,e\_tx-e\_tz)\,k} \\ -\frac{4\, c\_dl\,\rho\,\mathrm{D}\, u\_RN\_A\,(e\_tx+\mathrm{I}\,e\_tz)\,\zeta\, e\_ty\,\omega\left(e^{-k(\mathrm{I}x\_1-z\_1)}-e^{-k((\mathrm{I}e\_tx-e\_tz)\,L+\mathrm{I}x\_1-z\_1)}\right)}{3\,\pi\,(\mathrm{I}\,e\_tx-e\_tz)\,k} \\ \frac{4\, c\_dl\,\rho\,\mathrm{D}\, u\_RN\_A\left(\mathrm{I}\, e\_tx^2+\mathrm{I}\, e\_ty^2-e\_tx\, e\_tz\right)\zeta\,\omega\left(e^{-k(\mathrm{I}x\_1-z\_1)}-e^{-k((\mathrm{I}e\_tx-e\_tz)\,L+\mathrm{I}x\_1-z\_1)}\right)}{3\,\pi\,(\mathrm{I}\,e\_tx-e\_tz)\,k} \end{bmatrix} \tag{3.2.5}$$

2.3 Viscous drag Force Verification

> $\frac{8}{3\cdot \mathrm{pi}}\, c\_dl\cdot\, \frac{\mathrm{rho}}{2}\, \mathrm{D}\, u\_RN\_A\cdot \mathrm{I}\,\zeta\,\omega\, e^{kz}\, e^{-\mathrm{I}kx}\cdot L$

$$\frac{\frac{4\,\mathrm{I}}{3}\, c\_dl\,\rho\,\mathrm{D}\, u\_RN\_A\,\zeta\,\omega\, e^{kz}\, e^{-\mathrm{I}kx}\, L}{\pi} \tag{3.3.1}$$

> $simplify\left(subs\left(\left[c\_dl=1, \mathrm{D}=0.1, \mathrm{rho}=1025, L=0.1, \zeta=1, \omega=1.5, k=\frac{1.5^2}{9.81}, \mathrm{pi}=3.14, x=0, z=0, u\_RN\_A=\mathrm{sqrt}(2)\right], (3.3.1)\right)\right);$

$$9.232922933\ \mathrm{I} \tag{3.3.2}$$

> $simplify\left(subs\left(\left[c\_dl=1, \mathrm{D}=0.1, \mathrm{rho}=1025, L=\mathrm{sqrt}(3)\cdot 10, \zeta=1, \omega=1.5, k=\frac{1.5^2}{9.81}, \mathrm{pi}=3.14, x\_1=0, z\_1=0, e\_tx=\frac{-1}{\mathrm{sqrt}(3)}, e\_ty=\frac{-1}{\mathrm{sqrt}(3)}, e\_tz=\frac{-1}{\mathrm{sqrt}(3)}, u\_RN\_A=\mathrm{sqrt}(2)\right], (3.2.5)\right)\right);$

$$\begin{bmatrix} 380.6864532 + 97.58191766\ \mathrm{I} \\ -17.58814006 - 247.9282556\ \mathrm{I} \\ -363.0983134 + 150.3463379\ \mathrm{I} \end{bmatrix} \tag{3.3.3}$$

> $WL; simplify\left(subs\left(\left[c\_dl=1, \mathrm{D}=0.1, \mathrm{rho}=1025, L=\mathrm{sqrt}(3)\cdot 10, \zeta=1, \omega=1.5, k=\frac{1.5^2}{9.81}, \mathrm{pi}=3.14, x\_1=\frac{WL}{4}, z\_1=0, e\_tx=\frac{-1}{\mathrm{sqrt}(3)}, e\_ty=\frac{-1}{\mathrm{sqrt}(3)}, e\_tz=\frac{-1}{\mathrm{sqrt}(3)}, u\_RN\_A=\mathrm{sqrt}(2)\right], (3.2.5)\right)\right);$

$$27.48115200$$

$$\begin{bmatrix} 95.69335798 - 381.1655648\ \mathrm{I} \\ -247.8380105 + 18.81709821\ \mathrm{I} \\ 152.1446524 + 362.3484665\ \mathrm{I} \end{bmatrix} \tag{3.3.4}$$

> $simplify\left(subs\left(\left[c\_dl=1, \mathrm{D}=0.1, \mathrm{rho}=1025, L=0.1, \zeta=5, \omega=0.5, k=\frac{0.5^2}{9.81}, \mathrm{pi}=3.14, x=0, z=0, u\_RN\_A=5\ \mathrm{sqrt}(2)\right], (3.3.1)\right)\right);$

$$76.94102444\ \mathrm{I} \tag{3.3.5}$$

> $simplify\left(subs\left(\left[c\_dl=1, \mathrm{D}=1, \mathrm{rho}=1025, L=\mathrm{sqrt}(3)\cdot 10, \zeta=5, \omega=0.5, k=\frac{0.5^2}{9.81}, \mathrm{pi}=3.14, x\_1=0, z\_1=0, e\_tx=\frac{-1}{\mathrm{sqrt}(3)}, e\_ty=\frac{-1}{\mathrm{sqrt}(3)}, e\_tz=\frac{-1}{\mathrm{sqrt}(3)}, u\_RN\_A=5\cdot \mathrm{sqrt}(2)\right], (3.2.5)\right)\right);$

$$\begin{bmatrix} 82393.49851 - 29297.61420\ \mathrm{I} \\ -34057.26823 - 43576.57631\ \mathrm{I} \\ -48336.23029 + 72874.19041\ \mathrm{I} \end{bmatrix} \tag{3.3.6}$$

> $simplify\left(subs\left(\left[c\_dl=1, \mathrm{D}=1, \mathrm{rho}=1025, L=27, \zeta=5, \omega=0.5, k=\frac{0.5^2}{9.81}, \mathrm{pi}=3.14, x\_1=0, z\_1=0, e\_tx=\frac{-1}{\mathrm{sqrt}(2)}, e\_ty=\frac{+1}{\mathrm{sqrt}(2)}, e\_tz=0, u\_RN\_A=5\cdot \mathrm{sqrt}(2)\right], (3.2.5)\right)\right);$

$$\begin{bmatrix} 99820.53973 + 24774.06471\,I \\ 99820.53973 + 24774.06471\,I \\ -49548.1294 + 199641.0795\,I \end{bmatrix} \quad (3.3.7)$$

2.4 Viscous drag Torque

```
> simplify( 8/(3·pi) u_rn_A· c_d· rho/2 D·int(-(-L/2 + s)·v_RN(3,1)/exp(I omega t), s = 0..L) );
```

$$\frac{1}{3\pi k^2\left(-3\,e\_tx^2\,e\_tz + I\,e\_tx^3 - 3\,I\,e\_tx\,e\_tz^2 + e\_tz^3\right)}\left(2\,c\_d\,\omega\,\zeta\,u\_rn\_A\,\rho\,D\left(\left(I\,L\,e\_tx^4\,k + \left(-3\,k\,L\,e\_tz + 2\right)e\_tx^3 + \left(I\,e\_ty^2\,L\,k - 3\,I\,e\_tz^2\,L\,k + 4\,I\,e\_tz\right)e\_tx^2 + \left(-2\,L\,e\_ty^2\,e\_tz\,k + L\,e\_tz^3\,k + 2\,e\_ty^2 - 2\,e\_tz^2\right)e\_tx - I\left(k\,L\,e\_tz - 2\right)e\_tz\,e\_ty^2\right)e^{-k\left(\left(I\,e\_tx - e\_tz\right)L + I\,x\_1 - z\_1\right)} + \left(I\,L\,e\_tx^4\,k + \left(-3\,k\,L\,e\_tz - 2\right)e\_tx^3 + \left(I\,e\_ty^2\,L\,k - 3\,I\,e\_tz^2\,L\,k - 4\,I\,e\_tz\right)e\_tx^2 + \left(-2\,L\,e\_ty^2\,e\_tz\,k + L\,e\_tz^3\,k - 2\,e\_ty^2 + 2\,e\_tz^2\right)e\_tx - I\,e\_tz\left(k\,L\,e\_tz + 2\right)e\_ty^2\right)e^{-k\left(I\,x\_1 - z\_1\right)}\right)\right) \quad (3.4.1)$$

2.5 Viscous drag Torque verification

```
> simplify( subs( [c_d = 1, D = 0.1, rho = 1025, L = 10, ζ = 1, ω = 1.5, k = 1.5^2/9.81, pi = 3.14, x_1 = 0, z_1 = 0, e_tx = -1, e_ty = 0, e_tz = 0, u_rn_A = sqrt(2)], (3.4.1)) );
```

$$634.9225936 + 1406.601463\,I \quad (3.5.1)$$

```
> WL; simplify( subs( [c_d = 1, D = 0.1, rho = 1025, L = WL, ζ = 1, ω = 1.5, k = 1.5^2/9.81, pi = 3.14, x_1 = 0, z_1 = 0, e_tx = 1, e_ty = 0, e_tz = 0, u_rn_A = sqrt(2)], (3.4.1)) );
```

$$\begin{bmatrix} 27.48115200 \\ 11026.79530 - 109.3409184\,I \end{bmatrix} \quad (3.5.2)$$

```
> simplify( subs( [c_d = 1, D = 0.1, rho = 1025, L = WL, ζ = 1, ω = 1.5, k = 1.5^2/9.81, pi = 3.14, x_1 = WL/4, z_1 = 0, e_tx = 1, e_ty = 0, e_tz = 0, u_rn_A = sqrt(2)], (3.4.1)) );
```

$$-164.0080149 - 11026.11769\,I \quad (3.5.3)$$

```
> simplify( subs( [c_d = 1, D = 0.1, rho = 1025, L = 10·sqrt(2), ζ = 1, ω = 1.5, k = 1.5^2/9.81, pi = 3.14, x_1 = 0, z_1 = 0, e_tx = -1/sqrt(2), e_ty = -1/sqrt(2), e_tz = 0, u_rn_A = sqrt(2)], (3.4.1)) );
```

$$1269.845187 + 2813.202926\,I \quad (3.5.4)$$

```
> simplify( subs( [c_d = 1, D = 1, rho = 1025, L = 10, ζ = 5, ω = 0.5, k = 0.5^2/9.81, pi = 3.14, x_1 = 0, z_1 = 0, e_tx = -1, e_ty = 0, e_tz = 0, u_rn_A = 5·sqrt(2)], (3.4.1)) );
```

$$16181.06998 + 2073.036057\,I \quad (3.5.5)$$

```
> simplify( subs( [c_d = 1, D = 1, rho = 1025, L = 10·sqrt(2), ζ = 5, ω = 0.5, k = 0.5^2/9.81, pi = 3.14, x_1 = 0, z_1 = 0, e_tx = -1/sqrt(2), e_ty = -1/sqrt(2), e_tz = 0, u_rn_A = 5 sqrt(2)], (3.4.1)) );
```

$$32362.13994 + 4146.079223\,I \quad (3.5.6)$$

```
> evalf( simplify( subs( [c_d = 1, D = 1, rho = 1025, L = 27, ζ = 5, ω = 0.5, k = 0.5^2/9.81, pi = 3.14, x_1 = 0, z_1 = 0, e_tx = -1/sqrt(2), e_ty = 1/sqrt(2), e_tz = 0, u_rn_A = 5 sqrt(2)], (3.4.1)) ) );
```

$$219417.85 + 54456.448\,I \quad (3.5.7)$$

3. Added mass

3.1 Added mass translation

Now the relevant acceleration perpendicular to the centre line of the cylinder needs to be decomposed: $\frac{\partial \mathbf{u}_{RN}}{\partial t} = \mathbf{e}_t \times \left(\frac{\partial \mathbf{u}_R}{\partial t} \times \mathbf{e}_t\right)$,

```
> u_dc;
```

$$\begin{bmatrix} 0170 \\ 0 \\ c\_dz\,e^{I\omega t} - Omega\_d\_p\,e^{I\omega t}\,r\_so \end{bmatrix} \quad (4.1.1)$$

> $u\_dcN := simplify(CrossProduct(e\_t, CrossProduct(u\_dc, e\_t)))$;

$$u\_dcN := \begin{bmatrix} -e\_tz\, e^{I\omega t}\,(-r\_so\ Omega\_d\_p + c\_dz)\ e\_tx \\ -e\_tz\, e^{I\omega t}\,(-r\_so\ Omega\_d\_p + c\_dz)\ e\_ty \\ e^{I\omega t}\,(e\_tx^2 + e\_ty^2)\ (-r\_so\ Omega\_d\_p + c\_dz) \end{bmatrix} \tag{4.1.2}$$

To find the total force the cylinder needs to be integrated over its length. only the varying parts over the length will be integrated. This is only u_dRN. To do that an axis system (s) will be defined following the centre line of the cylinder. This is simularly as before. What is different is that the distance form position "s" to the centre point need to be calculated: $r\_so = s - \frac{L}{2}$

$$\_so = -\frac{L}{2} + s \tag{4.1.3}$$

> $u\_dcN := simplify\left(subs\left(r\_so = s - \frac{L}{2}, subs(z = z\_1 + s\cdot e\_tz, subs(x = x\_1 + s\cdot e\_tx, u\_dcN))\right)\right)$;

$$u\_dcN := \begin{bmatrix} -\frac{e\_tx\, e^{I\omega t}\,((L - 2\,s)\ Omega\_d\_p + 2\,c\_dz)\ e\_tz}{2} \\ -\frac{e\_ty\, e^{I\omega t}\,((L - 2\,s)\ Omega\_d\_p + 2\,c\_dz)\ e\_tz}{2} \\ \frac{e^{I\omega t}\,((L - 2\,s)\ Omega\_d\_p + 2\,c\_dz)\ (e\_tx^2 + e\_ty^2)}{2} \end{bmatrix} \tag{4.1.4}$$

> $u\_dcNds := simplify\left(Vector\left(\left[\int_0^L u\_dcN(1,1)\,ds, \int_0^L u\_dRN(2,1)\,ds, \int_0^L u\_dcN(3,1)\,ds\right]\right)\right)$;

$$u\_dcNds := \begin{bmatrix} -L\, e^{I\omega t}\, c\_dz\, e\_tx\, e\_tz \\ u\_dRN(2,1)\, L \\ L\, e^{I\omega t}\, c\_dz\, (e\_tx^2 + e\_ty^2) \end{bmatrix} \tag{4.1.5}$$

This results in the total force vector.

> $F\_n\_HM := simplify\left(c\_a\cdot rho\cdot \frac{pi\cdot D^2}{4} \cdot\sim u\_dcNds\right)$;

$$F\_n\_HM := \begin{bmatrix} -\frac{c\_a\, \rho\, \pi\, D^2\, L\, e^{I\omega t}\, c\_dz\, e\_tx\, e\_tz}{4} \\ \frac{c\_a\, \rho\, \pi\, D^2\, u\_dRN(2,1)\, L}{4} \\ \frac{c\_a\, \rho\, \pi\, D^2\, L\, e^{I\omega t}\, c\_dz\, (e\_tx^2 + e\_ty^2)}{4} \end{bmatrix} \tag{4.1.6}$$

for this calculation only the time independent z-component is relevant

> $simplify\left(\frac{subs((e\_tx^2 + e\_ty^2) = 1, F\_n\_HM(3,1))}{\exp(I\,omega\,t)}\right)$; $simplify\left(\frac{subs((e\_tx^2 + e\_ty^2) = 1, F\_n\_HM(3,1))}{\exp(I\,omega\,t)\cdot c\_dz}\right)$;

$$\frac{c\_a\, \rho\, \pi\, D^2\, L\, c\_dz}{4}$$

$$\frac{c\_a\, \rho\, \pi\, D^2\, L}{4} \tag{4.1.7}$$

3.2 Added innertia

> $aaa := CrossProduct\left(e\_t\cdot\left(-\frac{L}{2} + s\right), u\_dcN\right)$

$$aaa := \left[\left[\frac{\left(-\frac{L}{2} + s\right) e\_ty\, e^{I\omega t}\,((L - 2\,s)\ Omega\_d\_p + 2\,c\_dz)\ (e\_tx^2 + e\_ty^2)}{2} + \frac{\left(-\frac{L}{2} + s\right) e\_tz^2\, e\_ty\, e^{I\omega t}\,((L - 2\,s)\ Omega\_d\_p + 2\,c\_dz)}{2}\right], \left[-\frac{\left(-\frac{L}{2} + s\right) e\_tx\, e^{I\omega t}\,((L - 2\,s)\ Omega\_d\_p + 2\,c\_dz)\ (e\_tx^2 + e\_ty^2)}{2} - \frac{\left(-\frac{L}{2} + s\right) e\_tz^2\, e\_tx\, e^{I\omega t}\,((L - 2\,s)\ Omega\_d\_p + 2\,c\_dz)}{2}\right], \left[0\right]\right] \tag{4.2.1}$$

> $bbb := Vector\left(\left[simplify\left(c\_a\cdot rho\,\frac{pi\cdot D^2}{4}\int_0^L \frac{aaa(1,1)}{\exp(I\cdot omega\cdot t)}\,ds\right), simplify\left(c\_a\cdot rho\,\frac{pi\cdot D^2}{4}\int_0^L \frac{aaa(2,1)}{\exp(I\cdot omega\cdot t)}\,ds\right), simplify\left(c\_a\right.\right.$

$$\cdot\text{rho}\ \frac{\text{pi}\cdot D^2}{4}\int_0^L \frac{aaa(3,1)}{\exp(I\cdot\text{omega}\cdot t)}\,ds\Bigg)\Bigg]\Bigg)$$

$$bbb := \begin{bmatrix} -\frac{c\_a\,\rho\,\pi\,D^2\,e\_ty\,Omega\_d\_p\,(e\_tx^2+e\_ty^2+e\_tz^2)\,L^3}{48} \\ \frac{c\_a\,\rho\,\pi\,D^2\,e\_tx\,Omega\_d\_p\,(e\_tx^2+e\_ty^2+e\_tz^2)\,L^3}{48} \\ 0 \end{bmatrix} \tag{4.2.2}$$

>

> $Vector\left(\left[0, simplify\left(c\_a\cdot\text{rho}\ \frac{\text{pi}\cdot D^2}{4}\int_0^L -\left(-\frac{L}{2}+s\right)\cdot\frac{u\_dcN(2,1)}{\exp(I\cdot\text{omega}\cdot t)}\,ds\right), simplify\left(c\_a\cdot\text{rho}\ \frac{\text{pi}\cdot D^2}{4}\int_0^L -\left(-\frac{L}{2}+s\right)\cdot\frac{u\_dcN(3,1)}{\exp(I\cdot\text{omega}\cdot t)}\,ds\right)\right]\right)$

$$\begin{bmatrix} 0 \\ -\frac{c\_a\,\rho\,\pi\,D^2\,e\_ty\,Omega\_d\_p\,e\_tz\,L^3}{48} \\ \frac{c\_a\,\rho\,\pi\,D^2\,Omega\_d\_p\,(e\_tx^2+e\_ty^2)\,L^3}{48} \end{bmatrix} \tag{4.2.3}$$

> $simplify\left(c\_a\cdot\text{rho}\ \frac{\text{pi}\cdot D^2}{4}\int_0^L -\left(-\frac{L}{2}+s\right)\frac{subs\left((e\_tx^2+e\_ty^2)=1, u\_dcN(3,1)\right)}{\exp(I\cdot\text{omega}\cdot t)}\,ds\right)$

$$\frac{c\_a\,\rho\,\pi\,D^2\,Omega\_d\_p\,L^3}{48} \tag{4.2.4}$$

> $\frac{(4.2.4)}{Omega\_d\_p}$

$$\frac{c\_a\,\rho\,\pi\,D^2\,L^3}{48} \tag{4.2.5}$$

4. Damping

>

4.1 Translation

> $u\_c;$

$$\begin{bmatrix} 0 \\ 0 \\ c\_z\,e^{I\omega t} - Omega\_p\,e^{I\omega t}\,r\_so \end{bmatrix} \tag{5.1.1}$$

The velocity is decomposed in perpendicular direction to the cylinder centre line $\mathbf{u}_{RN} = \mathbf{e}_t \times (\mathbf{u}_R \times \mathbf{e}_t)$,

> $u\_cN := simplify(CrossProduct(e\_t, CrossProduct(u\_c, e\_t)));$

$$u\_cN := \begin{bmatrix} -e\_tz\,e^{I\omega t}\,(-Omega\_p\,r\_so + c\_z)\,e\_tx \\ -e\_tz\,e^{I\omega t}\,(-Omega\_p\,r\_so + c\_z)\,e\_ty \\ e^{I\omega t}\,(e\_tx^2+e\_ty^2)\,(-Omega\_p\,r\_so + c\_z) \end{bmatrix} \tag{5.1.2}$$

> $u\_cN := simplify\left(subs\left(r\_so = s - \frac{L}{2}, subs(z = z\_1 + s\cdot e\_tz, subs(x = x\_1 + s\cdot e\_tx, u\_cN))\right)\right);$

$$u\_cN := \begin{bmatrix} -\frac{e\_tx\,e^{I\omega t}\,((L-2\,s)\,Omega\_p + 2\,c\_z)\,e\_tz}{2} \\ -\frac{e\_ty\,e^{I\omega t}\,((L-2\,s)\,Omega\_p + 2\,c\_z)\,e\_tz}{2} \\ \frac{e^{I\omega t}\,((L-2\,s)\,Omega\_p + 2\,c\_z)\,(e\_tx^2+e\_ty^2)}{2} \end{bmatrix} \tag{5.1.3}$$

> $u\_cN\_ds := simplify\left(Vector\left(\left[\int_0^L \frac{u\_cN(1,1)}{\exp(I\,\text{omega}\,t)}\,ds, \int_0^L \frac{u\_cN(2,1)}{\exp(I\,\text{omega}\,t)}\,ds, \int_0^L \frac{u\_cN(3,1)}{\exp(I\,\text{omega}\,t)}\,ds\right]\right)\right);$

$$u\_cN\_ds := \begin{bmatrix} -L\,e\_tx\,e\_tz \\ -L\,c\_z\,e\_ty\,e\_tz \\ L\,c\_z\,(e\_tx^2+e\_ty^2) \end{bmatrix} \tag{5.1.4}$$

> $F\_VD\_c := \frac{8}{3 \cdot \mathrm{pi}} \, u\_rn\_A \cdot c\_d \cdot \frac{\mathrm{rho}}{2} \, \mathrm{D} \cdot \sim u\_cN\_ds(3, 1)$

$$F\_VD\_c := \frac{4 \, u\_rn\_A \, c\_d \, \rho \, \mathrm{D} \, L \, c\_z \left(e\_tx^2 + e\_ty^2\right)}{3 \, \pi} \tag{5.1.5}$$

> $\frac{subs\left(\left(e\_tx^2 + e\_ty^2\right) = 1, F\_VD\_c\right)}{c\_z}$

$$\frac{4 \, u\_rn\_A \, c\_d \, \rho \, \mathrm{D} \, L}{3 \, \pi} \tag{5.1.6}$$

4.2 Rotation

>

> $F\_VD\_c\_omega := simplify\left(\frac{8}{3 \cdot \mathrm{pi}} \, u\_rn\_A \cdot c\_d \cdot \frac{\mathrm{rho}}{2} \, \mathrm{D} \cdot \int_0^L - \left(-\frac{L}{2} + s\right) \cdot \frac{u\_cN(3, 1)}{\exp(I \, \mathrm{omega} \, t)} \, \mathrm{d}s\right)$

$$F\_VD\_c\_omega := \frac{u\_rn\_A \, c\_d \, \rho \, \mathrm{D} \, Omega\_p \left(e\_tx^2 + e\_ty^2\right) L^3}{9 \, \pi} \tag{5.2.1}$$

> $\frac{subs\left(\left(e\_tx^2 + e\_ty^2\right) = 1, F\_VD\_c\_omega\right)}{Omega\_p}$

$$\frac{u\_rn\_A \, c\_d \, \rho \, \mathrm{D} \, L^3}{9 \, \pi} \tag{5.2.2}$$

>

C.3. Verification based on a five buoys system

When this system is analysed the following eigenmodes and eigenvalues shown in equation C.1 and figure C.1 can be found. The first eigenmode refers to a coupled heave motion. It can be seen that the middle buoy has the most extreme displacement. The second and third eigenmode resemble a pitch motion. With the second eigenfrequency buoys 1, 2 and 3 move in opposite direction as buoy 4 and 5. With third eigenfrequency buoy 1 and 4 move in opposite direction as buoy 3 and 5. The fourth eigenfrequency resembles a flying movement where buoy 1 and 3 move in opposite direction as the other three buoys.

$$\omega_1 = 0.7316 \text{ rad/s} \begin{bmatrix} -0.2110 \\ -0.7793 \\ -0.2110 \\ -0.3897 \\ -0.3897 \end{bmatrix}, \omega_2 = 0.8145 \text{ rad/s} \begin{bmatrix} 0.0000 \\ 0.5774 \\ -0.0000 \\ -0.5774 \\ -0.5774 \end{bmatrix} \omega_3 = 0.8252 \text{ rad/s} \begin{bmatrix} 0.3717 \\ -0.0000 \\ -0.3717 \\ 0.6015 \\ -0.6015 \end{bmatrix},$$

$$\omega_4 = 0.8950 \text{ rad/s} \begin{bmatrix} 0.6749 \\ -0.2436 \\ 0.6749 \\ -0.1218 \\ -0.1218 \end{bmatrix} \omega_5 = 0.8978 \text{ rad/s} \begin{bmatrix} 0.6015 \\ 0.0000 \\ -0.6015 \\ -0.3717 \\ 0.3717 \end{bmatrix}, \quad \text{(C.1)}$$

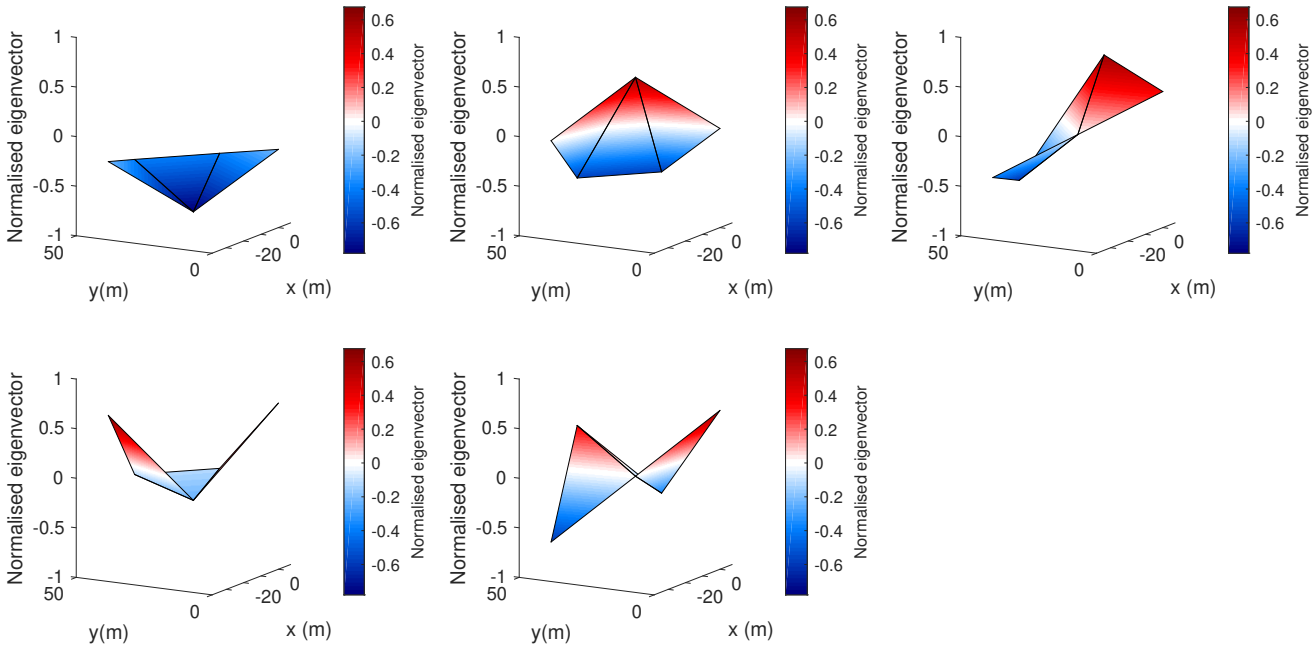

Figure C.1: Eigenmodes of a five buoys system

In figure C.2 the response of a five buoys system can be found. The vertical red dotted lines indicate the eigenfrequencies as shown in equation C.1. In the eigenmodes corresponding with the two lower eigenfrequencies an high motion of buoy 2 was indicated. This is also seen in the lower lower angular frequencies of the response plot. In the eigenmodes corresponding with the two higher eigenfrequencies an high motion of buoy 5 was indicated. This is again seen in figure C.2.

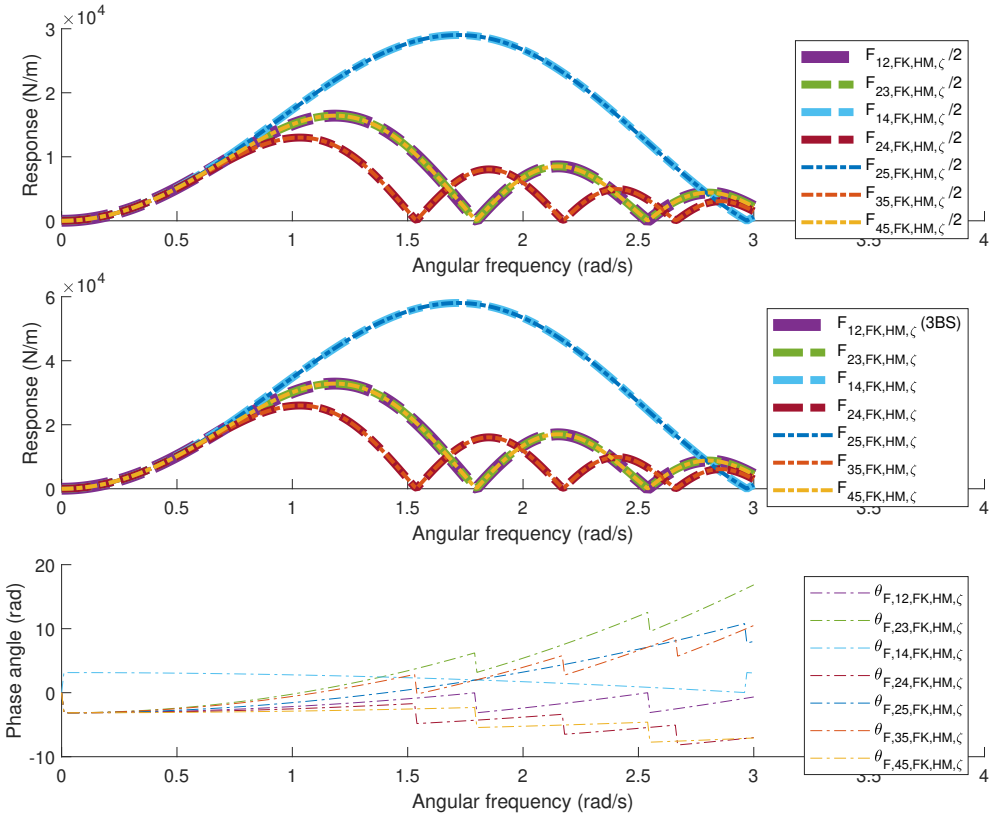

Figure C.3: Comparison of Froude-Krylov and hydrodynamic mass force between the three buoy (3BS) and five buoys system.

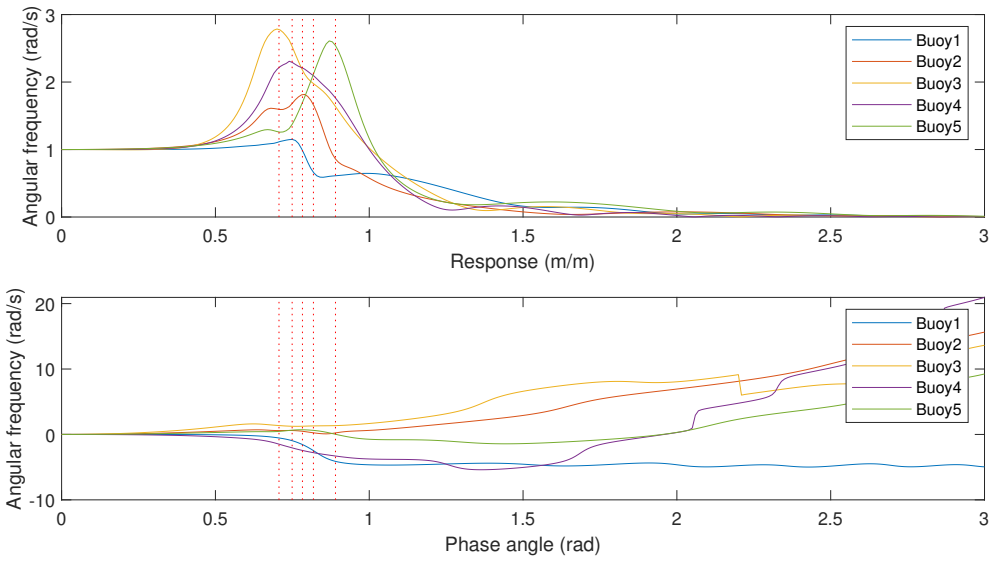

Figure C.2: Response of a five buoys system

Figure C.3 and Figure C.4 the Froude-Krylov and hydrodynamic mass force are shown. This indicates that the forces and moments have the same magnitude for the beams with the same orientation. The phase angle is different. Figure C.5 and Figure C.6 indicated the viscous drag force and moment on the different beams. These forces and moments do mainly depend on the magnitude of the relative

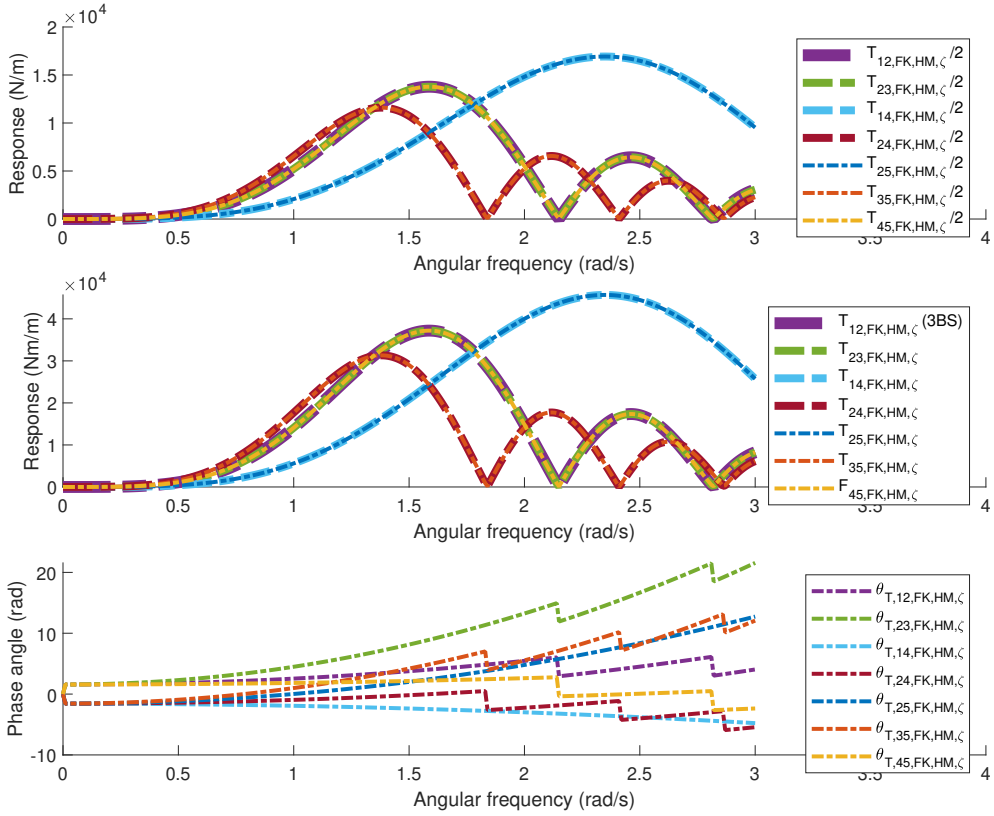

Figure C.4: Comparison of Froude-Krylov and hydrodynamic mass moment between the three buoy (3BS) and five buoys system.

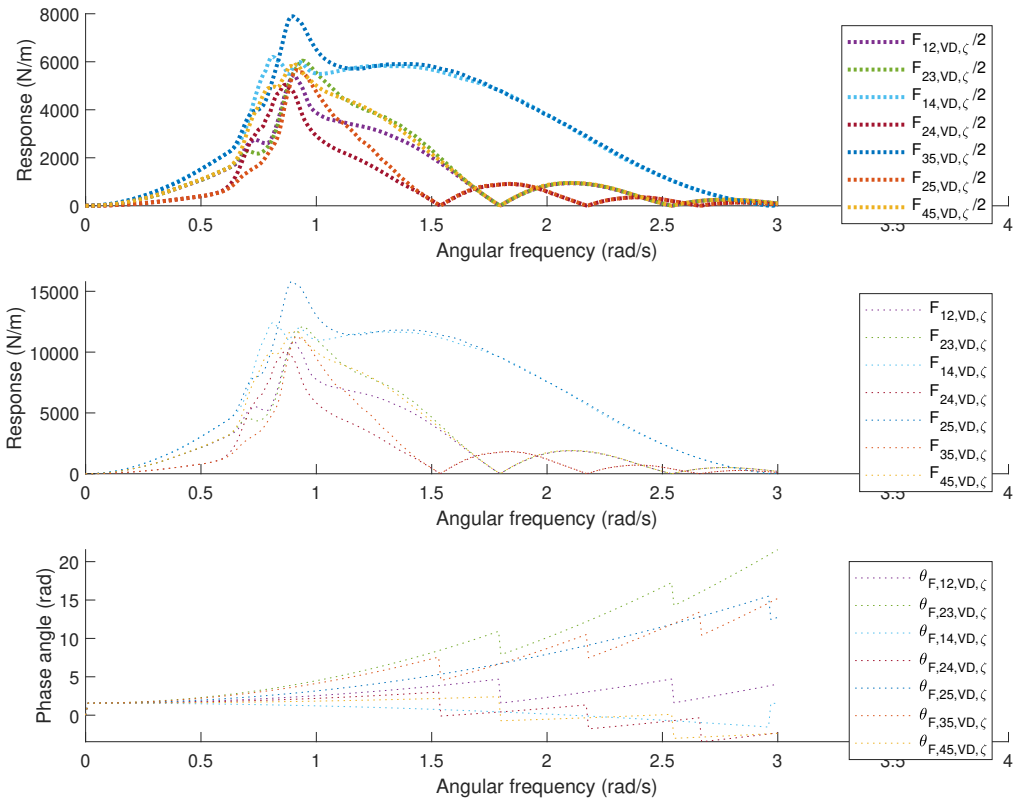

Figure C.5: Comparison of viscous drag force between the three buoy (3BS) and five buoys system.

velocity. This can be found in Figure C.7. The relative velocities, the force and the torque are in the same order of magnitude. Lastly, in Figure C.7 the Froude-Krylov forces on the bottom of the buoys. These are each time the same. Only the phase angle differs due to their position in x-direction.

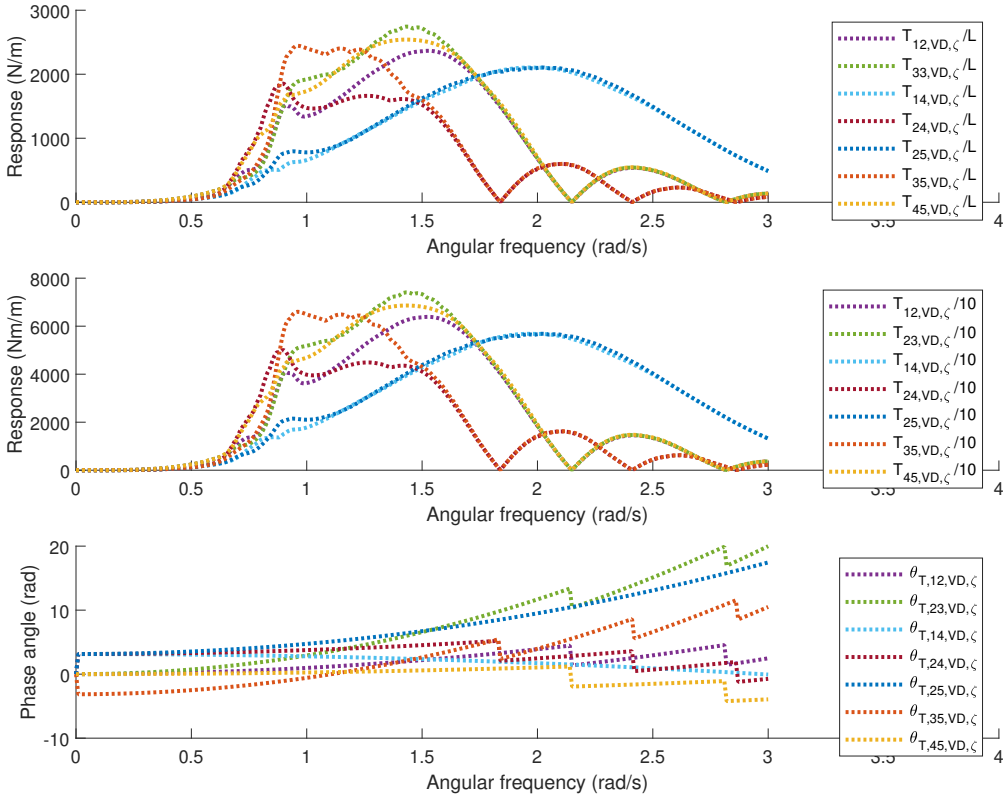

Figure C.6: Comparison of viscous drag moment between the three buoy and five buoys system.

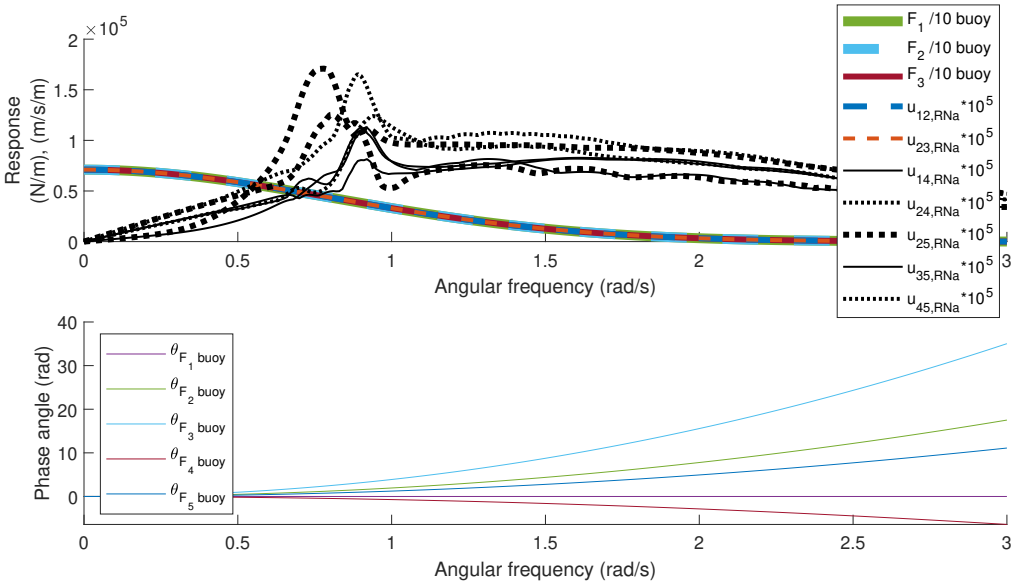

Figure C.7: Comparison of forces on the buoys and the relative velocity of the beams between the three buoy (3BS) and five buoys system.

D

Appendix: MATLAB code

This appendix contains the essential code that was necessary to obtain the results shown in this thesis. To speed up the process of simulations this code was further implemented in a bigger code so that multiple topologies and variations can be executed. Furthermore, code was written to easily assess the obtained data. The larger code can be obtained by contacting the author Andreas Feys or the supervisor of this thesis Dr.-Ing. S. Schreier.

Listing D.1: run.m code

```
1
2  clear;
3  % close all
4  t=1;
5  tic
6  Input
7  [BuoyCon,Pos1,Pos2,Resp_BuoyCon]=Connections(C,X,Y,DeptBeamVec,Respini);      % Finding coordinates and
       responce of start and end of beam
8  time(t)=toc;
9  t=t+1;
10 tic
11 BuildupMassMatrix
12 time(t)=toc;
13 t=t+1;
14 tic
15 BuildupStiffnessMatrix
16 time(t)=toc;
17 t=t+1;
18 tic
19 BuildupForceVectorFixed
20 time(t)=toc;
21 t=t+1;
22 % Qcc=zeros(NumIt,DimSystem,length(omega));
23 aa=0;
24 bb=2;
25 while bb>0.01 && aa<20
26 %     tic
27     aa=aa+1;
28     if aa < 2
29         [BuoyCon,Pos1,Pos2,Resp_BuoyCon]=Connections(C,X,Y,DeptBeamVec,Respini);
30     elseif aa <= 2
31         aaa1=A.*Respini+(1-A).*permute(Qcc(1,:,:),[2 3 1]);
32         [BuoyCon,Pos1,Pos2,Resp_BuoyCon]=Connections(C,X,Y,DeptBeamVec,aaa1);
33     else
34         aaa2=permute( A.*Qcc(aa-2,:,:)+(1-A).*Qcc(aa-1,:,:) ,[2 3 1]);
35         [BuoyCon,Pos1,Pos2,Resp_BuoyCon]=Connections(C,X,Y,DeptBeamVec,aaa2);      % Finding coordinates
               and responce of start and end of beam
36     end
37 %     time(t)=toc;
38 %     t=t+1;
39     tic
40     BuildupDampingsMatrix
41     time(t)=toc;
42     t=t+1;
43     tic
44     BuildupForceVectorDamping
45     time(t)=toc;
46     t=t+1;
47     tic
48     Calculations
49     time(t)=toc;
50     t=t+1;
51     tic
52     time(t)=toc;
53     t=t+1;
54     tic
55     Qcc(aa,:,:)=permute(Resp,[3,1,2]);
56     time(t)=toc;
57     t=t+1;
58     if aa > 1
59     bb=sum(abs(sum(permute(abs(Qcc(aa-1,:,:)-Qcc(aa,:,:)),[2 3 1]),2))./abs(sum(permute(abs(Qcc(aa-1,:,:))
           ,[2 3 1]),2)));
60     end
```

```
end
aa
bb
sum(time)
load chirp
sound(y,Fs)
```

Listing D.2: input.m code

```
%% Written by Andreas Feys for Graduation
% Program is build up to assess the response of a buoy and beam structure
% in regular waves in a frequency domain.

%% This script defines the input variables of the whole program
% Here the inputs will be explained
% Omegax: the frequency range for the calculations,
% C: topology matrix,
% TriangleMatrix defines the triangles
% X: x positions of the different buoys
% Y: y coordinates,
% D: buoy diameter matrix
% Draft: buoy draft matrix,
% l: beam length,
% L: beam length matrix

%% General inputs
global rho g omega Ampletude k c_d c_a
rho=1025;
g=9.81;
Ampletude=1; % Amplitude of incoming wave
omega=[0:0.01:3]; %Variation of omega to asses over.
k=omega.^2./g;      %k variation direct connection with omega
c_d=1.2;
c_a=1;
A=0.15;

% NumIt=10;
%% Structure inputs

BeamLength=27;
BeamDept=-2;
BeamDiameter=1;
BuoyDiameter=3;
BuoyDraft=-7.5;

%% 2 buoy system for verification
C=[ 1 1 1 0 0;...
    -1 1 1 1 1;...
    -1 -1 1 1 0;...
    0 -1 -1 1 1;...
    0 -1 0 -1 1];
DimSystem=length(C); %Dimension construction: #buoys

Xini=[0 0 0 sqrt(3)/2*27 sqrt(3)/2*27]';  % coordinates in relative grid with distance between buoys 1
Yini=[0 27 27*2 27*0.5 27*1.5]';
Zini=BuoyDraft*ones(length(Xini),1);
alpha=45;
Buoypositionmatrix=transpose(rotz(alpha)*[Xini'; Yini'; Zini']);
X=Buoypositionmatrix(:,1);
Y=Buoypositionmatrix(:,2);
Z=Buoypositionmatrix(:,3);

Respini=1*ones(length(X),length(omega)); % Initial responce for the buoys per omega
DiameterBuoy=BuoyDiameter*ones(DimSystem,1);%[3; 3];%

percentCritDamp=0.005;                                  %Percentage of critical damping applied on
    buoy
LengthBeam=abs(BeamLength*(C-eye(DimSystem)));          %length matrix beam
DiameterBeam=abs(BeamDiameter*(C-eye(DimSystem)));      %radius matrix beam
DeptBeam=BeamDept*abs(C-eye(DimSystem));               %Draft Vector buoy
DeptBeamVec=BeamDept*ones(DimSystem,1);

TriangleMatix=[1 2 3];
```

Listing D.3: Connections.m code

```
function [Combinaties,Pos1,Pos2,Responcecombinatie] = Connections(Topology,X,Y,DeptConnection,Responces)
% Function: Converts the topology to a matrix with every row two values of
% the X, Y, Responce for a beam.
% inputs: X and Y location of the buoys. Z: vector of the depth of the beams
% Response of the system of previous iteration, topology matrix of the system.

ddd=triu(Topology,1);% positive triangle without diagonal

l_inds = find(ddd); % find indices of non zero items
[row,col] = ind2sub(size(Topology),l_inds); %convert indices to coordinates resulting in a matrix with on
    every row two buoys that are directly connected. This is used to rearrange the position information
    of all connect buoys

Combinaties = [row col];
Xcom=X(Combinaties);                %for a 2 buoy system the vector must be transposed
Ycom=Y(Combinaties);                %for a 2 buoy system the vector must be transposed
Zcom=DeptConnection(Combinaties);   %for a 2 buoy system the vector must be transposed

```

```
Responcecombinatie=zeros([size(Combinaties) length(Responces)]); % The same reorganisation is done for the response

    for n=1:size(Combinaties,1)
        Responcecombinatie(n,1,:)=Responces(Combinaties(n,1),:);
        Responcecombinatie(n,2,:)=Responces(Combinaties(n,2),:);
    end

Pos1=[Xcom(:,1) Ycom(:,1) Zcom(:,1)]; % combining these coordinates for positions used in Morison calculations
Pos2=[Xcom(:,2) Ycom(:,2) Zcom(:,1)];
end
```

Listing D.4: BuildupMassMatrix.m code

```
%% Written by Andreas Feys for Graduation
% Program is build up to assess the response of a buoy and beam structure
% in regular waves in a frequency domain.

%% Masses and added masses from buoys (Part A)
Mbuoy=rho*pi*(DiameterBuoy.^2)/4.*abs(Z);                    %Vector of masses of the buoys
Mbuoyadded=AddedmassFK(abs(Z),DiameterBuoy);                 %Vector of added masses of the buoys
M1a_buoy=diag(Mbuoy+Mbuoyadded);                             %Sumation and make diagonal matrix

%% Masses and moment of inertias from beams (Part B and part C)
M1b_beam_dv4=pi*rho.*(DiameterBeam.^2/4).*LengthBeam/4;      %Mass matrix of beams

M1c=-1/12.*pi*rho.*(DiameterBeam.^2/4).*LengthBeam;           % Moment of inertia

M1d=diag(sum(M1b_beam_dv4));                                 %summation of rows mass matrix

M1e=diag(sum(-M1c));                                         %summation of rows inertia matrix times -1

M1=M1a_buoy+M1b_beam_dv4+M1c+M1d+M1e;                        %total mass matrix excluding Morison contribution

% M1=M1a_buoy+M1b_beam_dv4+M1d;                          %total mass matrix excluding Morison contribution

%% Build up of added mass from Morison

M2=zeros(DimSystem,DimSystem);                               %initialising a zero matrix for the added masses
M3=zeros(DimSystem,DimSystem);

for n=1:size(BuoyCon,1)
    % the for loop calculates the values per connecting beam.
    M2a=MorisonAddedHM(Pos1(n,:),Pos2(n,:),DiameterBeam(BuoyCon(n,1),BuoyCon(n,2)));
    M2(BuoyCon(n,1),BuoyCon(n,2),:)=1/4*M2a;                 %first the added mass is calculated for one connecting beam,
    % then they are divide by four and placed on the right position based
    % on the connecting buoys (making use of the connection matrix that is
    % based on the topology matrix.

    M3a=MorisonAddedHMTorque(Pos1(n,:),Pos2(n,:),DiameterBeam(BuoyCon(n,1),BuoyCon(n,2)));
    M3(BuoyCon(n,1),BuoyCon(n,2),:)=-M3a/LengthBeam(BuoyCon(n,1),BuoyCon(n,2))^2;
    % the same sequence is not executed for the moment of inertia due to
    % added mass.
end
    % the four loop only results in a matrix with the top triangle filled
M2=M2+permute(M2,[2 1 3]);                                   % the matrix is mirrored over its diagonal
M2_sum=sum(M2,2);                                            % the rows are summed
M2_diag=diag(M2_sum);
M2_tot=M2+M2_diag;                                           % and are added to the matrix

M3=M3+permute(M3,[2 1 3]);                                   % the same is done for the moment inertia part of the mass matrix
M3_sum=-sum(M3,2);
M3_diag=diag(M3_sum);
M3_tot=M3+M3_diag;

%% summation

% M=M1+M2_tot+M3_tot;
M=M1+M2_tot+M3_tot;                                          % now all sub matrices are added together resulting in the total mass matrix
```

Listing D.5: MorisonAddedHM.m code (2)

```
function [addedmass] = MorisonAddedHM(Pos1,Pos2,D)
% Written by Andreas Feys for graduation process
% Summary of this function
%   Imported globals: rho and c_a
%   Pos1: position of one end of on end of th cylinder (x, y, z)'
%   Pos2 position other end of cylinder,
%   D; diameter of cylinder,
%   addemass: output the force vector in vertical direction per given omega
% All units are in meter, newton, rad/s
% The time varying part is not included

global rho c_a
L=norm(Pos2-Pos1);
e_t=(Pos2-Pos1)/L;

addedmass=c_a * rho * pi * D ^ 2 * L * (e_t(1) ^ 2 + e_t(2) ^ 2) / 4;
end
```

Listing D.6: MorisonAddedHMTorque.m code

```
function [addedmass] = MorisonAddedHMTorque(Pos1,Pos2,D)
% Writen by Andreas Feys for graduation process
% Summary of this function
%   Inported globals:
%   rho, k, ampletude, omega and c_a
%   Pos1: position of one end of on end of th cylinder (x, y, z)'
%   Pos2 position other end of cylinder,
%   D; diameter of cylinder,
%   Moment of innertia due to added mass: output the force vector in vertical direction per given omega
% All units are in meter, newton, rad/s
% The time varying part is not included

global rho c_a
L=norm(Pos2-Pos1);
e_t=(Pos2-Pos1)/L;

addedmass=c_a * rho * pi * D ^ 2 * (e_t(1)^2+e_t(2)^2) * L ^ 3 / 48;


end
```

Listing D.7: BuildupStiffnessMatrix.m code

```
%% Written by Andreas Feys for Graduation
% Program is build up to assess the response of a buoy and beam structure
%  in regular waves in a frequency domain.
% This part of the program defines the stiffness matrix


Kbuoy=pi*rho*g*(DiameterBuoy.^2)/4;                         %Stiffness vector of the buoys
K=diag(Kbuoy);
```

Listing D.8: BuildupDampingsMatrix.m code

```
%% Written by Andreas Feys for Graduation
% Program is build up to assess the response of a buoy and beam structure
% in regular waves in a frequency domain.
% In this part the damping matrix will be determined

%% Damping due to buoys determined with critical damping
Kbuoy=pi*rho*g.*(DiameterBuoy.^2)/4;
bBuoy=percentCritDamp*2*sqrt(Kbuoy.*Mbuoy);                    %calculation damping based on critical
    damping taking into account the hard coded stiffness and mass
B1=diag(bBuoy);
B1_omega=repmat(B1,1,1,length(omega));     % for the calculations we need this in a 3D matrix


%% Damping due to VD force and Torque
B2=zeros(1,length(omega));
B2_omega=zeros(DimSystem,DimSystem,length(omega));
B3=zeros(1,length(omega));
B3_omega=zeros(DimSystem,DimSystem,length(omega));

for n=1:size(BuoyCon,1)
    Resp1=reshape(Resp_BuoyCon(n,1,:),1,length(omega));                    %reshape to right input for
        the Morison functions
    Resp2=reshape(Resp_BuoyCon(n,2,:),1,length(omega));
    B2=MorisonAddedVD(Pos1(n,:),Pos2(n,:),DiameterBeam(BuoyCon(n,1),BuoyCon(n,2)),Resp1,Resp2);
    B2_omega(BuoyCon(n,1),BuoyCon(n,2),:)=1/4*B2;

    B3=MorisonAddedVDTorque(Pos1(n,:),Pos2(n,:),DiameterBeam(BuoyCon(n,1),BuoyCon(n,2)),Resp1,Resp2);
    B3_omega(BuoyCon(n,1),BuoyCon(n,2),:)=-B3/LengthBeam(BuoyCon(n,1),BuoyCon(n,2))^2;
end
B2_omega=B2_omega+permute(B2_omega,[2 1 3]);
B2_omega_sum=sum(B2_omega,2);
B2_omega_diag=bsxfun(@times, eye(size(B2_omega(:,:,1))), B2_omega_sum);
B2_omega_tot=B2_omega+B2_omega_diag;

B3_omega=B3_omega+permute(B3_omega,[2 1 3]);
B3_omega_sum=-sum(B3_omega,2); % be aware of the minus here
B3_omega_diag=bsxfun(@times, eye(size(B3_omega(:,:,1))), B3_omega_sum);
B3_omega_tot=B3_omega+B3_omega_diag;

% B=B1_omega+B2_omega_tot+B3_omega_tot;
B=B1_omega+B2_omega_tot+B3_omega_tot;
```

Listing D.9: MorisonAddedVD.m code

```
function [addedmass] = MorisonAddedVD(Pos1,Pos2,D,Resp1,Resp2)
%% Written by Andreas Feys for Graduation
% Program is build up to assess the response of a buoy and beam structure
% in regular waves in a frequency domain.

% In this part the VD damping force coefficient due to the movement of the
% construction will be determined. Multiplying the coefficient that is
% outputted by this function with the velocity of the element will give the force

global rho c_d
L=norm(Pos2-Pos1);
e_t=(Pos2-Pos1)/L;

```

```
u_rn_A=MorisonMagnetudeUra(Pos1,Pos2,Resp1,Resp2);

addedmass=8/3/pi*c_d*rho/2*D*u_rn_A*L*(e_t(1)^2+e_t(2)^2);
end
```

Listing D.10: MorisonMagnetudeUra.m code

```
function [urn1b] = MorisonMagnetudeUra(Pos1,Pos2,Resp1,Resp2)
% Written by Andreas Feys for graduation process
% Summary of this function
%   Imported globals:
%   rho, k, ampletude, omega and c_a
%   Pos1: position of one end of on end of th cylinder (x, y, z)'
%   Pos2 position other end of cylinder,
%   Resp1 is the found response over previous iteration of buoy 1
%   Resp2 is the found response over previous iteration of buoy 2
%   D; diameter of cylinder,
%   Force: output the force vector in vertical direction per given omega
% All units are in meter, newton, rad/s
% The time varying part is not included

global k Ampletude omega

L=norm(Pos2-Pos1);      %calculation of beam length
e_t=(Pos2-Pos1)/L;      %calculation of tangent unit vector

s=[0:1/12:1];
T=[0:2/12*pi:2*pi];
urn1a=zeros(length(s),length(T),length(omega));

for S=1:length(s)
    for TT=1:length(T)
        urn1a(S,TT,:)= reshape(sqrt(real(Ampletude * omega .* exp(k * Pos1(3)) .* exp(-1j * k * (s(S) * L
            * e_t(1) + Pos1(1))) * exp( 1j * T(TT))*e_t(2)).^2 + real(1j * Ampletude * omega .* exp(k *
            Pos1(3)) .* exp(-1j * k * (s(S) * L * e_t(1) + Pos1(1))) * exp( 1j * T(TT)) - 1j * Resp1 * (
            1 - s(S) ) .* omega * exp( 1j * T(TT)) -  1j *  s(S) * Resp2 .* omega * exp( 1j *T(TT))).^2 )
            ,[1,1,length(omega)]);
%  urn1a(S,TT,:)=        reshape(

     abs(1j * Ampletude * omega .* exp(k * Pos1(3)) .* exp(-1j * k * (s(S) * L * e_t(1) + Pos1(1))) * exp(
      1j * T(TT)) - 1j * Resp1 * ( 1 - s(S) ) .* omega * exp( 1j * T(TT)) -  1j *  s(S) * Resp2 .* omega *
      exp( 1j *T(TT))),[1,1,length(omega)]);

    end
end
% urn1a
% max(max(urn1a))
urn1b=reshape(max(mean(urn1a,1),[],2),[1,length(omega)]);
end
```

Listing D.11: MorisonAddedVDTorque.m code

```
function [addedmass] = MorisonAddedVDTorque(Pos1,Pos2,D,Resp1,Resp2)
%UNTITLED2 Summary of this function goes here
%   Detailed explanation goes here

global rho c_d
L=norm(Pos2-Pos1);
e_t=(Pos2-Pos1)/L;

u_rn_A=MorisonMagnetudeUra(Pos1,Pos2,Resp1,Resp2);

addedmass=8/3/pi*c_d*rho/2*D*u_rn_A*L^3*(e_t(1)^2+e_t(2)^2)/12;
end
```

Listing D.12: BuildupForceVector.m code

```
%% Build up force matrix
% Written by Andreas Feys for Graduation
% Program is build up to assess the response of a buoy and beam structure
% in regular waves in a frequency domain.

global rho g k Ampletude omega

%% Froude Krylov Forces on buoys
Froude_KrylovVec=rho*g*Ampletude*exp(Z*k).*exp(-1i*X*k)*pi.*DiameterBuoy.^2/4;
Froude_KrylovVec2=rho*Z*pi.*DiameterBuoy.^2/4*-Ampletude*omega.^2.*exp(Z*k).*exp(-1i*X*k);
F1=Froude_KrylovVec;

%% Morison FK and HM

F2a_FKHM=zeros(DimSystem,DimSystem,length(omega));
T2b_FKHM=zeros(DimSystem,DimSystem,length(omega));

for n=1:size(BuoyCon,1)
    F2a_FKHM(BuoyCon(n,1),BuoyCon(n,2),:)=MorisonFKHM(Pos1(n,:)',Pos2(n,:)',DiameterBeam(BuoyCon(n,1),
        BuoyCon(n,2)))/2; %call function
    T2b_FKHM(BuoyCon(n,1),BuoyCon(n,2),:)=MorisonFKHMTorque(Pos1(n,:)',Pos2(n,:)',DiameterBeam(BuoyCon(n
        ,1),BuoyCon(n,2)))/LengthBeam(BuoyCon(n,1),BuoyCon(n,2));
end
F2a_FKHM=F2a_FKHM+permute(F2a_FKHM,[2 1 3]);
T2b_FKHM=T2b_FKHM+permute(T2b_FKHM,[2 1 3]);

```

```
25
26 %% Morison VD
27
28 F3a_VD=zeros(DimSystem,DimSystem,length(omega));
29 T3b_VD=zeros(DimSystem,DimSystem,length(omega));
30
31 for n=1:size(BuoyCon,1)
32     Resp1=reshape(Resp_BuoyCon(n,1,:),1,length(omega));                    %reshape to right imput for
           the morison functions
33     Resp2=reshape(Resp_BuoyCon(n,2,:),1,length(omega));
34     F3a_VD(BuoyCon(n,1),BuoyCon(n,2),:)=MorisonVD(Pos1(n,:)',Pos2(n,:)',DiameterBeam(BuoyCon(n,1),BuoyCon(
           n,2)),Resp1,Resp2)/2; %call function
35     T3b_VD(BuoyCon(n,1),BuoyCon(n,2),:)=MorisonVDTorque(Pos1(n,:)',Pos2(n,:)',DiameterBeam(BuoyCon(n,1),
           BuoyCon(n,2)),Resp1,Resp2)/LengthBeam(BuoyCon(n,1),BuoyCon(n,2));
36 end
37 F3a_VD=F3a_VD+permute(F3a_VD,[2 1 3]);
38 T3a_VD=T3b_VD+permute(T3b_VD,[2 1 3]);
39
40 % F=F1+sum(F2a_FKHM+T2b_FKHM+F3a_VD+F3a_VD,2);
41 F=F1+sum(F2a_FKHM+T2b_FKHM+F3a_VD+T3a_VD,2);
```

Listing D.13: MorisonFKHM.m code (2)

```
1  function [Force] = MorisonFKHM(Pos1,Pos2,D)
2  % Written by Andreas Feys for graduation process
3  % Summary of this function
4  %   Inported globals:
5  %   rho, k, ampletude, omega and c_a
6  %   Pos1: position of one end of on end of th cylinder (x, y, z)'
7  %   Pos2 position other end of cylinder,
8  %   D; diameter of cylinder,
9  %   Force: output the force vector in vertical direction per given omega
10 % All units are in meter, newton, rad/s
11 % The time varying part is not included
12
13 global rho k Ampletude omega c_a
14
15 % ampli=Ampletude
16 syms s x y z a a_n t Omega K
17 % s, coordinate along cylinder axis
18 % x y z global coordinate system
19 % e_t unit vector along cylinder axis with coordinates ex ey ez in global
20 % system
21 % a particle acceleration in fluid
22 % t time
23 % Omega, angular frequency
24 % K wavenumber
25
26 a = [1j*Ampletude .* Omega^2 .* exp(K .* z) .* exp(-1j .* K .* x);...   %definition of acceleration in
       fluid by Airy wave theory without time varying part
27     0;...
28     - Ampletude .* Omega^2 .* exp(K .* z) .* exp(-1j .* K .* x)];
29
30 L=norm(Pos2-Pos1);       %calculation of beam length
31 e_t=(Pos2-Pos1)/L;       %calculation of tangent unit vector
32
33 a_n=cross(e_t,cross(a,e_t));    %perpendicular acceleration
34
35 a_n=subs(a_n, [x, y, z], [Pos1(1)+s.*e_t(1), Pos1(2)+s.*e_t(2), Pos1(3)+s.*e_t(3)]);    %substitution
       before acceleration
36
37 a_n_int=int(a_n,s,0,L);    %integration of equation
38
39 F_n_FK=(1+c_a)*rho*pi*D^2/4*a_n_int;    %calculation of total force
40
41 Force=zeros(1,length(omega));
42 for v = 1:length(omega)
43     Force(v)=eval(subs(F_n_FK(3),[Omega, K],[omega(v), k(v)]));      % substitution of omega and k of
           symbolic toolbox for all desired omega's
44 end
45
46 end
```

Listing D.14: MorisonFKHMTorque.m code

```
1  function [Moment] = MorisonFKHMTorque(Pos1,Pos2,D)
2  % Written by Andreas Feys for graduation process
3  % Summary of this function
4  %   Inported globals:
5  %   rho, k, ampletude, omega and c_a
6  %   Pos1: position of one end of on end of th cylinder (x, y, z)'
7  %   Pos2 position other end of cylinder,
8  %   D; diameter of cylinder,
9  %   Force: output the force vector in vertical direction per given omega
10 % All units are in meter, newton, rad/s
11 % The time varying part is not included
12
13 global rho k Ampletude omega c_a
14
15 syms s x y z a a_n t Omega K r
16 % s, coordinate along cylinder axis
17 % x y z global coordinate system
18 % e_t unit vector along cylinder axis with coordinates ex ey ez in global
19 % system
```

```
% a particle acceleration in fluid
% t time
% Omega, angular frequency
% K wavenumber

a = [1j*Ampletude .* Omega^2 .* exp(K .* z) .* exp(-1j .* K .* x);...   %definition of acceleration in fluid by Airy wave theory without time varying part
    0;...
    - Ampletude .* Omega^2 .* exp(K .* z) .* exp(-1j .* K .* x)];

L=norm(Pos2-Pos1);      %calculation of beam length
e_t=(Pos2-Pos1)/L;      %calculation of tangent unit vector

a_n=cross(e_t,cross(a,e_t));    %perpendicular acceleration
a_n=subs(a_n, [x, y, z], [Pos1(1)+s.*e_t(1), Pos1(2)+s.*e_t(2), Pos1(3)+s.*e_t(3)]);    %substitution before acceleration

a_n_r=-(-L/2+s)*a_n(3);
a_n_r_int=int(a_n_r,s,0,L);
M_FKHM=(1+c_a)*rho*pi*D^2/4*a_n_r_int;
Moment=zeros(1,length(omega));
for v = 1:length(omega)
    Moment(:,v)=eval(subs(M_FKHM,[Omega, K],[omega(v), k(v)]));       % substitution of omega and k of symbolic toolbox for all desired omega's
end


end
```

Listing D.15: MorisonVD.m code

```
function [Force] = MorisonVD(Pos1,Pos2,D,Resp1,Resp2)
% Written by Andreas Feys for graduation process
% Summary of this function
%   Inported globals:
%   rho, k, ampletude, omega and c_a
%   Pos1: position of one end of on end of th cylinder (x, y, z)'
%   Pos2 position other end of cylinder,
%   Resp1 is the found response over previous iteration of buoy 1
%   Resp2 is the found response over previous iteration of buoy 2
%   D; diameter of cylinder,
%   Force: output the force vector in vertical direction per given omega
% All units are in meter, newton, rad/s
% The time varying part is not included

global rho k Ampletude omega c_d

syms s x y z a a_n t Omega K
% s, coordinate along cylinder axis
% x y z global coordinate system
% e_t unit vector along cylinder axis with coordinates ex ey ez in global
% system
% a particle acceleration in fluid
% t time
% Omega, angular frequegncy
% K wavenumber

v = [Ampletude .* Omega .* exp(K .* z) .* exp(-1j .* K .* x);...        %definition of acceleration in fluid by Airy wave theory without time varying part
    0;...
    1j * Ampletude .* Omega .* exp(K .* z) .* exp(-1j .* K .* x)];

L=norm(Pos2-Pos1);      %calculation of beam length
e_t=(Pos2-Pos1)/L;      %calculation of tangent unit vector

u_rn_A=MorisonMagnetudeUra(Pos1,Pos2,Resp1,Resp2);

v_n=cross(e_t,cross(v,e_t));

v_n=subs(v_n, [x, y, z], [Pos1(1)+s.*e_t(1), Pos1(2)+s.*e_t(2), Pos1(3)+s.*e_t(3)]);

v_n_int=int(v_n,s,0,L);

F_n_VD=8/3/pi*c_d*rho/2*D*u_rn_A*v_n_int(3);

Force=zeros(1,length(omega));
for v = 1:length(omega)
    Force(v)=eval(subs(F_n_VD(v),[Omega, K],[omega(v), k(v)]));
end

end
```

Listing D.16: MorisonVDTorque.m code

```
function [Moment] = MorisonVDTorque(Pos1,Pos2,D,Resp1,Resp2)
%UNTITLED2 Summary of this function goes here
%   Ampletude of the wave this is most probably 1 in meter,
%   omega: vector with the dedicated frequencies to calculate,
%   Pos1: position of one end of on end of th cylinder (x, y, z)'
%   Pos2 position other end of cylinder,
%   D; diameter of cylinder,
%   Resp1 response of one end of cylinder (x, y, z)' per frequency,
%   Resp2 response of second of cylinder
%   It calculates the moment around the third axis of the beam oriented
```

```
%   axis system

global rho k Ampletude omega c_d

syms s x y z a a_n t Omega K r
% s, coordinate along cylinder axis
% x y z global coordinate system
% e_t unit vecotr along cylinder axis with coordinates ex ey ez in global
% system
% v particle speed in fluid
% a particle acceleration in fluid
% t time
% Omega, angular frequency
% K wavenumber
% r indicating the distance till the middle of the beam in s direction


v = [Ampletude .* Omega .* exp(K .* z) .* exp(-1j .* K .* x);...
     0;...
     1j * Ampletude .* Omega .* exp(K .* z) .* exp(-1j .* K .* x)];

L=norm(Pos2-Pos1);
e_t=(Pos2-Pos1)/L;

u_rn_A=MorisonMagnetudeUra(Pos1,Pos2,Resp1,Resp2);
v_n=cross(e_t,cross(v,e_t));
v_n=subs(v_n, [x, y, z], [Pos1(1)+s.*e_t(1), Pos1(2)+s.*e_t(2), Pos1(3)+s.*e_t(3)]);

v_n_r=-(-L/2+s)*v_n(3);
v_n_r_int=int(v_n_r,s,0,L);
M_VD=8/3/pi*c_d*rho/2*D*u_rn_A*v_n_r_int;
Moment=zeros(1,length(omega));
for v = 1:length(omega)
     Moment(v)=eval(subs(M_VD(v),[Omega, K],[omega(v), k(v)]));
end
end
```

Listing D.17: Calculations.m code

```
%% Calculations:
% solving the differential equation
global omega
% obtaining the eigenmodes and the eigenfrequencies
[Evecs,Evals]=eig(K,M);
omega1=sqrt(Evals);
Evecnorm=Evecs.*(max(abs(Evecs),[],1).^-1);

% obtaining the frequency response per frequency
Resp=zeros(DimSystem,length(omega));
F=Ffixed+FDamp;

for a=1:length(omega)
     Zdyn=-M*(omega(a)).^2+1j*B(:,:,a).*omega(a)+K;
     Resp(:,a)=Zdyn\F(:,a);
end
```